Phase-Space Berry Phases in Chiral Magnets

Skyrmion Charge, Hall Effect, and Dynamics of Magnetic Skyrmions

Inaugural-Dissertation

zur

Erlangung des Doktorgrades

der Mathematisch-Naturwissenschaftlichen Fakultät

der Universität zu Köln

vorgelegt von

Robert Bamler

aus

München

Köln 2016

Berichterstatter:	Prof. Dr. Achim Rosch
(Gutachter)	Prof. Dr. Alexander Altland

Tag der mündlichen Prüfung: 11. Juli 2016

Abstract

The dynamics of electrons in solids is influenced by Berry phases in phase space (combined position and momentum space). Phase-space Berry phases lead to an effective force on the electrons, an anomalous contribution to the group velocity, and a correction to the density of states in phase space. In addition, Berry phases in position and in momentum space are related to topological winding numbers and can be used to characterize topologically distinct phases of matter. We study theoretically the effects of phase-space Berry phases in magnetic materials with weak spin-orbit coupling and a smoothly varying magnetization texture. Such magnetic textures appear generically in non-centrosymmetric magnetic materials with weak spin-orbit coupling due to a competition between the ferromagnetic exchange interaction and the weaker Dzyaloshinskii-Moriya interaction. In particular, the discovery of topologically stable whirls, so-called skyrmions, in the magnetization texture of these materials has attracted considerable attention due to prospects of applications in future magnetic storage devices.

In part I of this thesis, we investigate the influence of phase-space Berry phases on the equilibrium properties of electrons in chiral magnets with weak spin-orbit coupling. We show that the strength of the Dzyaloshinskii-Moriya interaction in the long-wavelength limit can be calculated from Berry phases in mixed position/momentum space and that the same Berry phases lead to an electric charge of skyrmions in metallic chiral magnets. In insulators, the skyrmion charge of magnetic skyrmions turns out to be proportional to the topologically quantized second Chern number in phase space. This establishes a link between skyrmions in chiral magnets and the charged excitations in integer quantum Hall systems with small Zeeman splitting.

In part II, we consider the Hall effect in the skyrmion lattice phase of chiral magnets in presence of spin-orbit coupling. It has been previously known that Berry phases in momentum space lead to the intrinsic part of the anomalous Hall effect, and that Berry phases in position space lead to an effective Lorentz force, resulting in the so-called topological Hall effect. By expanding the Kubo-Středa Formula for the Hall conductivity in gradients in position and momentum space, we show that the interplay between smooth magnetic textures and spin-orbit coupling leads to a previously disregarded contribution to the Hall effect, and we find a correction to the semiclassical formulation of the topological Hall effect.

In part III, we study the influence of phase-space Berry phases on the dynamics of skyrmions in chiral magnets. Berry phases in mixed position/momentum space lead to a dissipationless momentum transfer from conduction electrons to skyrmions that is proportional to an applied electric field and independent of the (spin or electric) current. We further show that the electric charge of skyrmions, discussed in part I, influences the skyrmion motion only via hydrodynamic drag and ohmic friction in metals. In insulators, the quantized skyrmion charge couples directly to an applied electric field.

Kurzzusammenfassung

Phasenraum-Berryphasen beeinflussen die Bewegung von Elektronen in Festkörpern. Sie führen zu einer effektiven Kraft auf die Elektronen, einem anomalen Beitrag zur Gruppengeschwindigkeit und einer Korrektur der Zustandsdichte im Phasenraum. Außerdem stehen Ortsraum- und Impulsraum-Berryphasen im Zusammenhang mit topologischen Windungszahlen, welche topologisch unterschiedliche Materiezustände unterscheiden. In dieser theoretischen Arbeit untersuchen wir die Effekte von Phasenraumberryphasen in magnetischen Materialien mit schwacher Spin-Bahn-Kopplung und einer glatten Magnetisierungstextur im Ortsraum. Solche magnetischen Texturen entstehen generisch in Magneten ohne Inversionszentrum (chiralen Magneten) mit schwacher Spin-Bahn-Kopplung aufgrund einer Konkurrenz zwischen ferromagnetischer Austauschwechselwirkung und der schwächern Dzyaloschinskii-Moriya-Wechselwirkung. Insbesondere hat die Entdeckung topologisch geschützter Wirbel der Magnetisierung, sogenannter Skyrmionen, aufgrund möglicher Anwendungen in zukünftigen magnetischen Datenspeichern große Aufmerksamkeit hervorgerufen.

In Teil I dieser Arbeit untersuchen wir den Einfluss von Phasenraumberryphasen auf die Gleichgewichtseigenschaften von Elektronen in chiralen Magneten mit schwacher Spin-Bahn-Kopplung. Wir zeigen dass die Stärke der Dzyaloshinskii-Moriya–Wechselwirkung im langwelligen Limes mithilfe von Berryphasen im gemischten Orts/Impulsraum berechnet werden kann und dass dieselben Berryphasen zu einer elektrischen Ladung von Skyrmionen in metallischen chiralen Magneten führen. In Isolatoren ist die Skyrmionenladung proportional zur topologisch quantisierten zweiten Chernzahl im Phasenraum. Mit dieser Erkenntnis schlagen wir eine Brücke zwischen Skyrmionen in chiralen Magneten und den geladenen Anregungen im ganzzahligen Quanten-Hall-Effekt bei schwacher Zeemanaufspaltung.

In Teil II beschäftigen wir uns mit dem Hall-Effekt in der Skyrmiongitterphase chiraler Magnete unter Berücksichtigung der Spin-Bahn-Kopplung. Es ist bereits bekannt dass Impulsraum-Berryphasen zur intrinsischen Komponente des anomalen Hall-Effekts führen, und dass Ortsraum-Berryphasen eine effektive Lorentzkraft generieren, welche zum sogenannten topologischen Hall-Effekt führt. Indem wir die Kubo-Středa-Formel für die Hallleitfähigkeit in Gradienten im Orts- und Impulsraum entwickeln zeigen wir, dass die Kombination aus der langwelligen magnetischen Textur und Spin-Bahn-Kopplung zu einem bisher unberücksichtigten Beitrag zum Hall-Effekt führen, und wir finden eine Korrektur zur semiklassischen Formel für den topologischen Hall-Effekt.

In Teil III untersuchen wir den Einfluss von Phasenraum-Berryphasen auf die Dynamic von Skyrmionen in chiralen Magneten. Berryphasen im gemischten Orts/Impulsraum führen zu einem dissipationslosen Impulsübertrag von den Leitungselektronen auf die Skyrmionen, der proportional zu einem angelegten elektrischen Feld und unabhängig

vom (Spin- oder Ladungs-)Strom ist. Wir zeigen weiterhin dass die elektrische Ladung von Skyrmionen (siehe Teil I) deren Bewegung in Metallen nur durch hydrodynamisches Mitschleppen (drag) und Ohmsche Reibung beeinflusst. In Isolatoren koppelt die quantisierte Skyrmionladung direkt an ein angelegtes elektrisches Feld.

Contents

1. Introduction

The concept of Berry phases is a fundamental aspect of quantum mechanics. Berry phases arise naturally in systems with many degrees of freedom whose dynamics are governed by different time scales, whenever the dynamics of the fast modes depends on the configuration of the slow modes. In such a scenario, which is ubiquitous in nature, the system picks up a geometric phase as the slow modes evolve in time and the fast modes follow adiabatically the changing environment dictated by the slow modes. The remarkable aspect of Berry phases is that they are insensitive to the velocity with which the slow modes change in time and depend only on the geometry of the trajectory [1]. A classical analog of the connection between geometry and dynamics can be seen in the Foucault pendulum. Due to the rotation of the earth, the orientation of the pendulum changes over the course of one day. Interestingly, the rotation angle per day of the pendulum is independent of the oscillation frequency of the pendulum or the angular velocity of the earth. It only depends on a geometric property: as the earth turns around its axis, the location at which the experiment is carried out encloses a certain solid angle on the surface of the earth. The orientation of the pendulum rotates by 2π minus the enclosed solid angle per day.

The notion of Berry phases has been employed in a wide variety of physical disciplines. Examples include solid state physics [2], quantum computing [3], and astrophysics [4]. In condensed matter physics, Berry phases influence the semiclassical dynamics of Bloch electrons, leading to additional forces [5], an anomalous contribution to the group velocity [6], and an effective change of the density of states in phase space [7]. Apart from their influence on the dynamics of the system, the close relation of Berry phases with the geometry of the configuration space provides new tools for the classification of different states of matter. In condensed matter physics, the topological properties of the band structure are characterized by Berry phases of Bloch electrons. For example, the topological winding number of the integer quantum Hall state is related to Berry phases of Bloch electrons in the magnetic Brillouin zone [8]. This classification of states of matter by Berry phases is not limited to momentum space. In 2009, Mühlbauer and collaborators discovered a novel magnetic state in the chiral magnet MnSi [9]. Here, the magnetization texture in the so-called skyrmion-lattice phase is characterized by a regular arrangement of smooth magnetic whirls (skyrmions) with a topologically protected winding number. It turns out that this position-space winding number translates to Berry phases picked up by conduction electrons as they traverse the magnetization texture. Mathematically, the Berry phase in position space is equivalent to a spin-dependent Ahronov-Bohm phase and it manifests itself in an emergent (spin-dependent) Lorentz force on the electrons. The effect can be measured in Hall experiments [10]. The counter force from the electrons on the skyrmions leads to a very efficient coupling of

spin currents and skyrmions [11, 12], which raises expectations for applications in novel spin-tronic devices.

Microscopically, the formation of smooth skyrmions in chiral magnets such as MnSi is a consequence of weak spin-orbit coupling. Spin-orbit coupling is also a common mechanism that generates Berry phases in momentum space. Thus, chiral magnets are prime materials to study in general the effects of Berry phases in phase space, i.e., combined position and momentum space. As quantum-mechanical phases are only detectable through interference, only Berry phases picked up on closed loops are physical. While Berry-phase effects corresponding to closed loops in either position or momentum space have been studied in separate systems to considerable extent, the same can not be said for Berry-phase effects involving both position and momentum space.

In this thesis, we study the effects of Berry phases in the whole phase space on skyrmions in chiral magnets. In part I (Chapters 5–6), we focus on equilibrium properties of electrons in a static and long-wavelength skyrmion lattice. Using both semiclassical arguments and a systematic gradient expansion of the Green's function, we show that the Dzyaloshinskii-Moriya interaction energy, which is responsible for magnetic texture, is a consequence of Berry phases in mixed position/momentum space. In addition, we show that these mixed phase-space Berry phases lead to an electric charge of skyrmions in metals. In insulators, the electric charge of skyrmions is given by the product of the Berry curvature in position and momentum space, and is quantized. An example of skyrmions with a quantized electric charge has been known from quantum Hall systems [13, 14]. We thus provide a link between the charge of skyrmions in quantum Hall systems and in metallic chiral magnets.

In part II (Chapters 7–8), we consider the transport of electrons in the presence of a static skyrmion lattice. Using again a systematic gradient expansion method, we derive a formula for the Hall conductivity in the presence of Berry phases in phase space. We find a previously disregarded contribution to the Hall conductivity that arises due to a combination of smooth modulations in position space and spin-orbit coupling. Even in absence of spin-orbit coupling, a comparison between our result for the topological Hall effect shows a correction to the semiclassical theory if more than one orbital band participate in the electronic transport.

In part III (Chapters 9–11), we turn to the dynamics of skyrmions in chiral magnets in the presence of an electric field. Starting from a single skyrmion with only a translational degree of freedom, we develop a general method to derive an equation of motion for the translational degree of freedom, taking Berry phases in the whole of phase space into account. Of particular focus is the influence of the electric charge of the skyrmion, derived in part I, on its dynamics. In metals, we find that the charge couples only via hydrodynamic drag and ohmic friction to an applied electric field. In insulators, the drag and friction forces vanish, and the quantized electric charge of the skyrmion couples instead directly to the applied electric field, as it would for an elementary particle.

2. Skyrmions in chiral magnets

2.1. Skyrmions as topologically stable objects

The concept of emergent degrees of freedom is ubiquitous in modern physics. It is based on the notion that "the whole is greater than the sum of its parts," usually attributed to Aristotle. A very general mechanism under which emergent degrees of freedom can arise is expressed by the Goldstone theorem. It is based on a local symmetry analysis of the constituent fields and it predicts the existence of bosonic low-energy degrees of freedom if the ground state in the thermodynamic limit breaks a local symmetry. For example, if many atoms are brought together and condense to a crystal, then the Goldstone theorem predicts the existence of three branches of acoustic phonons. Similarly, the emergent degree of freedom in a Bose-Einstein condensate is the phase of the global wave function. The Goldstone bosons are different from the individual degrees of freedom of the constituents since they exist only in the thermodynamic limit. For example, unlike the acoustic phonons in an infinitely extended solid, the vibrational modes of a two-atomic molecule have a finite energy gap to the ground state. Yet, the Goldstone bosons are merely a coherent superposition of individual degrees of freedom of the constituents. They can therefore be regarded as the quantized version of collective excitations.

A more intricate kind of emergent degree of freedom arises when not only the local value and the gradients of the fields are considered but rather the topology of the global field configuration is taken into account. In 1961, in an attempt to resolve the microscopic structure of nucleons in the core of an atom, Skyrme proposed a non-linear sigma model for the pion fields [15]. The three pion fields π^+, π^-, and π^0 are encoded in the three real parameters of a matrix $U \in SU(2)$ and the Lagrangian density is given by

$$\mathcal{L} \propto -\kappa^2 \frac{1}{2} \operatorname{Tr}\left((\partial^\mu U^\dagger)(\partial_\mu U)\right) + \frac{1}{16} \operatorname{Tr}\left([U^\dagger \partial^\mu U, U^\dagger \partial_\nu U]^2\right) \tag{2.1}$$

where ∂_μ and ∂^μ are covariant and contravariant derivatives in space time, respectively, and κ is a parameter of the model with mass dimension 1. The important observation of Skyrme was that the stationary points of the action $S = \int \mathrm{d}^4x\, \mathcal{L}$ are solitons, i.e., field configurations with finite energy that are inhomogeneous in a finite region of space and constant in the limit $|\mathbf{r}| \to \infty$. Moreover, Skyrme found an integer constant of motion, which he called particle number, and which can be understood as follows. Since U is constant for $|\mathbf{r}| \to \infty$, position space $\mathbb{R}^3$ can be compactified to the surface $\mathbb{S}^3$ of a four-dimensional sphere by identifying all points that are far away from any solitons. The matrix $U \in SU(2)$ can be parametrized as

$$U(t, \mathbf{r}) = \begin{pmatrix} \phi_1(t, \mathbf{r}) + i\phi_2(t, \mathbf{r}) & -\phi_3(t, \mathbf{r}) + i\phi_4(t, \mathbf{r}) \\ \phi_3(t, \mathbf{r}) + i\phi_4(t, \mathbf{r}) & \phi_1(t, \mathbf{r}) - i\phi_2(t, \mathbf{r}) \end{pmatrix} \tag{2.2}$$

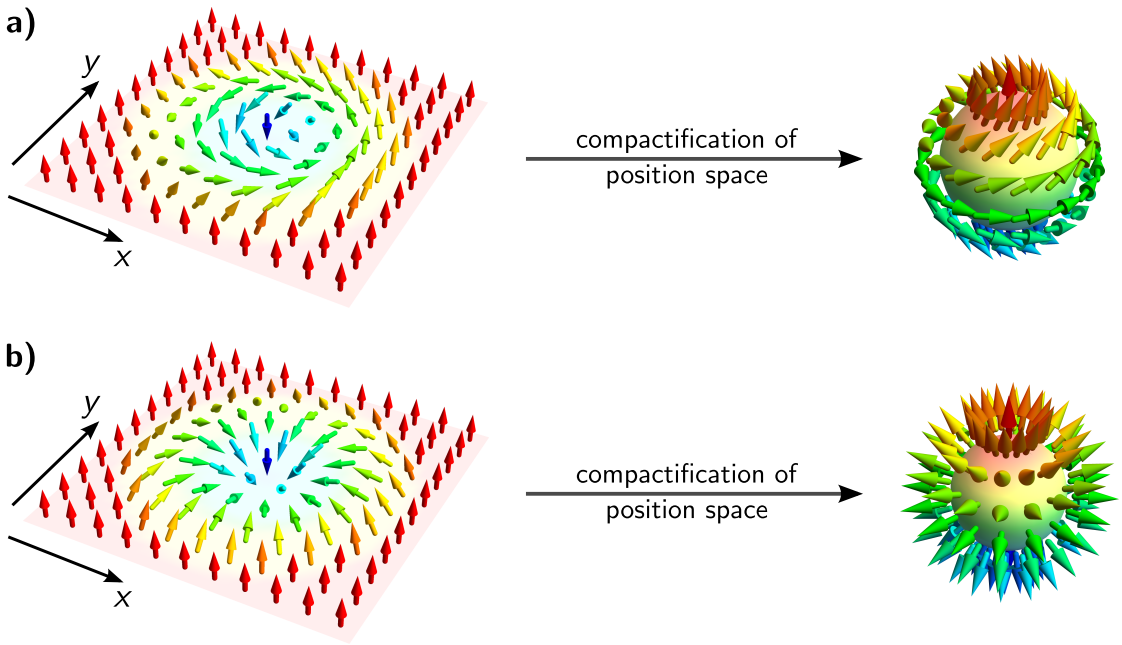

Figure 2.1.: Examples of two-dimensional skyrmions. In both cases, $\hat{\mathbf{M}}$ winds once around the unit sphere and both skyrmions have winding number $W = -1$ and can be continuously deformed into each other. Arrows are spaced in arbitrary distances not related to the lattice distance and colored according to their z component. a) Bloch-type skyrmion, typically found in bulk chiral magnets such as MnSi. b) Néel-type skyrmion, typically found in thin films.

where the real fields fields ϕ_α, $\alpha = 1, \ldots, 4$ have to satisfy the condition

$$\phi_1^2 + \phi_2^2 + \phi_3^2 + \phi_4^2 = 1. \tag{2.3}$$

Thus, for a fixed time t, the combined field $\boldsymbol{\phi} \equiv (\phi_1, \phi_2, \phi_3, \phi_4)$ defines a mapping from the compactified position space $\mathbb{S}^3$ to $\mathbb{S}^3$. Generally, the space of mappings from $\mathbb{S}^n$ to $\mathbb{S}^m$ separates into topologically disconnected classes, which form the n^{th} homotopy group of $\mathbb{S}^m$, or $\pi_n(\mathbb{S}^m)$ for short. In the present scenario we have $n = m = 3$ and since $\pi_n(\mathbb{S}^n)$ is always isomorphic to $\mathbb{Z}$ (for $n \geq 1$) [16], the field configuration at any given time can be labeled by an integer winding number,

$$W = \frac{1}{2\pi^2} \int \mathrm{d}^3 r \, \epsilon_{ijkl} \, \phi_i \frac{\partial \phi_j}{\partial r_x} \frac{\partial \phi_k}{\partial r_y} \frac{\partial \phi_l}{\partial r_z} \tag{2.4}$$

where ϵ_{ijkl} is the totally antisymmetric tensor. Time evolution, described on a classical level by the Euler-Lagrange equations of $\mathcal{L}$, is continuous and therefore the winding number is a constant of motion.

The integer winding number counts the number of times that $\boldsymbol{\phi}(\mathbf{r})$ covers $\mathbb{S}^3$ when $\mathbf{r}$ is varied over the whole space. A given field configuration with winding number W can

always be continuously deformed into a configuration of W "elementary" solitons that are located far away from each other. These elementary solitons are nowadays referred to as skrymions and their properties are similar to those of particles: skyrmions can move in space and they possess internal degrees of freedom in the sense that the field configuration can be deformed locally. However, continuous deformations cannot change the overall number of skyrmions since the winding number is a topological invariant. Thus, we started with a theory, Eq. (2.1), that contained the pion fields as the only particle fields, and we identified the topologically stable excitations of the pion field as a new emergent type of particles. In contrast to the collective excitations discussed above, skyrmions are not a coherent superposition of local excitations since they are not linear. Scaling a skyrmion solutions $\boldsymbol{\phi}$ by a factor of 2 does not lead to a configuration with two skyrmions but instead would violate the normalization condition Eq. (2.3).

The concept of topological excitations as emergent particles is not limited to three dimensions and it turns out that two-dimensional skrmions naturally appear in magnetic systems. These magnetic skyrmions are the topic of this thesis. The magnetization $\mathbf{M}(\mathbf{r})$ in a magnetic material is a three-component vector field. Below the transition temperature, the magnitude $|\mathbf{M}|$ of the magnetization becomes finite. Fluctuations of the magnitude are energetically expensive, while long-wavelength fluctuations of the direction $\hat{\mathbf{M}} := \mathbf{M}/|\mathbf{M}|$ are governed by the energy scale of crystal anisotropies, which is often much lower in bulk materials. It is therefore often a good approximation to assume a constant $|\mathbf{M}|$ and consider only the free energy as a function of $\hat{\mathbf{M}}$. Two kinds of two-dimensional skyrmions are depicted in Figure 2.1. Bloch-type skyrmions where $\hat{\mathbf{M}}$ winds like a screw on paths through the skyrmion center are typically found in bulk chiral magnets such as MnSi (Figure 2.1a). Néel-type skyrmions are often realized in thin films where inversion symmetry is broken by the existence of a substrate on only one side of the film (Figure 2.1b). Far away from the skyrmion, the magnetization is constant and we can again compactify position space to the sphere $\mathbb{S}^2$. The map $\hat{\mathbf{M}} : \mathbb{S}^2 \to \mathbb{S}^2$ has an integer winding number, which can be calculated from

$$W = \frac{1}{4\pi} \hat{\mathbf{M}} \cdot \left(\frac{\partial \hat{\mathbf{M}}}{\partial x} \times \frac{\partial \hat{\mathbf{M}}}{\partial y} \right). \tag{2.5}$$

The winding number counts the number of times that the unit sphere $\mathbb{S}^2$ is covered when $\mathbf{r}$ varies over the whole plane, as depicted in the right part of the Figure. One obtains the value of $W = -1$ for both configurations in Figure 2.1. The configurations are therefore sometimes called anti-skyrmions. Note, however, that the sign of W depends on the way in which the order parameter space $\mathbb{S}^2$ is embedded in $\mathbf{R}^3$. If we had looked at the two planes in Figure 2.1 from below, we would have obtained $W = 1$.

From a mathematical point of view, the winding number cannot be changed by continuous deformations of the magnetization texture. However, the topological protection only holds if the order parameter is always well-defined and the magnetization never vanishes. In real magnetic systems, the topological invariance of the winding number translates into an energy scale for a barrier that has to be overcome in order to change the winding number.

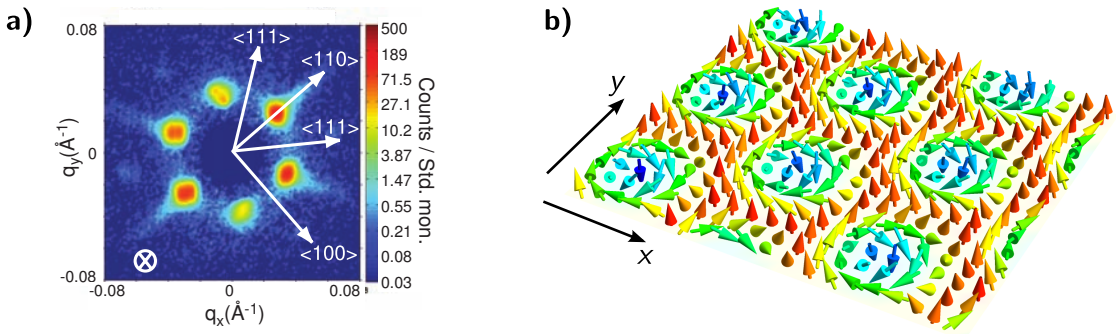

Figure 2.2.: Skyrmion lattice phase in MnSi; a) Typical intensity pattern in small angular neutron scattering experiments in the skyrmion lattice phase. Figure taken from Ref. [9]. The magnetic field points in the direction of the beam. White arrows indicate symmetry axes of the crystal. b) The superposition of three helices with coplanar wave vectors, an angle of 120° between each pair of wave vectors, and appropriate relative phases is a skyrmion lattice.

2.2. Skyrmion lattice phase in chiral magnets

In 1988, Bogdanov and Yablonskii [17] predicted that thermodynamically stable vortices, similar vortex lattices in super conductors, exist in magnetic materials with an easy-axis magnetic anisotropy. Their analysis was based on a mean-field calculation for a model with inversion-symmetric exchange interaction. In a later study by Bogdanov and Hubert [18], an exchange interaction with chiral asymmetry was considered in a similar model. The mean-field theory predicted the existence of a meta-stable hexagonal lattice of vortices. It is now known that, in the presence of a small external magnetic field, a lattice of skyrmions is stabilized by thermodynamic fluctuations in bulk magnetic materials with chiral asymmetry [9].

The first experimental discovery of a skyrmion lattice in magnetic materials was reported in 2009 by Mühlbauer and collaborators [9]. They examined a bulk sample of MnSi in the ordered phase close to the transition temperature using small angular neutron scattering (SANS). MnSi is a magnetic material with a transition temperature around 29.5 K whose crystal structure has no inversion symmetry. A small external magnetic field was applied parallel to the neutron beam. The recorded scattering image shows a pattern of six Brag peaks symmetrically aligned around the center (Figure 2.2a). Since neutrons couple primarily to the magnetization, the scattering intensity is proportional to the spin-spin correlation function in momentum space. Each pair of opposite brag peaks at wave-vectors $\mathbf{q}$ and $-\mathbf{q}$ corresponds to a helical spin configuration in position space with wavelength $2\pi/|\mathbf{q}|$ along the direction of $\mathbf{q}$. If the neutron beam is perpendicular to the magnetic field, only two Bragg peaks are observed, suggesting that the three Helices lie in the same plane perpendicular to the magnetic field. The superposition of three helices with 120° degree angle between each other results in a triangular lattice of skyrmions for appropriate relative phases between the helices (Figure

2.2b). The figure shows a cut through the system perpendicular to the applied magnetic field. The magnetization texture is translationally invariant in the direction along the magnetic field. It was confirmed by theoretical calculations that the skyrmion lattice is indeed the thermodynamically stable configuration.

In addition to SANS measurements, the existence of a skyrmion lattice phase in magnetic materials without inversion symmetry has now been confirmed with a number of complementary methods. These scattering experiments were later supported by observations of skyrmion lattices in real space using Lorentz Transmission Electron Microscopy for thin films [19], as well as magnetic force microscopy on the surface of bulk samples [20]. In addition to these direct observations, the phase boundaries to the skyrmion lattice can also be inferred from electron transport experiments. Here, the existence of a skyrmion lattice leads to a strong additional contribution to the Hall resistivity [21, 22]. We provide a more detailed discussion of the so-called topological Hall effect in Chapter 7.

The skyrmion lattice phase is not limited to MnSi and it has been observed in a variety of systems. The doped semiconductor $Fe_{1-x}Co_xSi$ was studied in [19, 23]. In thin films of FeGe [24], a skyrmion lattice phase was reported to exist up to approximately 260 K. A strategy to engineer thin-film structures that can host skyrmions at room temperature has been proposed in Ref. [25] and single skyrmions at room temperature have recently been observed by Boulle and collaborators [26]. The discovery of a skyrmion lattice in the insulating multiferroic compound Cu_2OSeO_3 [27] promises new possibilities to manipulate skyrmions via electric fields without resistive losses. All these systems have in common that the atomic structure has no inversion center. In thin films, inversion symmetry is broken due to the presence of a substrate on one side of the film. Bulk materials in which a skyrmion lattice phase has been observed all have a crystal structure whose space group has no inversion center, usually the $P2_13$ space group. Magnetic materials without inversion center are commonly referred to as chiral magnets. Each chiral magnet comes in two variants, a left-handed and a right-handed one, which are related to each other by space inversion. Due to the absence of inversion symmetry, the free energy functional $F[\mathbf{M}]$ contains non-inversion symmetric terms. In the Ginzburg-Landau theory of spontaneous symmetry breaking, one obtains $F[\mathbf{M}]$ by expanding in gradients of $\mathbf{M}$ and retaining all terms allowed by symmetry. Following the notation in [9], the free energy is given by

$$F[\mathbf{M}] = \int \mathrm{d}^3 r \, [r_0 \mathbf{M}^2 + J(\partial_i M_j)(\partial_i M_j) + 2D\mathbf{M} \cdot (\boldsymbol{\nabla} \times \mathbf{M}) + U(\mathbf{M}^2)^2 - \mathbf{B} \cdot \mathbf{M}]. \quad (2.6)$$

Here, $r_0 = 0$ marks the transition from the unordered to the ordered state on a mean-field level, D is the strength of the so-called Dzyaloshinskii-Moriya (DM) interaction, see below, J is the ferromagnetic exchange coupling, $U > 0$ is needed so that the free energy is bounded from below and $\mathbf{B}$ is the external magnetic field. The term proportional to D is odd under space inversion and therefore only allowed in chiral magnets. Its sign depends on the chirality of the crystal structure and it describes an anisotropic exchange interaction derived by Dzyaloshinksii and Moriya [28, 29]. The form of the DM

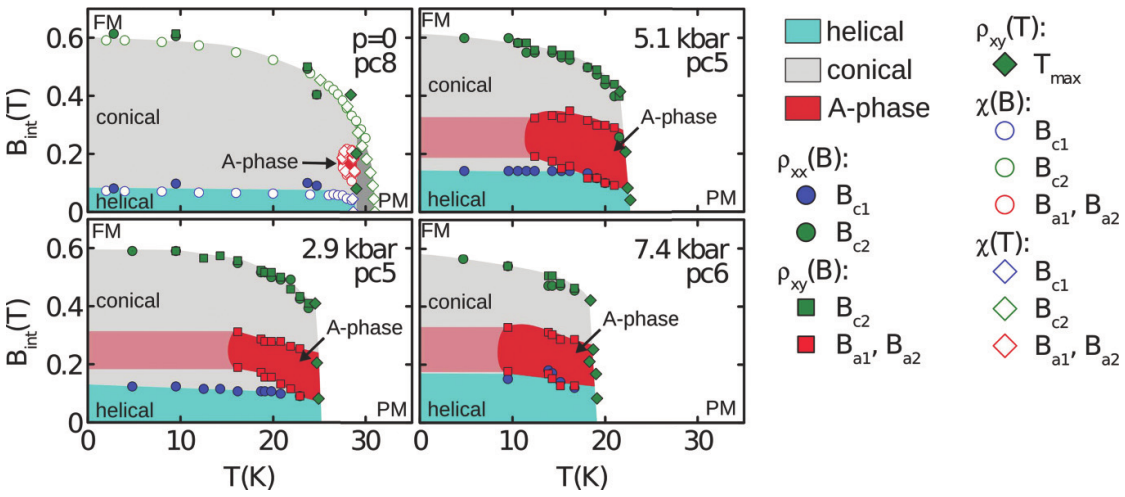

Figure 2.3.: Phase diagrams of MnSi at four different pressures from ambient pressure to 7.4 kbar. Figure taken from Ref. [30]. The skyrmion phase is labeled as "A-phase" for historical reasons. Phase boundaries are inferred from measurements of magnetoresistance ($\rho_{xx}(B)$), Hall effect ($\rho_{xy}(B)$ and $\rho_{xy}(T)$), and magnetic susceptibility ($\chi(B)$ and $\chi(T)$).

interaction with a scalar prefactor D in Eq. (2.6) is applicable to materials with cubic symmetries, as are all bulk materials mentioned above.

Three energy scales govern the physics of chiral magnets [9]. On the largest energy scale, the exchange interaction $J > 0$ penalizes gradients of the magnetization. On an intermediate scale, the DM interaction D favors maximally twisted spin structures. It is typically smaller than the exchange interaction since it is mediated by spin-orbit interaction, which is a relativistic effect. The competition between ferromagnetic exchange and DM interaction leads to helical structures with a wave vector of $q = D/J \sim \lambda_{\mathrm{so}}/a$ where $\lambda_{\mathrm{so}} \ll 1$ is the spin-orbit coupling strength and a is the lattice constant. On the lowest energy scale, crystal anisotropies, of higher order in λ_{so}, pin the orientation of helices along symmetry directions of the crystal for small external magnetic fields.

Phase diagram of MnSi. In Figure 2.3, we show the phase diagram of MnSi at four different pressures ranging from ambient pressure to 7.4 kbar. The figure is taken from Ref. [30]. The diagrams combine data from measurements of the Hall resistivity, magnetoresistance, and magnetic susceptibility, as indicated by the key. The general structure of the phase diagram is archetypal for all bulk chiral magnets. In thin films with magnetic field perpendicular to the sample, the skyrmion lattice phase typically extends down to lower temperatures because the conical phase cannot exist for geometrical reasons, see below. The following phases are indicated: At high temperatures, the system is in the unordered paramagnetic state (PM). At low external magnetic fields, the system orders in a helical state below the transition temperature. In this phase, the magnetization is

described by

$$\mathbf{M}(\mathbf{r}) = \mathbf{M}_1 \cos(\mathbf{q} \cdot \mathbf{r}) + \mathbf{M}_2 \sin(\mathbf{q} \cdot \mathbf{r}) \tag{2.7}$$

where $\mathbf{M}_1$, $\mathbf{M}_2$, and $\mathbf{q}$ are all perpendicular on each other. The wavelength $2\pi/|\mathbf{q}|$ of the helix in MnSi increases from 165 Å near the transition temperature to 180 Å for the lowest measured temperatures [31–33]. The direction of $\mathbf{q}$ is weakly pinned to along a [111] direction due to crystal anisotropies. In the diagram for $p = 0$, a narrow fluctuation disordered phase is indicated in dark gray. In this regime, mean-field theory would already predict an ordered state, but helical fluctuations with wave vectors $\mathbf{q}$ uniformely distributed on a sphere in momentum space give rise to corrections to the mean-field behavior and drive the transition weakly first order [31].

As the magnetic field is increased in the ordered state, the magnetization changes into a conical state. In this state the magnetization is again described by Eq. (2.7), but the wave vector $\mathbf{q}$ aligns parallel to the magnetic field and $\mathbf{M}_1$ and $\mathbf{M}_2$ are no longer perpendicular on $\mathbf{q}$ but obtain a component in direction of the magnetic field. The nature of the transition from the helical to the conical state depends on the orientation of the crystal. In the general case it is a crossover but it may be a second-order transition if the magnetic field is applied along a [111] direction [34]. The angle between $\mathbf{M}$ and $\mathbf{B}$ decreases with increasing magnetic field up to the point that the two are parallel and the system is in the ferromagnetic state.

The skyrmion lattice phase, labeled "A-phase" in Figure 2.3 for historical reasons, forms a small pocket close to the transition temperature at a small external field $B \sim 0.2\,\mathrm{T}$ at ambient pressure. The phase extends to lower temperatures as pressure is increased [30]. Due to the topological protection of skyrmions, the skyrmion lattice remains metastable if the system is prepared in the in the skyrmion lattice phase close to the transition temperature and then the temperature is lowered (field cooling). This is indicated by the light red shaded area. If the system is cooled down at zero magnetic field (zero-field cooling) and then the magnetic field is turned on, the system prefers the conical phase. The fate of a metastable skyrmion lattice when the magnetic field is slowly reduced and then inverted has been studied in Refs. [20,35]. In a three-dimensional sample, this "unwinding" happens by a process in which two skyrmions first merge at a single point in space at which the magnetization vanishes. This singular point then runs through the system like a zipper. It turns out that the singular point is a source or sink of an emergent magnetic field, see Section 4.1.

2.3. Recent trends

A major reason for the recent interest in magnetic skyrmions lies in their prospect for future data storage devices. The topological protection of skyrmions makes them promising candidates for non-volatile storage devices, especially since single skyrmions in a ferromagnetic background can be realized in thin magnetic films [25,26]. In addition, it turns out that skyrmions can be very efficiently manipulated with electric currents [12]. This has two reasons. First, skyrmions couple to currents via a particular gyro-coupling, which is related to the winding number of the skyrmion [11,36]. Second, unlike magnetic

bubbles, which have been known to exist in materials without chiral asymmetry since the 1970s [37], skyrmions in chiral magnets turn out to be rather rigid objects and forces on skyrmions couple predominantly to their translational mode rather than internal degrees of freedom [38]. In a numerical study, Fert and collaborators [39] proposed a setup by which a pattern of skyrmions that encodes a series of bits can be driven in a controlled way through a wire. Appropriately placed grooves in at the edge of the wire may help to control the placements of the skyrmions, or to nucleate skyrmions at sharp edges [40]. We study the dynamics of skyrmions with an emphasis on the influence of phase-space Berry phases in part III of this thesis (Chapters 9–11).

A different approach to the controlled manipulation of skyrmions is to selectedly create or destroy single skyrmions in a ferromagnetic background. In thin films, skyrmions can be created and destroyed by injecting a spin-polarized current from the magnetic tip of a scanning tunneling microscope [41,42]. Recent experiments by Hsu and collaborators [43] indicate that it may be possible to generate and destroy skyrmions by electric fields without a current. In part I of this thesis (Chapters 5–6), we show that skyrmions carry an electric charge, which might provide an explanation for this mechanism.

3. Berry phases

In 1983, Michael Berry made the observation [1] that the wave function of a quantum-mechanical system picks up a geometric phase when the parameters in the Hamiltonian are changed slowly. A similar geometrical phase had already been identified by Pancharatnam in 1956 in the context of classical optics [44]. This phase, today known as the Berry phase, influences the dynamics of the system and is ubiquitous in modern physics [2]. In this chapter, we discuss the mathematical and physical properties of Berry phases in a general setting. The application of these concepts onto chiral magnets is deferred to the next chapter.

This chapter is structured as follows. In Section 3.1, we discuss the general requirements that lead to the appearance of Berry phases in a physical system. We derive a general expression for the Berry phase in section 3.2 and discuss the range of its applicability in section 3.5. In Section 3.3, we discuss gauge invariance of Berry phase effects and give a geometric interpretation of the introduced quantities. In Section 3.4, we explicitly derive the Berry curvature for a spin in an external magnetic field. Finally, we discuss the validity of the adiabatic assumption in Section 3.5.

3.1. Origin of Berry phases in physical systems

If the Hamiltonian $H(t)$ of a quantum system depends on time, the instantaneous eigenstates of $H(t)$ are not stationary solutions of the time-dependent Schrödinger equation. However, if the time dependency of $H(t)$ is sufficiently slow (to be quantified in section 3.5) and if the energy levels are non-degenerate for all times, then the adiabatic theorem [45, 46] states that a system that is prepared in the n^{th} eigenstate of $H(t_0)$ at some initial time t_0 evolves in time by following the n^{th} eigenstate of $H(t)$ for $t \geq t_0$. Transitions into other eigenstates are exponentially suppressed as the time dependency of $H(t)$ becomes slower.

While the adiabatic theorem guarantees that the system remains in the n^{th} eigenstate of $H(t)$, it makes no statement about the phase factor $e^{i\varphi}$ that the wave function acquires if the Hamiltonian returns to its original form, i.e. if $H(t_1) = H(t_0)$ for some time $t_1 > t_0$. Berry's observation [1] was that the phase picked up by a quantum system under adiabatic time evolution can be understood as a sum of two contributions. First, the so-called *dynamical phase* is the straight-forward generalization of the phase acquired by a stationary state, and is given by the integral over time of the instantaneous eigenenergy divided by $\hbar$. Second, there is an additional contribution, which Berry denoted as the *geometrical phase*, and which is nowadays commonly referred to as the Berry phase. In contrast to the dynamical phase, the Berry phase depends only on the instantaneous

eigenstates of $H(t)$ and is insensitive to the eigenenergies.

The concept of Berry phases has been successfully applied in many branches of physics (see, e.g., Refs. [2–4]). This popularity may be explained by a combination of properties of the Berry phase.[1] First, Berry phases are physically measurable. Although the global phase factor of a wave function cannot be detected, Berry phases lead to interference when the adiabatic change from the initial Hamiltonian $H(t_0)$ to some final Hamiltonian $H(t')$ may be realized in more than one way. This is the generic situation if $H(t) \equiv H(\lambda_1(t), \ldots, \lambda_N(t))$ is an effective Hamiltonian for the fast modes of a system where the dynamics of some slow degrees of freedom $\lambda_i(t)$, $i = 1, \ldots, N$, is neglected (see below). In this case, the parameters λ_i may evolve from some initial to some final set of values on different trajectories. The different Berry phases picked up on these trajectories lead to interference and, ultimately, influence the effective equations of motion for the slow modes λ_i once their dynamics is reintroduced into the theory. As interference experiments can only measure phase differences, only differences between Berry phases are physical. In contrast, the Berry phase along a single (not closed) trajectory in parameter space depends on the choice of basis at the initial and final time. We will come back to this gauge degree of freedom in section 3.3.

Second, there exists an intuitive geometric interpretation of Berry phases, allowing for the application of powerful tools from differential geometry and from topology to quantum mechanical problems. The Berry phase along an infinitesimal path in parameter space $\{\lambda_i\}_{i=1,\ldots,N}$ may be interpreted as an affine connection, so that adiabatic time evolution becomes equivalent to parallel transport of the wave function along a path in parameter space [47]. While an affine connection depends on the local coordinate system (i.e., the choice of gauge), it gives rise to a gauge-independent quantity called the (Riemann) curvature tensor. In absence of degeneracies, the so-called Berry curvature is simply the Berry phase along an infinitesimal loop in parameter space. For a compact parameter space, the total curvature is a topological invariant, i.e. it only depends on global properties of the connection and is insensitive to local perturbations. This opens up powerful tools from the field of topology that can be used to explain physical phenomena and classify states of mater. For example, the quantization of the transverse conductivity in the quantum anomalous Hall effect [48] is a direct consequence of the quantization of the total Berry curvature in the Brillouin zone [8, 49].

Finally, Berry phases are ubiquitous in nature, since they appear whenever a quantum-mechanical system exhibits a clear separation of time scales. The time dependency of the Hamiltonian $H(t)$ may either be explicit due to an externally applied slowly time-dependent perturbation; or it may be an implicit time-dependency of an effective Hamiltonian for the fast degrees of freedom of a system whose constituents are governed by dynamics on clearly separated energy scales. Both scenarios are particularly common in condensed matter physics. Many experiments on solids, for example, measure macroscopic quantities such as thermal properties or transport coefficients in a macroscopic sample, while a microscopic description of the constituents is characterized by a much

[1] For an argumentation that focuses more on the mathematical properties of Berry phases, see also [2] and references therein.

smaller length scale (the lattice constant) and therefore much larger momenta and energies. In addition, the characteristic energy scales for the constituents themselves span a wide range from the Debye frequency for phonons ($\hbar\omega_D \sim 10 \ldots 100\,\mathrm{meV}$) to the band width of the electronic system ($\sim$ eV).

Let us illustrate the link between the separation of time scales and the appearance of a geometric phase by means of a classical analog. We consider a Foucault pendulum. Here, the two time scales are the short period τ of the oscillating pendulum and the long period T of the earth's rotation, which is a sidereal day (about four minutes short of a solar day). Except at the reversal points, the angular momentum $\mathbf{L}$ of the pendulum is primarily governed by the fast mode and therefore horizontally aligned. The gravitational force $\mathbf{F}_\mathrm{g}$ on the mass of the pendulum is downwards by definition, and therefore the torque $\dot{\mathbf{L}} = \mathbf{r} \times \mathbf{F}_\mathrm{g}$ is also in the horizontal plane ($\mathbf{r}$ points from the suspension point of the pendulum to the oscillating mass). However, the notion of "horizontal" changes slowly over time due to the rotation of the earth, and the angular momentum of the pendulum has to follow the horizontal plane. Microscopically, this process is mediated by a tiny torque due to the Coriolis force. It is rather cumbersome to solve the resulting equations of motion explicitly, since the Coriolis force depends on the velocity of the pendulum, which oscillates on the short time scale. To leading order in τ/T, it turns out that the direction of $\mathbf{L}$ follows the path that is defined by the smallest possible change consistent with the condition of staying in the horizontal plane [50]. The trajectory of the direction of $\mathbf{L}$ is therefore only governed by *geometric* aspects, namely the curvature of the surface of the earth and the latitude ϕ at which the experiment is carried out. It turns out that the direction of $\mathbf{L}$, and therefore the orientation of the pendulum, rotates by an angle of $2\pi \sin(\phi)$ per sidereal day, where ϕ is measured from the equator. This is precisely 2π minus the solid angle enclosed by the location of the experiment on the surface of the earth as it rotates around the earth's axis during one day.

In the classical example of the Foucault pendulum, the rotation angle can be observed directly. Quantum-mechanical phases, on the other hand, can only be observed if two wave functions interfere with each other. Therefore, Berry phases only play a role if the process that happens on the long time scale T is itself dynamic rather than externally imposed. Bloch electrons in an external electric field $\mathbf{E}$ are a prime example of such a separation of time scales. We may treat the electric field either in the current gauge, $\mathbf{E} = -\partial\mathbf{A}/\partial t$, where $\mathbf{A}(t)$ is the vector potential. This treatment is an example of an explicitly time-dependent Hamiltonian. The vector potential enters the Hamiltonian via the minimal coupling $\mathbf{p} = \boldsymbol{\pi} + e\mathbf{A}(t)$, where $\mathbf{p}$ and $\boldsymbol{\pi}$ are the kinetic and canonical momentum of the electrons with charge $-e$, respectively. A natural time scale τ_pert associated with the external perturbation is given by the time in which the difference $\mathbf{p} - \boldsymbol{\pi} = e\mathbf{A}(t)$ traverses the Brillouin zone once. This leads to the estimate

$$\frac{\hbar}{a} = e \left| \frac{\partial \mathbf{A}}{\partial t} \right| \tau_\mathrm{pert} = e|\mathbf{E}|\tau_\mathrm{pert} \tag{3.1}$$

where $a \sim$ Å is the lattice constant. Thus, the characteristic energy $\hbar/\tau_\mathrm{pert} = ea|\mathbf{E}|$ of the external perturbation is the energy an electron gains when it travels one lattice

constant in the direction of the electric field. Even for very large electric fields, this value is much smaller than the band separation $\Delta E \sim$ eV, which is the characteristic energy scale for electrons in the unperturbed system.

Alternatively, we could have described the external electric field in the potential gauge, $\mathbf{E} = -\boldsymbol{\nabla}\phi$, where $\phi(\mathbf{r})$ is the electric potential. In this treatment, the Hamiltonian is formally independent of time, but it gives rise to dynamics on two different time scales. The fast dynamics are described by the unperturbed Hamiltonian, whose eigenstates $\Psi_{n,\mathbf{k}}(\mathbf{r}) = e^{i\mathbf{k}\cdot\mathbf{r}}u_{n,\mathbf{k}}(\mathbf{r})$ are labeled by a band index n and a lattice momentum $\hbar\mathbf{k}$ and may be written as a product of a plane wave and a Bloch function $u_{n,\mathbf{k}}(\mathbf{r})$. The latter has the same periodicity as the atomic lattice. The electric potential $\phi(\mathbf{r})$ breaks the discrete translational symmetry and therefore the wave functions $\Psi_{n,\mathbf{k}}(\mathbf{r})$ are no longer stationary. If we require again that $ea|\mathbf{E}| \ll \Delta E$, then matrix elements $\langle\Psi_{n',\mathbf{k}'}|\phi(\mathbf{r})|\Psi_{n,\mathbf{k}}\rangle$ between two different bands $n \neq n'$ are small since the Bloch functions oscillate on a much shorter length scale than the electric potential. Thus, inter-band transitions are suppressed. On the other hand, intra-band matrix elements $\langle\Psi_{n,\mathbf{k}'}|\phi(\mathbf{r})|\Psi_{n,\mathbf{k}}\rangle$ between to close-by wave vectors $\mathbf{k}$ and $\mathbf{k}'$ are not suppressed (in a finite system) since the quickly oscillating factor $u^*_{n,\mathbf{k}'}(\mathbf{r})u_{n,\mathbf{k}}(\mathbf{r})$ in the integrand is almost everywhere positive for $\mathbf{k}' \approx \mathbf{k}$. To a good approximation, the effect of intra-band transitions can be described by a slow time evolution of the lattice wave vector $\mathbf{k}(t)$. The remaining (fast) degrees of freedom are captured by the Bloch function, which follows, in this approximation, adiabatically the trajectory of $\mathbf{k}(t)$ in the Brillouin zone. Thus, the electron dynamics in the presence of an external electric field is described by a time-dependent effective Hamiltonian $H^{\text{eff}}(t) = H(\mathbf{k}(t))$, where $H(\mathbf{k}) := e^{-i\mathbf{k}\cdot\mathbf{r}}He^{i\mathbf{k}\cdot\mathbf{r}}$ is the band Hamiltonian. We will see in section 5.1, that the time dependency of H^{eff} leads to Berry phases, which influence the trajectory of $\mathbf{k}(t)$.

3.2. Geometrical phase in a time-dependent system

In this section, we derive a general equation for the geometric phase picked up by a wave function under adiabatic time evolution due to a slowly time-dependent Hamiltonian. We follow the original derivation by Berry in [1].

We consider a quantum mechanical system whose Hamiltonian $H(\boldsymbol{\lambda}(t))$ depends on some time-dependent parameters $\boldsymbol{\lambda}(t) \equiv (\lambda_1(t), \ldots, \lambda_N(t)) \in M$, where the parameter space M is a real manifold. As discussed in the introduction to this chapter, the parameters $\boldsymbol{\lambda}(t)$ may either be externally applied time-dependent fields, or $H(\boldsymbol{\lambda}(t))$ may be the effective Hamiltonian of a more complicated system that contains some slow modes $\{\lambda_i(t)\}_{i=1,\ldots,N}$, whose dynamics is neglected for the moment. For example, if $\lambda_i \equiv k_i$ are the lattice wave vectors in an N-dimensional crystal, then M is the Brillouin zone, which is an N-torus. For fixed $\boldsymbol{\lambda}$, the Hamiltonian has eigenenergies $E_n(\boldsymbol{\lambda})$ and corresponding normalized eigenstates $|\Phi_n(\boldsymbol{\lambda})\rangle$, defined by

$$H(\boldsymbol{\lambda})|\Phi_n(\boldsymbol{\lambda})\rangle = E_n(\boldsymbol{\lambda})|\Phi_n(\boldsymbol{\lambda})\rangle, \qquad \langle\Phi_n(\boldsymbol{\lambda})|\Phi_n(\boldsymbol{\lambda})\rangle = 1. \tag{3.2}$$

We refer to $E_n(\boldsymbol{\lambda})$ and $|\Phi_n(\boldsymbol{\lambda})\rangle$ as the *instantaneous* eigenenergies and eigenstates,

respectively, and assume that the instantaneous eigenenergies are discrete and non-degenerate for all times. Note that Eq. (3.2) defines each instantaneous eigenstate only up to a global phase. We require that these phases are chosen such that the maps $\boldsymbol{\lambda} \mapsto |\Phi_n(\boldsymbol{\lambda})\rangle$ are differentiable. It is important to keep in mind that such a differentiable choice of instantaneous eigenstates is not always possible on the whole parameter space M (see example at the end of section 3.3). For the present purpose, however, we only require that the maps are differentiable on an open subset of M that contains the trajectory $\boldsymbol{\lambda}(t)$ during the (finite) time interval of interest, which is always possible.

Suppose that at some initial time t_0, the wave function $|\Psi\rangle$ of the system is prepared in the n^{th} instantaneous eigenstate, $|\Psi(t_0)\rangle \propto |\Phi_n(\boldsymbol{\lambda}(t_0))\rangle$. Time evolution is described by the Schrödinger equation,

$$i\hbar \frac{\partial}{\partial t} |\Psi(t)\rangle = H(\boldsymbol{\lambda}(t)) \, |\Psi(t)\rangle. \tag{3.3}$$

If $\boldsymbol{\lambda}(t)$ varies sufficiently slowly (see section 3.5), then $|\Psi(t)\rangle$ follows adiabatically the n^{th} instantaneous eigenstate. We thus make the ansatz

$$|\Psi(t)\rangle = e^{i\varphi(t)} \, |\Phi_n(\boldsymbol{\lambda}(t))\rangle \tag{3.4}$$

where $\varphi(t) \in \mathbb{R}$ is a yet to be determined phase. Combining Eqs. (3.2), (3.3) and (3.4) and projecting onto $\langle \Phi_n(\boldsymbol{\lambda}(t))|$ leads to

$$\frac{\partial \varphi(t)}{\partial t} = -\frac{E_n(\boldsymbol{\lambda}(t))}{\hbar} + \sum_{i=1}^{N} \frac{\partial \lambda_i}{\partial t} A_{n,i}(\boldsymbol{\lambda}(t)) \tag{3.5}$$

where

$$A_{n,i}(\boldsymbol{\lambda}) = i \langle \Phi_n(\boldsymbol{\lambda})| \frac{\partial}{\partial \lambda_i} |\Phi_n(\boldsymbol{\lambda})\rangle \tag{3.6}$$

is the i^{th} component of the *Berry connection* of the n^{th} energy level, which is real due to the normalization $\langle \Phi_n(\boldsymbol{\lambda})|\Phi_n(\boldsymbol{\lambda})\rangle = 1$. By integrating Eq. (3.5) we find for the phase picked up by a quantum state subject to adiabatic time evolution from t_0 to t_1,

$$\Delta\varphi_{0\to 1} \equiv \varphi(t_1) - \varphi(t_0) = -\frac{1}{\hbar} \int_{t_0}^{t_1} E_n(\boldsymbol{\lambda}(t)) \, \mathrm{d}t + \Delta\varphi_{\mathcal{C}} \tag{3.7}$$

with

$$\Delta\varphi_{\mathcal{C}} = \int_{\mathcal{C}} \mathrm{d}\boldsymbol{\lambda} \cdot \mathbf{A}_n \tag{3.8}$$

where $\mathcal{C} := \boldsymbol{\lambda}([t_0, t_1]) \subset M$ is the path in parameter space on which the parameters are varied and the notation $d\boldsymbol{\lambda} \cdot \mathbf{A}_n$ denotes the scalar product (i.e., sum over all components $i = 1, \ldots, N$).

Eq. (3.7) describes the phase under adiabatic time evolution as a sum of two contributions. The term involving the integral over time is called the dynamical phase. It generalizes the phase factor $e^{-iE_n t/\hbar}$ of a stationary state in a time-independent system

to the situation where the eigenenergy E_n depends slowly on time. The second term, $\Delta\varphi_{\mathcal{C}}$, is a correction to this naïve generalization. $\Delta\varphi_{\mathcal{C}}$ is the Berry phase for an adiabatic change of parameters along the path $\mathcal{C}$. Note that the Berry phase depends only on the (directed) contour $\mathcal{C}$ on which the parameters $\boldsymbol{\lambda}$ are varied, and is independent of the velocity with which $\boldsymbol{\lambda}(t)$ changes as a function of time (provided that the change remains adiabatic). For this reason, the Berry phase is sometimes called a geometrical phase. Note also that the Berry phase along the reversed path $\bar{\mathcal{C}}$ is given by $\Delta\varphi_{\bar{\mathcal{C}}} = -\Delta\varphi_{\mathcal{C}}$.

3.3. Gauge invariant formulation and geometric interpretation of Berry phases

The Berry connection, Eq. (3.6), cannot be a physically measurable quantity since it depends on the choice of phases for the instantaneous eigenstates $|\Phi_n(\boldsymbol{\lambda})\rangle$. The freedom to choose an arbitrary phase factor for each instantaneous eigenstate at all $\boldsymbol{\lambda} \in M$ constitutes a $U(1)$ gauge degree of freedom for the solutions of Eq. (3.2). For a given choice of phases, we may define an alternative set of instantaneous eigenstates via the gauge transformation

$$|\Phi_n(\boldsymbol{\lambda})\rangle \longmapsto e^{i\alpha_n(\boldsymbol{\lambda})}|\Phi_n(\boldsymbol{\lambda})\rangle \tag{3.9}$$

where $\alpha_n : M \to \mathbb{R}$ are arbitrary differentiable functions. The Berry connection, Eq. (3.6), changes under the gauge transformation,

$$A_{n,i}(\boldsymbol{\lambda}) \longmapsto A_{n,i}(\boldsymbol{\lambda}) - \frac{\partial\alpha_n(\boldsymbol{\lambda})}{\partial\lambda_i}. \tag{3.10}$$

Therefore, the Berry phase, Eq. (3.8), is also gauge dependent,

$$\Delta\varphi_{\mathcal{C}} \longmapsto \Delta\varphi_{\mathcal{C}} - \int_{\mathcal{C}} \mathrm{d}\boldsymbol{\lambda} \cdot \frac{\partial\alpha_n(\boldsymbol{\lambda})}{\partial\boldsymbol{\lambda}} = \Delta\varphi_{\mathcal{C}} - \alpha_n(\boldsymbol{\lambda}(t_1)) + \alpha_n(\boldsymbol{\lambda}(t_0)). \tag{3.11}$$

Eq. (3.11) simply reflects the fact that the gauge transformation, Eq. (3.9), changes the reference states to which the phases at times t_0 and t_1 are measured.

Berry curvature. When one derives semiclassical theories that include Berry phase effects, it is of advantage to formulate the semiclassical theory only in terms of gauge-invariant quantities. The gauge dependency of results obtained from a semiclassical theory can sometimes be quite subtle [51] if the semiclassical theory does not exclude gauge-dependent quantities right away. An important gauge-invariant quantity is given by the Berry phase along a loop in parameter space. If $\boldsymbol{\lambda}(t_1) = \boldsymbol{\lambda}(t_0)$, the last two terms on the right-hand side of Eq. (3.11) cancel and $\Delta\varphi_{\mathcal{C}}$ is gauge invariant. In the same way, the difference $\Delta\varphi_{\mathcal{C}_1} - \Delta\varphi_{\mathcal{C}_2}$ between the Berry phases along two different paths $\mathcal{C}_1$ and $\mathcal{C}_2$ with common start and end points is gauge invariant, since it is equal to the Berry phase $\Delta\varphi_{\mathcal{C}}$ picked up along the loop $\mathcal{C}$ that results from attaching the reverse of $\mathcal{C}_2$ to the end of the path $\mathcal{C}_1$ (Figure 3.1).

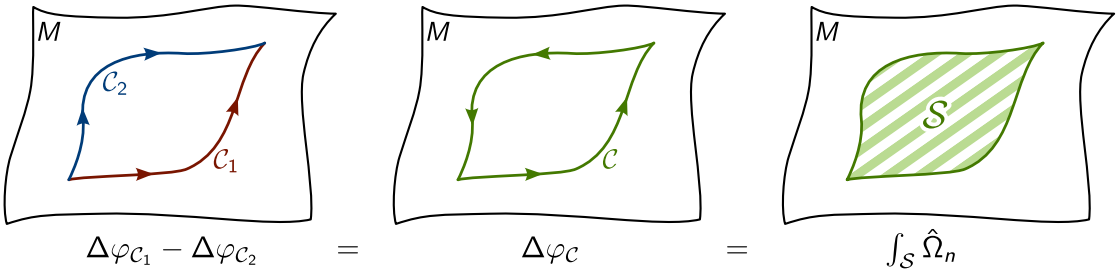

Figure 3.1.: The difference $\Delta\varphi_{\mathcal{C}_1} - \Delta\varphi_{\mathcal{C}_2}$ between the Berry phases along two paths $\mathcal{C}_1$ and $\mathcal{C}_2$ with common start and end points is gauge invariant since it is equal to the Berry phase $\Delta\varphi_{\mathcal{C}}$ along a loop $\mathcal{C}$ resulting from attaching the reverse of $\mathcal{C}_2$ to the end of $\mathcal{C}_1$. If $\mathcal{C}$ is contractible, then $\Delta\varphi_{\mathcal{C}}$ can be calculated by integrating the Berry curvature Ω_n over any surface $\mathcal{S}$ with $\partial\mathcal{S} = \mathcal{C}$, Eq. (3.12).

While the Berry phase along a loop $\mathcal{C} \subset M$ is gauge-invariant, it is difficult to include in a semiclassical theory due to its non-locality. This obstacle can be overcome if $\mathcal{C}$ can be contracted to a point, in which case the Berry phase along $\mathcal{C}$ can be expressed in terms of a local, gauge-invariant quantity known as *Berry curvature*. A contractible loop $\mathcal{C}$ can be expressed as the boundary $\partial\mathcal{S}$ of some surface $\mathcal{S} \subset M$. According to Stokes' theorem, one has for the Berry phase along $\mathcal{C}$,

$$\Delta\varphi_{\mathcal{C}} = \int_{\partial\mathcal{S}} d\boldsymbol{\lambda} \cdot \mathbf{A}_n = \frac{1}{\hbar} \int_{\mathcal{S}} \Omega_n \tag{3.12}$$

where the two-form

$$\Omega_n = \frac{1}{2} \sum_{i,j=1}^{N} \Omega_{n,ij}(\boldsymbol{\lambda})\, \mathrm{d}\lambda_i \wedge \mathrm{d}\lambda_j \qquad \text{with} \qquad \Omega_{n,ij}(\boldsymbol{\lambda}) = \frac{\partial A_j}{\partial \lambda_i} - \frac{\partial A_i}{\partial \lambda_j} \tag{3.13}$$

is the Berry curvature in the energy level n, which is invariant under the gauge transformation Eq. (3.10) ("$\wedge$" denotes the totally anti-symmetric wedge product). The components $\Omega_{n,ij} = -\Omega_{n,ji}$ of the Berry curvature form a skew symmetric tensor, usually referred to as the Berry curvature tensor, and satisfy the Jacobi identity

$$\frac{\partial \Omega_{n,ij}}{\partial \lambda_k} + \frac{\partial \Omega_{n,ki}}{\partial \lambda_j} + \frac{\partial \Omega_{n,jk}}{\partial \lambda_i} = 0 \tag{3.14}$$

which can be easily checked.

Intuitively, one can understand Eq. (3.12) by dividing the surface $\mathcal{S}$ into infinitely many infinitesimally small pairwise disjoint surfaces $\mathcal{S}_\alpha$ such that $\mathcal{S} = \bigcup_\alpha \mathcal{S}_\alpha$ (Figure 3.2 left). The (directed) path $\mathcal{C} = \partial\mathcal{S}$ is the sum over all directed paths $\partial\mathcal{S}_\alpha$ around the tiles $\mathcal{S}_\alpha$, as the paths along the boundaries between two neighboring tiles $\mathcal{S}_\alpha$ and $\mathcal{S}_{\alpha'}$ cancel due to opposite orientation (Figure 3.2 right). Thus, the Berry phase around the

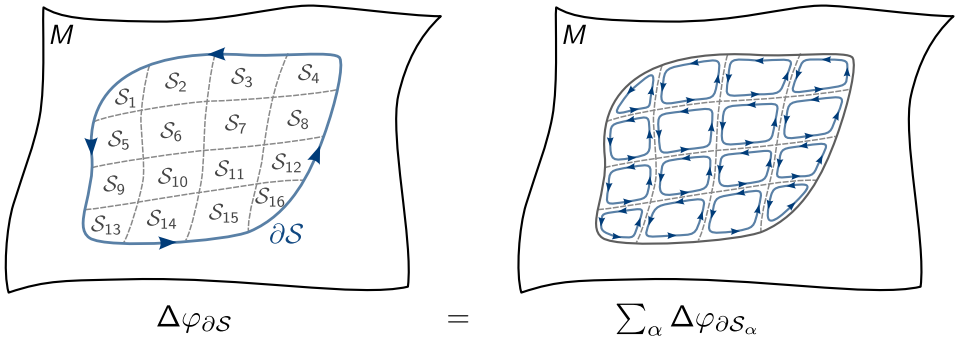

Figure 3.2.: The Berry curvature along the boundary ∂S of a surface $\mathcal{S}$ may be expressed by dividing $\mathcal{S}$ into small tiles $\mathcal{S}_\alpha$ (left), and summing over the Berry curvatures along the boundary of each tile (right). The paths along a shared boundary cancel due to opposite orientation.

whole surface $\mathcal{S}$ is equal to the sum of the Berry phases around each tile $\mathcal{S}_\alpha$. It is easy to see that, in the limit of infinitesimally small tiles, the Berry phase around a tile $\mathcal{S}_\alpha$ that lies in the plane spanned by λ_i and λ_j is given by the area of the tile multiplied by $\Omega_{n,ij}$.

Eq. (3.12) expresses the Berry phase along a loop $\mathcal{C}$ in terms of the local, gauge invariant Berry curvature. The relation holds for any loop $\mathcal{C}$ that can be contracted to a point (Figure 3.3 left). If $\mathcal{C}$ is not contractible (e.g., if M is a torus and $\mathcal{C}$ winds around one of its circles, see Figure 3.3 right), then there is no surface $\mathcal{S}$ with the property $\mathcal{C} = \partial\mathcal{S}$. Consequently, the Berry phase along a non-contractible loop cannot be expressed in terms of the Berry curvature Ω_n, and one has to resort to Eq. (3.8) to calculate $\Delta\varphi_\mathcal{C}$ from the Berry connection $\mathbf{A}_n$. This scenario is similar to the Aharonov-Bohm effect [52]. In momentum space, non-contractible trajectories exist since the Brillouin zone is a torus. The Berry-phase around the Brillouin zone of a one-dimensional crystal is known as the Zak phase [53]. It was recently observed in an ultracold gas of ^{87}Rb atoms [54].

Numerical evaluation of the Berry curvature. Combining Eqs. (3.6) and (3.13), the components of the Berry curvature are given by

$$\Omega_{n,ij}(\boldsymbol{\lambda}) = i\left(\frac{\partial\langle\Phi_n|}{\partial\lambda_i}\frac{\partial|\Phi_n\rangle}{\partial\lambda_j} - \frac{\partial\langle\Phi_n|}{\partial\lambda_j}\frac{\partial|\Phi_n\rangle}{\partial\lambda_i}\right) = -2\,\mathrm{Im}\left[\frac{\partial\langle\Phi_n|}{\partial\lambda_i}\frac{\partial|\Phi_n\rangle}{\partial\lambda_j}\right] \tag{3.15}$$

where we refrained from writing out the parameter $\boldsymbol{\lambda}$ of the instantaneous eigenvectors in order to improve readability. Eq. (3.15) can be used to calculate the Berry curvature for a given Hamiltonian $H(\boldsymbol{\lambda})$ if the instantaneous eigenvectors $|\Phi_n(\boldsymbol{\lambda})\rangle$ are differentiable in the chosen gauge. However, this is not always the case. In a numeric calculation, one may be tempted to rasterize the parameter space and find the instantaneous eigenvectors for all points $\boldsymbol{\lambda}$ on a grid with finite spacing, replacing derivatives by difference

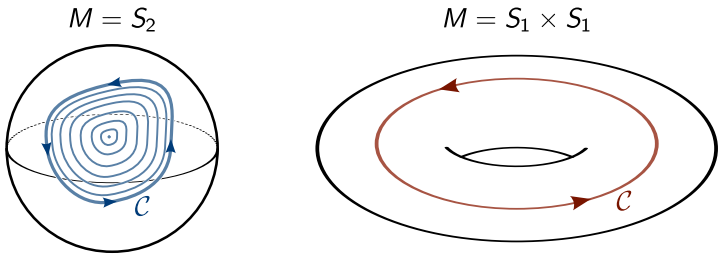

Figure 3.3.: Left: If the parameter space M is simply connected (e.g., $M = S_2$ is the surface of a sphere), then every loop $\mathcal{C} \subset M$ can be smoothly contracted to a point. The surface $\mathcal{S}$ that is covered by the loop during its contraction to a point has the property $\partial\mathcal{S} = \mathcal{C}$, such that Eq. (3.12) applies. Right: Example of a non-contractible loop $\mathcal{C}$ on a torus $M = S_1 \times S_1$, which is not simply connected. Here, Eq. (3.12) cannot be applied to calculate the Berry curvature along the loop.

quotients. Since the numerical diagonalization routine may produce eigenvectors with arbitrary phases, the difference quotients can become arbitrarily large. Even in analytical calculations, a choice of gauge such that $|\Phi_n(\boldsymbol{\lambda})\rangle$ is differentiable on the whole parameter space M does not always exist.

For a finite-dimensional Hilbert space, a numerically more stable expression for $\Omega_{n,ij}$ can be obtained by using the relation

$$(E_m - E_n)\,\langle\Phi_m|\frac{\partial|\Phi_n\rangle}{\partial\lambda_i} = \delta_{mn}\frac{\partial E_n}{\partial\lambda_i} - \left\langle\Phi_m\middle|\frac{\partial H}{\partial\lambda_i}\middle|\Phi_n\right\rangle, \tag{3.16}$$

which can be found by carrying out the derivatives on both sides of the equation

$$\langle\Phi_m|\frac{\partial}{\partial\lambda_i}(H|\Phi_n\rangle) = \langle\Phi_m|\frac{\partial}{\partial\lambda_i}(E_n|\Phi_n\rangle). \tag{3.17}$$

Inserting an identity operator $\mathbb{1} = \sum_m |\Phi_m\rangle\langle\Phi_m|$ in-between the two derivatives on the right-hand side of Eq. (3.15) and using Eq. (3.16) leads to

$$\Omega_{n,ij}(\boldsymbol{\lambda}) = -2\sum_{m\neq n}\mathrm{Im}\left[\frac{\langle\Phi_n|\frac{\partial H}{\partial\lambda_i}|\Phi_m\rangle\langle\Phi_m|\frac{\partial H}{\partial\lambda_j}|\Phi_n\rangle}{(E_m - E_n)^2}\right], \tag{3.18}$$

where the term with $m = n$ drops out of the sum since it is real. Eq. (3.18) suggests to interpret the Berry curvature as consequence of virtual transitions into different energy levels m. Even though we restrict the wave function to a single energy level n by assuming adiabatic time evolution, the presence of other energy levels $m \neq n$ is essential for a non-vanishing Berry curvature. Generically, we expect a large Berry curvature if off-diagonal elements of the Hamiltonian in the basis of instantaneous eigenstates change rapidly and if energy levels come close to each other, e.g. at an avoided crossing of energy levels (see example in section 4.3).

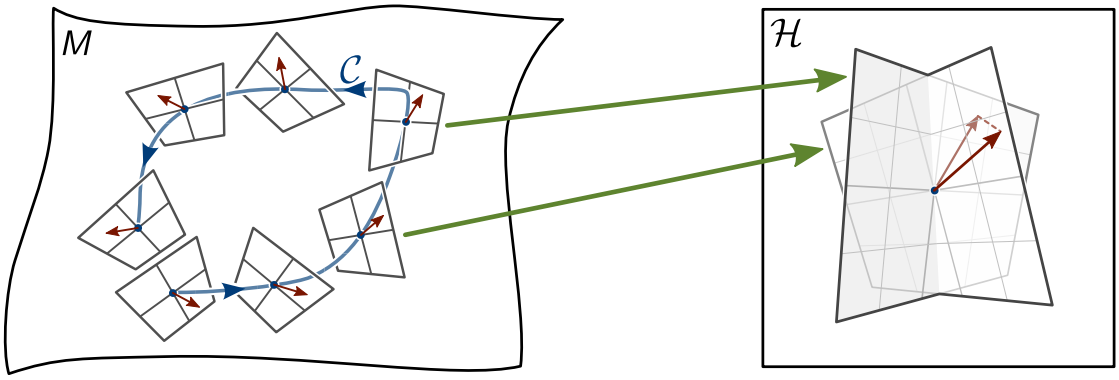

Figure 3.4.: Left: The complex line bundle $\mathcal{B}_n$, Eq. (3.19), is defined by attaching a one-dimensional complex vector space, here depicted as two-dimensional (real) planes, to each point $\boldsymbol{\lambda} \in M$. A reference state $|\psi(t)\rangle$ (red arrows) changes its direction under parallel transport along a loop $\mathcal{C} \subset M$ due to the holonomy of the parallel transport. Right: $\mathcal{B}_n$ admits for a natural parallel transport because all attached complex vector spaces are subspaces of the same Hilbert space $\mathcal{H}$. The natural parallel transport is defined by minimizing the distance (dashed red line) between $|\psi(t)\rangle$ and $|\psi(t+\mathrm{d}t)\rangle$, while keeping the norm of the state constant (Eq. (3.20)).

Geometric interpretation. The Berry phase along a loop $\mathcal{C}$ admits for a simple geometric interpretation. This has been pointed out in an article by Simon [47], which we summarize in the following. If we prepare the wave function $|\Psi\rangle$ of a system at time t_0 in the n^{th} instantaneous eigenstate, $|\Psi(t_0)\rangle = |\Phi_n(\boldsymbol{\lambda}(t_0))\rangle$, then the adiabatic theorem restricts the space of accessible wave functions for all $t \geq t_0$ to the n^{th} eigenspace of $H(\boldsymbol{\lambda}(t))$. This attaches (in absence of degeneracies) a one-dimensional complex vector space to each point $\boldsymbol{\lambda} \in M$, thus defining the complex line bundle (c.f., Figure 3.4 left)

$$\mathcal{B}_n := \{(\boldsymbol{\lambda}, |\phi\rangle) \,:\, \boldsymbol{\lambda} \in M \wedge H(\boldsymbol{\lambda})|\phi\rangle = E_n(\boldsymbol{\lambda})|\phi\rangle\}. \tag{3.19}$$

In order to define a phase picked up by $|\Psi(t)\rangle$ as $\boldsymbol{\lambda}(t)$ varies over time, we have to compare the state $|\Psi(t)\rangle$ to some reference state that also lies in the n^{th} eigenspace of $H(\boldsymbol{\lambda}(t))$. We cannot use the initial state $|\Psi(t_0)\rangle$ as the reference state since the eigenspaces of $H(\boldsymbol{\lambda})$ may depend on $\boldsymbol{\lambda}$. In section 3.2, we used the state $|\Phi_n(\boldsymbol{\lambda}(t))\rangle$ as a reference, but, as discussed above, $|\Phi_n(\boldsymbol{\lambda}(t))\rangle$ is only defined up to an arbitrary phase, thus rendering the relative phase between $|\Phi_n(\boldsymbol{\lambda}(t))\rangle$ and $|\Psi(t)\rangle$ gauge dependent. A gauge-independent reference state $|\psi(t)\rangle$ is defined by *parallel transport* of the initial state $|\Psi(t_0)\rangle$ along the trajectory $\boldsymbol{\lambda}(t)$ in the line bundle $\mathcal{B}_n$ (Figure 3.4 left). While many definitions of parallel transport are conceivable, $\mathcal{B}_n$ admits for a natural definition of parallel transport [55] as it is embedded in the product space $M \times \mathcal{H}$, where $\mathcal{H}$ is the Hilbert space. The natural parallel transport is defined by the property that it minimizes the rate of change $||\partial|\psi(t)\rangle/\partial t||$ under the boundary condition that $|\psi(t)\rangle$ is normalized and lies in the n^{th}

eigenspace of $H(\boldsymbol{\lambda}(t))$ for all t (Figure 3.4 right). This is equivalent to the condition[2]

$$\langle\psi(t)|\frac{\partial|\psi(t)\rangle}{\partial t} \equiv -\frac{\partial\langle\psi(t)|}{\partial t}|\psi(t)\rangle = 0. \tag{3.20}$$

One can calculate the phase that the wave function $|\Psi(t)\rangle$ picks up relative to the reference state $|\psi(t)\rangle$ following the same steps that lead to Eq. (3.7) and finds that it consists only of the dynamical phase. Thus, the choice of reference state $|\psi(t)\rangle$, defined by the natural parallel transport of the initial wave function along the trajectory $\boldsymbol{\lambda}(t)$, gauges away the Berry phase.

Let us now consider the case that the trajectory $\boldsymbol{\lambda}(t)$ describes a loop in the parameter space M, i.e., $\boldsymbol{\lambda}(t_1) = \boldsymbol{\lambda}(t_0)$ for some $t_1 > t_0$. Since the Berry phase along a loop is gauge invariant, it cannot be eliminated by a clever choice of gauge. Indeed, measuring phases relative to the reference state $|\psi(t)\rangle$ is not the same as a gauge transformation of the form of Eq. (3.9) if the trajectory is a loop. The reason is that, in general, $|\psi(t_1)\rangle \neq |\psi(t_0)\rangle$. While both $|\psi(t_1)\rangle$ and $|\psi(t_0)\rangle$ lie in the n^{th} eigenspace of $H(\boldsymbol{\lambda}(t_1)) = H(\boldsymbol{\lambda}(t_0))$, they may differ by a phase. The property that a vector is not invariant under parallel transport along a loop is known as *holonomy* of the chosen parallel transport. In case of a contractible loop, the holonomy is a measure of the *curvature* of a surface enclosed by the loop. The relative phase between $|\psi(t_1)\rangle$ and $|\psi(t_0)\rangle$ can easily be calculated by parameterizing $|\psi(t)\rangle = e^{i\varphi(t)}|\Phi_n(\boldsymbol{\lambda}(t))\rangle$. Inserting into Eq. (3.20) and combining with Eq. (3.6) shows that the phase picked up under parallel transport of the initial wave function $|\Psi(t_0)\rangle$ along a loop $\mathcal{C}$ in parameter space is precisely the Berry phase $\Delta\varphi_{\mathcal{C}}$, Eq. (3.8).

The above geometric picture justifies the choice of the names "Berry connection" and "Berry curvature". The Berry connection $\mathbf{A}_n$ is related to an affine connection on the complex line bundle $\mathcal{B}_n$ in the sense that it defines parallel transport of a vector $|\psi\rangle$ along a trajectory $\boldsymbol{\lambda}(t)$ by

$$|\psi(t + \mathrm{d}t)\rangle = \mathcal{T}(t + \mathrm{d}t\,, t)\,|\psi(t)\rangle \tag{3.21}$$

where the operator

$$\mathcal{T}(t + \mathrm{d}t\,, t) = |\Phi_n(\boldsymbol{\lambda}(t + \mathrm{d}t))\rangle \left(1 + \mathrm{d}t\,\frac{\lambda_j(t)}{\partial t}\, iA_{n,j}(\boldsymbol{\lambda}(t))\right) \langle\Phi_n(\boldsymbol{\lambda}(t))| + \mathcal{O}(\mathrm{d}t^2) \tag{3.22}$$

transports $|\psi\rangle$ from the one-dimensional complex vector space attached to $\boldsymbol{\lambda}(t)$ to the one attached to $\boldsymbol{\lambda}(t + \mathrm{d}t)$. It is easy to see that Eqs. (3.21)–(3.22) are equivalent to Eq. (3.20). Thus, we identify $iA_{n,j}$ as the natural affine connection on $\mathcal{B}_n$ [56].[3] In

[2] The fact that Eq. (3.20) minimizes $||\partial|\psi(t)\rangle/\partial t||$ can be seen by writing an alternative normalized trial wave function as $|\psi'(t)\rangle = e^{i\gamma(t)}|\psi(t)\rangle$ and observing that Eq. (3.20) ensures $||\partial|\psi'(t)\rangle/\partial t||^2 = ||\partial|\psi(t)\rangle/\partial t||^2 + (\partial\gamma/\partial t)^2$.

[3] Note that $iA_{n,j}$ defines a different affine connection on each line bundle $\mathcal{B}_n$ and that the affine connection carries only a single index j instead of three indices since the attached vector spaces are one-dimensional, i.e. the sum over all basis vectors is trivial. For the same reason, the Berry curvature $\Omega_{n,ij}$ of the energy level n carries only two (rather than of four) indices i, j.

physics context, it is common to leave the factor of i out of the definition and to denote $A_{n,j}$ as the Berry connection. The curvature associated with the connection $A_{n,j}$ is precisely the Berry curvature.

3.4. Example

We conclude the discussion of the Berry curvature with the calculation of Ω for a spin in a time-dependent external magnetic field $\mathbf{B}(t)$. This was originally discussed in [1]. Here, we use a more general approach that requires only the knowledge of the anti-commutation relations of angular momentum operators and can therefore more easily be generalized to other symmetry groups than $SU(2)$.

We consider a particle with total spin quantum number $s \in \{0, \frac{1}{2}, 1, \frac{3}{2}, \ldots\}$, i.e., $\mathbf{S}^2|\Psi\rangle = \hbar^2 s(s+1)|\Psi\rangle$ for all states $|\Psi\rangle$ in the Hilbert space. Here, $\mathbf{S}$ is the vector of spin operators, whose components satisfy the commutation relations of the Lie-algebra $\mathfrak{su}(2)$,

$$[S_i, S_j] = i\hbar\epsilon_{ijk}S_k \tag{3.23}$$

with the totally anti-symmetric tensor ϵ. The Hamiltonian of a spin in an external magnetic field $\mathbf{B}$ is given by

$$H(\mathbf{B}) = -\gamma\mathbf{B}\cdot\mathbf{S} \tag{3.24}$$

where γ is the gyromagnetic ratio of the particle carrying the spin (for electrons, $\gamma = qg/(2m)$ with electron charge $q = -e$, mass m, and g-factor $g \approx 2$). To keep the energy spectrum non-degenerate, we restrict the discussion to the case where $\mathbf{B} \neq \mathbf{0}$, i.e., the parameter space is $M = \mathbb{R}^3 \setminus \{\mathbf{0}\}$. Thus, for any $\mathbf{B} \in M$, there exists a $g_{\mathbf{B}} \in SU(2)$ that rotates the vector $\mathbf{B}$ into the z-direction, i.e.,

$$H(\mathbf{B}) = -\gamma|\mathbf{B}|\, U(g_{\mathbf{B}})\, S_z\, U(g_{\mathbf{B}}^{-1}) = -\gamma|\mathbf{B}|\, U(g(\mathbf{B}))\, S_z\, U^\dagger(g_{\mathbf{B}}) \tag{3.25}$$

where U is the $(2s+1)$-dimensional irreducible representation of $SU(2)$. Thus, the eigenvectors and eigenvalues of $H(\mathbf{B})$ are given by

$$|\Phi_m(\mathbf{B})\rangle = U(g_{\mathbf{B}})\,|m\rangle \quad \text{and} \quad E_m(\mathbf{B}) = -m\hbar\gamma|\mathbf{B}| \tag{3.26}$$

respectively, where $|m\rangle$ denotes the eigenvectors of S_z and $m \in \{-s, -s+1, \ldots, s\}$. The choice of $g_{\mathbf{B}} \in SU(2)$ admits a gauge degree of freedom since the spin quantization axis is invariant under rotation around itself. Therefore, the map $\mathbf{B} \mapsto |\Phi_m(\mathbf{B})\rangle$ is also gauge dependent. As we will see below, there is no gauge such that the map $\mathbf{B} \mapsto |\Phi_m(\mathbf{B})\rangle$ is differentiable on the whole parameter space M. Nevertheless, for a given $\mathbf{B} \in M$, we can always choose a gauge such that the map is differentiable on an open neighborhood of $\mathbf{B}$. Then, by inserting Eq. (3.24) into the identity

$$\langle\Phi_m(\mathbf{B})|(H(\mathbf{B}) - E_m(\mathbf{B}))|\Phi_m(\mathbf{B})\rangle = 0 \tag{3.27}$$

and differentiating with respect to B_α, one finds

$$\langle\Phi_m(\mathbf{B})|S_\alpha|\Phi_m(\mathbf{B})\rangle = m\hbar\frac{B_\alpha}{|\mathbf{B}|}. \tag{3.28}$$

Differentiating both sides of Eq. (3.28) by B_β leads to

$$\frac{\partial\langle\Phi_m(\mathbf{B})|}{\partial B_\beta} S_\alpha \left|\Phi_m(\mathbf{B})\right\rangle + \left\langle\Phi_m(\mathbf{B})\right| S_\alpha \frac{\partial|\Phi_m(\mathbf{B})\rangle}{\partial B_\beta} = m\hbar\left(\frac{\delta_{\alpha\beta}}{|\mathbf{B}|} - \frac{B_\alpha B_\beta}{|\mathbf{B}|^3}\right). \tag{3.29}$$

Since the Lie-algebra $\mathfrak{su}(2)$ is spanned by the generators $\{\frac{i}{\hbar}S_x, \frac{i}{\hbar}S_y, \frac{i}{\hbar}S_z\}$, and U is a representation of $SU(2)$, its derivatives can be written as

$$\frac{\partial U(g_\mathbf{B})}{\partial B_\beta} = \frac{i}{\hbar} f_{\beta\gamma} S_\gamma U(g_\mathbf{B}) \tag{3.30}$$

with some (gauge-dependent) real coefficients $f_{\beta\gamma}$. Thus, we find from Eq. (3.26),

$$\frac{\partial\left|\Phi_m(\mathbf{B})\right\rangle}{\partial B_\beta} = \frac{\partial U(g_\mathbf{B})}{\partial B_\beta}\left|m\right\rangle = \frac{i}{\hbar} f_{\beta\gamma} S_\gamma \left|\Phi_m(\mathbf{B})\right\rangle. \tag{3.31}$$

Inserting into Eq. (3.29) leads to

$$i f_{\beta\gamma}\left\langle\Phi_m(\mathbf{B})\right|[S_\alpha, S_\gamma]\left|\Phi_m(\mathbf{B})\right\rangle = m\hbar^2\left(\frac{\delta_{\alpha\beta}}{|\mathbf{B}|} - \frac{B_\alpha B_\beta}{|\mathbf{B}|^3}\right) \tag{3.32}$$

and thus, using Eqs. (3.23) and (3.28),

$$\epsilon_{\alpha\gamma\delta}\, f_{\beta\gamma}\, B_\delta = \frac{B_\alpha B_\beta}{|\mathbf{B}|^2} - \delta_{\alpha\beta}. \tag{3.33}$$

Finally, we find for the components of the Berry curvature Ω_m in the coordinates $\{B_x, B_y, B_z\}$,

$$\begin{aligned}
\Omega_{m,ij}(\mathbf{B}) &\overset{(3.15)}{=} i\left(\frac{\partial\langle\Phi_m(\mathbf{B})|}{\partial B_i}\frac{\partial\left|\Phi_m(\mathbf{B})\right\rangle}{\partial B_j} - \frac{\partial\langle\Phi_m(\mathbf{B})|}{\partial B_j}\frac{\partial\left|\Phi_m(\mathbf{B})\right\rangle}{\partial B_i}\right) \\
&\overset{(3.31)}{=} \frac{i}{\hbar^2}\, f_{i\alpha}\, f_{j\beta}\left\langle\Phi_m(\mathbf{B})\right|[S_\alpha, S_\beta]\left|\Phi_m(\mathbf{B})\right\rangle \\
&\overset{(3.23)}{=} -\frac{1}{\hbar}\,\epsilon_{\alpha\beta\gamma}\, f_{i\alpha}\, f_{j\beta}\left\langle\Phi_m(\mathbf{B})\right|S_\gamma\left|\Phi_m(\mathbf{B})\right\rangle \\
&\overset{(3.28)}{=} -\frac{m}{|\mathbf{B}|}\,\epsilon_{\alpha\beta\gamma}\, f_{i\alpha}\, f_{j\beta}\, B_\gamma \\
&= -\frac{m}{|\mathbf{B}|^3}\,\epsilon_{\mu\nu\lambda}\,\epsilon_{\mu\alpha\rho}\,\epsilon_{\nu\beta\gamma}\, f_{i\alpha}\, f_{j\beta}\, B_\lambda B_\rho B_\gamma \\
&\overset{(3.33)}{=} -\frac{m}{|\mathbf{B}|^3}\,\epsilon_{\mu\nu\lambda}\, B_\lambda\left(\frac{B_\mu B_i}{|\mathbf{B}|^2} - \delta_{\mu i}\right)\left(\frac{B_\nu B_j}{|\mathbf{B}|^2} - \delta_{\nu j}\right) \\
&= -m\,\epsilon_{ijk}\,\frac{B_k}{|\mathbf{B}|^3}.
\end{aligned} \tag{3.34}$$

If we restrict the parameter space to the surface of a sphere $\mathcal{S}_B \subset M$ of radius $B > 0$ around the degeneracy at $\mathbf{B} = \mathbf{0}$, then the right-hand side of Eq. (3.34) is simply

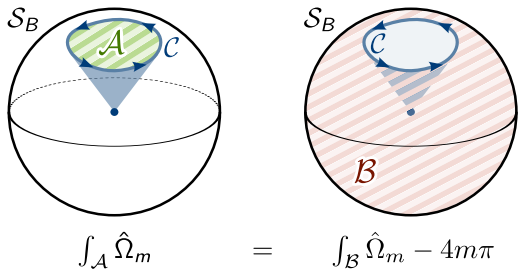

Figure 3.5.: The Berry phase along a loop $\mathcal{C}$ picked up by a particle in a magnetic field $\mathbf{B}$, Eq. (3.24), is given by $(-m)$ times the solid angle covered by $\mathcal{C}$. Here, m is the magnetic quantum number. Since both surfaces $\mathcal{A}$ (left) and $\mathcal{B}$ (right) have $\mathcal{C}$ as their boundaries, the Berry phase may be calculated by integrating over either one of the two and is only defined up to a multiple of $4m\pi$, see Eq. (3.36). Note that $\mathcal{A}$ and $\mathcal{B}$ have opposite orientation relative to the sphere $\mathcal{S}_B$ since they lie on opposite sides of the oriented path $\mathcal{C}$.

$(-m/B^2)$ times the volume form on $\mathcal{S}_B$. Therefore, the Berry phase along a loop $\mathcal{C} \subset M$ is given by $(-m)$ times the solid angle covered by a surface $\mathcal{A}$ whose boundary is $\mathcal{C}$ (Figure 3.5 left) and the integral of the total Berry curvature over $\mathcal{S}_B$ is, independently of the radius B, given by

$$\int_{\mathcal{S}_B} \Omega_m = -4\pi m. \tag{3.35}$$

Thus, in analogy to electromagnetism, the degeneracy at $\mathbf{B} = \mathbf{0}$ can be regarded as a point-source of Berry flux of strength $(-m)$ in band m. A loop $\mathcal{C} \subset \mathcal{S}_B$ divides $\mathcal{S}_B$ into two disjoint surfaces $\mathcal{A}$ and $\mathcal{B}$ (Figure 3.5). The Berry phase $\Delta\varphi_{\mathcal{C}}$ along the loop may be calculated by integrating Ω_m either over $\mathcal{A}$ or over $\mathcal{B}$, leading, in general, to different values for $\Delta\varphi_{\mathcal{C}}$,

$$\Delta\varphi_{\mathcal{C}} = \begin{cases} \int_{\mathcal{A}} \Omega_m & \text{or} \\ \int_{\mathcal{B}} \Omega_m = \int_{\mathcal{A}} \Omega_m + 4\pi m \end{cases} \tag{3.36}$$

if the orientations of $\mathcal{A}$ and $\mathcal{B}$ are chosen appropriately. This apparent contradiction is resolved by the fact that there is no gauge such that the eigenvectors $|\Phi_m(\mathbf{B})\rangle$ are differentiable on the whole sphere $\mathcal{S}_B$. Therefore, there always exists some (gauge-dependent) point $\mathbf{B}' \in \mathcal{S}_B$ where the Berry connection, Eq. (3.6), is not well-defined and Stokes theorem, Eq. (3.12), cannot be applied if $\mathbf{B}'$ lies in the integration region. This does not impair our results, however, since we can always shift $\mathbf{B}'$ between $\mathcal{A}$ and $\mathcal{B}$ with an appropriate gauge transformation without changing Ω_m (where it is defined). Therefore, both branches in Eq. (3.36) have to be regarded as valid choices for the Berry curvature along $\mathcal{C}$. Physically, only the phase factor $e^{i\Delta\varphi_{\mathcal{C}}}$ is relevant, which is independent of the choice of branch in Eq. (3.36) since $2m \in \mathbb{Z}$.

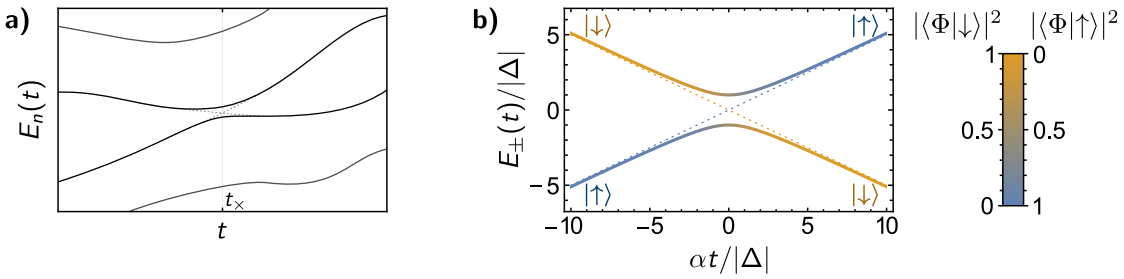

Figure 3.6.: a) Generic case of an avoided crossing of energy levels $E_n(t)$. In the simplest case, only two energy levels are close to each other at $t \approx t_\times$ and all other energy levels may be neglected. The dashed lines depict energy levels in absence of hybridization. b) Energy levels of the model Hamiltonian Eq. (3.37). Colors show overlap with the corresponding energy levels for $\Delta = 0$ (dashed lines), as indicated in the legend.

3.5. Quantification of adiabaticity

The derivation of the Berry phase in section 3.2 is based on the assumption of adiabaticity, i.e. we assumed that the wave function remains proportional to the n^{th} instantaneous eigenstate for all times (Eq. (3.4)). One can show that time evolution is indeed adiabatic if the parameters change slowly. In the strict limit of infinitely slowly traversal of the path $\mathcal{C} \subset M$, this holds even in the presence of a finite number of points $\boldsymbol{\lambda}_\alpha \in \mathcal{C}$ where the Hamiltonian $H(\boldsymbol{\lambda}_\alpha)$ is degenerate [46]. If the parameters $\boldsymbol{\lambda}(t)$ change with a finite rate, however, the time evolution is no longer strictly adiabatic and transitions to other instantaneous eigenstates may occur. These transitions are most prominent if the instantaneous eigenvector $|\Phi_n(\boldsymbol{\lambda}(t))\rangle$ changes rapidly, which happens generically in the vicinity of an avoided crossing of energy levels (Figure 3.6). To estimate under which conditions the assumption of adiabatic time evolution is still a good approximation, let us consider the transition probability between two instantaneous eigenstates when the Hamiltonian $H(t)$ is tuned through an avoided crossing of energy levels. This process is known as Landau-Zener tunneling [57–60].

First, we set up a minimal model for an avoided crossing of energy levels, following the arguments in [57]. In the simplest case of an avoided crossing, only two energy levels are close to each other at some time $t \approx t_\times$, while all other energy levels are well separated (Figure 3.6a). In this case, only the transition amplitudes between the two almost-crossing energy levels are large and we may model the system by a time-dependent two-level Hamiltonian $H(t)$. Without hybridization, the two energy levels $E_\downarrow(t)$ and $E_\uparrow(t)$ cross each other at $t = t_\times$. Since the transition rate is large only in the vicinity of $t_\times$, we may linearize $E_\uparrow(t) - E_\downarrow(t) = \alpha(t - t_\times)$ with some rate $\alpha > 0$. The degeneracy at $t = t_\times$ is lifted by a small hybridization Δ, which we assume to be constant since it is only relevant during the short period of time when the two energy levels are close to each other. In order to write down $H(t)$ explicitly, we choose a basis where, for $t \to \pm\infty$, the eigenstates are the canonical basis vectors $|\uparrow\rangle = (1, 0)^T$ and

$|\downarrow\rangle = (0,1)^T$. With the simplifications that we may always set $t_\times = 0$ and shift both energies such that $E_\downarrow(t) = -E_\uparrow(t)$, we arrive at the model Hamiltonian (c.f., Figure 3.6b)

$$H(t) = \begin{pmatrix} \frac{1}{2}\alpha t & \Delta \\ \Delta^* & -\frac{1}{2}\alpha t \end{pmatrix} \tag{3.37}$$

where Δ^* denotes the complex conjugate of Δ.

The Hamiltonian, Eq. (3.37), has instantaneous eigenenergies $E_\pm(t) = \pm\sqrt{\frac{1}{4}\alpha^2 t^2 + |\Delta|^2}$ and the corresponding instantaneous eigenstates $|\Phi_+(t)\rangle$ ($|\Phi_-(t)\rangle$) carry the state $|\downarrow\rangle$ ($|\uparrow\rangle$) from $t \to -\infty$ to the state $|\uparrow\rangle$ ($|\downarrow\rangle$) for $t \to +\infty$, respectively (see Figure 3.6b). However, the wave function $|\Psi(t)\rangle$ of a system that is prepared in the eigenstate $|\Phi_-(t)\rangle$ at time $t \to -\infty$ will have a finite overlap with $|\Phi_+(t)\rangle$ at time $t \to +\infty$. The probability of such a non-adiabatic transition,

$$P_{\text{n.a.}} := \lim_{t\to\infty} |\langle\Phi_+(t)|\Psi(t)\rangle|^2 \tag{3.38}$$

has been studied independently by Landau, Zener, Stueckelberg, and Majorana in 1932 [57–60] (for a more modern derivation, see [61]). For the Hamiltonian in Eq. (3.37), the exact result is

$$P_{\text{n.a.}} = e^{-2\pi|\Delta|^2/(\hbar\alpha)}. \tag{3.39}$$

Thus, non-adiabatic transitions between instantaneous eigenstates are exponentially suppressed if the rate of change $\alpha \ll |\Delta|^2/\hbar$, where $2|\Delta|$ is the minimal separation between the two energy levels. For the methods developed in this thesis, it will be most natural to express the Hamiltonian in the basis of instantaneous eigenstates $|\Phi_\pm(t)\rangle$ (as opposed to the constant basis $\{|\uparrow\rangle, |\downarrow\rangle\}$ used in Eq. (3.37)). While the Hamiltonian, Eq. (3.37), is by definition diagonal in the basis of $|\Phi_\pm(t)\rangle$, its time-derivative has off-diagonal terms that mediate (real or virtual) transitions between instantaneous eigenstates. We already saw that virtual transitions between instantaneous eigenstates influence adiabatic time evolution (Eq. (3.18)). Non-adiabatic corrections can be interpreted as real transitions. For the model in Eq. (3.37), one finds,

$$\left|\left\langle\Phi_-(t)\right|\frac{\partial H(t)}{\partial t}\left|\Phi_+(t)\right\rangle\right| = \frac{\alpha}{\sqrt{4+\alpha^2 t^2/|\Delta|^2}} \tag{3.40}$$

and therefore,

$$P_{\text{n.a.}} = e^{-\pi/(4\max_t(\kappa_{\text{n.a.}}(t)))} \tag{3.41}$$

where $\max_t(\cdots)$ denotes the maximum value over all times and the dimensionless parameter

$$\kappa_{\text{n.a.}}(t) := \frac{\hbar\left|\left\langle\Phi_-(t)\right|\frac{\partial H(t)}{\partial t}\left|\Phi_+(t)\right\rangle\right|}{(E_+(t)-E_-(t))^2} \tag{3.42}$$

quantifies non-adiabaticity. Adiabatic time evolution is a good approximation if $\kappa_{\text{n.a.}}(t) \ll 1$ for all times.

In this thesis, we study the electronic properties in magnetic materials with a smooth magnetization texture. The smooth inhomogeneity leads to Berry phase effects within each band and, in principle, also to non-adiabatic transitions between different bands. The relevance of the latter may be estimated by substituting $\frac{\partial H}{\partial t} \approx v_F \frac{\partial H}{\partial r} + \dot{k}\frac{\partial H}{\partial k}$ in Eq. (3.42) where v_F is a characteristic group velocity of the electrons, $\dot{k} \approx eE/\hbar$ with electric field E and elementary charge e, and H is the band-Hamiltonian that depends on some averaged position coordinate r (c.f., section 5.1). The range of validity of our methods is characterized by $\kappa_{\text{n.a.}} \ll 1$.

4. Phase-space Berry phases in chiral magnets

Berry phases play an important role in chiral magnets for two reasons. First, chiral magnets with weak spin-orbit coupling exhibit a smooth magnetization texture below the transition temperature (section 2.2). In the reference frame of a moving electron, the smooth spatial inhomogeneity of the magnetization acts like a slowly time-dependent exchange field (c.f., Eq. (3.24)), leading to Berry-phase effects in position space [62, 63]. Second, spin-orbit coupling leads to a non-vanishing Berry curvature in momentum space, which can be detected in measurements of the anomalous Hall effect [30]. The presence of *both* position and momentum-space Berry phases makes chiral magnets ideal example systems to study the effects of Berry phases in combined phase space $\{(\mathbf{r}, \mathbf{k})\}$. In general, Berry-phase effects in phase space are described by an antisymmetric 6×6 Berry curvature tensor $\Omega_{n,ij}$, whose off-diagonal blocks describe the geometric phases picked up by a wave packet on an infinitesimal loop in the plane spanned by position direction r_i and momentum direction k_j. If an explicit, slow time dependency of the Hamiltonian is allowed, the Berry curvature becomes a 7×7 tensor where the additional entries describe an emergent electric field in direct and in reciprocal space.

In this chapter, we present the origin and physical interpretation of Berry phases in position and momentum space (sections 4.1 and 4.2, respectively), and introduce simple models to estimate the relative strengths of position-, momentum-, and mixed position/momentum-space Berry phases in chiral magnets (section 4.3).

4.1. Position-space Berry phases and emergent electrodynamics

It was pointed out by Volovik [64] in 1986 that the total mass current in an itinerant magnet is the sum of two momenta: the momentum due to coherent motion (i.e., motion of the magnetization texture) and the momentum due to incoherent motion of the electrons. While the total mass current is well-defined, the partitioning between coherent and incoherent motion depends on a gauge. Thus, when either of the two components (coherent or incoherent motion) is treated in isolation, the natural description involves a gauge theory, where the gauge field shifts the canonical momentum. In the following, we summarize the derivation of the emergent gauge theory for the electron motion. We follow the conventions for signs and prefactors in Refs. [30, 65], which differ from some earlier treatments [62, 63] of emergent electrodynamics in chiral magnets.

Emergent electrodynamics. We consider a model for non-interacting electrons in a smooth background magnetization $\mathbf{M}(t,\mathbf{r})$. The single-particle Hamiltonian for the electrons is given by

$$H = -\frac{\hbar^2\boldsymbol{\nabla}^2}{2m} + \mathbf{B}^{\mathrm{ex}}(t,\mathbf{r})\cdot\boldsymbol{\sigma} \tag{4.1}$$

where $\boldsymbol{\sigma}$ is the vector of Pauli matrices and the exchange field $\mathbf{B}^{\mathrm{ex}}(t,\mathbf{r}) = -J\mathbf{M}(t,\mathbf{r})$ is proportional to the strength $J>0$ of the exchange coupling and the local magnetization $\mathbf{M}(t,\mathbf{r})$. The second term on the right-hand side of Eq. (4.1) is diagonalized by a local unitary transformation $U(t,\mathbf{r})$,

$$U^\dagger(t,\mathbf{r})\,\mathbf{B}^{\mathrm{ex}}(t,\mathbf{r})\cdot\boldsymbol{\sigma}\,U(t,\mathbf{r}) = |\mathbf{B}^{\mathrm{ex}}(t,\mathbf{r})|\sigma_z\ , \tag{4.2}$$

which we can always choose such that $\det U = 1$. Physically, $U(t,\mathbf{r})$ rotates the spin-quantization axis from the z-axis to the direction of the local exchange field. By parameterizing the two-component wave function $\Psi(t,\mathbf{r}) = U(t,\mathbf{r})\chi(t,\mathbf{r})$, one can check that $\Psi(t,\mathbf{r})$ satisfies the time-dependent Schrödinger equation with Hamiltonian H if the two-component spinor $\chi(t,\mathbf{r})$ satisfies the relation

$$i\hbar\,\partial_t\chi(t,\mathbf{r}) = \left[\frac{(-i\hbar\boldsymbol{\nabla} - \hbar\boldsymbol{\mathcal{A}}^{\mathrm{r}}(t,\mathbf{r}))^2}{2m} + |\mathbf{B}^{\mathrm{ex}}(t,\mathbf{r})|\sigma_z - \hbar\mathcal{A}^{\mathrm{t}}(t,\mathbf{r})\right]\chi(t,\mathbf{r}) \tag{4.3}$$

with the 2×2 matrix $\mathcal{A}^{\mathrm{t}}$ and the vector of 2×2 matrices $\boldsymbol{\mathcal{A}}^{\mathrm{r}} \equiv (\mathcal{A}^{\mathrm{r}}_x, \mathcal{A}^{\mathrm{r}}_y, \mathcal{A}^{\mathrm{r}}_z)$, defined by

$$\mathcal{A}^{\mathrm{t}}(t,\mathbf{r}) = i\,U^\dagger(t,\mathbf{r})\frac{\partial U(t,\mathbf{r})}{\partial t} \qquad \text{and} \qquad \boldsymbol{\mathcal{A}}^{\mathrm{r}}(t,\mathbf{r}) = i\,U^\dagger(t,\mathbf{r})\frac{\partial U(t,\mathbf{r})}{\partial \mathbf{r}}. \tag{4.4}$$

The matrices $\mathcal{A}^{\mathrm{t}}$ and $\boldsymbol{\mathcal{A}}^{\mathrm{r}}$ are hermitian since

$$0 = i\partial_\alpha \mathbb{1} = i\partial_\alpha(U^\dagger U) = \mathcal{A}_\alpha - \mathcal{A}_\alpha^\dagger \tag{4.5}$$

where α denotes either time or a space direction, and traceless since

$$\operatorname{tr}\mathcal{A}_\alpha = i\partial_\alpha(\operatorname{tr}\ln U) = i\partial_\alpha(\ln\det U) = 0. \tag{4.6}$$

Eq. (4.3) can be shown to be equivalent to the time-dependent Schrödinger Equation by multiplying both sides from the left with U and carrying out the derivatives of $\chi \equiv U^\dagger\Psi$ in space (time) order by order. In each step, the additional term from the basis transformation is canceled by the term $-\hbar\boldsymbol{\mathcal{A}}^{\mathrm{r}}$ ($\hbar\mathcal{A}^{\mathrm{t}}$). For example, one obtains for the first term on the right-hand side of Eq. (4.3),

$$\begin{aligned}
\frac{1}{2m}U(-i\hbar\boldsymbol{\nabla} - \hbar\boldsymbol{\mathcal{A}}^{\mathrm{r}})^2U^\dagger\Psi &= \frac{\hbar^2}{2m}U(-i\boldsymbol{\nabla} - \boldsymbol{\mathcal{A}}^{\mathrm{r}})\big(-i(\boldsymbol{\nabla}U^\dagger) - iU^\dagger\boldsymbol{\nabla} - \boldsymbol{\mathcal{A}}^{\mathrm{r}}U^\dagger\big)\Psi \\
&= \frac{\hbar^2}{2m}U(-i\boldsymbol{\nabla} - \boldsymbol{\mathcal{A}}^{\mathrm{r}})\big(iU^\dagger(\boldsymbol{\nabla}U)U^\dagger - iU^\dagger\boldsymbol{\nabla} - \boldsymbol{\mathcal{A}}^{\mathrm{r}}U^\dagger\big)\Psi \\
&= \frac{\hbar^2}{2m}U(-i\boldsymbol{\nabla} - \boldsymbol{\mathcal{A}}^{\mathrm{r}})(-iU^\dagger\boldsymbol{\nabla}\Psi) \\
&= \frac{\hbar^2}{2m}U\big(U^\dagger(\boldsymbol{\nabla}U)U^\dagger - U^\dagger\boldsymbol{\nabla} + i\boldsymbol{\mathcal{A}}^{\mathrm{r}}U^\dagger\big)\boldsymbol{\nabla}\Psi \\
&= -\frac{\hbar^2}{2m}\boldsymbol{\nabla}^2\Psi
\end{aligned} \tag{4.7}$$

where, in the second and the fourth line, we inserted an identity operator $U^\dagger U = \mathbb{1}$ and used the relation $U(\boldsymbol{\nabla} U^\dagger) = -(\boldsymbol{\nabla} U)U^\dagger$, which follows from the unitarity of U.

If the direction of $\mathbf{B}^{\mathrm{ex}}(t,\mathbf{r})$ is constant in space and time, then we can choose $U(t,\mathbf{r}) =$ const. and thus $\mathcal{A}_\alpha \equiv 0$. In this limit, Eq. (4.3) is the Schrödinger equation of a spin-$\frac{1}{2}$ particle in a collinear external Zeemann field of strength $|\mathbf{B}^{\mathrm{ex}}(t,\mathbf{r})|$ in z direction. We denote the spin state $|{\downarrow}\rangle$ ($|{\uparrow}\rangle$) defined by $\sigma_z |{\downarrow}\rangle = -|{\downarrow}\rangle$ ($\sigma_z |{\uparrow}\rangle = |{\uparrow}\rangle$) as majority (minority) spin, respectively. In the original basis, the majority spin state $U(t,\mathbf{r})\,|{\downarrow}\rangle$ describes a particle with spin $\mathbf{S} = \frac{\hbar}{2}\boldsymbol{\sigma}$ in direction opposite to $\mathbf{B}^{\mathrm{ex}}(t,\mathbf{r})$, whereas the spin of a particle in the minority spin state $U(t,\mathbf{r})\,|{\uparrow}\rangle$ points in the direction of $\mathbf{B}^{\mathrm{ex}}(t,\mathbf{r})$.

If, on the other hand, the exchange field is not collinear, then $\mathcal{A}_\alpha \neq 0$ in general and the canonical momentum $-i\hbar\boldsymbol{\nabla}$ of the electron is no longer a conserved quantity. In this case, Eq. (4.3) has a structure that is formally similar to the Schrödinger equation of a charged particle in electromagnetic fields with vector potential $\propto \boldsymbol{\mathcal{A}}^{\mathrm{r}}$ and scalar potential $\propto -\mathcal{A}^{\mathrm{t}}$. However, in contrast to conventional electromagnetism, the potentials $\propto \mathcal{A}_\alpha$ in Eq. (4.3) are 2×2 matrices whose off-diagonal elements mediate transitions between majority and minority spin. The strength of these spin-flip processes depends on the ratio of two energy scales: the Fermi energy $\epsilon_F \sim \hbar v_F k_F$ with Fermi velocity v_F and Fermi momentum $\hbar k_F$, and the energy scale ϵ_{mod} due to spatial and temporal modulations of the magnetic texture. The modulations enter Eq. (4.3) via the matrices $\mathcal{A}^{\mathrm{t}}$ and $\boldsymbol{\mathcal{A}}^{\mathrm{r}}$. From Eqs. (4.3)–(4.4), we obtain the estimate

$$\epsilon_{\mathrm{mod}} \sim v_F |\boldsymbol{\mathcal{A}}^{\mathrm{r}}| + \left|\mathcal{A}^{\mathrm{t}}\right| \sim \frac{\hbar v_F}{\xi_{\mathrm{mod}}} + \frac{\hbar v_M}{\xi_{\mathrm{mod}}} \tag{4.8}$$

where ξ_{mod} is the characteristic length scale on which the magnetization varies in space, e.g., the pitch length $\sim 165\ldots180\,\text{Å}$ in MnSi. Further, v_M is the velocity of the motion of the magnetic texture assuming that $\mathbf{M}(t,\mathbf{r}) = \mathbf{M}_0(\mathbf{r} - \mathbf{v}_M t)$ moves like a rigid body. In principle, a third energy scale $\epsilon_{\mathrm{scatt.}} \sim \hbar/\tau$, related to the amount of scattering processes, is also relevant. Here, τ is the quasi-particle life-time. We assume that the related energy scale $\hbar/\tau$ is much smaller than the band width such that the quasi-particle picture applies.

The second term on the right-hand side of Eq. (4.8) is subleading since v_M is always smaller than v_F. For a smooth magnetization texture, one has $\xi_{\mathrm{mod}} \gg a$, where $a \sim 1/k_F$ is the lattice constant. Therefore,

$$\epsilon_{\mathrm{mod}} \sim \frac{\hbar v_F}{\xi_{\mathrm{mod}}} \ll \hbar v_F k_F \sim \epsilon_F. \tag{4.9}$$

Thus, for a smooth magnetization texture, we may treat the matrices $\mathcal{A}^{\mathrm{t}}$ and $\boldsymbol{\mathcal{A}}^{\mathrm{r}}$ in Eq. (4.3) perturbatively. To linear order, only the diagonal matrix elements contribute. Since $\mathcal{A}_\alpha$ is hermitian and traceless, see Eqs. (4.5)–(4.6), the projection onto its diagonal elements is given by $-\langle{\downarrow}|\mathcal{A}_\alpha(t,\mathbf{r})|{\downarrow}\rangle\,\sigma_z$. Inserting into Eq. (4.3) leads to the effective Schrödinger equation

$$i\hbar\,\partial_t \chi_\sigma(t,\mathbf{r}) = \left[\frac{(-i\hbar\boldsymbol{\nabla} - q_\sigma^{\mathrm{em}}\mathbf{A}^{\mathrm{em}}(t,\mathbf{r}))^2}{2m} + q_\sigma^{\mathrm{em}}\left(V^{\mathrm{em}}(t,\mathbf{r}) - \frac{|\mathbf{B}^{\mathrm{ex}}(t,\mathbf{r})|}{q_\downarrow^{\mathrm{em}}}\right)\right]\chi_\sigma(t,\mathbf{r}) \tag{4.10}$$

for $\sigma \in \{\uparrow,\downarrow\}$, with so-called emergent charges $q^{\mathrm{em}}_{\uparrow} = -q^{\mathrm{em}}_{\downarrow}$, the emergent vector potential

$$\mathbf{A}^{\mathrm{em}}(t,\mathbf{r}) = \frac{\hbar}{q^{\mathrm{em}}_{\downarrow}} \langle\downarrow|\boldsymbol{\mathcal{A}}^{\mathrm{r}}(t,\mathbf{r})|\downarrow\rangle = \frac{i\hbar}{q^{\mathrm{em}}_{\downarrow}} \langle\downarrow|U^{\dagger}(t,\mathbf{r})\boldsymbol{\nabla}U(t,\mathbf{r})|\downarrow\rangle\,, \tag{4.11}$$

and the emergent scalar potential

$$V^{\mathrm{em}}(t,\mathbf{r}) = -\frac{\hbar}{q^{\mathrm{em}}_{\downarrow}} \langle\downarrow|\mathcal{A}^{\mathrm{t}}(t,\mathbf{r})|\downarrow\rangle = -\frac{i\hbar}{q^{\mathrm{em}}_{\downarrow}} \langle\downarrow|U^{\dagger}(t,\mathbf{r})\partial_t U(t,\mathbf{r})|\downarrow\rangle\,. \tag{4.12}$$

While $q^{\mathrm{em}}_{\downarrow}$ drops out of Eq. (4.10), it is convention to set $q^{\mathrm{em}}_{\downarrow} = \frac{1}{2}$ and $q^{\mathrm{em}}_{\uparrow} = -\frac{1}{2}$ for the majority and minority state of a spin-$\frac{1}{2}$ particle, respectively [30, 63].

Position-space Berry curvature. The emergent potentials $\mathbf{A}^{\mathrm{em}}$ and V^{em} are the gauge fields corresponding to the gauge degree of freedom $U(t,\mathbf{r}) \mapsto U(t,\mathbf{r})e^{i\varphi(t,\mathbf{r})\sigma_z}$, where $\varphi(t,\mathbf{r})$ is an arbitrary real-valued function. The gauge fields can be interpreted in two ways: On the one hand, Eq. (4.10) is the Schrödinger equation of a charged particle in external orbital electromagnetic fields (in addition to a collinear Zeemann field of strength $|\mathbf{B}^{\mathrm{ex}}(t,\mathbf{r})|$). In this sense, $\mathbf{A}^{\mathrm{em}}$ and V^{em} play the role of emergent electromagnetic potentials, which influence the motion of electrons in the same way that actual electromagnetic potentials would. Note, however, that the emergent charge $q^{\mathrm{em}}_{\sigma} = \pm\frac{1}{2}$ depends on the spin. The corresponding gauge-independent emergent electromagnetic fields are given by

$$\mathbf{B}^{\mathrm{em}}(\mathbf{r},t) = \boldsymbol{\nabla} \times \mathbf{A}^{\mathrm{em}}(\mathbf{r},t); \qquad \mathbf{E}^{\mathrm{em}}(\mathbf{r},t) = -\boldsymbol{\nabla}V^{\mathrm{em}}(\mathbf{r},t) - \partial_t \mathbf{A}^{\mathrm{em}}(\mathbf{r},t). \tag{4.13}$$

On the other hand, the gauge fields $\mathbf{A}^{\mathrm{em}}$ and V^{em} may also be interpreted as the components of the Berry connection in space-time. If we ignore the kinetic part of the Hamiltonian, Eq. (4.1), and treat $\mathbf{r}$ and t as external parameters, then the diagonal components of the matrices $\boldsymbol{\mathcal{A}}^{\mathrm{r}}$ and $\mathcal{A}^{\mathrm{t}}$ are just the Berry connection in space and time in the two local spin-eigenstates, see Eq. (3.6). For the corresponding Berry curvature $\Omega^{\mathrm{tr,tr}}_{\sigma}$ in space-time, we obtain from Eq. (4.13)

$$\Omega^{\mathrm{tr,tr}}_{\sigma,\alpha\beta} = \partial_\alpha A^{\mathrm{x}}_{\sigma,\beta} - \partial_\beta A^{\mathrm{x}}_{\sigma,\alpha} = \frac{q^{\mathrm{em}}_{\sigma}}{\hbar} \begin{pmatrix} 0 & -E^{\mathrm{em}}_x & -E^{\mathrm{em}}_y & -E^{\mathrm{em}}_z \\ E^{\mathrm{em}}_x & 0 & B^{\mathrm{em}}_z & -B^{\mathrm{em}}_y \\ E^{\mathrm{em}}_y & -B^{\mathrm{em}}_z & 0 & B^{\mathrm{em}}_x \\ E^{\mathrm{em}}_z & B^{\mathrm{em}}_y & -B^{\mathrm{em}}_x & 0 \end{pmatrix}_{\alpha\beta} \tag{4.14}$$

which is reminiscent of the electromagnetic field-strength tensor. A simple expression for the components of $\Omega^{\mathrm{tr,tr}}_{\sigma}$ can be obtained by transforming Eq. (3.34) from the space of magnetic fields $\mathbf{B}$ into space-time, identifying the spin-operator $\mathbf{S} = \frac{\hbar}{2}\boldsymbol{\sigma}$ and $\mathbf{B} = -\frac{2}{\hbar\gamma}\mathbf{B}^{\mathrm{ex}} = \frac{2J}{\hbar\gamma}\mathbf{M}$. One obtains

$$\Omega^{\mathrm{tr,tr}}_{\sigma,\alpha\beta}(t,\mathbf{r}) = -q_\sigma\, \epsilon_{ijk} \frac{\partial M_i}{\partial x_\alpha} \frac{\partial M_j}{\partial x_\beta} \frac{M_k}{|\mathbf{M}|^3} = -q^{\mathrm{em}}_{\sigma}\, \hat{\mathbf{M}} \cdot \left(\frac{\partial \hat{\mathbf{M}}}{\partial x_\alpha} \times \frac{\partial \hat{\mathbf{M}}}{\partial x_\beta} \right) \tag{4.15}$$

where $\hat{\mathbf{M}}(t,\mathbf{r}) := \mathbf{M}(t,\mathbf{r})/|\mathbf{M}(t,\mathbf{r})|$. The right-hand side of Eq. (4.15) is $(-4\pi q_\sigma)$ times the winding number density of the magnetization in the plane spanned by the space-time directions α and β (cf., Eq. (2.5)). For a Skyrmion lattice in the (r_x, r_y)-plane, where each Skyrmion contributes -1 to the total winding number, the total flux of emergent magnetic field in the z direction works out to be $+4\pi\hbar$ per Skyrmion. The emergent magnetic field influences the motion of electrons with majority spin $\downarrow$ and electric charge $-e$ in the same way as an actual magnetic field with flux $\frac{q_\downarrow^{\mathrm{em}}}{-e} \cdot 4\pi\hbar = -\Phi_0$ per Skyrmion would, where $\Phi_0 = 2\pi\hbar/e$ is the magnetic flux quantum. In MnSi, the wavelength of the magnetic modulation close to the transition temperature is given by $\lambda_S \approx 165\,\text{Å}$ [31], and and one obtains the value $\frac{q_\downarrow^{\mathrm{em}}}{-e}\langle B_z^{\mathrm{em}}\rangle \approx -13\,\mathrm{T}$ for the average emergent magnetic field [30]. The emergent magnetic field can be detected experimentally as an additional contribution to the Hall effect that appears only in the skyrmion lattice phase, see Section 7.1.

4.2. Berry phases in momentum space and anomalous velocity

In a study of the Hall effect in ferromagnets, Karplus and Luttinger [6] found already in 1954 that the group velocity of electrons in a crystal in presence of an external electric field differs from the semiclassically expected value of $\frac{\partial \epsilon_{n\mathbf{k}}}{\hbar\,\partial\mathbf{k}}$, where $\epsilon_{n\mathbf{k}}$ is the energy dispersion of band n. They obtained an additional term, called "anomalous velocity", which they were able to explain either by the fact that the electric field $\mathbf{E}$ changes the Bloch states of the crystal, or, equivalently, in terms of virtual transitions between different bands mediated by $\mathbf{E}$ (cf., discussion following Eq. (3.18)).

Berry curvature in the Brillouin zone. In the more modern framework of Berry phases, the anomalous velocity can be understood as the product of the electric field $\mathbf{E}$ with the Berry curvature in momentum space. We review the definition of the momentum-space Berry curvature, wee Eq. (4.20) below, following arguments by Xiao, Chang, and Niu [2]. In local density approximation, electrons in a crystal are described by a periodic single-particle Hamiltonian H. According to the Bloch theorem (see any textbook on solid state theory, e.g., Ref. [66]), the eigenfunctions $\Psi_{n\mathbf{k}}(\mathbf{r})$ of H are labeled by a band index n and a crystal momentum $\hbar\mathbf{k}$ and can be written as a product

$$\Psi_{n\mathbf{k}}(\mathbf{r}) = e^{i\mathbf{k}\cdot\mathbf{r}}\, u_{n\mathbf{k}}(\mathbf{r}) \tag{4.16}$$

where $u_{n\mathbf{k}}(\mathbf{r})$ is the lattice-periodic part of the Bloch wave function, satisfying

$$u_{n\mathbf{k}}(\mathbf{r}+\mathbf{R}) = u_{n\mathbf{k}}(\mathbf{r}) \tag{4.17}$$

for all lattice vectors $\mathbf{R}$. From the eigenvalue equation $H\Psi_{n\mathbf{k}}(\mathbf{r}) = \epsilon_{n\mathbf{k}}\Psi_{n\mathbf{k}}(\mathbf{r})$ it follows that the functions $u_{n\mathbf{k}}(\mathbf{r})$ satisfy the relation

$$H(\mathbf{k})u_{n\mathbf{k}}(\mathbf{r}) = \epsilon_{n\mathbf{k}}u_{n\mathbf{k}}(\mathbf{r}). \tag{4.18}$$

where the band Hamiltonian $H(\mathbf{k})$ is defined by

$$H(\mathbf{k}) = e^{-i\mathbf{k}\cdot\mathbf{r}} H e^{i\mathbf{k}\cdot\mathbf{r}}. \tag{4.19}$$

Here, the Hamiltonian H on the right-hand side is understood as a differential operator that acts, according to the usual product rule of differentiation, both on $e^{i\mathbf{k}\cdot\mathbf{r}}$ and on any state on which $H(\mathbf{k})$ is applied. Thus, starting from a single eigenvalue equation for the wave functions $\Psi_{n\mathbf{k}}(\mathbf{r})$, we arrived at a whole family of eigenvalue equations, Eq. (4.18), labeled by a parameter $\mathbf{k} \in \mathrm{BZ}$, where BZ is the Brillouin zone of the crystal. In compensation for the larger number of eigenvalue equations, the Hilbert space for the eigenfunctions $u_{n,\mathbf{k}}(\mathbf{r})$ is restricted by the boundary condition Eq. (4.17). We emphasize that the boundary condition is independent of $\mathbf{k}$ and therefore the Hilbert spaces of $H(\mathbf{k})$ for all $\mathbf{k}$ can be identified.

In the language of section 3.2, the states $|u_{n\mathbf{k}}\rangle$ with $\langle\mathbf{r}|u_{n\mathbf{k}}\rangle = u_{n\mathbf{k}}(\mathbf{r})$ are the instantaneous eigenstates of the band Hamiltonian $H(\mathbf{k})$. Since $\mathbf{k}$ is only well-defined up to a reciprocal lattice vector, one has to identify opposite edges of the Brillouin zone with each other, so that the Brillouin zone has the topology of a d-dimensional torus, where d is the spatial dimension. If $\mathbf{k}$ varies slowly in time (e.g., due to an external electric field $\mathbf{E}$), the wave function explores a finite part of the Brillouin zone and its dynamics are influenced by the Berry curvature $\Omega_n^{\mathrm{k,k}}$ in momentum space, whose components are

$$\begin{aligned}\Omega_{n,ij}^{\mathrm{k,k}}(\mathbf{k}) &\overset{(3.15)}{=} -2\,\mathrm{Im}\left[\frac{\partial\langle u_{n,\mathbf{k}}|}{\partial k_i}\frac{\partial|u_{n,\mathbf{k}}\rangle}{\partial k_j}\right] \\ &\overset{(3.18)}{=} -2\sum_{m\neq n}\mathrm{Im}\left[\frac{\langle u_{n,\mathbf{k}}|\frac{\partial H(\mathbf{k})}{\partial k_i}|u_{m,\mathbf{k}}\rangle\ \langle u_{m,\mathbf{k}}|\frac{\partial H(\mathbf{k})}{\partial k_j}|u_{n,\mathbf{k}}\rangle}{(\epsilon_{n,\mathbf{k}}-\epsilon_{m,\mathbf{k}})^2}\right].\end{aligned} \tag{4.20}$$

It turns out that the group velocity of a wave packet in band n contains a term $v_{n,i}^{\mathrm{anom}} = \frac{e}{\hbar}\Omega_{n,ij}^{\mathrm{k,k}} E_j$ [5, 67], in agreement with the anomalous velocity found by Karplus and Luttinger. We defer a review of the derivation to Section 5.1. In the present section, we focus instead on the physical origin of a non-vanishing Berry curvature $\Omega_n^{\mathrm{k,k}}$ in momentum space.

Requirements for a non-vanishing momentum-space Berry curvature. In order to obtain a complete list of physical mechanisms that can lead to a non-vanishing momentum-space Berry curvature we first derive a set of conditions under which the momentum-space Berry curvature vanishes. Then, we show that relaxing any of the conditions can indeed generate a non-vanishing momentum-space Berry curvature. We consider non-interacting electrons with an effective single-particle (Kohn-Sham) Hamiltonian H. The corresponding band Hamiltonian $H(\mathbf{k})$, Eq. (4.19), transforms under time-reversal $\mathcal{T}$ and spatial inversion $\mathcal{P}$ as

$$H(\mathbf{k}) \overset{\mathcal{T}}{\longmapsto} \sigma_y (H(-\mathbf{k}))^* \sigma_y \qquad \text{and} \qquad H(\mathbf{k}) \overset{\mathcal{P}}{\longmapsto} H(-\mathbf{k}) \tag{4.21}$$

where the star denotes complex conjugation and σ_y is the second Pauli matrix, acting on the spin degree of freedom of the electrons. We start from the simplest case of a non-magnetic system in absence of an external magnetic field and neglect, for the moment, spin-orbit coupling. In this scenario, the Hamiltonian is essentially spinless and therefore $H(\mathbf{k})$ commutes with σ_y. The combined space-time inversion $\mathcal{TP}$ therefore maps $H(\mathbf{k})$ to $(H(\mathbf{k}))^*$ and, if we assume that the system is invariant under $\mathcal{TP}$, then $H(\mathbf{k})$ is real. Thus, if $u_{n,\mathbf{k}}(\mathbf{r})$ solves the eigenvalue equation $(H(\mathbf{k}) - \epsilon_{n,\mathbf{k}})u_{n,\mathbf{k}}(\mathbf{r}) = 0$, then so does the complex conjugate $u^*_{n,\mathbf{k}}(\mathbf{r})$ and we can choose all eigenfunctions $u_{n,\mathbf{k}}(\mathbf{r})$ to be real-valued. It is clear from Eq. (4.20) that the Berry curvature vanishes for real-valued eigenfunctions. In conclusion, we find that $\Omega^{\mathrm{k,k}}_{n,ij} = 0$ for a non-magnetic inversion-symmetric system in absence of a magnetic field when spin-orbit coupling is neglected. By reading this statement in reverse we identify four mechanisms that can lead to a non-vanishing momentum-space Berry curvature.

(i) *Break $\mathcal{T}$ symmetry explicitly with an orbital magnetic field.* A magnetic field $\mathbf{B} = \boldsymbol{\nabla} \times \mathbf{A}$ breaks the discrete translational invariance of the system, thus invalidating the Bloch theorem, Eqs. (4.16)–(4.17). However, if the number of magnetic flux quanta per atomic unit cell is a rational number m/n, then a generalized Bloch theorem holds in a unit cell that is enlarged by a factor of n. This case has been studied by Thouless and collaborators [8] and it turns out that the Brillouin zone that corresponds to the enlarged unit cell has a non-vanishing Berry curvature $\Omega^{\mathrm{k,k}}_n$. In presence of an external electric field $\mathbf{E}$, the Berry curvature leads to an anomalous velocity perpendicular to $\mathbf{E}$ and $\mathbf{B}$, which manifests itself in a non-vanishing Hall conductivity, as expected due to the magnetic field. The case of an irrational number of magnetic flux quanta per atomic unit cell in a perfectly clean system has been studied by Hofstadter [68].

(ii) *Break $SU(2)$ symmetry with a spin-dependent potential.* An effective Zeeman coupling $\mathbf{B}^{\mathrm{Z}} \cdot \boldsymbol{\sigma}$ that breaks the spin-symmetry can be achieved either explicitly by an external magnetic field or spontaneously by exchange interaction in a magnetic system. If the effective Zeeman field $\mathbf{B}^{\mathrm{Z}}(\mathbf{r})$ is collinear, it alone cannot lead to a momentum-space Berry curvature. In this case we can choose a coordinate system such that $\mathbf{B}^{\mathrm{Z}} \cdot \boldsymbol{\sigma} = |\mathbf{B}^{\mathrm{Z}}|\sigma_z$. The band Hamiltonian $H(\mathbf{k})$ is thus diagonal in the eigenbasis of σ_z and, assuming that inversion symmetry $\mathcal{P}$ is still present and neglecting spin-orbit coupling, $H(\mathbf{k})$ is still real. The same arguments as in the spinless case thus lead to a vanishing Berry curvature in momentum space in case of a collinear Zeeman field. In case of a smooth but non-collinear $\mathbf{B}^{\mathrm{Z}}(\mathbf{r})$, a rotation of the local spin-quantization axis into the direction of $\mathbf{B}^{\mathrm{Z}}(\mathbf{r})$ introduces an emergent orbital magnetic field $\mathbf{B}^{\mathrm{em}}$, as reviewed in section 4.1. According to the discussion following Eq. (4.15), the number of emergent magnetic flux quanta per magnetic unit cell in case of a spatially periodic $\mathbf{B}^{\mathrm{Z}}(\mathbf{r})$ is an integer, so that the problem can be mapped to case (i) above. Thus, if we had done the discussion of the Hamiltonian in Eq. (4.1) by applying the Bloch theorem in the magnetic unit cell, then no emergent magnetic field would have appeared and we would instead

have obtained a non-vanishing Berry curvature in momentum space. Physically observable phenomena, such as the topological Hall effect (see section 7.1) [63], can in principle be explained in either picture. The perturbative approach of section 4.1 is preferable over an explicit calculation in the magnetic unit cell if the magnetization varies only smoothly on the atomic length scale so that the magnetic unit cell is too large to allow for an efficient treatment (e.g., in the Skyrmion lattice phase of MnSi, the magnetic unit cell contains on the order of 10^4 atoms [69]).

(iii) *Break $SU(2)$ symmetry by including spin-orbit coupling.* The argument below Eq. (4.21) for a vanishing Berry curvature in momentum space was based on the assumption that $H(\mathbf{k})$ commutes with σ_y. This assumption breaks down if spin-orbit coupling is taken into account. Spin-orbit coupling is described by an extra term

$$H_{\mathrm{so}} = -\frac{i\hbar^2}{4m^2c^2}\,\epsilon_{ijk}\,\sigma_i\frac{\partial V(\mathbf{r})}{\partial r_j}\frac{\partial}{\partial r_k} \tag{4.22}$$

in the Hamiltonian H, where m is the bare electron mass, c the speed of light, ϵ the totally antisymmetric tensor, $\boldsymbol{\sigma}$ the vector of Pauli matrices acting on the spin degree of freedom of the electrons, and V the effective crystal potential within the approximation of non-interacting electrons. In the band Hamiltonian, Eq. (4.19), the corresponding term reads

$$H_{\mathrm{so}}(\mathbf{k}) = \frac{\hbar}{4m^2c^2}\,\epsilon_{ijk}\,\sigma_i\frac{\partial V(\mathbf{r})}{\partial r_j}\left(\hbar k_k - i\hbar\frac{\partial}{\partial r_k}\right). \tag{4.23}$$

Spin-orbit coupling is a relativistic effect and matrix elements $\langle u_{m,\mathbf{k}}|H_{\mathrm{so}}(\mathbf{k})|u_{n,\mathbf{k}}\rangle$ are usually small compared to the non-relativistic part of the Hamiltonian, although it can become larger for heavy atoms. Treating $H_{\mathrm{so}}(\mathbf{k})$ perturbatively, we can write the unperturbed Bloch functions as $|u^{(0)}_{n,\mathbf{k}}\rangle = |u^{(0)}_{\tilde{n},\mathbf{k}}\rangle\,|\sigma\rangle$ where $n \equiv (\tilde{n},\sigma)$ is a combined band index for orbital degrees of freedom $\tilde{n}$ and spin $\sigma \in \{\uparrow,\downarrow\}$, and $|u^{(0)}_{\tilde{n},\mathbf{k}}\rangle$ is the (purely orbital) eigenstate of the spinless unperturbed band Hamiltonian. To first order in perturbation theory, one finds

$$H_{\mathrm{so}}(\mathbf{k}) \approx \sum_{\tilde{n}} \mathbf{g}^{\mathrm{so}}_{\tilde{n}}(\mathbf{k})\cdot\boldsymbol{\sigma}\;|u^{(0)}_{\tilde{n},\mathbf{k}}\rangle\;\langle u^{(0)}_{\tilde{n},\mathbf{k}}| \tag{4.24}$$

where the vectors

$$\mathbf{g}^{\mathrm{so}}_{\tilde{n}}(\mathbf{k}) = \frac{\hbar}{4m^2c^2}\;\langle u^{(0)}_{\tilde{n},\mathbf{k}}|(\boldsymbol{\nabla}V)\times(-i\hbar\boldsymbol{\nabla}+\hbar\mathbf{k})|u^{(0)}_{\tilde{n},\mathbf{k}}\rangle \tag{4.25}$$

can be regarded as a Zeeman field in reciprocal space. The calculation of the Berry curvature in momentum space is analogous to the derivation of the position-space Berry curvature, Eq. (4.15), and yields the result

$$\Omega^{\mathrm{k,k}}_{\tilde{n},\sigma}(\mathbf{k}) = \pm\frac{1}{2}\hat{\mathbf{g}}_{\tilde{n}}\cdot\left(\frac{\partial\hat{\mathbf{g}}_{\tilde{n}}}{\partial k_i}\times\frac{\partial\hat{\mathbf{g}}_{\tilde{n}}}{\partial k_j}\right) \tag{4.26}$$

where $\hat{\mathbf{g}}_{\tilde{n}}(\mathbf{k}) = \mathbf{g}_{\tilde{n}}(\mathbf{k})/|\mathbf{g}_{\tilde{n}}(\mathbf{k})|$ and the plus (minus) sign is for $\boldsymbol{\sigma}$ parallel (anti-parallel) to $\mathbf{g}_{\tilde{n}}$, respectively. The right-hand side of Eq. (4.26) is the winding number density of the vector field $\mathbf{g}_{\tilde{n}}(\mathbf{k})$. Its integral over two-dimensional cuts of the Brillouin zone is quantized to integer multiples of 2π [2]. In two-dimensional insulators, this property translates to a quantized transverse conductivity called quantum anomalous Hall effect [48, 49]. The preparation and study of materials with strong spin-orbit coupling that are insulating in the bulk is of central interest in the field of topological insulators.

(iv) *Break $\mathcal{P}$ symmetry.* In order to break space-inversion symmetry, the atomic unit cell has to contain at least two atoms which are either of a different element or located at positions that are inequivalent under space-inversion. This leads to an iso-spin degree of freedom $\boldsymbol{\tau}$, and the band Hamiltonian $H(\mathbf{k})$ will, in general, couple $\mathbf{k}$ and $\boldsymbol{\tau}$, in a similar way in which spin-orbit coupling couples $\mathbf{k}$ and spin $\boldsymbol{\sigma}$, see Eq. (4.24). In general, this iso-spin-orbit coupling leads to a non-vanishing Berry curvature in momentum space by a similar argument as discussed for scenario (iii) above. Thus, a material without inversion symmetry can have a non-zero Berry curvature in momentum space even in absence of spin-orbit coupling.

4.3. Berry phases in mixed position/momentum space

Chiral magnets like MnSi exhibit an inhomogeneous magnetization texture, which leads to a Berry curvature in position space (section 4.1). The chiral magnetization texture is realized because the magnetization knows about the chirality of the underlying atomic crystal structure due to spin-orbit coupling. At the same time, both chirality (i.e., absence of inversion symmetry) and spin-orbit coupling are also sources of a Berry curvature in momentum space, see Section 4.2. Due to the presence of both position-space and momentum-space Berry phases, chiral magnets are ideal systems to study in a more general setting the effects of Berry phases in phase space. The Berry phase is only gauge-invariant along a loop in parameter space, and the combination of both position and momentum dependence of the Hamiltonian allows for new types of loops that lie in planes spanned by one position and one momentum direction. This can be seen in the Berry curvature Ω_n of a given band n, whose components form an anti-symmetric 7×7 tensor,

$$\Omega_{n,ij} = -2\,\mathrm{Im}\left[\frac{\partial\langle n,t,\mathbf{r},\mathbf{k}|}{\partial\xi_i}\frac{\partial|n,t,\mathbf{r},\mathbf{k}\rangle}{\partial\xi_j}\right] = \begin{pmatrix} 0 & \Omega_n^{\mathrm{t,r}} & \Omega_n^{\mathrm{t,k}} \\ \Omega_n^{\mathrm{r,t}} & \Omega_n^{\mathrm{r,r}} & \Omega_n^{\mathrm{r,k}} \\ \Omega_n^{\mathrm{k,t}} & \Omega_n^{\mathrm{k,r}} & \Omega_n^{\mathrm{k,k}} \end{pmatrix}_{ij} . \tag{4.27}$$

Here, $\xi \equiv (t, \mathbf{r}, \mathbf{k})$ is a coordinate in combined time, position, and momentum space, and $|n, t, \mathbf{r}, \mathbf{k}\rangle$ is the n^{th} eigenstate of a band Hamiltonian $H(t, \mathbf{r}, \mathbf{k})$ that depends on time t and crystal momentum $\hbar\mathbf{k}$, as well as on an average position $\mathbf{r}$. The precise definition of $H(t, \mathbf{r}, \mathbf{k})$ will be the subject of Sections 5.1 and 6.1. For the discussion at hand, it is sufficient to require that $H(t, \mathbf{r}, \mathbf{k})$ is a smooth function of $\mathbf{r}$ on the atomic length scale and a smooth function of t on the time scale of the inverse Fermi energy. The space-time

part of the tensor on the right-hand side of Eq. (4.27) was discussed in Section 4.1, see Eqs. (4.14)–(4.15). The 3×3 block $\Omega_n^{\mathrm{k,k}}$ is the Berry curvature in momentum space, see Eq. (4.26). The new components $\Omega^{\mathrm{t,k}} = -(\Omega^{\mathrm{k,t}})^T$ and $\Omega^{\mathrm{r,k}} = -(\Omega^{\mathrm{k,r}})^T$ only appear in systems with Berry phases in both space-time and momentum space. In the following, we discuss the relative magnitudes of the components of the Berry curvature by means of two model systems.

Minimal model for phase-space Berry phases with a single orbital band. In the simplest model of a chiral magnet, the orbital bands are energetically well-separated and only the spin-degree of freedom $\boldsymbol{\sigma}$ leads to Berry phases. In Ref. [65], we discussed a toy model for chiral magnets with a single orbital band with energy dispersion $\epsilon_{\mathbf{k}}$. The Hamiltonian is given by

$$H(\mathbf{r}, \mathbf{k}) = \epsilon_{\mathbf{k}} + [\mathbf{B}^{\mathrm{ex}}(\mathbf{r}) + \mathbf{g}^{\mathrm{so}}(\mathbf{k})] \cdot \boldsymbol{\sigma} = \epsilon_{\mathbf{k}} + \mathbf{n}(\xi) \cdot \boldsymbol{\sigma} \tag{4.28}$$

where $\mathbf{B}^{\mathrm{ex}}$ is the exchange field as in section 4.1, $\mathbf{g}^{\mathrm{so}}$ is defined in Eq. (4.25) and is a consequence of spin-orbit coupling, and $\mathbf{n} := \mathbf{B}^{\mathrm{ex}} + \mathbf{g}^{\mathrm{so}}$. For weak spin orbit coupling, $|\mathbf{B}^{\mathrm{ex}}| > |\mathbf{g}^{\mathrm{so}}|$, so that $\mathbf{n}(\xi)$ never vanishes and the energy levels are never degenerate. The Berry curvature is given by the winding number density of $\mathbf{n}$,

$$\Omega_{\sigma,ij} = q_\sigma^{\mathrm{em}}\, \hat{\mathbf{n}} \cdot (\partial_i \hat{\mathbf{n}} \times \partial_j \hat{\mathbf{n}}) = \frac{q_\sigma^{\mathrm{em}}}{|\mathbf{n}|^3}\, \mathbf{n} \cdot (\partial_i \mathbf{n} \times \partial_j \mathbf{n}) \tag{4.29}$$

where i and j run over time, position, and momentum, $\hat{\mathbf{n}} := \mathbf{n}/|\mathbf{n}|$, and, as in section 4.1, $\sigma = \downarrow$ and $\sigma = \uparrow$ denote majority and minority spin configuration with emergent charges $q_\downarrow^{\mathrm{em}} = \frac{1}{2}$ and $q_\uparrow^{\mathrm{em}} = -\frac{1}{2}$, respectively. For simplicity, we assume that the magnetic texture $\mathbf{B}^{\mathrm{ex}}(t, \mathbf{r}) = \mathbf{B}_0^{\mathrm{ex}}(\mathbf{r} - \mathbf{v}_M t)$ moves as a rigid structure with some velocity $\mathbf{v}_M$. Thus, $\Omega_{n,i}^{\mathrm{r,t}} = \Omega_{n,ij}^{\mathrm{r,r}} v_{M,j}$ and $\Omega_{n,i}^{\mathrm{k,t}} = \Omega_{n,ij}^{\mathrm{k,r}} v_{M,j}$, and we can focus on the 6×6 tensor

$$\Omega_{\sigma,ij}^{\mathrm{x,x}} = \begin{pmatrix} \Omega_\sigma^{\mathrm{r,r}} & \Omega_\sigma^{\mathrm{r,k}} \\ \Omega_\sigma^{\mathrm{k,r}} & \Omega_\sigma^{\mathrm{k,k}} \end{pmatrix}_{ij}. \tag{4.30}$$

where the label "x" denotes phase-space, i.e., combined position and momentum space. To estimate the relative strengths of the components of $\Omega_\sigma^{\mathrm{x,x}}$, we consider the limit where spin-orbit coupling is weak compared to the ferromagnetic exchange interaction. More precisely, we assume that the dimensionless parameter $\lambda_{\mathrm{so}} \sim |\mathbf{g}^{\mathrm{so}}|/|\mathbf{B}^{\mathrm{ex}}| \ll 1$ is small. In chiral magnets, the length scale ξ_{mod} of modulations in position space is controlled by a competition between ferromagnetic exchange interaction and Dzyaloshinskii-Moriya interaction. The latter is a consequence of spin-orbit coupling and one finds $\xi_{\mathrm{mod}} \sim a/\lambda_{\mathrm{so}}$ where a is the atomic lattice constant [9]. Thus, spatial derivatives $\partial/\partial r_i$ in Eq. (4.29)

are generically of order $\lambda_{\rm so}/a$. Expanding Eq. (4.29) to leading order in $\lambda_{\rm so}$, we find

$$\Omega^{\rm r,r}_{\sigma,ij} \approx \frac{q^{\rm em}_\sigma}{|\mathbf{B}^{\rm ex}|^3}\,\mathbf{B}^{\rm ex}\cdot\left(\frac{\partial \mathbf{B}^{\rm ex}}{\partial r_i}\times\frac{\partial \mathbf{B}^{\rm ex}}{\partial r_j}\right) \sim \lambda^2_{\rm so} \tag{4.31}$$

$$\Omega^{\rm k,k}_{\sigma,ij} \approx \frac{q^{\rm em}_\sigma}{|\mathbf{B}^{\rm ex}|^3}\,\mathbf{B}^{\rm ex}\cdot\left(\frac{\partial \mathbf{g}^{\rm so}}{\partial k_i}\times\frac{\partial \mathbf{g}^{\rm so}}{\partial k_j}\right) \sim \lambda^2_{\rm so} \tag{4.32}$$

$$\Omega^{\rm r,k}_{\sigma,ij} = -\Omega^{\rm k,r}_{\sigma,ji} \approx \frac{q^{\rm em}_\sigma}{|\mathbf{B}^{\rm ex}|^3}\,\mathbf{B}^{\rm ex}\cdot\left(\frac{\partial \mathbf{B}^{\rm ex}}{\partial r_i}\times\frac{\partial \mathbf{g}^{\rm so}}{\partial k_j}\right) \sim \lambda^2_{\rm so}. \tag{4.33}$$

Minimal model for phase-space Berry phases with orbital degrees of freedom. If two orbital bands are energetically close to each other, then the Berry curvature is no longer perturbative in the spin-orbit coupling strength $\lambda_{\rm so}$. We consider a system with two orbital bands, whose dispersion relations in absence of exchange and spin-orbit coupling are given by $\epsilon_{+,\mathbf{k}}$ and $\epsilon_{-,\mathbf{k}}$, respectively (Figure 4.1a). For simplicity, we assume that $\epsilon_{+,\mathbf{k}}$ and $\epsilon_{-,\mathbf{k}}$ are separated by a direct gap Δ. Since a simultaneous shift of the energies of all bands does not affect the Berry curvature, we may further simplify that $\epsilon_{+,\mathbf{k}} = -\epsilon_{-,\mathbf{k}} > 0$. Each orbital band comes in two spin configurations. The Hamiltonian is given by

$$H(\mathbf{r},\mathbf{k}) = H_0(\mathbf{r},\mathbf{k}) + H_{\rm so}(\mathbf{k}) \quad \text{with} \quad H_0(\mathbf{r},\mathbf{k}) = \tau_z\,\epsilon_{+,\mathbf{k}} + \mathbf{B}^{\rm ex}(\mathbf{r})\cdot\boldsymbol{\sigma} \tag{4.34}$$

where the spin-orbit coupling part $H_{\rm so}(\mathbf{k})$ is defined in Eq. (4.23), $\mathbf{B}^{\rm ex}(\mathbf{r})$ is a smoothly position-dependent exchange field as in Eq. (4.28), and the operator τ_z acts only on the orbital degree of freedom and has eigenvalue $+1$ for the upper and -1 for the lower orbital band. We denote the eigenstates of $H_0(\mathbf{r},\mathbf{k})$ by $|u^{(0)}_{\tau\sigma}(\mathbf{r},\mathbf{k})\rangle$, where $\tau = \text{“}+\text{”}$ ($\tau = \text{“}-\text{”}$) labels the upper (lower) orbial band and $\sigma = \uparrow$ ($\sigma = \downarrow$) labels the spin-configuration parallel (anti-parallel) to $\mathbf{B}^{\rm ex}(\mathbf{r})$, see Figure 4.1b and 4.1c. We restrict the discussion again to the limit where spin-orbit coupling is weak compared to exchange interaction, i.e., all matrix elements of $H_{\rm so}(\mathbf{k})$ are much smaller than $|\mathbf{B}^{\rm ex}|$.

If $\Delta \gg 2|\mathbf{B}^{\rm ex}|$, the orbital bands are energetically well-separated (Figure 4.1b) and, to leading order in the spin-orbit coupling strength, the Hamiltonian, Eq. (4.34), decouples into two copies of the Hamiltonian in Eq. (4.28).

We now focus on the case $\Delta < 2|\mathbf{B}^{\rm ex}|$ (Figure 4.1c). The large exchange field separates the two bands $|u^{(0)}_{-,\downarrow}\rangle$ and $|u^{(0)}_{+,\uparrow}\rangle$ from the rest of the spectrum and the Berry curvature in these Bands is again described by relations similar to Eqs. (4.31)–(4.33). The remaining two bands $|u^{(0)}_{-,\uparrow}\rangle$ and $|u^{(0)}_{+,\downarrow}\rangle$, however, show a qualitatively new behavior. If $H_{\rm so}(\mathbf{k})$ is neglected, there exist points in momentum space where the two bands are degenerate (Figure 4.1c). Spin-orbit coupling, $H_{\rm so}(\mathbf{k})$, leads to a hybridization of $|u^{(0)}_{-,\uparrow}\rangle$ and $|u^{(0)}_{+,\downarrow}\rangle$. Therefore, the energies of the eigenstates $|u_n(\mathbf{r},\mathbf{k})\rangle$ of the full Hamiltonian with spin-orbit coupling exhibit an avoided crossing[1] (Figure 4.1d). In order to estimate the

[1] For a generic Hamiltonian on a finite-dimensional Hilbert space in the absence of symmetries, it is sufficient to fine-tune three parameters in order to realize an accidental degeneracy. Therefore,

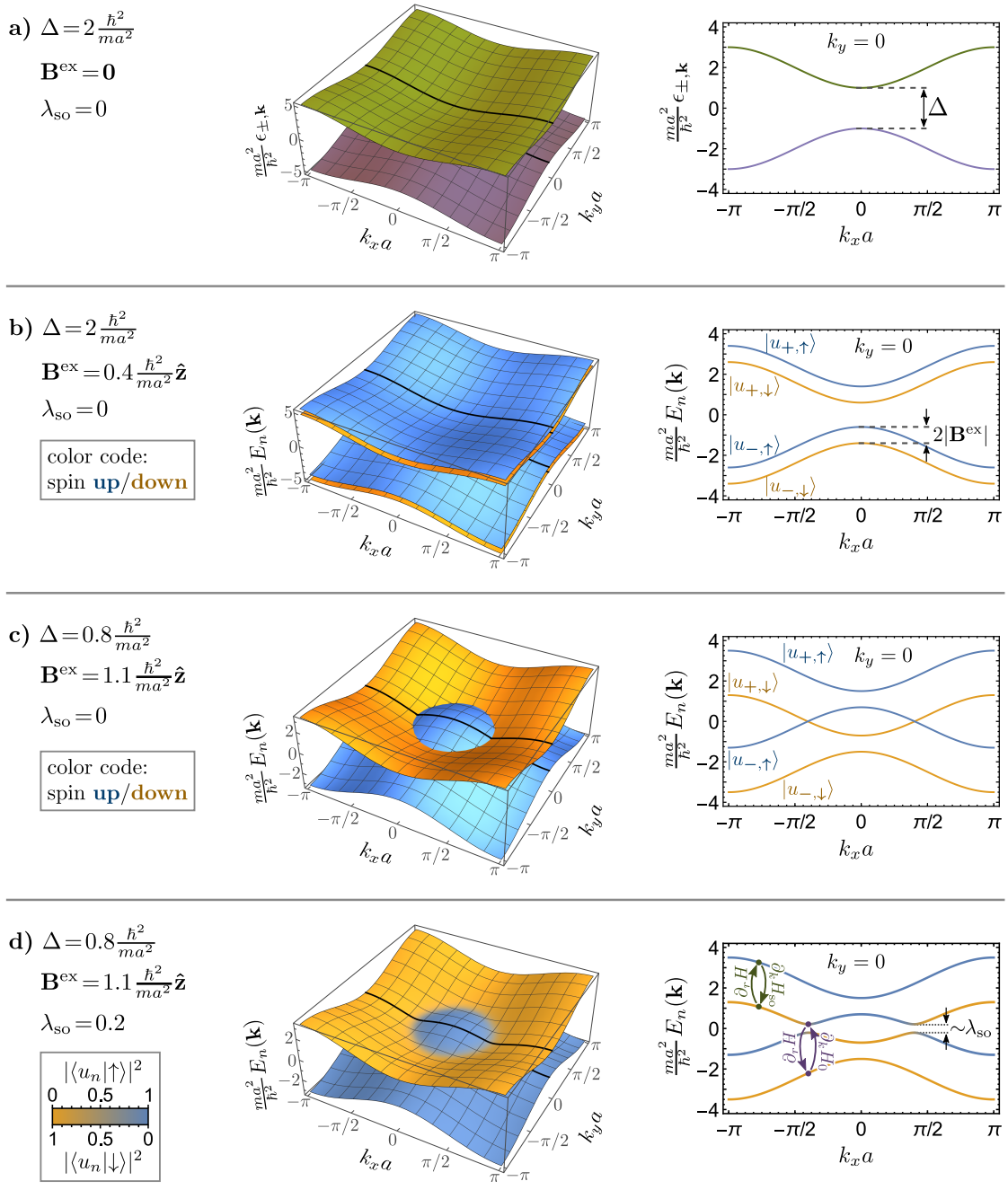

Figure 4.1.: Band structure for the Hamiltonian in Eqs. (4.34), (4.37), and (4.38) with constant $\mathbf{B}^{\mathrm{ex}}$. The right plots show a cut through the Brillouin zone at $k_y = 0$ (black lines in 3d plots). In c) and d), the 3d plots show only the central two bands. a) Spinless limit. b) Case $\Delta \gg 2|\mathbf{B}^{\mathrm{ex}}|$. c) If $\Delta < 2|\mathbf{B}^{\mathrm{ex}}|$, the central two bands cross in absence of spin-orbit coupling. d) Weak spin-orbit coupling $\lambda_{\mathrm{so}} \ll 1$ lifts the degeneracy; arrows indicate virtual transitions that contribute to leading order in λ_{so} to $\Omega_n^{\mathrm{r,k}}$, see main text.

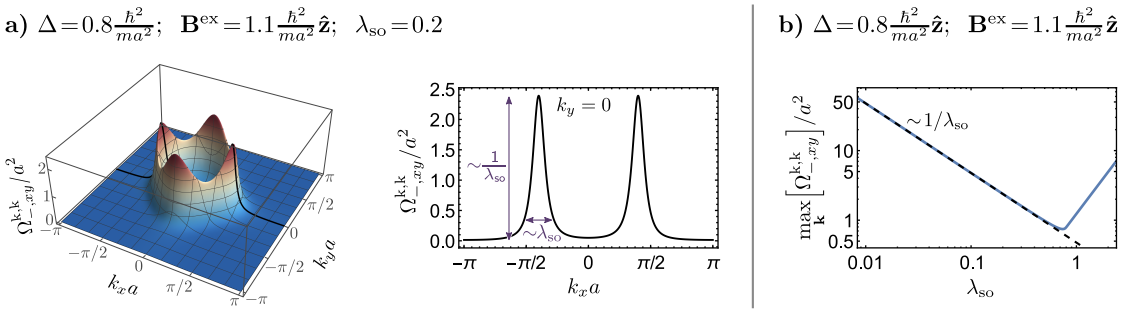

Figure 4.2.: Momentum-space Berry curvature $\Omega^{\mathrm{k,k}}_{-,xy}$ for the lower one of the two almost-crossing bands in Figure 4.1d. The Hamiltonian is given in Eqs. (4.34), (4.37), and (4.38) with constant $\mathbf{B}^{\mathrm{ex}}$. The other one of the two almost-crossing bands has Berry curvature $\Omega^{\mathrm{k,k}}_{+,xy} = -\Omega^{\mathrm{k,k}}_{-,xy}$. a) $\Omega^{\mathrm{k,k}}_{-,xy}$ for a fixed spin-orbit coupling strength $\lambda_{\mathrm{so}} = 0.2$. The right plot shows a cut through the Brillouin zone at $k_y = 0$ (black line in the 3d plot). In contrast to Figure 4.1d, the colors in the 3d plot do not carry any additional information. b) Maximum of $\Omega^{\mathrm{k,k}}_{-,xy}$ over the whole Brillouin zone as a function of λ_{so}. For small λ_{so}, $\max_{\mathbf{k}}[\Omega^{\mathrm{k,k}}_{-,xy}]$ is proportional to $1/\lambda_{\mathrm{so}}$ (straight dashed line), see Eq. (4.42).

magnitude of the phase-space Berry curvature $\Omega^{\mathrm{x,x}}_n$ in the two almost-crossing bands, we write $\Omega^{\mathrm{x,x}}_n$ in the from of Eq. (3.18),

$$\Omega^{\mathrm{rk,rk}}_{n,ij} \equiv \begin{pmatrix} \Omega^{\mathrm{r,r}}_n & \Omega^{\mathrm{r,k}}_n \\ \Omega^{\mathrm{k,r}}_n & \Omega^{\mathrm{k,k}}_n \end{pmatrix}_{ij} = -2 \sum_{m \neq n} \mathrm{Im}\left[\frac{\langle u_n | (\partial_i H) | u_m \rangle \, \langle u_m | (\partial_j H) | u_n \rangle}{(E_m - E_n)^2} \right] \tag{4.35}$$

where i and j run over the coordinates of position $\mathbf{r}$ and momentum $\mathbf{k}$, $E_n(\mathbf{r}, \mathbf{k})$ is the dispersion relation of the full Hamiltonian including exchange and spin-orbit coupling, and we suppressed the $(\mathbf{r}, \mathbf{k})$-dependency of $|u_n\rangle$, H, and E_n. The position-space Berry curvature $\Omega^{\mathrm{r,r}}_n$ contains two spatial derivatives. For a chiral magnet with small spin-orbit coupling parameter $\lambda_{\mathrm{so}} \ll 1$, we therefore find with the same arguments that lead to Eq. (4.31),

$$\Omega^{\mathrm{r,r}}_n \sim \lambda^2_{\mathrm{so}} \tag{4.36}$$

The momentum-space Berry curvature $\Omega^{\mathrm{k,k}}_n$ varies strongly over the Brillouin zone. Figure 4.2a shows $\Omega^{\mathrm{k,k}}_n(\mathbf{k})$ for a toy model defined on a two-dimensional square lattice.

despite spin-orbit coupling, a two-dimensional (three-dimensional) model of the form of Eq. (4.34) generally remains degenerate on lines (three-dimensional submanifolds) in the four-dimensional (six-dimensional) phase-space $\{(\mathbf{r}, \mathbf{k})\}$. At the remaining degeneracy points, Berry phases are not a good concept because the assumption of adiabatic time evolution breaks down. If the degeneracy points are excluded from the parameter space, they can be regarded as δ-like sources and sinks of Berry flux (cf., section 3.4). For the discussion at hand, we assume that the Fermi surface contains no degeneracy points, i.e., the Fermi energy lies within one of the bands in Figure 4.1d).

The Hamiltonian is given by Eq. (4.34) with $\mathbf{B}^{\mathrm{ex}}$ in z-direction and

$$\epsilon_{+,\mathbf{k}} = \frac{\hbar^2}{ma^2}(2 - \cos(k_x a) - \cos(k_y a)) + \frac{\Delta}{2}; \tag{4.37}$$

$$H_{\mathrm{so}}(\mathbf{k}) = \lambda_{\mathrm{so}} \left|\mathbf{B}^{\mathrm{ex}}\right| \tau_x \left(\sigma_x \sin(k_x a) + \sigma_y \sin(k_y a)\right) \tag{4.38}$$

where m is the effective electron mass, a the lattice constant and the operator τ_x is defined by $\tau_x |u^{(0)}_{\pm,\sigma}\rangle = |u^{(0)}_{\mp,\sigma}\rangle$. Projecting this model onto the subspace spanned by $|u^{(0)}_{-,\uparrow}\rangle$ and $|u^{(0)}_{+,\downarrow}\rangle$, one finds the effective 2×2 Hamiltonian

$$H^{\mathrm{eff}}(\mathbf{k}) = \mathbf{g}^{\mathrm{eff}}(\mathbf{k}) \cdot \boldsymbol{\gamma} \tag{4.39}$$

where $\boldsymbol{\gamma}$ is a vector of Pauli matrices acting in the subspace spanned by $|u^{(0)}_{-,\uparrow}\rangle$ and $|u^{(0)}_{+,\downarrow}\rangle$, and

$$\mathbf{g}^{\mathrm{eff}}(\mathbf{k}) = \begin{pmatrix} \lambda_{\mathrm{so}} \left|\mathbf{B}^{\mathrm{ex}}\right| \sin(k_x a) \\ \lambda_{\mathrm{so}} \left|\mathbf{B}^{\mathrm{ex}}\right| \sin(k_y a) \\ \left|\mathbf{B}^{\mathrm{ex}}\right| - \epsilon_{+,\mathbf{k}} \end{pmatrix}. \tag{4.40}$$

The Berry curvature for this specific model is the winding number density of $\mathbf{g}^{\mathrm{eff}}(\mathbf{k})$,

$$\Omega^{\mathrm{k,k}}_{\pm,xy}(\mathbf{k}) = \mp \frac{\mathbf{g}^{\mathrm{eff}}(\mathbf{k}) \cdot \left[(\partial_{k_x} \mathbf{g}^{\mathrm{eff}}(\mathbf{k})) \times (\partial_{k_y} \mathbf{g}^{\mathrm{eff}}(\mathbf{k}))\right]}{2|\mathbf{g}^{\mathrm{eff}}(\mathbf{k})|^3} \tag{4.41}$$

where the upper (lower) sign corresponds to the upper (lower) band, respectively. The Berry curvature $\Omega^{\mathrm{k,k}}_{\pm,xy}(\mathbf{k})$ has a pronounced peak in the vicinity of the avoided crossing, where the denominator on the right-hand side of Eq. (4.41) becomes small (Figure 4.2a). By writing out the right-hand side of Eq. (4.41) explicitly, one finds (see also Figure 4.2b)

$$\Omega^{\mathrm{k,k}}_{\pm} \sim \begin{cases} 1/\lambda_{\mathrm{so}} & \text{close to the avoided crossing} \\ \lambda^2_{\mathrm{so}} & \text{away from the avoided crossing.} \end{cases} \tag{4.42}$$

These estimates are not limited to the specific form of $H_{\mathrm{so}}(\mathbf{k})$, Eq. (4.38), as can be seen by the following arguments. Close to the avoided crossing, the denominator in Eq. (4.35) is of order λ^2_{so} since the energy splitting is a consequence of spin-orbit coupling. In the numerator, off-diagonal matrix elements of $\partial_k H_0$ become large because the states $|u_n\rangle$ interpolate between $|u^{(0)}_{+\downarrow}\rangle$ and $|u^{(0)}_{-\uparrow}\rangle$ as $\mathbf{k}$ scans through the avoided crossing. However, for the momentum-momentum component of the Berry curvature, at least one of the two matrix-elements in Eq. (4.35) must come from $\partial_k H_{\mathrm{so}} \sim \lambda_{\mathrm{so}}$ since the term where both matrix elements come from $\partial_k H_0$ does not contribute to the Berry curvature (it corresponds to a reduction of the parameter space to the one-dimensional space of $\epsilon_{\pm,\mathbf{k}}$, and there is no curvature in one dimension). This implies $\Omega^{\mathrm{k,k}}_{\pm} \sim 1/\lambda_{\mathrm{so}}$ close to the avoided crossing. Far away from the avoided crossing, the denominator in Eq. (4.35) is independent of λ_{so} and off-diagonal matrix elements of $\partial_k H_0$ are suppressed by a factor of λ_{so} each because the states $|u_n\rangle$ and $|u_m\rangle$ are well-approximated by the unperturbed

states $|u^{(0)}_{\pm,\sigma}\rangle$. This confirms that also the second case covered in Eq. (4.42) applies beyond the specific model of Eqs. (4.37)–(4.38).

We emphasize that $\Omega^{\mathrm{k,k}}_{\pm}$ is non-perturbative in λ_{so} in the vicinity of an avoided crossing (Eq. (4.42); see also [70]). This is the case even though our model, Eq. (4.34), relies on spin-orbit coupling to generate a non-vanishing $\Omega^{\mathrm{k,k}}_{\pm}$ in the first place. Note that, while $\Omega^{\mathrm{k,k}}_{\pm} \sim 1/\lambda_{\mathrm{so}}$ close to an avoided crossing, the width of the region around the avoided crossing where this estimate applies is of order λ_{so} (Figure 4.2a). This is consistent with the fact that the total Berry flux of a two-dimensional cut through the Brillouin zone is quantized.

Finally, we turn to the Berry curvature $\Omega^{\mathrm{r,k}}_n$ in mixed position/momentum-space. The expression for $\Omega^{\mathrm{r,k}}_n$ in Eq. (4.35) contains one spatial derivative $\partial_r H \sim \lambda_{\mathrm{so}}$. The denominator is always of order $|\mathbf{B}^{\mathrm{ex}}|^2$ since $\partial_r H = \partial_r \mathbf{B}^{\mathrm{ex}} \cdot \boldsymbol{\sigma}$ couples only states within the same orbital band. In Eq. (4.35), $\Omega^{\mathrm{r,k}}_n$ is expressed in terms of virtual transitions between the bands $n \to m \to n$, which are mediated by the operators $\partial_r H$ and $\partial_k H$, respectively. Exactly which kinds of virtual transitions are allowed depends on whether $\mathbf{k}$ is close to the avoided crossing (see purple arrows in Figure 4.1d), or far away from it (green arrows in Figure 4.1d). Away from the avoided crossing, the states $|u_n\rangle$ are well-approximated by the unperturbed states $|u^{(0)}_{\pm,\sigma}\rangle$, and thus $\partial_r H$ couples only states with opposite spin. The only contribution to the matrix elements of $\partial_k H$ between states with opposite spin comes from $\partial_k H_{\mathrm{so}}$, since $\partial_k H_0$ is spin-independent (green arrows in Figure 4.1d). This leads to a suppression of $\Omega^{\mathrm{r,k}}_n$ away from the avoided crossing by another factor of λ_{so}. Close to the avoided crossing, the states $|u^{(0)}_{+,\downarrow}\rangle$ and $|u^{(0)}_{-,\uparrow}\rangle$ hybridize and therefore $\partial_r H$ also mediates transitions between states whose spin components have a non-vanishing overlap (purple arrows in Figure 4.1d). The matrix element of $\partial_k H$ is in this case dominated by $\partial_k H_0$, which is independent of λ_{so}. In conclusion, we find

$$\Omega^{\mathrm{r,k}}_{\pm} \sim \begin{cases} \lambda_{\mathrm{so}} & \text{close to the avoided crossing} \\ \lambda^2_{\mathrm{so}} & \text{away from the avoided crossing.} \end{cases} \tag{4.43}$$

4.4. Relevance of phase-space Berry phases in chiral magnets

Due to the combination of both a smooth magnetic texture and weak spin-orbit coupling the physics of chiral magnets is influenced by Berry phases in phase space. It is well-established that the Berry curvature in position space, $\Omega^{\mathrm{r,r}}_n$, plays an important role, allowing for a natural explanation of the so-called topological Hall effect [63] (see section 7.1). Position-space Berry phases affect also the dynamics of the magnetization [62], leading, e.g., to a gyro-coupling $\mathbf{G} \times \dot{\mathbf{R}} = \mathbf{F}$ between the velocity $\dot{\mathbf{R}}$ of Skyrmions and an external force $\mathbf{F}$ [11] (see section 9.1). Here, the gyro-coupling vector $\mathbf{G}$ is proportional to the emergent magnetic field $\mathbf{B}^{\mathrm{em}}$.

Measurements on MnSi [30] show a large signal of the anomalous Hall resistivity (see section 7.1), which is an indication that the electron dynamics is also strongly influenced by the momentum-space Berry curvature $\Omega^{\mathrm{k,k}}_n$. This is in agreement with our qualitative

estimates in section 4.3, which showed that all components $\Omega_n^{\mathrm{r,r}}$, $\Omega_n^{\mathrm{k,k}}$, and $\Omega_n^{\mathrm{r,k}}$ of the phase-space Berry curvature are quadratic in the small spin-orbit coupling strength λ_{so} as long as $\mathbf{k}$ lies far away from any avoided band crossing. In this regime, our results for the two-band model, Eqs. (4.36), (4.42), and (4.43), agree with the results we obtained in the simpler one-band model, Eqs. (4.31)–(4.33). While the position-space Berry curvature $\Omega_n^{\mathrm{r,r}} \sim \lambda_{\mathrm{so}}^2$ remains small regardless of details of the band structure (Eq. (4.36)), the Berry curvatures in momentum-space and in mixed position/momentum-space, $\Omega_n^{\mathrm{k,k}}$ and $\Omega_n^{\mathrm{r,k}}$, are enhanced if spin-orbit coupling leads to an avoided crossing of otherwise degenerate bands (Eqs. (4.42) and (4.43)). These kinds of avoided crossings appear to be a typical feature of the band structure of chiral magnets [71]. Therefore, one should expect that $\Omega_n^{\mathrm{k,k}}$ and $\Omega_n^{\mathrm{r,k}}$ play an important role in the physics of chiral magnets. Yet, in contrast to the position-space Berry curvature $\Omega_n^{\mathrm{r,r}}$, the roles of $\Omega_n^{\mathrm{k,k}}$ and especially $\Omega_n^{\mathrm{r,k}}$ in chiral magnets have not yet enjoyed the same attention in the literature.

Part I.

Dzyaloshinskii-Moriya interaction and the electric charge of skyrmions

5. Semiclassical approach to energy and charge density in chiral magnets

Chiral magnets exhibit phases with a smooth magnetization texture due to Dzyaloshinskii-Moriya (DM) interactions (see Section 2.2). As discussed in section 4.3, the combination of a smooth magnetization texture and spin-orbit (SO) interaction leads a Berry curvature $\Omega_n^{\mathrm{x,x}}$ in phase space $x \equiv (\mathbf{r}, \mathbf{k})$ that is non-vanishing for all three combinations of position/momentum directions, i.e. $\Omega_n^{\mathrm{r,r}}$, $\Omega_n^{\mathrm{k,k}}$, and $\Omega_n^{\mathrm{r,k}}$ are all non-zero. It is well-established that the diagonal blocks, $\Omega_n^{\mathrm{r,r}}$ and $\Omega_n^{\mathrm{k,k}}$, strongly influence the physics of chiral magnets, leading to the topological [22] and the anomalous Hall effect [70, 72], respectively (see Section 7.1). On the other hand, physical consequences of the off-diagonal block $\Omega_n^{\mathrm{r,k}}$ of the Berry curvature tensor in chiral magnets have received less attention. For antiferromagnets with a smooth spin texture, it has been argued by Cheng and Niu [73] that $\Omega_n^{\mathrm{r,k}}$ crucially influences the dynamics electrons. In this and the following chapter we will argue that Berry phases in mixed position/momentum space determine the strength of DM interactions in chiral magnets and lead to an electric charge of skyrmions. We thereby identify phase-space Berry phases as a mechanism that generates magnetic textures, and we establish ties between Skyrmions in chiral magnets and skyrmions in quantum Hall systems at filling factor $\nu \approx 1$, which carry a quantized electric charge [13, 14]. We have published the results of this and the following chapter in Ref. [65].

We use two complementary approaches to treat the effects of a smooth magnetic texture on the equilibrium electronic properties of chiral magnets. In the present chapter, we employ a semiclassical method, which has the advantage that its intermediate results can be interpreted classically as the equations of motion for the center-of-mass coordinates of a wave packet. The semiclassical approach is, however, only valid to lowest order in gradients of the magnetization texture. In chapter 6, we will present an alternative approach based on a gradient expansion of the Green's function, which is consistent with the semiclassical approach and extends the range of validity to higher orders in the gradients. The higher order terms are crucial in insulating systems, where the leading contribution to the electric charge of skyrmions is of second order.

This chapter is organized as follows. We review the semiclassical theory of wave-packet dynamics in the presence of Berry phases in Sections 5.1 and 5.2 and show how these results affect the energy and charge density in chiral magnets in Section 5.3. We continue with analytical results for model systems (section 5.4) and conclude with numerical results for the strength of DM interactions and the electric charge of skyrmions in MnSi (Section 5.5).

5.1. Semiclassical dynamics of wave packets

As discussed in section 4.3, the combination of smooth magnetic textures and SO coupling in chiral magnets leads to a Berry curvature $\Omega_n^{\mathrm{x,x}}$ in phase space $x \equiv (\mathbf{r}, \mathbf{k})$. In this section, we summarize the results from two articles, by Sundaram and Niu [5] and by Xiao, Shi, and Niu [7], in which the influence of $\Omega_n^{\mathrm{x,x}}$ on the semiclassical dynamics of electrons was derived. We illustrate the derivation at the example of a magnet with a smooth magnetization texture in external electromagnetic fields, treating the electromagnetic potentials on an equal footing with the smooth magnetization. This has the advantage that all terms in the resulting semiclassical equations of motion will directly be independent of the electromagnetic gauge.

The semiclassical equations of motion of an electron in d-dimensional space are a generalization of the classical equations of motion. In absence of a magnetic field, the latter are given by

$$\frac{\mathrm{d}r_i}{\mathrm{d}t} = \frac{\partial \mathcal{H}(t, \mathbf{r}, \mathbf{p})}{\partial p_i} \qquad \text{and} \qquad \frac{\mathrm{d}p_i}{\mathrm{d}t} = -\frac{\partial \mathcal{H}(t, \mathbf{r}, \mathbf{p})}{\partial r_i} \tag{5.1}$$

where $\mathbf{r}$, $\mathbf{p}$, and t are position, momentum, and time, respectively, and $\mathcal{H}(t, \mathbf{r}, \mathbf{p}) = \mathbf{p}^2/(2m) - e\phi(t, \mathbf{r})$ is the Hamilton function of an electron with mass m and charge $-e$ in an electric potential $\phi(t, \mathbf{r})$. A more compact way of writing Eq. (5.1) is

$$\frac{\mathrm{d}x_i}{\mathrm{d}t} = J_{ij} \frac{\partial \mathcal{H}(t, x)}{\hbar\, \partial x_j} \tag{5.2}$$

where $x \equiv (\mathbf{r}, \mathbf{k})$ with $\mathbf{k} := \mathbf{p}/\hbar$ is the particle's coordinate in $2d$-dimensional phase space and J is the canonical symplectic form,

$$J = \begin{pmatrix} 0 & \mathbb{1}_{d\times d} \\ -\mathbb{1}_{d\times d} & 0 \end{pmatrix} \tag{5.3}$$

with $\mathbb{1}_{d\times d}$ being the identity in d-dimensional space. At this stage, the factor of $\hbar$ drops out of Eq. (5.2). We include it here to simplify the notation when we generalize to semiclassical dynamics below.

Semiclassical approximation. For electrons in a periodic crystal, the coherence length is typically much larger than the lattice constant, rendering a purely classical description useless in most cases. However, one can often obtain good predictions for physical quantities within a semiclassical approximation. Semiclassical theories are ubiquitous in solid state physics. For example, even a seemingly purely classical theory such as the Drude formula for the electric conductivity is usually applied with a renormalized electron mass, which is a quantum-mechanical effect due to coherent scattering off the crystal potential. In a semiclassical approximation, the motion of electrons is described by classical equations of motion similar to Eq. (5.2), i.e., differential equations for the trajectory of a point in $2d$-dimensional phase space, as opposed to an equation for the

evolution of a wave function in Hilbert space. Quantum-mechanical effects are taken into account by modifications of Eq. (5.2), and by an appropriate re-quantization rule.

Due to the uncertainty principle, the phase-space coordinates $\mathbf{r}$ and $\mathbf{k}$ cannot be simultaneously known to arbitrary precision. Therefore, the semiclassical equations of motion are differential equations for the center-of-mass coordinates $x_\mathrm{c} \equiv (\mathbf{r}_\mathrm{c}, \mathbf{k}_\mathrm{c})$ of a wave packet. In a naïve semiclassical treatment, one might be tempted to simply replace the classical Hamilton function $\mathcal{H}(t, x)$ in Eq. (5.2) by the expectation value $\langle \Psi_{t,\mathbf{r}_\mathrm{c},\mathbf{k}_\mathrm{c}} | H(t) | \Psi_{t,\mathbf{r}_\mathrm{c},\mathbf{k}_\mathrm{c}} \rangle$ of the Hamiltonian operator in an appropriate wave packet state $|\Psi_{t,\mathbf{r}_\mathrm{c},\mathbf{k}_\mathrm{c}}\rangle$, see below. We shall see, however, that this naïve substitution misses important effects if the crystal is subject to smooth modulations, such as small external electromagnetic fields or a smooth magnetization texture. In particular, an equation of motion of the form of Eq. (5.1) cannot include the emergent Lorentz force $\frac{\mathrm{d}\mathbf{p}_\mathrm{c}}{\mathrm{d}t} = q_\sigma^\mathrm{em} \frac{\mathrm{d}\mathbf{r}_\mathrm{c}}{\mathrm{d}t} \times \mathbf{B}^\mathrm{em}$ one expects due to the emergent magnetic field $\mathbf{B}^\mathrm{em}$ discussed in section 4.1, nor does it include the anomalous velocity $\frac{\mathrm{d}\mathbf{r}_\mathrm{c}}{\mathrm{d}t} \propto \mathbf{E}$ discussed in section 4.2.

Sundaram and Niu [5] derived the effective equations of motion for wave packets in a smoothly perturbed crystal using a variational approach over wave packets. It turns out that the smooth modulations lead to three modifications of the semiclassical description:

(i) a correction $\delta\mathcal{E}_n^{(1)}$ to the energy of the wave packet;

(ii) terms proportional to the Berry curvature $\Omega_n^{\mathrm{x,x}}$ in the equations of motion for the center-of-mass coordinates x_c; among others, these terms account for the emergent magnetic field $\mathbf{B}^\mathrm{em}$ and the anomalous velocity (see sections 4.1 and 4.2, respectively); and

(iii) a correction to the density of states in phase space that restores particle number conservation [7].

The derivation of (i) and (ii) in Ref. [5] is based on wave packates that have a narrow support in both position and momentum space at all times. The non-zero width of the wave packets in phase space is taken into account only to leading order in gradients of the smooth modulations, and the fact that the wave function disperses (spreads out) over time is neglected. In addition, the derivation neglects (real) inter-band transitions, which is a good approximation in the adiabatic limit $\kappa_\mathrm{n.a.} \ll 1$, see Eq. (3.42).

Model. We review the derivation of items (i) and (ii) above from Ref. [5] and the derivation of (iii) from Ref. [7], using the example of a magnet with a smooth magnetization texture $\mathbf{M}(t, \mathbf{r})$ (Figure 5.1a). In preparation for Section 7.2, we also include external electromagnetic fields $\mathbf{E} = -\boldsymbol{\nabla}\phi - \partial_t \mathbf{A}$ and $\mathbf{B} = \boldsymbol{\nabla} \times \mathbf{A}$, and assume that the potentials ϕ and $\mathbf{A}$ vary smoothly in time and space. In the approximation of non-interacting electrons, the single-particle Hamiltonian is given by

$$H(t) = \frac{(-i\hbar\boldsymbol{\nabla} + e\mathbf{A}(t, \mathbf{r}))^2}{2m} + V(\mathbf{r}) + H_\mathrm{so} + \mathbf{B}^\mathrm{ex}(t, \mathbf{r}) \cdot \boldsymbol{\sigma} - e\phi(t, \mathbf{r}) \tag{5.4}$$

Here, m and $-e$ are the bare mass and the charge of the electron, respectively, V is the lattice-periodic effective potential, $\boldsymbol{\sigma}$ is the vector of Pauli matrices acting on the spin

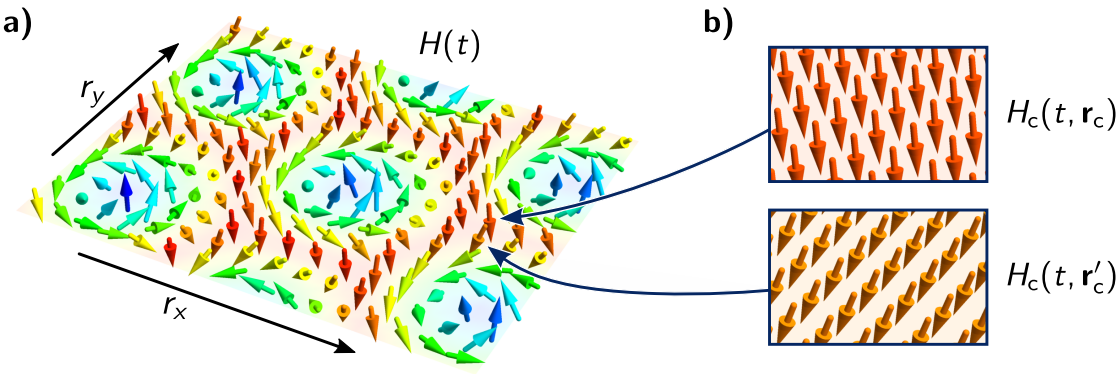

Figure 5.1.: a) Smooth magnetization texture $\mathbf{M}(t, \mathbf{r})$ in the skyrmion lattice phase of a chiral magnet. The magnetization enters in the definition of the microscopic Hamiltonian $H(t)$, Eq. (5.4). Arrows are colored as a function of their out-of-plane component. The spacing between the arrows is not related to the atomic lattice constant a, which is much smaller in the case of MnSi. b) The local Hamiltonian $H_c(t, \mathbf{r}_c)$, Eq. (5.5), is constructed by periodic continuation of $H(t)$ around a given point $\mathbf{r}_c$. Formally, one separates the potentials that enter the definition of H into periodic fields and smooth modulation fields, and keeps the values of the modulation fields fixed in the definition of H_c.

degree of freedom, and H_{so} is the SO coupling term defined in Eq. (4.22). Further, the exchange field $\mathbf{B}^{ex}(t, \mathbf{r}) = -J\mathbf{M}(t, \mathbf{r})$ depends on to the strength $J > 0$ of the exchange coupling and the local magnetization $\mathbf{M}(t, \mathbf{r})$. The fields ϕ, $\mathbf{A}$, and $\mathbf{B}^{ex}$ introduce smooth modulations into the otherwise lattice-periodic system. We assume that the modulation fields vary on a length scale ξ_{mod}, defined by the smallest one of the distances over which either ϕ changes on the order of the band gap, $e\mathbf{A}$ traverses the Brillouin zone, or the direction of $\mathbf{B}^{ex}$ twists by 360°. In contrast, $V(\mathbf{r})$ is lattice periodic, i.e., it varies on the length scale of the lattice constant a. The semiclassical approximation is applicable if $\xi_{mod} \gg a$.

Local Hamiltonian. For each position $\mathbf{r}_c$, one defines a local Hamiltonian by evaluating, in Eq. (5.4), the modulation fields ϕ, $\mathbf{A}$, and $\mathbf{B}^{ex}$ at the fixed position $\mathbf{r}_c$ (Figure 5.1b),

$$H_c(t, \mathbf{r}_c) = \frac{(-i\hbar\boldsymbol{\nabla} + e\mathbf{A}(t, \mathbf{r}_c))^2}{2m} + V(\mathbf{r}) + H_{so} + \mathbf{B}^{ex}(t, \mathbf{r}_c) \cdot \boldsymbol{\sigma} - e\phi(t, \mathbf{r}_c). \tag{5.5}$$

Here, the gradient $\boldsymbol{\nabla}$ acts only on $\mathbf{r}$ and not on $\mathbf{r}_c$, so that $H_c(t, \mathbf{r}_c)$ depends only parametrically on $\mathbf{r}_c$. For fixed t and $\mathbf{r}_c$, the local Hamiltonian $H_c(t, \mathbf{r}_c)$ is lattice periodic and therefore its eigenstates $|\Phi\rangle$ are Bloch functions. In order to obtain a formulation of the semiclassical theory that is independent of the electromagnetic gauge, we label the Bloch functions by their *kinetic* lattice momentum $\hbar\mathbf{k}$, i.e.,

$$\Phi_{n,t,\mathbf{r}_c,\mathbf{k}}(\mathbf{r}) = e^{i(\mathbf{k} - \frac{e}{\hbar}\mathbf{A}(t,\mathbf{r}_c))\cdot\mathbf{r}}\, u_{n,t,\mathbf{r}_c,\mathbf{k}}(\mathbf{r}) \tag{5.6}$$

where n is the band index and the lattice-periodic part $u_{n,t,\mathbf{r}_\mathrm{c},\mathbf{k}}(\mathbf{r})$ is independent of the electromagnetic gauge. Formally, the fact that two different wave vectors $\mathbf{k}$ and $\mathbf{k}-\frac{e}{\hbar}\mathbf{A}$ appear on the right-hand side of Eq. (5.6) may be regarded as being merely a peculiar way to label the Bloch functions Φ. In particular, we emphasize that u is still strictly lattice-periodic.[1]

The lattice-periodic part $u_{n,t,\mathbf{r}_\mathrm{c},\mathbf{k}}(\mathbf{r})$ of the Bloch functions satisfy the eigenvalue equation

$$\tilde{H}_\mathrm{c}(t,\mathbf{r}_\mathrm{c},\mathbf{k})\,u_{n,t,\mathbf{r}_\mathrm{c},\mathbf{k}}(\mathbf{r}) = \mathcal{E}_n^{(0)}(t,\mathbf{r}_\mathrm{c},\mathbf{k})\,u_{n,t,\mathbf{r}_\mathrm{c},\mathbf{k}}(\mathbf{r}) \tag{5.7}$$

where we define the gauge-invariant local band Hamiltonian as

$$\tilde{H}_\mathrm{c}(t,\mathbf{r}_\mathrm{c},\mathbf{k}) = e^{-i(\mathbf{k}-\frac{e}{\hbar}\mathbf{A})\cdot\mathbf{r}}\,H_\mathrm{c}(t,\mathbf{r}_\mathrm{c})\,e^{i(\mathbf{k}-\frac{e}{\hbar}\mathbf{A})\cdot\mathbf{r}} + e\phi(t,\mathbf{r}_\mathrm{c}) \tag{5.8}$$

Note that both $\tilde{H}_\mathrm{c}(t,\mathbf{r}_\mathrm{c},\mathbf{k})$ and the local eigenenergy $\mathcal{E}_n^{(0)}(t,\mathbf{r}_\mathrm{c},\mathbf{k})$ are functions of the kinetic momentum $\hbar\mathbf{k}$, and are defined in such a way that they are both independent of the electromagnetic potentials ϕ and $\mathbf{A}$. We point out that the local band Hamiltonian $\tilde{H}_\mathrm{c}(t,\mathbf{r}_\mathrm{c},\mathbf{k})$ is not the same as the Wigner-transformed Hamiltonian $\tilde{H}(t,\mathbf{r},\mathbf{k})$ we will introduce in Section 6.2 (see there for a comparison between the two).

Energy correction. The main idea of the derivation of the semiclassical equations of motion, Ref. [5], is to vary over wave packets that contain only contributions from a single band n. For a given time t and point $x_\mathrm{c}\equiv(\mathbf{r}_\mathrm{c},\mathbf{k}_\mathrm{c})$ in phase space, one constructs a wave packet

$$\Psi_{t,\mathbf{r}_\mathrm{c},\mathbf{k}_\mathrm{c}}(\mathbf{r}) = \int \mathrm{d}^d k\; a(\mathbf{k})\Phi_{n,t,\mathbf{r}_\mathrm{c},\mathbf{k}}(\mathbf{r}) \tag{5.9}$$

where the complex envelope function $a(\mathbf{k})$ is chosen such that (i) it reproduces the correct expectation value of the position operator, i.e., $\langle\Psi_{t,\mathbf{r}_\mathrm{c},\mathbf{k}_\mathrm{c}}|\mathbf{r}|\Psi_{t,\mathbf{r}_\mathrm{c},\mathbf{k}_\mathrm{c}}\rangle = \mathbf{r}_\mathrm{c}$; (ii) its support in reciprocal space is small compared to the size $\sim 1/a$ of the Brillouin zone; and (iii) it is centered around $\mathbf{k}_\mathrm{c}$, i.e., $\int \mathrm{d}^d k\,\mathbf{k}|a(\mathbf{k})|^2 = \mathbf{k}_\mathrm{c}$ (with normalization $\int \mathrm{d}^d k\,|a(\mathbf{k})|^2 = 1$). In this sense, $x_\mathrm{c}\equiv(\mathbf{r}_\mathrm{c},\mathbf{k}_\mathrm{c})$ is the center-of-mass coordinate of the wave packet in phase space, where $\hbar\mathbf{k}_\mathrm{c}$ is its "physical" momentum: A measurement of the gauge-invariant momentum operator $\hat{\mathbf{p}} = -i\hbar\boldsymbol{\nabla} + e\mathbf{A}$ in the wave-packet state $|\Psi_{t,\mathbf{r}_\mathrm{c},\mathbf{k}_\mathrm{c}}\rangle$ would yield a value close to $\hbar\mathbf{k}_\mathrm{c}$ (modulo reciprocal lattice vectors). According to the uncertainty principle, the narrow support of $a(\mathbf{k})$ in momentum space implies that the wave packet $|\Psi_{t,\mathbf{r}_\mathrm{c},\mathbf{k}_\mathrm{c}}\rangle$ extends over many unit cells in position space. The semiclassical approach is based on the assumption that the part of the system that is probed by $|\Psi_{t,\mathbf{r}_\mathrm{c},\mathbf{k}_\mathrm{c}}\rangle$ is well approximated by the local Hamiltonian $H(t,\mathbf{r}_\mathrm{c})$. This is the case if the width Δr of the wave packet in position space is small compared to the length scale ξ_mod of the smooth modulations. In summary, we assume that the following hierarchy of length scales holds

$$a \ll \Delta r \ll \xi_\mathrm{mod}. \tag{5.10}$$

[1] Notice that $\mathbf{A}$ in Eq. (5.6) is evaluated at the fixed position $\mathbf{r}_\mathrm{c}$. This is different than in the case of the magnetic Bloch theorem, in which the functions u are no longer lattice periodic (see, e.g., [8]). In the situation discussed here, the local Hamiltonian $H_\mathrm{c}(t,\mathbf{r}_\mathrm{c})$ does not have a magnetic field, because $\mathbf{A}$ is a constant in Eq. (5.5).

We split the expectation value of the energy into two terms,

$$\mathcal{E}_n(t,\mathbf{r}_\mathrm{c},\mathbf{k}_\mathrm{c}) := \langle\Psi_{t,\mathbf{r}_\mathrm{c},\mathbf{k}_\mathrm{c}}|H(t)|\Psi_{t,\mathbf{r}_\mathrm{c},\mathbf{k}_\mathrm{c}}\rangle = \langle\Psi_{t,\mathbf{r}_\mathrm{c},\mathbf{k}_\mathrm{c}}|H_\mathrm{c}(t,\mathbf{r}_\mathrm{c})|\Psi_{t,\mathbf{r}_\mathrm{c},\mathbf{k}_\mathrm{c}}\rangle + \delta\mathcal{E}_n^{(1)}(t,\mathbf{r}_\mathrm{c},\mathbf{k}_\mathrm{c}) \tag{5.11}$$

with

$$\delta\mathcal{E}_n^{(1)}(t,\mathbf{r}_\mathrm{c},\mathbf{k}_\mathrm{c}) = \langle\Psi_{t,\mathbf{r}_\mathrm{c},\mathbf{k}_\mathrm{c}}|(H(t)-H_\mathrm{c}(t,\mathbf{r}_\mathrm{c}))|\Psi_{t,\mathbf{r}_\mathrm{c},\mathbf{k}_\mathrm{c}}\rangle\,. \tag{5.12}$$

Using Eqs. (5.7)–(5.8) and the fact that the envelope function $a(\mathbf{k})$ is peaked around $\mathbf{k}\approx\mathbf{k}_\mathrm{c}$, we find for the first term on the right-hand side of Eq. (5.11),

$$\langle\Psi_{t,\mathbf{r}_\mathrm{c},\mathbf{k}_\mathrm{c}}|H(t)|\Psi_{t,\mathbf{r}_\mathrm{c},\mathbf{k}_\mathrm{c}}\rangle \approx \mathcal{E}_n^{(0)}(t,\mathbf{r}_\mathrm{c},\mathbf{k}_\mathrm{c}) - e\phi(t,\mathbf{r}_\mathrm{c}). \tag{5.13}$$

The second term on the right-hand side of Eq. (5.11) is a correction due to gradients of the modulation fields $\mathbf{A}$, and $\mathbf{B}^\mathrm{ex}$. The evaluation of this term in Ref. [5] yields to leading order in the gradients,

$$\delta\mathcal{E}_n^{(1)}(t,\mathbf{r}_\mathrm{c},\mathbf{k}_\mathrm{c}) \approx -\sum_{i=1}^{d}\mathrm{Im}\left[\frac{\partial\langle u_{n,t,\mathbf{r}_\mathrm{c},\mathbf{k}}|}{\partial r_{\mathrm{c},i}}\left(\mathcal{E}_n^{(0)}(t,\mathbf{r}_\mathrm{c},\mathbf{k}_\mathrm{c})-\tilde{H}_\mathrm{c}(t,\mathbf{r}_\mathrm{c},\mathbf{k}_\mathrm{c})\right)\frac{\partial|u_{n,t,\mathbf{r}_\mathrm{c},\mathbf{k}}\rangle}{\partial k_i}\right]\Bigg|_{\mathbf{k}=\mathbf{k}_\mathrm{c}} \tag{5.14}$$

which we rewrite with the help of Eq. (3.16) in a form that is more convenient for numerical evaluation,

$$\delta\mathcal{E}_n^{(1)}(t,\mathbf{r}_\mathrm{c},\mathbf{k}_\mathrm{c}) \approx -\sum_{i=1}^{d}\sum_{m\neq n}\mathrm{Im}\left[\frac{\langle u_{n,t,\mathbf{r}_\mathrm{c},\mathbf{k}_\mathrm{c}}|\frac{\partial\tilde{H}_\mathrm{c}}{\partial r_{\mathrm{c},i}}|u_{m,t,\mathbf{r}_\mathrm{c},\mathbf{k}_\mathrm{c}}\rangle\ \langle u_{m,t,\mathbf{r}_\mathrm{c},\mathbf{k}_\mathrm{c}}|\frac{\partial\tilde{H}_\mathrm{c}}{\partial k_i}|u_{n,t,\mathbf{r}_\mathrm{c},\mathbf{k}_\mathrm{c}}\rangle}{\mathcal{E}_n^{(0)}(t,\mathbf{r}_\mathrm{c},\mathbf{k}_\mathrm{c})-\mathcal{E}_m^{(0)}(t,\mathbf{r}_\mathrm{c},\mathbf{k}_\mathrm{c})}\right] \tag{5.15}$$

where the derivatives of the local band Hamiltonian $\tilde{H}_\mathrm{c}$, Eq. (5.8), are evaluated at $(t,\mathbf{r}_\mathrm{c},\mathbf{k}_\mathrm{c})$. The energy correction $\delta\mathcal{E}_n^{(1)}$ is sometimes called magnetic energy because it contains a term of the form $-\mathbf{m}\cdot(\boldsymbol{\nabla}\times\mathbf{A})$. Here, $\mathbf{m}$ can be identified as the magnetization of the single electron under consideration, which couples to the external magnetic field $\mathbf{B}=\boldsymbol{\nabla}\times\mathbf{A}$.

Equations of motion. The time evolution of the wave packet $|\Psi_{t,\mathbf{r}_\mathrm{c},\mathbf{k}_\mathrm{c}}\rangle$ is described by the Hamiltonian, Eq. (5.4). Solutions of the time-dependent Schrödinger Equation are stationary points of the action $S=\int\mathrm{d}t\,L$ with Lagrangian

$$L[|\Psi\rangle] = \langle\Psi|\left(i\hbar\frac{\mathrm{d}}{\mathrm{d}t}-H(t)\right)|\Psi\rangle\,. \tag{5.16}$$

Semiclassical equations of motion for the trajectory $x_\mathrm{c}(t)\equiv(\mathbf{r}_\mathrm{c}(t),\mathbf{k}_\mathrm{c}(t))$ in phase space are obtained by restricting the domain of L to wave packets of the form of Eq. (5.9). As

discussed above, this ansatz neglects inter-band scattering and the dispersion (spreading) of wave packets. One obtains

$$\begin{aligned} L(t, x_\mathrm{c}, \dot{x}_\mathrm{c}) \equiv L[|\Psi_{t,\mathbf{r}_\mathrm{c},\mathbf{k}_\mathrm{c}}\rangle] &= \langle \Psi_{t,\mathbf{r}_\mathrm{c},\mathbf{k}_\mathrm{c}} | \left(i\hbar \frac{\mathrm{d}}{\mathrm{d}t} - H(t) \right) | \Psi_{t,\mathbf{r}_\mathrm{c},\mathbf{k}_\mathrm{c}} \rangle \\ &= -\mathcal{E}_n(t, x_\mathrm{c}) + e\phi(t, \mathbf{r}_\mathrm{c}) + i\hbar \langle \Psi_{t,\mathbf{r}_\mathrm{c},\mathbf{k}_\mathrm{c}} | \left(\frac{\partial}{\partial t} + \dot{\mathbf{r}}_\mathrm{c} \cdot \frac{\partial}{\partial \mathbf{r}_\mathrm{c}} + \dot{\mathbf{k}}_\mathrm{c} \cdot \frac{\partial}{\partial \mathbf{k}_\mathrm{c}} \right) | \Psi_{t,\mathbf{r}_\mathrm{c},\mathbf{k}_\mathrm{c}} \rangle \\ &\approx -\mathcal{E}_n + e\phi + \hbar \mathcal{A}^\mathrm{t} + \dot{\mathbf{r}}_\mathrm{c} \cdot (\hbar \mathbf{k}_\mathrm{c} + \hbar \boldsymbol{\mathcal{A}}^\mathrm{r} - e\mathbf{A}) + \dot{\mathbf{k}}_\mathrm{c} \cdot \hbar \boldsymbol{\mathcal{A}}^\mathrm{k} \end{aligned} \tag{5.17}$$

where, in the last step, we used again the fact that the envelope function $a(\mathbf{k})$ is peaked at $\mathbf{k}_\mathrm{c}$. In Eq. (5.17), $\mathcal{A}^\mathrm{t}$, $\boldsymbol{\mathcal{A}}^\mathrm{r}$, and $\boldsymbol{\mathcal{A}}^\mathrm{k}$ are the components of the Berry connection for the local band Hamiltonian $\tilde{H}_\mathrm{c}(t, \mathbf{r}_\mathrm{c}, \mathbf{r}_\mathrm{c})$, as defined in Eq. (3.6). Explicitly,

$$\mathcal{A}^\mathrm{t} = i \langle u_{n,t,x_\mathrm{c}} | \frac{\partial}{\partial t} | u_{n,t,x_\mathrm{c}} \rangle \quad \text{and} \quad \mathcal{A}^\mathrm{x}_i \equiv (\boldsymbol{\mathcal{A}}^\mathrm{r}, \boldsymbol{\mathcal{A}}^\mathrm{k})_i = i \langle u_{n,t,x_\mathrm{c}} | \frac{\partial}{\partial x_{\mathrm{c},i}} | u_{n,t,x_\mathrm{c}} \rangle \tag{5.18}$$

where the partial time derivative is evaluated at constant x_c. The semiclassical equations of motion for the center-of-mass coordinates $x_\mathrm{c} \equiv (\mathbf{r}_\mathrm{c}, \mathbf{k}_\mathrm{c})$ in phase space are obtained from the Euler-Lagrange equations for $L(t, x_\mathrm{c}, \dot{x}_\mathrm{c})$. One finds

$$\left. \frac{\mathrm{d}r_{\mathrm{c},i}}{\mathrm{d}t} \right|_n = \frac{\partial \mathcal{E}_n}{\hbar\, \partial k_{\mathrm{c},i}} - \Omega^{\mathrm{k,t}}_{n,i} - \Omega^{\mathrm{k,r}}_{n,ij} \dot{r}_{\mathrm{c},j} - \Omega^{\mathrm{k,k}}_{n,ij} \dot{k}_{\mathrm{c},j}; \tag{5.19}$$

$$\hbar \left. \frac{\mathrm{d}k_{\mathrm{c},i}}{\mathrm{d}t} \right|_n = -\frac{\partial \mathcal{E}_n}{\partial r_{\mathrm{c},i}} - eE_i + \hbar\, \Omega^{\mathrm{r,t}}_{n,i} + \left(\hbar\, \Omega^{\mathrm{r,r}}_{n,ij} - e\epsilon_{ijl} B_l \right) \dot{r}_{\mathrm{c},j} + \hbar\, \Omega^{\mathrm{r,k}}_{n,ij} \dot{k}_{\mathrm{c},j} \tag{5.20}$$

where the notation "$|_n$" is merely a reminder that $\mathbf{r}_\mathrm{c}$ and $\mathbf{k}_\mathrm{c}$ are the center-of-mass coordinates of a wave packet formed from band n, and that the semiclassical equations of motion are different in different bands. On the right-hand sides of Eqs. (5.19)–(5.20), we used the electric field $\mathbf{E} = -\boldsymbol{\nabla}\phi - \partial_t \mathbf{A}$, the magnetic field $\mathbf{B} = \boldsymbol{\nabla} \times \mathbf{A}$, and the usual definition of the Berry curvature (cf., Eq. (3.13)),

$$\Omega^{\mathrm{x,t}}_{n,i} = \frac{\partial \mathcal{A}^\mathrm{t}}{\partial x_\mathrm{c,i}} - \frac{\partial \mathcal{A}^\mathrm{x}_i}{\partial t} \qquad \text{and} \qquad \Omega^{\mathrm{x,x}}_{n,ij} \equiv \begin{pmatrix} \Omega^{\mathrm{r,r}}_n & \Omega^{\mathrm{r,k}}_n \\ \Omega^{\mathrm{k,r}}_n & \Omega^{\mathrm{k,k}}_n \end{pmatrix}_{ij} = \frac{\partial \mathcal{A}^\mathrm{x}_j}{\partial x_\mathrm{c,i}} - \frac{\partial \mathcal{A}^\mathrm{x}_i}{\partial x_\mathrm{c,j}}. \tag{5.21}$$

The first term on the right-hand side of Eqs. (5.19) and (5.20), respectively, is analogous to the classical equations of motion, Eq. (5.1), where the Hamilton function $\mathcal{H}$ is replaced by the energy expectation value $\mathcal{E}_n \approx \mathcal{E}^{(0)}_n + \delta\mathcal{E}^{(1)}_n$. The remaining terms are gradient corrections. The Berry curvatures $\Omega^{\mathrm{r,t}}_n$ and $\Omega^{\mathrm{r,r}}_n$ appear in the same places as the electric and magnetic field, respectively. Indeed, by inserting Eq. (4.14), one obtains an emergent Lorentz force $\mathbf{F}^\mathrm{em}_\sigma = q^\mathrm{em}_\sigma (\mathbf{E}^\mathrm{em} + \dot{\mathbf{r}}_\mathrm{c} \times \mathbf{B}^\mathrm{em})$ in the majority (minority) band $\sigma = \downarrow$ ($\sigma = \uparrow$) of a chiral magnet, where q^em_σ, $\mathbf{E}^\mathrm{em}$, and $\mathbf{B}^\mathrm{em}$ are the emergent charge, emergent electric field, and emergent magnetic field, respectively (see Section 4.1). Similarly, the momentum-space Berry curvature $\Omega^{\mathrm{k,k}}_n$ in Eq. (5.19) plays the role of a magnetic field in reciprocal space. The term $v^\mathrm{anom}_{n,i} = -\Omega^{\mathrm{k,k}}_{n,ij} \dot{k}_{\mathrm{c},j} \approx \frac{e}{\hbar} \Omega^{\mathrm{k,k}}_{n,ij} E_j$ is the anomalous velocity discussed in section 4.2, which is perpendicular to $\mathbf{E}$ due to the skew-symmetry of $\Omega^{\mathrm{k,k}}_n$.

In a more compact form, Eqs. (5.19)–(5.20) can be written as

$$(J_{ij} - \Omega'^{\mathrm{x,x}}_{n,ij})\dot{x}_{\mathrm{c},j} = -\frac{\partial \mathcal{E}_n}{\hbar\, \partial x_{\mathrm{c},i}} + \Omega'^{x,t}_{n,i} \tag{5.22}$$

where the primed Berry curvatures are the same as the unprimed ones defined in Eq. (5.21), except for the components

$$\Omega'^{\mathrm{r,t}}_{n,i} := \Omega^{\mathrm{r,t}}_{n,i} - \frac{e}{\hbar}E_i \qquad \text{and} \qquad \Omega'^{\mathrm{r,r}}_{n,ij} := \Omega^{\mathrm{r,r}}_{n,ij} - \frac{e}{\hbar}\epsilon_{ijl}B_l \; . \tag{5.23}$$

Using the anti-symmetry of J and $\Omega^{\mathrm{x,x}}_n$, Eq. (5.22) is equivalent, to linear order in $\Omega'^{\mathrm{x,x}}_n$, to

$$\dot{x}_{\mathrm{c},i} = (J - J\Omega'^{\mathrm{x,x}}_n J)_{ij} \left(\frac{\partial \mathcal{E}_n}{\hbar\, \partial x_{\mathrm{c},j}} - \Omega'^{x,t}_{n,j} \right) \tag{5.24}$$

5.2. Correction to the density of states.

The semiclassical equation of motion, Eq. (5.22), describes the dynamics of a single electron in phase space. To calculate measurable quantities in a many-electron system, one needs to sum over all occupied states. This requires an appropriate (re-)quantization scheme. For example, the expectation value of single-particle observable $\hat{O}$ at time t is given by

$$\langle \hat{O} \rangle_t = \sum_n \int \mathrm{d}^{2d}x_{\mathrm{c}}\, D_n(t, x_{\mathrm{c}}) f_n(t, x_{\mathrm{c}})\, \langle \Phi_{n,t,\mathbf{r}_{\mathrm{c}},\mathbf{k}_{\mathrm{c}}} | \hat{O} | \Phi_{n,t,\mathbf{r}_{\mathrm{c}},\mathbf{k}_{\mathrm{c}}} \rangle \; . \tag{5.25}$$

Here, n is the band index, the distribution function f_n is the expectation value of the number of particles in band n at point x_{c} in phase space ($0 \leq f_n(t, x_{\mathrm{c}}) \leq 1$ for fermions), and $D_n(t, x_{\mathrm{c}})$ is the density of states in phase space at time t. In absence of Berry-phases, the latter is a constant, $D_n = (2\pi)^{-d}$. This can be seen, for example, by restricting the system to a cube of volume L^d and performing the limit $L \to \infty$. On a more fundamental level, the constant D_n is a consequence of the fact that, in absence of Berry phases, $\mathbf{r}$ and $\mathbf{k}$ satisfy canonical Poisson brackets $\{r_i, \hbar k_j\} = \delta_{ij}$, see below and Ref. [74]. It has been pointed out by Xiao, Shi, and Niu [7] that a constant D_n is, however, incompatible with the semiclassical equations of motion Eq. (5.22) as soon as either $\Omega'^{\mathrm{r,k}} \neq 0$ or both $\Omega'^{\mathrm{r,r}} \neq 0$ and $\Omega'^{\mathrm{k,k}} \neq 0$. As we will see below, a constant D_n in this case would violate the conservation of the total number of particles,

$$N(t) = \sum_n \int \mathrm{d}^{2d}x_{\mathrm{c}}\, D_n(t, x_{\mathrm{c}}) f_n(t, x_{\mathrm{c}}). \tag{5.26}$$

Liouville theorem and particle number conservation. In a consistent semiclassical theory, the total particle number N has to be conserved. Assuming a non-interacting system, the distribution function $f_n(t, x_{\mathrm{c}})$ at a given time t can be expressed in terms of

$f_n(t_0, x_\mathrm{c})$ at some reference time t_0 by integration of the equation of motion, Eq. (5.22),

$$\begin{aligned} f_n(t, x_\mathrm{c}) &= \int \mathrm{d}^{2d}x'_\mathrm{c}\, \delta\left(x'_\mathrm{c} + \int_{t_0}^{t} \dot{x}_\mathrm{c}(t')\,\mathrm{d}t' - x_\mathrm{c}\right) f_n(t_0, x'_\mathrm{c}) \\ &= f_n\left(t_0, x_\mathrm{c} - \int_{t_0}^{t} \dot{x}_\mathrm{c}(t')\,\mathrm{d}t'\right) \end{aligned} \tag{5.27}$$

Thus, we have

$$\frac{\partial f_n(t, x_\mathrm{c})}{\partial t} = -\frac{\partial f_n(t, x_\mathrm{c})}{\partial x_{\mathrm{c},i}} \dot{x}_{\mathrm{c},i} \tag{5.28}$$

and the time derivative of the total particle number is

$$\begin{aligned} \frac{\mathrm{d}N}{\mathrm{d}t} &= \sum_n \int \mathrm{d}^{2d}x_\mathrm{c} \left[\frac{\partial D_n(t, x_\mathrm{c})}{\partial t} f_n(t, x_\mathrm{c}) - D_n(t, x_\mathrm{c}) \frac{\partial f_n(t, x_\mathrm{c})}{\partial x_{\mathrm{c},i}} \dot{x}_{\mathrm{c},i}\right] \\ &= \sum_n \int \mathrm{d}^{2d}x_\mathrm{c} \left[\frac{\partial D_n(t, x_\mathrm{c})}{\partial t} + \frac{\partial D_n(t, x_\mathrm{c})}{\partial x_{\mathrm{c},i}} \dot{x}_{\mathrm{c},i} + D_n(t, x_\mathrm{c}) \frac{\partial \dot{x}_{\mathrm{c},i}}{\partial x_{\mathrm{c},i}}\right] f_n(t, x_\mathrm{c}) \end{aligned} \tag{5.29}$$

where we integrated by parts in the last step.

In a purely classical system governed by the Hamilton equations of motion, Eq. (5.2), the last term in the bracket on the right-hand side of Eq. (5.29) vanishes due to the Liouville theorem, $\partial \dot{x}_i / \partial x_i = 0$, which is a direct consequence of Eq. (5.2) and the fact that J_{ij}, Eq. (5.3), is constant and skew-symmetric. Therefore, in absence of Berry phases, the right-hand side of Eq. (5.29) vanishes for a constant phase-space density $D_n = (2\pi)^{-d}$, as it should.

Under the semiclassical dynamics described by Eq. (5.22), the factor $\partial \dot{x}_{\mathrm{c},i} / \partial x_{\mathrm{c},i}$ does not vanish in general. The correct density of states D_n in this case is specified by the partial differential equation that results from setting the right-hand side of Eq. (5.29) to zero for all $f_n(t, x_\mathrm{c})$. In Ref. [7], the solution

$$D_n(t, x_\mathrm{c}) = \frac{\sqrt{\det(J - \Omega'^{\mathrm{x,x}}_n(t, x_\mathrm{c}))}}{(2\pi)^d} \tag{5.30}$$

was proposed. Here, the numerator is known as the Pfaffian of the skew-symmetric matrix $M := J - \Omega'^{\mathrm{x,x}}_n$, which is analytic in the components of $\Omega'^{\mathrm{x,x}}_n$ despite the appearance of the square root [75]. A derivation of Eq. (5.30) was given in Ref. [74] (see also our alternative derivation in Appendix B in Ref. [65]). To convince ourselves that Eq. (5.30) is indeed the correct density of states, we first consider the limit where all modulation fields are switched off at some reference time t_0. Therefore, $\Omega'^{\mathrm{r,r}}_n = 0 = \Omega'^{\mathrm{r,k}}_n$ at time t_0 and one finds that Eq. (5.30) correctly reduces to the classical density of states $D_n = (2\pi)^{-d}$. We now ramp up the modulation fields adiabatically from time t_0 to $t > t_0$ and send $t_0 \to -\infty$. A direct calculation shows that Eq. (5.30) sets the right-hand side of Eq. (5.29) to zero for all $f_n(t, x_\mathrm{c})$, as claimed. This can be checked by using Eq. (5.22), the Jacobi identity (Eq. (3.14)), and the relation

$$\frac{\partial \det(M)}{\partial x_{\mathrm{c},i}} = \det(M)\,\mathrm{tr}\left[M^{-1} \frac{\partial M}{\partial x_{\mathrm{c},i}}\right] \tag{5.31}$$

which follows from the identity $\log\det(M) = \mathrm{tr}\log(M)$. Thus, Eq. (5.30) satisfies the defining partial differential equation and the correct initial condition for the density of states in phase space.

Formally, Eq. (5.30) restores particle number conservation under the dynamics of Eq. (5.22) *exactly*. We emphasize, however, that the semiclassical equation of motion, Eq. (5.22), is only valid to leading order in the gradient corrections $\Omega'^{\mathrm{x,x}}_n$ and $\Omega'^{\mathrm{x,t}}_n$. Therefore, the density of states, Eq. (5.30), is in general also only valid to first order in the components of $\Omega'^{\mathrm{x,x}}_n$. To first order, one obtains

$$D_n(t, x_\mathrm{c}) \approx \frac{1}{(2\pi)^d}\left(1 - \mathrm{Tr}\Big[\Omega^{\mathrm{r,k}}_n(t, x_\mathrm{c})\Big]\right) + \mathcal{O}\left((\Omega'^{\mathrm{x,x}}_n)^2\right) \tag{5.32}$$

where $\mathrm{Tr}\left[\Omega^{\mathrm{r,k}}_n\right] = \sum_{i=1}^{d} \Omega^{\mathrm{r,k}}_{n,ii}$.

5.3. Berry-phase effects on energy and charge density

While the semiclassical equation of motion, Eq. (5.22), describes the *dynamics* of electrons, the energy shift $\delta\mathcal{E}_n$, Eq. (5.14), and the density of states D_n, Eq. (5.30), affect also equilibrium properties. In the remaining sections of this chapter, we discuss the effects of phase-space Berry phases on the energy and charge density of chiral magnets, which we published in Ref. [65]. Within the semiclassical approximation, the free energy of a non-interacting many-particle system is given by $F = \int f(\mathbf{r}_\mathrm{c})\,\mathrm{d}^d r_\mathrm{c}$ with the free energy density

$$f(\mathbf{r}_\mathrm{c}) = -k_B T \sum_n \int \mathrm{d}^d k_\mathrm{c}\; D_n(x_\mathrm{c}) \ln\Big(1 + e^{-(\mathcal{E}_n(x_\mathrm{c})-\mu)/(k_B T)}\Big) \approx f^{(0)}(\mathbf{r}_\mathrm{c}) + \delta f^{(1)}(\mathbf{r}_\mathrm{c}). \tag{5.33}$$

Here, k_B is the Boltzmann constant, T the temperature, μ the chemical potential, $D(x_\mathrm{c})$ is the semiclassical density of states in phase space, see Eq. (5.32), and $\mathcal{E}_n(x_\mathrm{c})$ is the energy expectation value of a wave packet with center-of-mass coordinates $x_\mathrm{c} \equiv (\mathbf{r}_\mathrm{c}, \mathbf{k}_\mathrm{c})$, see Eq. (5.11). In absence of phase-space Berry phases, the free energy density reduces to

$$f^{(0)}(\mathbf{r}_\mathrm{c}) = -k_B T \sum_n \int \frac{d^d k_\mathrm{c}}{(2\pi)^d}\; \ln\Big(1 + e^{-(\mathcal{E}^{(0)}_n(x_\mathrm{c})-\mu)/(k_B T)}\Big). \tag{5.34}$$

Berry-phases in mixed position/momentum space lead to a change of the energy density. To leading order in the gradient terms, we obtain

$$\begin{aligned}\delta f^{(1)}(\mathbf{r}_\mathrm{c}) = \sum_n \int \frac{\mathrm{d}^d k_\mathrm{c}}{(2\pi)^d} \Big[&\delta\mathcal{E}^{(1)}_n(x_\mathrm{c})\; n_F(\mathcal{E}^{(0)}_n(x_\mathrm{c}) - \mu) \\ &+ k_B T\, \mathrm{Tr}\Big(\Omega^{\mathrm{r,k}}_n(x_\mathrm{c})\Big) \ln\Big(1 + e^{-(\mathcal{E}^{(0)}_n(x_\mathrm{c})-\mu)/(k_B T)}\Big)\Big]\end{aligned} \tag{5.35}$$

where $n_F(\epsilon) = 1/(1 + e^{\epsilon/(k_B T)})$ is the Fermi distribution and $\delta\mathcal{E}^{(1)}_n$ and $\Omega^{\mathrm{r,k}}_n$ are defined in Eqs. (5.15) and (5.21), respectively. Note that both terms on the right-hand side of

Eq. (5.35) are non-zero only in the presence of both SO interaction and a smooth spatial inhomogeneity (magnetization texture). We will identify $\delta f^{(1)}$ as the DM energy in the next section.

The charge density $\rho(\mathbf{r}_\mathrm{c})$ is also influenced by Berry phases. To leading order in the gradient correction terms, we obtain[2]

$$\begin{aligned}\delta\rho^{(1)}(\mathbf{r}_\mathrm{c}) &= e\,\frac{\partial\delta f^{(1)}(\mathbf{r}_\mathrm{c})}{\partial\mu} = \\ &= -e\sum_n\int\frac{\mathrm{d}^d k_\mathrm{c}}{(2\pi)^d}\Big[\delta\mathcal{E}_n^{(1)}(x_\mathrm{c})n_F'(\mathcal{E}_n^{(0)}(x_\mathrm{c})-\mu) - \mathrm{Tr}\Big(\Omega_n^{\mathrm{r,k}}(x_\mathrm{c})\Big)n_F(\mathcal{E}_n^{(0)}(x_\mathrm{c})-\mu))\Big]\end{aligned} \tag{5.36}$$

where $n_F'(\epsilon) = \partial n_F(\epsilon)/\partial\epsilon$.

Electrostatic screening. In Eq. (5.36), the correction to the charge density was calculated at fixed μ and the effect of screening due to Coulomb interaction was ignored. In a metal, Coulomb interactions lead to screening of charges (see, e.g., Ref. [76]) and the total charge density $\delta\rho^{\mathrm{tot}}(\mathbf{r}_\mathrm{c}) \approx \delta\rho^{(1)}(\mathbf{r}_\mathrm{c}) + \delta\rho^{\mathrm{sc}}(\mathbf{r}_\mathrm{c})$ is a sum of the charge density $\delta\rho^{(1)}(\mathbf{r}_\mathrm{c})$ due to phase-space Berry curvatures and a redistribution

$$\delta\rho^{\mathrm{sc}}(\mathbf{r}_\mathrm{c}) = -e^2\nu_F\delta V(\mathbf{r}_\mathrm{c}) \tag{5.37}$$

of charges due to screening. Here, ν_F is the density of states at the Fermi level and δV is the electrostatic screening potential, which is related to the total charge density via the Maxwell relation

$$-\epsilon_0\boldsymbol{\nabla}^2\delta V(\mathbf{r}_\mathrm{c}) = \rho^{\mathrm{tot}}(\mathbf{r}_\mathrm{c}) \tag{5.38}$$

where ϵ_0 is the permittivity of the vacuum. To solve Eqs. (5.37)–(5.38) for $\delta\rho^{\mathrm{tot}}$, we go to Fourier space and obtain

$$\delta\rho_\mathbf{q}^{\mathrm{tot}} = -q^2\lambda_{\mathrm{TF}}^2\delta\rho_\mathbf{q}^{\mathrm{sc}} = -q^2\lambda_{\mathrm{TF}}^2\left(\delta\rho_\mathbf{q}^{\mathrm{tot}} - \delta\rho_\mathbf{q}^{(1)}\right) \tag{5.39}$$

where $\mathbf{q}$ is the wave vector and $\lambda_{\mathrm{TF}} = \sqrt{\epsilon_0/(e^2\nu_F)}$ the Thomas-Fermi screening length. Therefore,

$$\delta\rho_\mathbf{q}^{\mathrm{tot}} = \frac{q^2\lambda_{\mathrm{TF}}^2}{q^2\lambda_{\mathrm{TF}}^2+1}\delta\rho_\mathbf{q}^{(1)} \tag{5.40}$$

where $\mathbf{q}$ is the wave vector. In good metals and for long-wavelength skyrmions, one has $q\lambda_{\mathrm{TF}} \ll 1$ (see numerical results below). Therefore, the denominator on the right-hand side of Eq. (5.40) is close to unity and we obtain in position space

$$\delta\rho^{\mathrm{tot}}(\mathbf{r}_\mathrm{c}) \approx -\lambda_{\mathrm{TF}}^2\boldsymbol{\nabla}^2\delta\rho^{(1)}(\mathbf{r}_\mathrm{c}). \tag{5.41}$$

[2] We are using SI units here with electron charge $-e$, which is a different sign convention than in Ref. [65].

As expected, the total charge of the system $\int \mathrm{d}^3 r_\mathrm{c}\, \delta\rho^\mathrm{tot}(\mathbf{r}_\mathrm{c})$ vanishes when screening is taken into account, and the charge density $\delta\rho^\mathrm{tot}(\mathbf{r}_\mathrm{c})$ that includes screening effects is positive (negative) when the charge density $\delta\rho^{(1)}$ due to phase-space Berry phases has a maximum (minimum). While screening happens only at the Fermi surface, the unscreened charge density $\delta\rho^{(1)}$ has contributions both from the Fermi surface and the Fermi sea, see Eq. (5.35). Therefore, $\delta\rho^{(1)}$ is still an interesting quantity to estimate the amount of charge-redistribution due to phase-space Berry phases. Moreover, there is no screening in insulators and we will show in chapter 6.3 that Berry phases in phase space lead to a quantized skyrmion charge in insulators. Interestingly, Eq. (5.30) for the density of states D_n in phase space turns out to be valid beyond the linear order in $\Omega_n^{\mathrm{x,x}}$ in insulators (this is not true for metals, though).

5.4. DM energy and skyrmion charge in a minimal model

In order to estimate qualitatively how the Berry-phase corrections to the energy and the skyrmion charge depend on the strength of SO interaction, we consider the minimal model of a chiral magnet without avoided band crossings, Eq. (4.28), with a time-independent exchange field $\mathbf{B}^\mathrm{ex}(\mathbf{r})$ and a SO-coupling field $\mathbf{g}^\mathrm{so}(\mathbf{k})$. We obtain the local band Hamiltonian by evaluating Eq. (4.28) at the center-of-mass coordinates $x_\mathrm{c} \equiv (\mathbf{r}_\mathrm{c}, \mathbf{k}_\mathrm{c})$,

$$\tilde{H}_\mathrm{c}(\mathbf{r}_\mathrm{c}, \mathbf{k}_\mathrm{c}) = \epsilon_{\mathbf{k}_\mathrm{c}} + [\mathbf{B}^\mathrm{ex}(\mathbf{r}_\mathrm{c}) + \mathbf{g}^\mathrm{so}(\mathbf{k}_\mathrm{c})] \cdot \boldsymbol{\sigma} =: \epsilon_{\mathbf{k}_\mathrm{c}} + \mathbf{n}(x_\mathrm{c}) \cdot \boldsymbol{\sigma} \tag{5.42}$$

with $\mathbf{n} = \mathbf{B}^\mathrm{ex} + \mathbf{g}^\mathrm{so}$. The Berry curvature in phase space is given by the winding number density of $\mathbf{n}(x_\mathrm{c})$, Eq. (4.29). In particular, one has $\Omega_\downarrow^{\mathrm{x,x}} = -\Omega_\uparrow^{\mathrm{x,x}}$ where $\sigma = \downarrow$ and $\sigma = \uparrow$ denote the majority and minority spin configuration, respectively (see section 4.1). From Eq. (5.14), we obtain for the energy shift,

$$\delta\mathcal{E}_\uparrow^{(1)}(x_\mathrm{c}) = \delta\mathcal{E}_\downarrow^{(1)}(x_\mathrm{c}) = |\mathbf{n}|\, \mathrm{Tr}\Big[\Omega_\uparrow^{r,k}\Big]. \tag{5.43}$$

DM interaction strength. From Eq. (5.35), we obtain for the correction to the free energy density,

$$\delta f^{(1)}(\mathbf{r}_\mathrm{c}) = \int \frac{\mathrm{d}^d k_\mathrm{c}}{(2\pi)^d}\, \mathrm{Tr}\Big[\Omega_\uparrow^{\mathrm{r,k}}\Big] \Bigg[|\mathbf{n}| \left(n_F(\mathcal{E}_\uparrow^{(0)} - \mu) + n_F(\mathcal{E}_\downarrow^{(0)} - \mu) \right) + k_B T \ln\left(\frac{1 + e^{-(\mathcal{E}_\uparrow^{(0)} - \mu)/(k_B T)}}{1 + e^{-(\mathcal{E}_\downarrow^{(0)} - \mu)/(k_B T)}} \right) \Bigg]. \tag{5.44}$$

We consider the limit of a small band splitting compared to the Fermi energy and expand in $\mathcal{E}_\uparrow^{(0)} - \mathcal{E}_\downarrow^{(0)} = 2|\mathbf{n}| \ll \mu$. The first two terms in the expansion cancel and we obtain to leading order

$$\delta f^{(1)}(\mathbf{r}_\mathrm{c}) \approx \frac{2}{3} \int \frac{\mathrm{d}^d k_\mathrm{c}}{(2\pi)^d}\, |\mathbf{n}|^3\, \mathrm{Tr}\Big[\Omega_\uparrow^{\mathrm{r,k}}\Big] n_F''(\epsilon_{\mathbf{k}_\mathrm{c}} - \mu). \tag{5.45}$$

To make further progress, we assume, as in section 4.3, that SO interactions are small compared to the exchange interaction and expand to leading order in the SO-interaction strength $\lambda_{\rm so} \sim |\mathbf{g}^{\rm so}|/|\mathbf{B}^{\rm ex}| \ll 1$. In this limit, $\Omega_{\uparrow}^{\rm r,k} \sim \lambda_{\rm so}^2$ is given by Eq. (4.33) and we obtain

$$\delta f^{(1)}(\mathbf{r}_{\rm c}) = D_{ij} \left(\hat{\mathbf{B}}^{\rm ex}(\mathbf{r}_{\rm c}) \times \frac{\partial \hat{\mathbf{B}}^{\rm ex}(\mathbf{r}_{\rm c})}{\partial r_{{\rm c},j}} \right)_i \tag{5.46}$$

where $\hat{\mathbf{B}}^{\rm ex} = \mathbf{B}^{\rm ex}/|\mathbf{B}^{\rm ex}|$ and

$$D_{ij} \approx -\frac{|\mathbf{B}^{\rm ex}|^2}{3} \int \frac{\mathrm{d}^d k_{\rm c}}{(2\pi)^d} \, \frac{\partial g_i^{\rm so}}{\partial k_j} n_F''(\epsilon_{\mathbf{k}_{\rm c}} - \mu) \, . \tag{5.47}$$

In a cubic lattice, such as MnSi, the vector field $\mathbf{g}^{\rm so}(\mathbf{k})$ (Eq. (4.25)) is covariant under rotations by 120° around the [111] direction, i.e. cyclic permutations of the directions x, y, and z. This implies $D_{ij} \propto \delta_{ij}$ in a cubic system. In order to obtain a qualitative estimate, we recall that $\mathbf{g}^{\rm so}$ varies on the order of the SO interaction energy $E_{\rm so} \sim \lambda_{\rm so}|\mathbf{B}^{\rm ex}|$. For an order-of-magnitude, we approximate $|\partial g_i^{\rm so}/\partial k_j| \sim E_{\rm so} a$ where a is the atomic lattice constant. Assuming a cubic crystal structure, we obtain,

$$D_{ij} = -D\delta_{ij} \qquad \text{with} \qquad D \sim E_{\rm so} \frac{1}{a^{d-1}} \frac{B_0^2}{E_F^2}. \tag{5.48}$$

Inserting into Eq. (5.46), we find for the Berry-phase contribution to the total free Energy,

$$\delta F^{(1)} := \int \mathrm{d}^d r_{\rm c} \, \delta f^{(1)}(\mathbf{r}_{\rm c}) \approx D \int \mathrm{d}^d r_{\rm c} \, \hat{\mathbf{M}} \cdot (\boldsymbol{\nabla} \times \hat{\mathbf{M}}) \tag{5.49}$$

where $\hat{\mathbf{M}} = -\hat{\mathbf{B}}^{\rm ex}$ is the unit vector in the direction of the magnetization $\mathbf{M} \propto -\mathbf{B}^{\rm ex}$. We identify $\delta F^{(1)}$ as the DM interaction (cf., Eq. (2.6)). The relation between phase-space Berry phases and Dzyaloshinskii-Moriya interaction was also pointed out in Ref. [77]. As expected, the DM interaction strength D, Eq. (5.48), is proportional to the energy scale $E_{\rm so}$ of SO interactions and quadratic in the magnetization.

Skyrmion charge. For the Berry-phase correction to the charge density, we obtain from Eq. (5.46)

$$\delta\rho^{(1)}(\mathbf{r}_{\rm c}) = e\frac{\partial f^{(1)}(\mathbf{r}_{\rm c})}{\partial \mu} \approx e\frac{\partial D_{ij}}{\partial \mu} \left(\hat{\mathbf{B}}^{\rm ex}(\mathbf{r}_{\rm c}) \times \frac{\partial \hat{\mathbf{B}}^{\rm ex}(\mathbf{r}_{\rm c})}{\partial r_{{\rm c},j}} \right)_i . \tag{5.50}$$

In section 2.2, we discussed the experimental observation of the skyrmion lattice phase in MnSi. The magnetization texture is well described by [9, 78]

$$\mathbf{B}^{\rm ex}(\mathbf{r}) = B_0 \, \hat{\mathbf{z}} + B_1 \sum_{n=0}^{2} \Big[(\hat{\mathbf{z}} \times \hat{\boldsymbol{\xi}}_n) \sin\Big(q_0 \, \hat{\boldsymbol{\xi}}_n \cdot \mathbf{r}\Big) + \hat{\mathbf{z}} \cos\Big(q_0 \, \hat{\boldsymbol{\xi}}_n \cdot \mathbf{r}\Big) \Big] . \tag{5.51}$$

where $q_0 \approx 2\pi/(190\,\text{Å})$, $\hat{\mathbf{z}} = (0,0,1)$ is the unit vector in the direction of a small external magnetic field that stabilizes the skyrmion lattice, $\hat{\boldsymbol{\xi}}_n = (\cos(2\pi n/3), \sin(2\pi n/3), 0)$,

and, according to mean-field calculations [9], $B_1/B_0 \approx -1.5$. See Figure 5.1a for an illustration. Since the non-collinear magnetization texture results from a competition between DM interactions (which are a consequence of SO interactions) and ferromagnetic exchange interactions, q_0 is proportional to $|\mathbf{g}^{\mathrm{so}}|/|\mathbf{B}^{\mathrm{ex}}| \sim \lambda_{\mathrm{so}}$. For our estimate, we set $q_0 = \lambda_{\mathrm{so}} 2\pi/a$. The area of a single skyrmion in the (x, y)-plane is proportional to $(2\pi/q_0)^2$. Thus, we obtain from Eqs. (5.50) for the electric charge of a skyrmion per atomic layer in z direction (without screening),

$$\delta Q^{(1)} := a \int\limits_{\text{skyrmion}} \mathrm{d}r_{\mathrm{c},x}\, \mathrm{d}r_{\mathrm{c},y}\, \delta\rho^{(1)}(\mathbf{r}_{\mathrm{c}}) \sim e\frac{B_0^3}{E_F^3} \tag{5.52}$$

where the integral runs over a single magnetic unit cell in the plane perpendicular to the small external magnetic field. Note that the skyrmion charge $\delta Q^{(1)}$ is independent of the SO coupling strength λ_{so}, since the smallness of the charge density $\delta\rho^{(1)} \sim \lambda_{\mathrm{so}}^2$ is compensated by the large size $\mathcal{O}(1/\lambda_{\mathrm{so}}^2)$ of the skyrmions. This qualitative result is confirmed by *ab initio* calculations that use the real band structure of MnSi (see next section), as long as screening is neglected.

5.5. Numerical results for DM energy and skyrmion charge in MnSi

Numerical values for the DM interaction strength D and the skyrmion charge $\delta Q^{(1)}$ in the skyrmion lattice phase of MnSi were obtained from *ab initio* methods by our collaborators F. Freimuth and Y. Mokrousov [65]. The calculations were done for the left-handed crystal structure, with the atomic coordinates from Ref. [71].

Method. While the semiclassical description we reviewed in section 5.1 was originally derived for non-interacting systems, it can also be applied to interacting systems by using density functional theory (DFT). In DFT, the interacting Hamiltonian H is mapped to a noninteracting one using the following iterative procedure [79]. According to the Hohenberg-Kohn theorem [80, 81], the ground-state $|\Psi[n(\mathbf{r})]\rangle$ of H is completely determined by the electron density $n(\mathbf{r})$. Therefore, finding the ground state of H is equivalent to finding the density profile $n(\mathbf{r})$ that minimizes the energy functional $E[n] := \langle\Psi[n(\mathbf{r})]|H|\Psi[n(\mathbf{r})]\rangle$. The minimization of $E[n]$ for the interacting Hamiltonian H can be mapped to a minimization of the energy of non-interacting electrons in an external potential $V[n](\mathbf{r})$. Here, $V[n](\mathbf{r})$ is a functional of the density $n(\mathbf{r})$ and contains an exchange-correlation term that has to be approximated in practice. The results presented in this section were obtained in a relativistic calculation in local density approximation [82], i.e., the exchange-correlation at any given position $\mathbf{r}$ is approximated by the exchange-correlation in a system with homogeneous electron density and collinear magnetization in a fixed direction. From the ground state $|\Phi\rangle$ of the non-interacting system (with spin-orbit coupling), the density $n'(\mathbf{r}) = \langle\Phi|\psi^\dagger(\mathbf{r})\psi(\mathbf{r})|\Phi\rangle$ is obtained. This density is inserted back into the original problem and the procedure is iterated until a

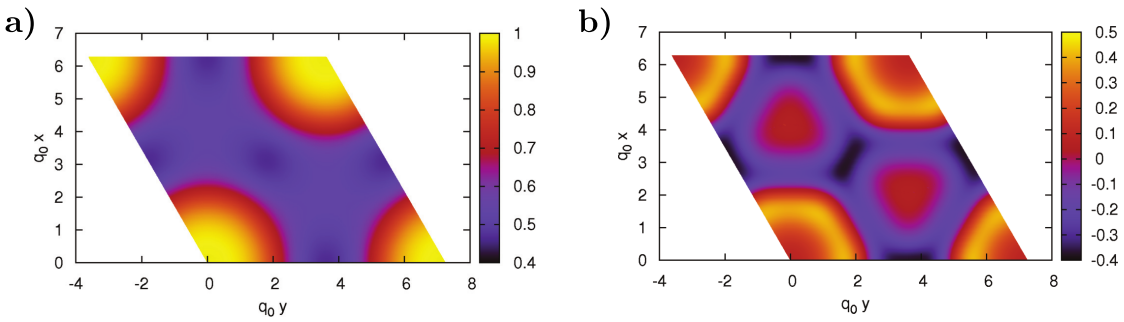

Figure 5.2.: Berry-phase correction to the charge density in MnSi without and with screening. Both figures are taken from Ref. [65]. a) Normalized free energy density $\delta F^{(1)}(\mathbf{r}_c)/\delta F^{(1)}(\mathbf{0})$ and normalized charge density $\delta\rho^{(1)}(\mathbf{r}_c)/\delta\rho^{(1)}(\mathbf{0})$ within the magnetic unit cell, without the effect of screening. The minimal charge density $\delta\rho^{(1)}(\mathbf{0}) = -1.95 \times 10^{-6}\,\mathrm{e/\AA^3}$ (for electrons with charge $-e$) and the minimal free energy density $\delta F^{(1)}(\mathbf{0}) = -0.0018\,\mathrm{meV/\AA^3}$ are both at the center of the skyrmion, which is located at the origin. b) Screened charge density $\delta\rho^{\mathrm{tot}}(\mathbf{r}_c)$ within the magnetic unit cell. The minimal charge density at the center of the skyrmion (origin) is $\delta\rho^{\mathrm{tot}}(\mathbf{0}) = -1.07 \times 10^{-10}\,\mathrm{e/\AA^3}$.

self-consistent solution is obtained. The resulting single-particle Hamiltonian with the self-consistent effective potential $V(\mathbf{r})$ is called Kohn-Sham Hamiltonian. We point out that, even though our semiclassical treatment of Berry-phase effects on the charge and energy density are based on the assumption of noninteracting electrons, the numerical results are exact to linear order in spatial gradients even for the real interacting system, provided that the exact Kohn-Sham Hamiltonian is used.

The calculations were performed in states with collinear magnetization $\mathbf{M} = \mathbf{M}(\mathbf{r}_c)$. The effective single-particle Kohn-Sham Hamiltonian is given by the local Hamiltonian $H_c(\mathbf{r}_c)$, Eq. (5.5), with $\mathbf{A} = \mathbf{0}$ and $\phi = 0$. Here, the effective potential V, the electric field $\mathbf{E} = -\boldsymbol{\nabla}V$ that appears in H_{so} (Eq. (4.22)), and the strength of the exchange field $\mathbf{B}^{\mathrm{ex}}(\mathbf{r}_c)$ were both approximated by their values without SO interaction. We refer to Appendix A of Ref. [65] for details of the numerical parameters.

Results. From the periodic part $|u_{n,t,\mathbf{r}_c,\mathbf{k}}\rangle$ of the eigenstates of the effective single-particle Hamiltonian H_c, the energy correction $\delta\mathcal{E}_n^{(1)}$ and the components of the Berry curvature $\Omega_n^{\mathrm{r,k}}$ were obtained using Eqs. (3.18) and (5.14). The energy and charge density are given by Eqs. (5.35) and (5.36), respectively, and can again be cast into the form of Eq. (5.46) and (5.50), respectively, by using the chain rule,

$$\frac{\partial H_c}{\partial r_i} = \frac{\partial H_c}{\partial \hat{B}_j^{\mathrm{ex}}} \frac{\partial \hat{B}_j^{\mathrm{ex}}}{\partial r_i}. \tag{5.53}$$

The DFT calculations yield, to a good approximation, $D_{ij} \approx -D\delta_{ij}$ with DM interaction strength

$$D = -4.1\,\mathrm{meV\,\AA}/a^3 \tag{5.54}$$

where a^3 is the volume of the eight-atom unit cell with lattice constant $a = 4.558\,\text{Å}$. An experimental value for D can be extracted from the free energy $F(q) \propto Dq + Jq^2$ in the helical phase of MnSi, which has a minimum for a helix with wave vector $q_0 = -D/(2J)$. Using $q_0 = 2\pi/(190\,\text{Å})$ and the exchange coupling $J = 52\,\mathrm{meV\,\AA}^2/a^3$ from neutron scattering experiments [69], one obtains an experimental value of $D = -3.4\,\mathrm{meV\,\AA/a}^3$, in good agreement with our result.

Due to the lattice symmetry, the energy and charge density are proportional to each other and we show both in the same plot, Figure 5.2a, using the magnetization texture from Eq. (5.51). Both $\delta f^{(1)}(\mathbf{r}_\mathrm{c})$ and $\delta\rho^{(1)}(\mathbf{r}_\mathrm{c})$, Eqs. (5.46) and (5.50), are maximal in the center of the skyrmion, located at the origin in Figure 5.2. By integrating $\delta\rho^{(1)}(\mathbf{r}_\mathrm{c})$ over the magnetic unit cell, we obtain a total skyrmion charge[3] of $\delta Q^{(1)} = -0.25e$. However, this result neglects Coulomb interactions, which lead screening of charges on the length-scale of the Thomas-Fermi screening length $\lambda_\mathrm{TF} = \sqrt{\epsilon_0/(e^2\nu_F)}$, see Eq. (5.41). From our DFT calculations, we obtain $\nu_F \approx 0.11/(\mathrm{eV\,\AA}^3)$ and therefore $\lambda_\mathrm{TF} \approx 0.224\,\text{Å} \ll 1/q_0$. The short λ_TF leads to a strong suppression of the charge density $\rho^\mathrm{tot} \approx -\lambda_\mathrm{TF}^2 \boldsymbol{\nabla}^2 \delta\rho^{(1)}$, see Fig. 5.2b.

[3] Note again the different sign convention than in Ref. [77]. In this thesis, SI units with electron charge $-e$ are used.

6. Skyrmion charge from a gradient expansion

In this chapter, we extend our discussion of the electric charge of skyrmions beyond the semiclassical approximation used in chapter 5. To do so, we introduce a complementary method to calculate electronic properties in systems with a smooth magnetization texture, which is based on a systematic gradient expansion of the Green's function. To leading order, the gradient expansion is equivalent to the semiclassical approximation, while higher order contributions lead to corrections to the semiclassical picture. In insulators, we argue that the total electric charge of a skyrmion is quantized and given by the second-order term of the gradient expansion.

This chapter is organized as follows. In section 6.1, we introduce the so-called Wigner representation of quantum-mechanical operators, which separates oscillations on the atomic length scale from modulations on a long length scale. In section 6.2, we use the Wigner representation to expand the equilibrium Green's function of an inhomogeneous system in terms of only local quantities. We use this gradient expansion in section 6.3 to calculate the electric charge of skyrmions in metals and in insulators and we compare to the results obtained within the semiclassical treatment of chapter 5. Parts of this chapter can also be found in our publication, Ref. [65].

6.1. Wigner transformation on a lattice

In this section, we present an efficient representation of quantum-mechanical operators in a system with modulations on a long length scale, such as a smooth magnetization texture. This so-called Wigner representation is defined in Eq. (6.5) below. The remaining parts of this chapter are devoted to some technical issues of the Wigner transformation in presence of a lattice. The impatient reader may decide to skip those more technical parts and return to them once problems with Wigner transformations turn up in calculations.

We consider an operator $\hat{A}$ that is approximately periodic in space on a short length scale set by the lattice constant a, but that is subject to smooth modulations on a length scale $\xi_{\mathrm{mod}} \gg a$. For example, consider the Hamiltonian of a magnet with a smooth magnetization texture. Our aim is to find a representation of $\hat{A}$ in which dependencies on the two length scales are separated into two different coordinates. While periodic systems are most efficiently described in momentum space, modulations on the long length scale ξ_{mod} are more naturally expressed in position space. The Wigner representation uses both position and momentum coordinates. In the literature, the Wigner transform of a

function $f(\mathbf{r}_1, \mathbf{r}_2)$ that depends on two position coordinates is commonly defined as the Fourier transform w.r.t. the relative coordinate $\mathbf{r}_1 - \mathbf{r}_2$ (see, e.g., [83, 84]),

$$\tilde{f}(\mathbf{r}, \mathbf{k}) := \int \mathrm{d}^d\rho \, e^{-i\mathbf{k}\cdot\boldsymbol{\rho}} \, f\Big(\mathbf{r} + \frac{\boldsymbol{\rho}}{2}, \mathbf{r} - \frac{\boldsymbol{\rho}}{2}\Big) \qquad \text{(without a lattice).} \tag{6.1}$$

One can recover the original function $f(\mathbf{r}_1, \mathbf{r}_2)$ from its Wigner transform via the inverse transformation

$$f(\mathbf{r}_1, \mathbf{r}_2) = \int \frac{\mathrm{d}^d k}{(2\pi)^d} \, e^{i\mathbf{k}\cdot(\mathbf{r}_1 - \mathbf{r}_2)} \, \tilde{f}\left(\frac{\mathbf{r}_1 + \mathbf{r}_2}{2}, \mathbf{k}\right) \qquad \text{(without a lattice).} \tag{6.2}$$

In presence of a lattice, however, the definition Eq. (6.1) does not lead to the intended separation of length scales. While Eq. (6.1) encodes short-wavelength oscillations w.r.t. the relative coordinate $\mathbf{r}_1 - \mathbf{r}_2$ in the $\mathbf{k}$-dependency of $\tilde{f}$ as intended, short-wavelength oscillations w.r.t. the center-of-mass coordinate $(\mathbf{r}_1 + \mathbf{r}_2)/2$ still manifest themselves in the $\mathbf{r}$-dependency of $\tilde{f}$. In particular, the Wigner transform $\tilde{G}(\omega; \mathbf{r}, \mathbf{k})$ of the Green's function of an almost-periodic system would oscillate as a function of $\mathbf{r}$ on the short length-scale a if one used the definition in Eq. (6.1).

Definition of the Wigner transform on a lattice. In order to separate the two length scales $\xi_{\mathrm{mod}} \gg a$ into position and momentum dependency, respectively, we use an alternative definition of the Wigner transform in the presence of a lattice. Our description will be valid for a single-particle operator

$$\hat{A} = \hat{A}[\lambda_1(\mathbf{r}), \lambda_2(\mathbf{r}), \ldots] \tag{6.3}$$

that is a functional of some smooth modulation fields $\lambda_i(\mathbf{r})$, which vary on the length scale ξ_{mod}. If all modulation fields are constant in space, $\hat{A}$ becomes exactly periodic in space with periodicities (in the d space dimensions) on the order of a. An example of an operator of the form of Eq. (6.3) is given by the Hamiltonian of our model of a chiral magnet, Eq. (5.4), with time-independent modulation fields $\mathbf{B}^{\mathrm{ex}}$, $\mathbf{A}$, and ϕ. We require that the Hamiltonian $H[\lambda_1(\mathbf{r}), \lambda_2(\mathbf{r}), \ldots]$ of the system is also of the form of Eq. (6.3), and we introduce a reference Hamiltonian $H_0 := H[\Lambda_1, \Lambda_2, \cdots]$, which is obtained by fixing all modulations fields $\lambda_i(\mathbf{r})$ to constant values Λ_i. The eigenstates $\{|n, \mathbf{k}\rangle\}$ of H_0 form a complete set of basis states, and we will use these states as reference states to express the Wigner transform. Since H_0 is a periodic Hamiltonian, its eigenstates are Bloch states,

$$\langle \mathbf{r} | n, \mathbf{k} \rangle = e^{i\mathbf{k}\cdot\mathbf{r}} \, u_{n,\mathbf{k}}(\mathbf{r}) \tag{6.4}$$

where $u_{n,\mathbf{k}}(\mathbf{r})$ is lattice periodic. We assumed that the vector potential $\mathbf{A}$ was set to zero when we fixed the modulation fields to constant values, so that the kinetic and the canonical momentum coincide (cf., discussion below Eq. (5.6)). An important property of the reference states $|n, \mathbf{k}\rangle$ defined in this way is that they are differentiable by $\mathbf{k}$ even at the boundary of the Brillouin zone (BZ), where $\mathbf{k}$ is "wrapped around" to the opposite side of the BZ (see Figure 6.1). This is the main reason why we constructed the

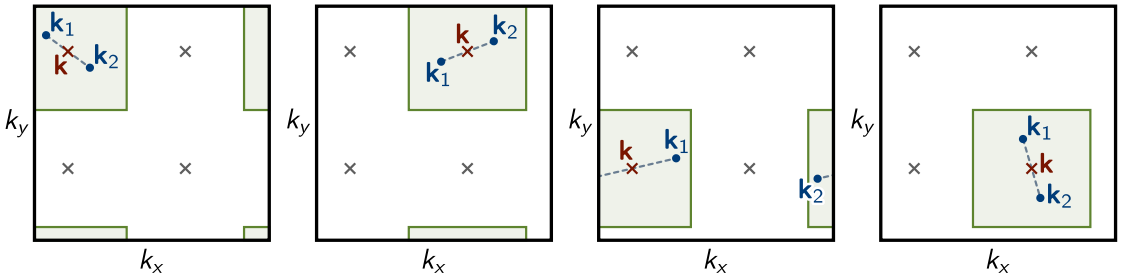

Figure 6.1.: Central wave vector $\mathbf{k}$ in the definition of the Wigner transform, Eq. (6.5). Each of the four subplots depicts the 1st BZ and two lattice wave-vectors $\mathbf{k}_1$ and $\mathbf{k}_2$. Due to the periodic boundary conditions, all four crosses are viable candidates for the center point $\mathbf{k} = (\mathbf{k}_1 + \mathbf{k}_2)/2$ in each plot. By restricting the domain of the $\mathbf{q}$-integration in Eq. (6.5) to the 1st BZ, we make sure that, for any pair of wave vectors $\mathbf{k}_1$ and $\mathbf{k}_2$, the matrix element $\langle m, \mathbf{k}_1 | \hat{A} | n, \mathbf{k}_2 \rangle$ contributes to the WT $\tilde{A}_{mn}(\mathbf{r}, \mathbf{k})$ for exactly one $\mathbf{k}$, marked red in the figure. The shaded areas indicate which wave vectors $\mathbf{k}_1$ and $\mathbf{k}_2$ contribute to the WT at the same wave vector $\mathbf{k}$. By choosing an inversion-symmetric BZ, we make sure that matrix elements with small momentum transfer $|\mathbf{k}_1 - \mathbf{k}_2| \ll 2\pi/a$ always contribute to the WT at a wave vector $\mathbf{k}$ close to $\mathbf{k}_1$ and $\mathbf{k}_2$ (modulo reciprocal lattice vectors). While this requirement is not strictly necessary for Eqs. (6.10) and (6.19) to be valid, it guarantees that $\mathbf{k}$ can be interpreted as an approximately conserved (lattice) wave vector if the Hamiltonian $\tilde{H}(\mathbf{r}, \mathbf{k})$ depends smoothly on $\mathbf{r}$.

reference states explicitly from the eigenstates of a reference Hamiltonian H_0 instead of using, e.g., plain waves with momentum $\mathbf{k}$ wrapped back into the first Brillouin zone. On the other hand, the above choice of reference states is accompanied by the complication that for a band n with non-trivial topology (non-zero Chern number) there is always some momentum $\mathbf{k}_0$ where $|n, \mathbf{k}_0\rangle$ is not differentiable (cf., discussion below Eq. (3.36)). As we will discuss below, this does not invalidate our definition of the Wigner transform, though.

We define the Wigner transform of the operator $\hat{A}$ to be the matrix-valued function

$$\tilde{A}_{mn}(\mathbf{r}, \mathbf{k}) := \int' \frac{\mathrm{d}^d q}{(2\pi)^d} \, e^{i\mathbf{q}\cdot\mathbf{r}} \left\langle m, \mathbf{k} + \frac{\mathbf{q}}{2} \middle| \hat{A} \middle| n, \mathbf{k} - \frac{\mathbf{q}}{2} \right\rangle \tag{6.5}$$

where $\mathbf{k}$ lies in the first Brillouin zone (1st BZ), the integration runs over the 1st BZ, and the momenta $\mathbf{k} \pm \frac{\mathbf{q}}{2}$ are implicitly folded back into the 1st BZ. The prime on the integral symbol indicates that we require the integration region for $\mathbf{q}$ to be inversion-symmetric around the origin in momentum space. Thus, $\mathbf{k} + \frac{\mathbf{q}}{2}$ and $\mathbf{k} - \frac{\mathbf{q}}{2}$ both run over the same region in momentum space, which is only half as big as the 1st BZ (see Figure 6.1). While it is common convention to choose an inversion-symmetric BZ anyway, sometimes a rhomboid with $\mathbf{k} = \mathbf{0}$ at one of its corners is used in calculations. Here, we explicitly

require an inversion-symmetric integration region for $\int' \mathrm{d}^d q$ because $\mathbf{q}$ is the difference between the lattice momenta of the two Bloch states on the right-hand side of Eq. (6.5). Since the BZ is a torus, differences between any two momenta are only defined modulo reciprocal lattice vectors (Figure 6.1). By restricting both $\mathbf{k} + \frac{\mathbf{q}}{2}$ and $\mathbf{k} - \frac{\mathbf{q}}{2}$ to a region of half the Brillouin zone size, centered around $\mathbf{k}$, we make sure that the difference is always measured along the shortest path. In particular, this implies that, for any two wave vectors $\mathbf{k}_1, \mathbf{k}_2 \in \mathrm{BZ}$, the matrix element $\langle m, \mathbf{k}_1 | \hat{A} | n, \mathbf{k}_2 \rangle$ contributes to the WT $\tilde{A}(\mathbf{r}, \mathbf{k})$ at exactly one wave vector $\mathbf{k}$.

Motivation for the definition of the Wigner transform. Our definition of the Wigner transform, Eq. (6.5), provides the desired separation of length scales so that variations on the long length scale ξ_{mod} are encoded in the $\mathbf{r}$-dependency of $\tilde{A}_{mn}(\mathbf{r}, \mathbf{k})$, while oscillations on the atomic length scale a only influence the $\mathbf{k}$-dependency and the matrix structure. This can be seen from the fact that $\tilde{A}_{mn}(\mathbf{r}, \mathbf{k})$ encodes only properties of the operator $\hat{A}$ that are detectable by wave packets from bands m and n which are concentrated in phase space around position $\mathbf{r}$ and (lattice) momentum $\mathbf{k}$. A Gaussian wave packet around point $(\mathbf{r}, \mathbf{k})$ in $2d$-dimensional phase space is given by

$$|\Phi_{n,\mathbf{r},\mathbf{k}}\rangle = \int \frac{\mathrm{d}^d k'}{(2\pi)^d} \, a(\mathbf{k}') \, \big|n, \mathbf{k}'\big\rangle \tag{6.6}$$

with the envelope function

$$a(\mathbf{k}') = \left(\frac{\sqrt{2\pi}}{\Delta k} \right)^{d/2} e^{-\frac{(\mathbf{k}'-\mathbf{k})^2}{4(\Delta k)^2} - i\mathbf{k}'\cdot\mathbf{r}} \tag{6.7}$$

where the width Δk in momentum space is chosen such that $1/\xi_{\mathrm{mod}} \ll \Delta k \ll 1/a$ so that $|\Phi_{n,\mathbf{r},\mathbf{k}}\rangle$ is peaked both in position and in momentum space. Strictly speaking, $a(\mathbf{k}')$ is understood to be periodically continued in momentum space, so that the Gaussian peak wraps around the BZ if $\mathbf{k}$ is located near the edge of the BZ. Assuming that the periodic part $\big|u_{n,\mathbf{k}'}\big\rangle$ of the Bloch states depends sufficiently smoothly on $\mathbf{k}'$, one finds for the expectation value of the position operator, $\langle \Phi_{n,\mathbf{r},\mathbf{k}} | \hat{\mathbf{r}} | \Phi_{n,\mathbf{r},\mathbf{k}} \rangle \approx \mathbf{r}$. The exact expectation value of the position operator depends on the gauge and may deviate from $\mathbf{r}$ at most by a distance on the order of a, provided that the reference states depend smoothly on momentum. We accept this small deviation here in return for a simple definition of the Wigner transform, keeping in mind that whenever we interpret a Wigner transformed function $\tilde{A}(\mathbf{r}, \mathbf{k})$ physically, $\mathbf{r}$ is to be regarded as a coarse-grained position that cannot be resolved beyond the atomic scale. This has implications on the gauge-dependency of $\tilde{A}$ discussed at the end of this section.

The matrix element of an operator $\hat{A}$ between two wave packets that are both centered

around $(\mathbf{r}, \mathbf{k})$ in phase space is given by

$$\begin{aligned}\langle \Phi_{m,\mathbf{r},\mathbf{k}} | \hat{A} | \Phi_{n,\mathbf{r},\mathbf{k}} \rangle &= \int \frac{\mathrm{d}^d k_1'}{(2\pi)^d} \int \frac{\mathrm{d}^d k_2'}{(2\pi)^d}\, a^*(\mathbf{k}_1')\, a(\mathbf{k}_2')\, \langle m, \mathbf{k}_1' | \hat{A} | n, \mathbf{k}_2' \rangle \\ &= \int \frac{\mathrm{d}^d k'}{(2\pi)^d} \int \frac{\mathrm{d}^d q}{(2\pi)^d}\, a^*\Big(\mathbf{k}' + \frac{\mathbf{q}}{2}\Big)\, a\Big(\mathbf{k}' - \frac{\mathbf{q}}{2}\Big) \Big\langle m, \mathbf{k}' + \frac{\mathbf{q}}{2} \Big| \hat{A} \Big| n, \mathbf{k}' - \frac{\mathbf{q}}{2} \Big\rangle \end{aligned} \tag{6.8}$$

where all momentum integrations are over the first Brillouin zone and momentum arguments of Bloch states are implicitly wrapped back into the 1st BZ. If $\hat{A}$ is of the form of Eq. (6.3), then it mediates only small momentum transfer (modulo reciprocal lattice vectors) and the matrix element on the last line of Eq. (6.8) vanishes unless $q \lesssim 1/\xi_{\mathrm{mod}}$. Assuming further that the matrix element depends smoothly on the central momentum $\mathbf{k}$, we can use the fact that the envelope function $a(\mathbf{k}')$ is strongly peaked at $\mathbf{k}$ and approximate $\mathbf{k}' \approx \mathbf{k}$ in the matrix element. Thus, the two momentum integrations factorize,

$$\begin{aligned}\langle \Phi_{m,\mathbf{r},\mathbf{k}} | \hat{A} | \Phi_{n,\mathbf{r},\mathbf{k}} \rangle \approx & \left[\left(\frac{\sqrt{2\pi}}{\Delta k} \right)^d \int \frac{\mathrm{d}^d k'}{(2\pi)^d}\, e^{-\frac{(\mathbf{k}'-\mathbf{k})^2}{2(\Delta k)^2}} \right] \times \\ & \times \left[\int \frac{\mathrm{d}^d q}{(2\pi)^d} e^{-\frac{q^2}{8(\Delta k)^2} + i\mathbf{q}\cdot\mathbf{r}} \Big\langle m, \mathbf{k} + \frac{\mathbf{q}}{2} \Big| \hat{A} \Big| n, \mathbf{k} - \frac{\mathbf{q}}{2} \Big\rangle \right] \\ \approx & \tilde{A}_{mn}(\mathbf{r}, \mathbf{k}) \end{aligned} \tag{6.9}$$

where the integral over $\mathbf{k}'$ evaluates approximately to 1 since we assumed that the peak-width Δk is small compared to the size of the BZ. For $q \lesssim 1/\xi_{\mathrm{mod}} \ll \Delta k$, the factor $e^{-\frac{q^2}{8(\Delta k)^2}} \approx 1$ in the $\mathbf{q}$-integration can be dropped and the right-hand side of Eq. (6.9) reduces to $\tilde{A}_{mn}(\mathbf{r}, \mathbf{k})$. Thus, in the limit $a/\xi_{\mathrm{mod}} \to 0$, the Wigner transform $\tilde{A}_{mn}(\mathbf{r}, \mathbf{k})$ is the matrix element of $\hat{A}$ between two wave packets localized around point $(\mathbf{r}, \mathbf{k})$ in phase space.

Inverse Wigner transformation. Eq. (6.5) defines the Wigner transformation $\tilde{A}_{mn}(\mathbf{r}, \mathbf{k})$ of an operator $\hat{A}$ by a Fourier transform in the relative momentum coordinate. In order to recover the matrix elements of the oberator $\hat{A}$ in the reference basis from $\tilde{A}$, one has to perform the inverse Fourier transform,

$$\langle m, \mathbf{k}_1 | \hat{A} | n, \mathbf{k}_2 \rangle \approx \int \mathrm{d}^d r\, e^{-i(\mathbf{k}_1 - \mathbf{k}_2)\cdot\mathbf{r}} \tilde{A}_{mn}\Big(\mathbf{r}, \frac{\mathbf{k}_1 + \mathbf{k}_2}{2}\Big). \tag{6.10}$$

The inverse transformation is not exact, however, due to the fact that the $\mathbf{q}$-integration in Eq. (6.5) is restricted to a finite area. This issue has been discussed by Genske and Rosch [85] for the Wigner transform of a function $A(t_1, t_2)$ that depends on two times. In their discussion, a filter function was introduced in the defining integrand for the Wigner

transform, which is equal to one if the both t_1 and t_2 are close to the central time. In our definition of the Wigner transformation we effectively introduced a hard-edge filter function by the fact that the contributions where $\mathbf{k} \pm \frac{\mathbf{q}}{2}$ is more than half a reciprocal lattice vector away from $\mathbf{k}$ are cut off from the integral in Eq. (6.5). Eq. (6.10) is a good approximation for the inverse Wigner transformation if the matrix elements of the operator $\mathbf{A}$ fall of rapidly for large momentum transfer $\mathbf{q}$. This is valid if the separation of length scales $\xi_{\mathrm{mod}} \gg a$ holds.

If $\hat{A}$ is the Hamiltonian of the system, then matrix elements with large momentum transfer on the order of reciprocal lattice vectors are related to Landau-Zener tunneling (see Section 3.5). The gradient expansion derived in the next section will therefore not be able to account for Landau-Zener tunneling. This should not come as a surprise since the Landau-Zenter tunnelling probability, Eqs. (3.41)–(3.42) is non-analytic in the parameter $\kappa_{\mathrm{n.a.}}$.

Gauge-dependency. The basis states $|n, \mathbf{k}\rangle$ are only defined up to a gauge transformation

$$|n, \mathbf{k}\rangle \longmapsto |n, \mathbf{k}\rangle' := e^{i\varphi_n(\mathbf{k})} |n, \mathbf{k}\rangle \tag{6.11}$$

where φ_n is a family of real-valued functions. For the Wigner transform, we find to leading order in gradients of φ_n,

$$\begin{aligned} |m, \mathbf{k}\rangle \, \tilde{A}_{mn}(\mathbf{r}, \mathbf{k}) \, \langle n, \mathbf{k}| = \int \frac{\mathrm{d}^d q}{(2\pi)^d} \, e^{i\mathbf{q}\cdot\mathbf{r} + i(\varphi_m(\mathbf{k}+\frac{\mathbf{q}}{2}) - \varphi_m(\mathbf{k})) - i(\varphi_n(\mathbf{k}-\frac{\mathbf{q}}{2}) - \varphi_n(\mathbf{k}))} \times \\ \times |m, \mathbf{k}\rangle' \, {}'\left\langle m, \mathbf{k} + \frac{\mathbf{q}}{2} \middle| \hat{A} \middle| n, \mathbf{k} - \frac{\mathbf{q}}{2} \right\rangle' \, {}'\langle n, \mathbf{k}| \\ \approx |m, k\rangle' \, \tilde{A}'_{mn} \left(\mathbf{r} + \frac{1}{2} \frac{\partial(\varphi_m(\mathbf{k}) + \varphi_n(\mathbf{k}))}{\partial \mathbf{k}}, \mathbf{k} \right) {}'\langle n, \mathbf{k}| \end{aligned} \tag{6.12}$$

where the Wigner transform in the new gauge, $\tilde{A}'_{mn}(\mathbf{r}', \mathbf{k})$, is defined by

$$\tilde{A}'_{mn}(\mathbf{r}', \mathbf{k}) = \int \frac{\mathrm{d}^d q}{(2\pi)^d} \, e^{i\mathbf{q}\cdot\mathbf{r}'} \, {}'\left\langle m, \mathbf{k} + \frac{\mathbf{q}}{2} \middle| \hat{A} \middle| n, \mathbf{k} - \frac{\mathbf{q}}{2} \right\rangle' \tag{6.13}$$

and we neglected terms with higher-order derivatives. In Eq. (6.12), $\tilde{A}'_{mn}(\mathbf{r}', \mathbf{k})$ is evaluated at position $\mathbf{r}' = \mathbf{r} + \frac{1}{2}\frac{\partial}{\partial \mathbf{k}}(\varphi_m + \varphi_n)$. The difference between $\mathbf{r}$ and $\mathbf{r}'$ is a consequence of the fact that the Wigner transform is a function of the canonical position. To first order in the gradients, the canonical position differs from the kinetic (i.e., physical) position by the momentum-space Berry connection $\boldsymbol{\mathcal{A}}_{n,\mathbf{k}} = i \, \langle u_{n,\mathbf{k}} | \frac{\partial}{\partial \mathbf{k}} | u_{n,\mathbf{k}} \rangle$, which changes under the gauge transformation Eq. (6.11).

Note that the interpretation, Eq. (6.9), of the Wigner transformation in terms of wave-packets is only valid in a gauge in which the periodic part $|u_{n,\mathbf{k}}\rangle$ of the Bloch states depends smoothly on $\mathbf{k}$ (only then are the wave packets localized in position space). For gauge transformations that preserve this property, the shift in position $\mathbf{r}' - \mathbf{r}$ is at most on the order of the lattice constant a, which cannot be resolved by the wave

packets defined in Eq. (6.6). In the following, we will therefore interpret the parameter $\mathbf{r}$ of a Wigner transform $\tilde{A}(\mathbf{r},\mathbf{k})$ as a coarse-grained physical position that does not resolve oscillations on the atomic length scale a, and we will thus neglect the gauge-dependency of $\mathbf{r}$ when we interpret, e.g., the charge density $\rho(\mathbf{r})$ physically. The fact that $\tilde{A}(\mathbf{r},\mathbf{k})$ is a function of the canonical position $\mathbf{r}$ is related to the non-constant density of states in the presence of phase-space Berry phases (see section 5.2): If the momentum-space Berry curvature $\boldsymbol{\mathcal{A}}_{n,\mathbf{k}}$ depends on position $\mathbf{r}$, then close-by points of the kinetic position $\mathbf{r}-\boldsymbol{\mathcal{A}}_{n,\mathbf{k}}$ increase or reduce in density by moving closer together or further apart. We will show in Section 6.3 that the resulting change of charge density $\delta\rho(\mathbf{r})$ is correctly captured by our method even though we neglect the gauge dependency of $\mathbf{r}$. The only downside is that the precise position where the increased or decreased charge density appears cannot be resolved beyond the length scale $a \ll \xi_{\mathrm{mod}}$.

There is a subtle issue with the choice of gauge for the Wigner transform $\tilde{A}_{mn}(\mathbf{r},\mathbf{k})$ in case of a topologically non-trivial band structure. If either of the bands m or n has a non-zero Chern number, the Bloch states of that band cannot be differentiable by $\mathbf{k}$ on the whole Brillouin zone. To make sure that $\tilde{A}_{mn}(\mathbf{r},\mathbf{k})$ is differentiable on an open neighborhood of $\mathbf{k}$, we choose a gauge such that all Bloch states are differentiable on the whole region accessible to $\mathbf{k}\pm\frac{\mathbf{q}}{2}$ in Eq. (6.5), i.e., we push the singularities of $\boldsymbol{\nabla}_k\,|n,\mathbf{k}\rangle$ out of the integration region. Using this gauge, we define $\tilde{A}_{mn}(\mathbf{r},\mathbf{k})$ according to Eq. (6.5) for all $\mathbf{k}\in\mathcal{U}_1$ where the open region $\mathcal{U}_1\subset\mathrm{BZ}$ is defined by the condition that $\mathbf{k}$ is more than half a reciprocal lattice vector away from all singularities. Once $\mathbf{k}$ comes closer than half a reciprocal lattice vector to a singularity, a different gauge has to be used, which will become a valid choice on some other open region $\mathcal{U}_2\subset\mathrm{BZ}$. Thus, for topologically non-trivial bands, one has to cover the BZ with a finite set of open regions $\mathcal{U}_i$ and define $\tilde{A}_{mn}(\mathbf{r},\mathbf{k})$ for $\mathbf{k}\in\mathcal{U}_i$ using an appropriate gauge on each patch. Whenever two patches $\mathcal{U}_i$ and $\mathcal{U}_j$ overlap, the two corresponding definitions for $\tilde{A}_{mn}(\mathbf{r},\mathbf{k})$ have to agree on the intersection $\mathcal{U}_i\cap\mathcal{U}_j$. The author is not aware of a rigorous proof that this procedure is always possible.

6.2. Local Green's function and gradient expansion

Based on the Wigner transform introduced in the preceding section, we derive in this section a perturbative expression of the Green's function of an almost-periodic system. We consider a time-independent system of non-interacting electrons whose single-particle Hamiltonian H is of the form of Eq. (6.3). The equilibrium Green's function is defined by

$$G_{\sigma_1,\sigma_2}(i\hbar\omega_n;\mathbf{r}_1,\mathbf{r}_2) = -\frac{1}{\mathcal{Z}}\int_0^\beta \mathrm{d}\tau\, e^{i\omega_n\tau}\,\mathrm{Tr}\Big[e^{-(\beta-\tau)\mathcal{H}}\,\psi_{\sigma_1}(\mathbf{r}_1)\,e^{-\tau\mathcal{H}}\,\psi^\dagger_{\sigma_2}(\mathbf{r}_2)\Big] \tag{6.14}$$

where $\mathcal{Z}=\mathrm{Tr}\big[e^{-\beta\mathcal{H}}\big]$ is the partition function, $\beta=1/(k_BT)$ is the inverse temperature, $\omega_n=2\pi(n+\frac{1}{2})k_BT/\hbar$ is a fermionic Matsubara frequency, $\psi^\dagger_\sigma(\mathbf{r})$ ($\psi_\sigma(\mathbf{r})$) creates (annihilates) an electron with spin σ at position $\mathbf{r}$, and $\mathcal{H}=\int\mathrm{d}^dr\,\psi^\dagger(\mathbf{r})H\psi(\mathbf{r})$ is the Hamiltonian

in second quantized form. The Green's function satisfies the matrix relation

$$(i\hbar\omega_n \mathbb{1}_{\text{spin}} - H_{\mathbf{r}_1})\, G(i\omega_n; \mathbf{r}_1, \mathbf{r}_2) = \mathbb{1}_{\text{spin}}\, \delta(\mathbf{r}_1 - \mathbf{r}_2) \tag{6.15}$$

where the notation $H_{\mathbf{r}_1}$ indicates that the Hamiltonian acts as a differential operator on the argument $\mathbf{r}_1$ of the Green's function, and $\mathbb{1}_{\text{spin}}$ is the identity operator in spin space. Thus, the Green's function can formally be obtained by inversion of the single-particle Hamiltonian,

$$\hat{G}(i\hbar\omega_n) = (i\omega_n - H)^{-1} \tag{6.16}$$

where $\hat{G}(i\omega_n)$ is understood as an operator on the single-particle Hilbert space,

$$\hat{G}(i\omega_n) := \sum_{\sigma_1,\sigma_2} \int \mathrm{d}^d r_1 \int \mathrm{d}^d r_2\ |\sigma_1, \mathbf{r}_1\rangle\, G_{\sigma_1,\sigma_2}(i\omega_n; \mathbf{r}_1, \mathbf{r}_2)\, \langle\sigma_2, \mathbf{r}_2| \tag{6.17}$$

where $|\sigma, \mathbf{r}\rangle$ are eigenstates of the position operator and of the z-component of the spin operator.

Moyal product. If H is lattice-periodic, the operator inversion on the right-hand side of Eq. (6.16) can be reduced to the inversion of a matrix in band space using Bloch theorem. If H is not lattice-periodic, it is in general difficult to calculate its inverse $\hat{G}(i\omega_n)$ exactly. However, one can use a perturbative expansion of $\hat{G}(i\omega_n)$ if H is of the form of Eq. (6.3), i.e., if there is a separation of the length scales a and $\xi_{\text{mod}} \gg a$ of the lattice constant and smooth modulations, respectively. To make the separation of length scales explicit, we use Wigner representation and denote by $\tilde{H}(\mathbf{r}, \mathbf{k})$ and $\tilde{G}(i\omega_n; \mathbf{r}, \mathbf{k})$ the Wigner transform, defined in Eq. (6.5), of H and $\hat{G}(i\omega_n)$, respectively. In Wigner representation, Eq. (6.15) becomes

$$\sum_l (i\hbar\omega_n \delta_{ml} - \tilde{H}_{ml}(\mathbf{r}, \mathbf{k})) \circ \tilde{G}_{lj}(i\omega_n; \mathbf{r}, \mathbf{k}) = \delta_{mj}. \tag{6.18}$$

where the symbol "$\circ$" denotes the so-called Moyal product [83, 86], which is defined for the Wigner transforms of two operators $\hat{A}$ and $\hat{B}$ by

$$\tilde{A}(\mathbf{r}, \mathbf{k}) \circ \tilde{B}(\mathbf{r}, \mathbf{k}) := \tilde{A}(\mathbf{r}, \mathbf{k})\, e^{\frac{i}{2}(\overleftarrow{\partial_{\mathbf{r}}}\cdot\overrightarrow{\partial_{\mathbf{k}}} - \overleftarrow{\partial_{\mathbf{k}}}\cdot\overrightarrow{\partial_{\mathbf{r}}})}\ \tilde{B}(\mathbf{r}, \mathbf{k}) = \tilde{A}(x)\, e^{\frac{i}{2} J_{ij} \overleftarrow{\partial_i}\overrightarrow{\partial_j}}\ \tilde{B}(x). \tag{6.19}$$

Here, the exponential function is understood as a formal power series and the symbol $\overleftarrow{\partial}$ ($\overrightarrow{\partial}$) denotes a partial derivative that acts on the function to the left (right). In the last equality in Eq. (6.19), we introduce a shorthand notation where $x \equiv (\mathbf{r}, \mathbf{k})$ is the combined phase-space coordinate, J is the canonical symplectic form defined in Eq. (5.3), and summation over repeated indices is implied. Eq. (6.19) can be shown by explicitly inserting the definition of Wigner transform for both $\tilde{A}$ and $\tilde{B}$ and integrating by parts.

Gradient expansion of the Green's function. In order to calculate local properties of the inhomogeneous system, we express the Wigner transform $\tilde{G}(i\omega_n; x)$ of the Green's function in a perturbative gradient expansion by truncating the exponential series in

Eq. (6.19). Both terms in the exponent in Eq. (6.19) involve one differentiation in position and one in momentum space. We expect that all Wigner transforms vary on a length scale ξ_{mod} in position space and on a scale of $1/a$ in momentum space, so that an expansion of the exponential series in Eq. (6.19) corresponds to an expansion in $a/\xi_{\mathrm{mod}} \ll 1$.

Technically, we write $\tilde{G}(i\omega_n; x)$ as

$$\tilde{G}(i\omega_n; x) \approx \tilde{G}^{(0)}(i\omega_n; x) + \tilde{G}^{(1)}(i\omega_n; x) + \tilde{G}^{(2)}(i\omega_n; x) + \mathcal{O}(\partial_{\mathbf{r}}^3) \tag{6.20}$$

where the superscript denotes the total order of spatial gradients. In this chapter, our aim is to calculate the leading order contribution to the charge density in a skyrmion, which turns out to be linear in $\partial_{\mathbf{r}}$ in metals and quadratic in insulators (see Section 6.3). Therefore, we truncate the expansion in Eq. (6.20) after the second order.

Local Green's function. To zero'th order in the gradients, we obtain from Eqs. (6.18)–(6.20),

$$\tilde{G}^{(0)}(i\omega_n; x) = (i\hbar\omega_n - \tilde{H}(x))^{-1} =: \tilde{g}(i\omega_n; x). \tag{6.21}$$

Here, the notation $(\cdots)^{-1}$ is to be understood as a pointwise inversion of $(i\omega_n - \tilde{H}(x))$, which is a matrix in band space for every point x in phase space. Computationally, the pointwise inversion of a band-matrix is an easier operation than the original operator inversion in the full Hilbert space, Eq. (6.16). We refer to $\tilde{g}(i\omega_n; x)$ as the *local Green's function*, since a truncation of Eq. (6.19) at zero'th order is analogous to a local density approximation.

Gradient corrections. To first order in the gradients, Eqs. (6.18)–(6.20) yield the relation

$$\tilde{g}^{-1}(i\omega_n; x)\, \tilde{G}^{(1)}(i\omega_n; x) + \frac{i}{2} J_{ij}\, (\partial_i \tilde{g}^{-1}(i\omega_n; x))\, (\partial_j \tilde{g}(i\omega_n; x)) = 0 \tag{6.22}$$

which can be solved for $\tilde{G}^{(1)}(i\omega_n; x)$,

$$\tilde{G}^{(1)} = \frac{i}{2} J_{ij}\, \tilde{g}\, (\partial_i \tilde{H})\, \tilde{g}\, (\partial_j \tilde{H})\, \tilde{g} \equiv \tag{6.23}$$

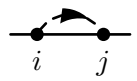

where we omitted all dependencies on ω_n and x to improve readability, with the understanding that all matrix inversions are again pointwise. In the last step in Eq. (6.23), we introduce a pictorial notation. Each solid line in our diagrams corresponds to a local Green's function $\tilde{g}$, a vertex with label i represents a factor of $\partial_i \tilde{H}$, and a dashed arrow from vertex i to vertex j denotes multiplication with $\frac{i}{2} J_{ij}$ and summation over i and j.

The second-order part of Eqs. (6.18)–(6.20) is

$$\tilde{g}^{-1}\, \tilde{G}^{(2)} + \frac{i}{2} J_{ij}\, (\partial_i \tilde{g}^{-1})\, (\partial_j \tilde{G}^{(1)}) + \frac{1}{2}\left(\frac{i}{2}\right)^2 J_{ij} J_{kl}\, (\partial_i \partial_k \tilde{g}^{-1})\, (\partial_j \partial_l \tilde{g}) = 0 \tag{6.24}$$

which has the solution (using the pictorial notation introduced in Eq. (6.23))

$\tilde{G}^{(2)} =$ 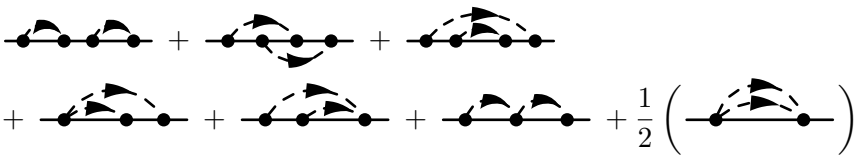 (6.25)

where, e.g., the first diagram on the second line represents the term

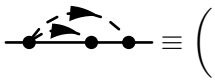 $\equiv \left(\frac{i}{2}\right)^2 J_{ij} J_{kl}\; \tilde{g}\,(\partial_i \partial_k \tilde{H})\,\tilde{g}\,(\partial_j \tilde{H})\,\tilde{g}\,(\partial_l \tilde{H})\,\tilde{g}.$ (6.26)

Comparison between local Hamiltonian $\tilde{H}_\mathbf{c}$ and Wigner transformed Hamiltonian $\tilde{H}$. In Eq. (6.21), we defined the local Green's function $\tilde{g}(i\omega_n; \mathbf{r}, \mathbf{k})$ as the pointwise inverse of $(i\omega_n - \tilde{H}(\mathbf{r}, \mathbf{k}))$. Thus, for a fixed position $\mathbf{r}_\mathrm{c}$, $\tilde{g}(i\omega_n; \mathbf{r}_\mathrm{c}, \mathbf{k})$ is the Green's function of a (fictitious) homogeneous system described by the band Hamiltonian $\tilde{H}(\mathbf{r}_\mathrm{c}, \mathbf{k})$. While, in this sense, $\tilde{H}(\mathbf{r}_\mathrm{c}, \mathbf{k})$ describes electron dynamics locally in the vicinity of $\mathbf{r}_\mathrm{c}$, it is worth noting the differences between $\tilde{H}(\mathbf{r}_\mathrm{c}, \mathbf{k})$ and the local band Hamiltonian $\tilde{H}_\mathrm{c}(\mathbf{r}_\mathrm{c}, \mathbf{k})$ defined in Eqs. (5.5) and (5.8). As an example, we consider the time-independent Hamiltonian

$$H = H_0 + \mathbf{B}^\mathrm{ex}(\mathbf{r}) \cdot \boldsymbol{\sigma} \tag{6.27}$$

where H_0 is lattice periodic, the exchange field $\mathbf{B}^\mathrm{ex}$ varies on a length scale ($\xi_\mathrm{mod} \gg a$), and $\boldsymbol{\sigma}$ is the vector of Pauli matrices. The local Hamiltonian, Eq. (5.5), is obtained by evaluating $\mathbf{B}^\mathrm{ex}$ at position $\mathbf{r}_\mathrm{c}$. Its eigenstates are the Bloch states $|\Phi_{n,\mathbf{r}_\mathrm{c},\mathbf{k}}\rangle$ defined in Eq. (5.6), so that, in its eigenbasis, the local band Hamiltonian $\tilde{H}_\mathrm{c}(\mathbf{r}_\mathrm{c}, \mathbf{k})$, Eq. (5.8), is the matrix-valued function

$$\Big(\tilde{H}_\mathrm{c}(\mathbf{r}_\mathrm{c}, \mathbf{k})\Big)_{mn} \equiv \langle \Phi_{m,\mathbf{r}_\mathrm{c},\mathbf{k}} | (H_0 + \mathbf{B}^\mathrm{ex}(\mathbf{r}_\mathrm{c})) | \Phi_{n,\mathbf{r}_\mathrm{c},\mathbf{k}} \rangle = \delta_{mn}\, \mathcal{E}_n^{(0)}(\mathbf{r}_\mathrm{c}, \mathbf{k}). \tag{6.28}$$

In order to compare the local band Hamiltonian $\tilde{H}_\mathrm{c}$ to the Wigner transformed Hamiltonian $\tilde{H}$, we express the exchange field in terms of its Fourier transform $\tilde{\mathbf{B}}^\mathrm{ex}(\mathbf{q})$,

$$\mathbf{B}^\mathrm{ex}(\mathbf{r}) = \int \frac{\mathrm{d}^d q}{(2\pi)^d}\, \tilde{\mathbf{B}}^\mathrm{ex}(\mathbf{q})\, e^{i\mathbf{q}\cdot\mathbf{r}} \tag{6.29}$$

and evaluate $\tilde{H}$ at position $\mathbf{r}_\mathrm{c}$ in the same basis states $|\Phi_{n,\mathbf{r}_\mathrm{c},\mathbf{k}}\rangle$,

$$\begin{aligned}\tilde{H}_{mn}(\mathbf{r}_\mathrm{c}, \mathbf{k}) = \langle \Phi_{m,\mathbf{r}_\mathrm{c},\mathbf{k}} | H_0 | \Phi_{n,\mathbf{r}_\mathrm{c},\mathbf{k}} \rangle + \int \frac{\mathrm{d}^d q}{(2\pi)^d} \int \frac{\mathrm{d}^d q'}{(2\pi)^d} \int \mathrm{d}^d r'\, e^{i\mathbf{q}\cdot\mathbf{r}_\mathrm{c} + i(\mathbf{q}'-\mathbf{q})\cdot\mathbf{r}'} \times \\ \times\, u^*_{m,\mathbf{r}_\mathrm{c},\mathbf{k}+\frac{\mathbf{q}}{2}}(\mathbf{r}')\, \tilde{\mathbf{B}}^\mathrm{ex}(\mathbf{q}') \cdot \boldsymbol{\sigma}\, u_{n,\mathbf{r}_\mathrm{c},\mathbf{k}-\frac{\mathbf{q}}{2}}(\mathbf{r}')\end{aligned} \tag{6.30}$$

where u is the lattice-periodic part of the Bloch functions Φ. Assuming that $\tilde{\mathbf{B}}^{\mathrm{ex}}(\mathbf{q}')$ is non-vanishing only for small momenta $q' \lesssim 1/\xi_{\mathrm{mod}} \ll 1/a$ and neglecting Umklapp-scattering off the magnetic texture, the integral over $\mathbf{r}'$ vanishes unless $\mathbf{q} = \mathbf{q}'$. Therefore, we find

$$\tilde{H}_{mn}(\mathbf{r}_{\mathrm{c}}, \mathbf{k}) = \langle \Phi_{m,\mathbf{r}_{\mathrm{c}},\mathbf{k}} | H_0 | \Phi_{n,\mathbf{r}_{\mathrm{c}},\mathbf{k}} \rangle + \int \frac{\mathrm{d}^d q}{(2\pi)^d} \, e^{i\mathbf{q}\cdot\mathbf{r}_{\mathrm{c}}} \, \tilde{\mathbf{B}}^{\mathrm{ex}}(\mathbf{q}) \cdot \langle u_{m,\mathbf{r}_{\mathrm{c}},\mathbf{k}+\frac{\mathbf{q}}{2}} | \boldsymbol{\sigma} | u_{n,\mathbf{r}_{\mathrm{c}},\mathbf{k}-\frac{\mathbf{q}}{2}} \rangle \, . \tag{6.31}$$

If one neglects the momentum-dependency of the lattice-periodic states $|u_{n,\mathbf{r}_{\mathrm{c}},\mathbf{k}\pm\frac{\mathbf{q}}{2}}\rangle$, then the right-hand side of Eq. (6.31) reduces to the local band Hamiltonian, Eq. (6.28). Gradient corrections lead to differences between $\tilde{H}$ and $\tilde{H}_{\mathrm{c}}$. Expanding the matrix-element on the right-hand side of Eq. (6.31) to first order in $\mathbf{q}$, one obtains

$$\tilde{H}_{mn}(\mathbf{r}_{\mathrm{c}}, \mathbf{k}) \approx \Big(\tilde{H}_{\mathrm{c}}(\mathbf{r}_{\mathrm{c}}, \mathbf{k}) \Big)_{mn} - i \, \frac{\partial B_i^{\mathrm{ex}}(\mathbf{r})}{\partial r_{\mathrm{c},j}} \, \langle u_{m,\mathbf{r}_{\mathrm{c}},\mathbf{k}} | \, \sigma_i \frac{\partial \, | u_{n,\mathbf{r}_{\mathrm{c}},\mathbf{k}} \rangle}{\partial k_j} + \mathcal{O}((a/\xi_{\mathrm{mod}})^2). \tag{6.32}$$

If H_0 is spin-independent (i.e., without SO-coupling), the states $|u_{n,\mathbf{r}_{\mathrm{c}},\mathbf{k}}\rangle$ are eigenstates of $\mathbf{B}^{\mathrm{ex}}(\mathbf{r}_{\mathrm{c}}) \cdot \boldsymbol{\sigma}$ for all n and $\mathbf{k}$, so that

$$\tilde{H}_{mn}(\mathbf{r}_{\mathrm{c}}, \mathbf{k}) \approx \Big(\tilde{H}_{\mathrm{c}}(\mathbf{r}_{\mathrm{c}} - \boldsymbol{\mathcal{A}}^{\mathrm{k}}_{mn}(\mathbf{r}_{\mathrm{c}}, \mathbf{k}), \mathbf{k}) \Big)_{mn} + \mathcal{O}((a/\xi_{\mathrm{mod}})^2) \tag{6.33}$$

where the hermitian matrix

$$\boldsymbol{\mathcal{A}}^{\mathrm{k}}_{mn}(\mathbf{r}_{\mathrm{c}}, \mathbf{k}) := i \, \langle u_{m,\mathbf{r}_{\mathrm{c}},\mathbf{k}} | \, \frac{\partial \, | u_{n,\mathbf{r}_{\mathrm{c}},\mathbf{k}} \rangle}{\partial \mathbf{k}} \tag{6.34}$$

contains the momentum-space Berry connection on its diagonal components. In a chiral magnet, SO-coupling is smaller than exchange interaction by a factor of $\sim a/\xi_{\mathrm{mod}}$, so that Eq. (6.33) is even valid in presence of SO-coupling.

Therefore, we find that, in the limit $a/\xi_{\mathrm{mod}} \to 0$, the Wigner transformed Hamiltonian $\tilde{H}$ coincides with the local band Hamiltonian $\tilde{H}_{\mathrm{c}}$. To first order in the spatial gradients, the two Hamiltonians differ only due to the fact that we defined $\tilde{H}$ as a function of the canonical position, see also discussion below Eq. (6.13). To second order in the spatial gradients, the Wigner transformed Hamiltonian $\tilde{H}$ and the local band Hamiltonian $\tilde{H}_{\mathrm{c}}$ are different. Philosophically, $\tilde{H}_{\mathrm{c}}(\mathbf{r}_{\mathrm{c}}, \mathbf{k})$ is an educated guess of a lattice-periodic Hamiltonian around which the full Hamiltonian, Eq. (6.27), can be efficiently expanded in order to describe physical properties in the vicinity of $\mathbf{r}_{\mathrm{c}}$. The Wigner-transformed Hamiltonian $\tilde{H}(\mathbf{r}, \mathbf{k})$, on the other hand, is an effective Hamiltonian that is "felt" by wave packets centered around a position close to $\mathbf{r}$, where the exact center-of-mass position of the wave packets depends on the gauge. We allowed for a small deviation $\sim a$ between $\mathbf{r}$ and the exact center-of-mass position of the wave packets in order to simplify the definition of the Wigner transform.

6.3. Skyrmion charge

In this section, we derive general expressions for the charge density due to phase-space Berry phases in metals and in insulators, based on the gradient expansion of the Wigner transformed Green's function $\tilde{G}(i\omega_n; \mathbf{r}, \mathbf{k})$. As discussed in section 6.1, the position argument $\mathbf{r}$ of any Wigner transform is to be understood as a coarse-grained position, and does not resolve fluctuations beyond atomic resolution. Therefore, we calculate in this section a coarse-grained charge density $\rho(\mathbf{R})$, which is only defined on lattice sites $\mathbf{R} \in \mathcal{L}$ by

$$\rho(\mathbf{R}) := -e \sum_m \langle\langle \phi_m^\dagger(\mathbf{R}) \phi_m(\mathbf{R}) \rangle\rangle, \qquad \mathbf{R} \in \mathcal{L} \tag{6.35}$$

where $-e$ is the electron charge, $\langle\langle \cdots \rangle\rangle$ denotes both thermal and quantum-mechanical averaging, and $\phi_m^\dagger(\mathbf{R})$ ($\phi_m(\mathbf{R})$) creates (annihilates) an electron in an orbital that is concentrated around lattice site $\mathbf{R}$ and that contains only states from band m. Specifically, we use the Wannier states, which are created by

$$\phi_m^\dagger(\mathbf{R}) := \int \frac{\mathrm{d}^d k}{(2\pi)^d} \, e^{-i\mathbf{k}\cdot\mathbf{R}} \, a_{m,\mathbf{k}}^\dagger, \qquad \mathbf{R} \in \mathcal{L} \tag{6.36}$$

where $a_{m,\mathbf{k}}^\dagger$ creates an electron in the basis state $|m, \mathbf{k}\rangle$ defined in Eq. (6.4). Since the Wannier states form an orthonormal basis of the single-particle Hilbert space, the total charge of the system is given by $Q = \sum_{\mathbf{R}\in\mathcal{L}} \rho(\mathbf{R})$. For a sufficiently smooth gauge of the reference states $|m, \mathbf{k}\rangle$, the Wannier states are localized in space around $\mathbf{R}$, which justifies the interpretation of $\rho(\mathbf{R})$ as a coarse-grained local charge density.[1]

Combining Eqs. (6.35)–(6.36), we find,

$$\begin{aligned}
\rho(\mathbf{R}) &= -e \sum_m \int \frac{\mathrm{d}^d k_1}{(2\pi)^d} \int \frac{\mathrm{d}^d k_2}{(2\pi)^d} \, e^{i(\mathbf{k}_1 - \mathbf{k}_2)\cdot\mathbf{R}} \, \langle\langle a_{m,\mathbf{k}_2}^\dagger a_{m,\mathbf{k}_1} \rangle\rangle \\
&= -e \, \frac{1}{\beta} \sum_{\omega_n} \sum_m \int \frac{\mathrm{d}^d k_1}{(2\pi)^d} \int \frac{\mathrm{d}^d k_2}{(2\pi)^d} \, e^{i(\mathbf{k}_1 - \mathbf{k}_2)\cdot\mathbf{R}} \, \langle m, \mathbf{k}_1 | \hat{G}(i\omega_n) | m, \mathbf{k}_2 \rangle \\
&= -e \, \frac{1}{\beta} \sum_{\omega_n} \sum_m \int \frac{\mathrm{d}^d k}{(2\pi)^d} \int \frac{\mathrm{d}^d q}{(2\pi)^d} \, e^{i(\mathbf{q}+\mathbf{g})\cdot\mathbf{R}} \, \left\langle m, \mathbf{k} + \frac{\mathbf{q}}{2} \middle| \hat{G}(i\omega_n) \middle| m, \mathbf{k} - \frac{\mathbf{q}}{2} \right\rangle
\end{aligned} \tag{6.37}$$

where $\beta = 1/(k_B T)$ is the inverse temperature, $\hat{G}(i\omega_n)$ is defined in Eq. (6.17), all momentum integrations run over the 1st BZ, and momentum arguments to the Bloch states $|m, \mathbf{k} \pm \frac{\mathbf{q}}{2}\rangle$ are implicitly folded back into the 1st BZ. In the last line of Eq. (6.37), the reciprocal lattice vector $\mathbf{g}$ compensates for the fact that, in the second line of Eq. (6.37), $\mathbf{k}_1 - \mathbf{k}_2$ may run outside of the 1st BZ. Since we defined $\rho(\mathbf{R})$ only for lattice sites $\mathbf{R} \in \mathcal{L}$, we have $e^{i\mathbf{g}\cdot\mathbf{R}} = 1$ and we conclude, using Eq. (6.5),

$$\rho(\mathbf{R}) = -e \, \frac{1}{\beta} \sum_{\omega_n} \int \frac{\mathrm{d}^d k}{(2\pi)^d} \, \mathrm{Tr}\Big[\tilde{G}(i\omega_n; \mathbf{R}, \mathbf{k})\Big] \tag{6.38}$$

[1] We point out, however, that a gauge where all Wannier states are localized close to a given point $\mathbf{R}$ in space does not necessarily exist in case of a topologically non-trivial band structure.

where the trace runs over all bands.

Charge density in metals. We obtain a perturbative expression for the charge density by inserting the gradient expansion of the Green's function, Eq. (6.20), into Eq. (6.38). To zero'th order in the spatial gradients, the local Green's function $\tilde{g}(i\omega_n; \mathbf{R}, \mathbf{k}) = (i\hbar\omega_n - \tilde{H}(\mathbf{R}, \mathbf{k}))^{-1}$ is given by the pointwise inverse of the Wigner transformed Hamiltonian (Eq. (6.21)). Therefore, the zero-order charge density $\rho^{(0)}(\mathbf{R})$ is the average charge density one would find in a lattice-periodic system with band Hamiltonian $\tilde{H}(\mathbf{R}, \mathbf{k})$ for fixed $\mathbf{R}$.

In metals, the leading-order correction $\delta\rho^{(1)}(\mathbf{R})$ to the charge density is first order in the spatial gradients. Inserting Eq. (6.23) into Eq. (6.38) and evaluating the Matsubara summation, we find

$$\delta\rho^{(1)}(\mathbf{R}) = e\frac{i}{2}J_{ij}\int\frac{\mathrm{d}^d k}{(2\pi)^d}\int_{-\infty}^{\infty}\frac{\mathrm{d}\epsilon}{2\pi i}\, n_F(\epsilon-\mu)\ \mathrm{Tr}\Big[\tilde{g}^R(\partial_i\tilde{H})\tilde{g}^R(\partial_j\tilde{H})\tilde{g}^R - \tilde{g}^A(\partial_i\tilde{H})\tilde{g}^A(\partial_j\tilde{H})\tilde{g}^A\Big] \tag{6.39}$$

where μ is the chemical potential, $n_F(\epsilon-\mu) = 1/(1+e^{\beta(\epsilon-\mu)})$ is the Fermi function, and $\tilde{g}^R$ ($\tilde{g}^A$) is the retarded (advanced) local Green's function, i.e., the local Green's function $\tilde{g}$ evaluated at frequencies $\epsilon/\hbar + i0^+$ ($\epsilon/\hbar - i0^+$) just above (below) the real axis. Using the cyclicity of the trace and the relations $2i\,\mathrm{Im}[\tilde{g}] = \tilde{g}^R - \tilde{g}^A$ and $\partial\tilde{g}^{R/A}/\partial\epsilon = -(\tilde{g}^{R/A})^2$ leads to,

$$\delta\rho^{(1)}(\mathbf{R}) = ieJ_{ij}\int\frac{\mathrm{d}^d k}{(2\pi)^d}\int_{-\infty}^{\infty}\frac{\mathrm{d}\epsilon}{2\pi}\, n_F(\epsilon-\mu)\ \mathrm{Tr}\Big[(\tilde{g}^A)^2(\partial_i\tilde{H})\,\mathrm{Im}[\tilde{g}](\partial_j\tilde{H}) - \frac{\partial\,\mathrm{Im}[\tilde{g}]}{\partial\epsilon}(\partial_i\tilde{H})\tilde{g}^R(\partial_j\tilde{H})\Big] \tag{6.40}$$

We integrate by parts over ϵ in the second term in the trace and use the anti-symmetry of J_{ij} to arrive at

$$\delta\rho^{(1)}(\mathbf{R}) = ieJ_{ij}\int\frac{\mathrm{d}^d k}{(2\pi)^d}\int_{-\infty}^{\infty}\frac{\mathrm{d}\epsilon}{2\pi}\Big(-n_F(\epsilon-\mu)\,\mathrm{Tr}\Big[\mathrm{Im}[\tilde{g}]\,(\partial_i\tilde{H})\,\big((\tilde{g}^R)^2+(\tilde{g}^A)^2\big)\,(\partial_j\tilde{H})\Big] + n_F'(\epsilon-\mu)\,\mathrm{Tr}\Big[\mathrm{Im}[\tilde{g}]\,(\partial_i\tilde{H})\,\tilde{g}^R\,(\partial_j\tilde{H})\Big]\Big) \tag{6.41}$$

where $n_F'(\epsilon-\mu) = \partial n_F(\epsilon-\mu)/\partial\epsilon$. Since $\tilde{g}^{R/A}(\epsilon/\hbar; x) = (\epsilon - \tilde{H}(x) \pm i0^+)^{-1}$, one has $\mathrm{Im}[\tilde{g}(\epsilon/\hbar; x)] = -\pi\delta(\epsilon - \tilde{H}(x))$ in a non-interacting system. To use this relation, we recall that the Wigner transformed Hamiltonian $\tilde{H}(x)$ defines a hermitian operator in band space for each point x in phase space and we evaluate the traces on the right-hand side of Eq. (6.41) in the local eigenstates $|\tilde{n}, x\rangle$ of $\tilde{H}(x)$, which are defined by the eigenvalue relation

$$\tilde{H}(x)\,|\tilde{n}, x\rangle = \mathcal{E}^{(0)}_{\tilde{n}}(x)\,|\tilde{n}, x\rangle\,. \tag{6.42}$$

We find

$$\begin{aligned}\delta\rho^{(1)}(\mathbf{R}) =& ieJ_{ij}\int\frac{\mathrm{d}^d k}{(2\pi)^d}\sum_{\tilde{n}}\sum_{\tilde{m}\neq\tilde{n}}\langle\tilde{n},x|\partial_i\tilde{H}|\tilde{m},x\rangle\,\langle\tilde{m},x|\partial_j\tilde{H}|\tilde{n},x\rangle\times\\ &\times\left(\frac{n_F(\mathcal{E}^{(0)}_{\tilde{n}}(x)-\mu)}{(\mathcal{E}^{(0)}_{\tilde{n}}(x)-\mathcal{E}^{(0)}_{\tilde{m}}(x))^2}-\frac{n_F'(\mathcal{E}^{(0)}_{\tilde{n}}(x)-\mu)}{2(\mathcal{E}^{(0)}_{\tilde{n}}(x)-\mathcal{E}^{(0)}_{\tilde{m}}(x))}\right)\\ =&-e\sum_{\tilde{n}}\int\frac{\mathrm{d}^d k}{(2\pi)^d}\left[\delta\mathcal{E}^{(1)}_{\tilde{n}}(x)\,n_F'(\mathcal{E}^{(0)}_{\tilde{n}}(x)-\mu)-\mathrm{Tr}\Big(\Omega^{\mathrm{r,k}}_{\tilde{n}}(x)\Big)\,n_F(\mathcal{E}^{(0)}_{\tilde{n}}(x)-\mu))\right]\end{aligned}\tag{6.43}$$

where, in the first line, terms with $\tilde{m}=\tilde{n}$ do not contribute due to the skew-symmetry of J_{ij} and, in the second line, we identified the energy correction $\delta\mathcal{E}^{(1)}_{\tilde{n}}(x)$ and the mixed position/momentum space Berry curvature $\Omega^{\mathrm{r,k}}_{\tilde{n}}(x)$. Here, $\delta\mathcal{E}^{(1)}_{\tilde{n}}(x)$ and $\Omega^{\mathrm{r,k}}_{\tilde{n}}(x)$ are defined in Eqs. (5.15) and (3.18), respectively, where the Hamiltonian is inserted in Wigner representation, $\tilde{H}(x)$. As discussed at the end of section 6.2, $\tilde{H}(x)$ is equal to the the local band Hamiltonian $\tilde{H}_c(x)$ up to gradient corrections. Therefore, to leading order in the spatial gradients, Eq. (6.43) confirms the semiclassical result Eq. (5.36), as expected. This no longer holds for higher orders, however. For example, within the semiclassical approach, the second-order contribution to the charge density (which is obtained by expanding the semiclassical density of states in phase space, Eq. (5.30), to second order in the Berry curvature) differs from the second-order term in the gradient expansion (which is obtained by inserting $\tilde{G}^{(2)}$, Eq. (6.25), into Eq. (6.38)). The difference is evident from the fact that the expression for $\tilde{G}^{(2)}$ contains second-order derivatives (vertices with two attached dashed arrows in Eq. (6.25)), which do not appear in the semiclassical theory.

DM interaction strength. Similar to the charge density, the free energy density may also be calculated from the gradient expansion of the Green's function. The leading order correction is

$$\delta f^{(1)}(\mathbf{R}) = -k_B T\sum_{\omega_n}\int\frac{\mathrm{d}^d k}{(2\pi)^d}\,\mathrm{Tr}\log[-k_B T\,\tilde{G}^{(1)}(i\omega_n;x)].\tag{6.44}$$

where $\tilde{G}^{(1)}$ is given in Eq. (6.23). We checked by explicit evaluation that Eq. (6.44) confirms the semiclassical result Eq. (5.35).

Quantized total skyrmion charge in insulators. If the chemical potential μ lies in a band gap, the Fermi-surface term (proportional to $\delta\mathcal{E}^{(1)}_{\tilde{n}}$) in Eq. (6.43) vanishes in the limit $T\to 0$. While the Fermi-sea term (proportional to $\mathrm{Tr}[\Omega^{\mathrm{r,k}}_{\tilde{n}}]$) may contribute to the local charge density, it turns out that it does not contribute to the total charge $\delta Q=\int\mathrm{d}^d r\,\delta\rho(\mathbf{r})$ of a single skyrmion in an insulator.[2] For the contribution to δQ due

[2] The total charge of the system is $Q=\sum_{\mathbf{R}\in\mathcal{L}}\rho(\mathbf{R})$. We approximate the sum by an integral, assuming a smooth magnetization texture. The coarse-grained charge density $\rho(\mathbf{r})$ at arbitrary position $\mathbf{r}\in\mathbb{R}^d$ is defined by replacing the lattice position $\mathbf{R}$ by $\mathbf{r}$ in Eq. (6.38), which provides a smooth interpolation of $\rho(\mathbf{R})$.

to $\Omega^{\mathrm{r,k}}_{\tilde{n},xx}$, for example, the integral $\int \mathrm{d}r_x \int \frac{\mathrm{d}k_x}{2\pi}\, \Omega^{\mathrm{r,k}}_{\tilde{n},xx}$ is a first Chern number and therefore quantized. When r_y is chosen far away from the skyrmion, the integral vanishes due to the absence of spatial modulations. Therefore, it vanishes everywhere.

The leading-order contribution to the total charge of skyrmions in insulators is second order in the spatial gradients. By inserting $\tilde{G}^{(2)}$, Eq. (6.25) into Eq. (6.38), we show in Appendix A.1 that the second-order contribution to the total charge of a skyrmion is

$$\delta Q^{(2)} = -\frac{e\hbar}{12}\,\mathcal{I}_{ijkl} \int \frac{\mathrm{d}^{2d}x}{(2\pi)^d} \int_{-\infty}^{\infty} \frac{\mathrm{d}\omega}{2\pi}\, \mathrm{Tr}\Big[\tilde{g}\,(\partial_i \tilde{H})\,\tilde{g}\,(\partial_j \tilde{H})\,\tilde{g}\,(\partial_k \tilde{H})\,\tilde{g}\,(\partial_l \tilde{H})\,\tilde{g}\Big]_{i\omega_n \to \mu/\hbar + i\omega}. \tag{6.45}$$

where all local Green's functions are evaluated at complex frequency $\mu/\hbar + i\omega$ and $\mathcal{I}$ is an anti-symmetric tensor in $2d$-dimensional phase space,

$$\mathcal{I}_{ijkl} = \begin{cases} \epsilon_{ijkl} & \text{in } d = 2 \text{ dimensions} \\ \frac{1}{2}\epsilon_{ijklqr} J_{qr} & \text{in } d = 3 \text{ dimensions.} \end{cases} \tag{6.46}$$

Here, ϵ is the canonical totally anti-symmetric tensor in $2d$-dimensional phase space with the convention $\epsilon_{r_x,r_y,k_x,k_y} = 1$ and $\epsilon_{r_x,r_y,r_z,k_x,k_y,k_z} = 1$ for $d = 2$ and $d = 3$, respectively. In two dimensions, $\delta Q^{(2)}$ is quantized as expected for an insulator, since the right-hand side of Eq. (6.45) is the second Chern number associated with the local Green's function $\tilde{g}$.[3] With a calculation similar to Appendix C of Ref. [87], Eq. (6.45) can be written as

$$\delta Q^{(2)} = e\frac{\mathcal{I}_{ijkl}}{8} \int \frac{\mathrm{d}^{2d}x}{(2\pi)^d}\, \mathrm{Tr}\Big[\hat{\Omega}_{ij}\hat{\Omega}_{kl}\Big] \tag{6.47}$$

where, for each pair of phase-space directions i and j, the (in general) non-Abelian Berry curvature $\hat{\Omega}_{ij}$ is a matrix in the space of occupied bands, whose elements are given by

$$\langle x,\tilde{n}|\hat{\Omega}_{ij}|x,\tilde{m}\rangle = i\sum_{\tilde{n}'} \frac{\langle x,\tilde{n}|\frac{\partial \tilde{H}}{\partial x_i}|x,\tilde{n}'\rangle\,\langle x,\tilde{n}'|\frac{\partial \tilde{H}}{\partial x_j}|x,\tilde{m}\rangle - \langle x,\tilde{n}|\frac{\partial \tilde{H}}{\partial x_j}|x,\tilde{n}'\rangle\,\langle x,\tilde{n}'|\frac{\partial \tilde{H}}{\partial x_i}|x,\tilde{m}\rangle}{\Big(\mathcal{E}^{(0)}_{\tilde{n}}(x) - \mathcal{E}^{(0)}_{\tilde{n}'}(x)\Big)\Big(\mathcal{E}^{(0)}_{\tilde{m}}(x) - \mathcal{E}^{(0)}_{\tilde{n}'}(x)\Big)}. \tag{6.48}$$

where $\tilde{n}$ and $\tilde{m}$ are occupied bands and $\tilde{n}'$ runs over all (occupied and empty) bands (one can show that the divergent terms for $\tilde{n}' = \tilde{n}$ and for $\tilde{n}' = \tilde{m}$ cancel, see Appendix C of Ref. [87]). The diagonal part of $\hat{\Omega}_{ij}$ is the Abelian Berry curvature, see Eq. (3.18). The (in general) non-Abelian nature of the Berry curvature did not affect the first-order terms $\delta\rho^{(1)}$ and $\delta f^{(1)}$ discussed so far, since off-diagonal matrix elements of $\hat{\Omega}_{ij}$ only play a role when the trace is taken over a product of at least two Berry curvatures, as is the case in Eq. (6.47).

It turns out that, if all winding numbers due to non-Abelian Berry curvatures vanish, Eq. (6.47) coincides with the charge one obtains by expanding the semiclassical density of states, Eq. (5.30), to second order in Ω and integrating over space and momentum.

[3] See, e.g., Eq. (53) in Ref. [87].

Thus, while the semiclassical theory is generally only valid to linear order in the spatial gradients, it predicts the correct result beyond linear order in the specific case of the total skyrmion charge in an insulator at filling factor 1. For larger filling factors, however, non-Abelian Berry curvatures have to be taken into account in general, see Eqs. (6.47)–(6.48).

We show in Appendix A.2 that, for a single occupied band in $d = 2$ dimensions, the right-hand side of Eq. (6.47) reduces to the product of two quantized winding numbers,

$$\delta Q^{(2)} = \sigma_{xy} \Phi_0 \tag{6.49}$$

where

$$\sigma_{xy} = \frac{e^2}{\hbar} \int \frac{\mathrm{d}^2 k}{(2\pi)^2} \, \Omega_{xy}^{\mathrm{k,k}} \tag{6.50}$$

is the quantized Hall conductivity and

$$\Phi_0 = \frac{\hbar}{e} \int \mathrm{d}^2 r \, \Omega_{xy}^{\mathrm{r,r}} = \pm \frac{2\pi\hbar}{e} \tag{6.51}$$

is the total emergent magnetic flux (the real-space winding number of the skyrmion).

Eq. (6.49) is a well-known result in the context of quantum Hall systems at filling factor close to $\nu = 1$ [13,88]. In a two-dimensional electron gas in a strong perpendicular magnetic field, the degeneracy of each Landau level is equal to the number of magnetic flux quanta in the system. Since each skyrmion carries a quantized emergent magnetic flux $\frac{q^{\mathrm{em}}}{e} \int \mathrm{d}^2 r \, B_z^{\mathrm{em}} = \frac{\hbar}{e} \int \mathrm{d}^2 r \, \Omega_{xy}^{\mathrm{r,r}} = \Phi_0$ (cf., Eq. (4.14)), the system can increase the degeneracy of each Landau level by one by forming a skyrmion. This is energetically favorable if ν lies slightly above an integer value and the ferromagnetic exchange energy is large compared to the Zeeman splitting [13, 88–90]. Evidence for the formation of skyrmions in a quantum Hall system has been observed in GaAs/AlGaAs quantum wells [14].

In $d = 3$ dimensions, skyrmions form line defects and the total charge of a skyrmion is proportional to its length L. In Appendix A.3, we show that the skyrmion charge per length in a three-dimensional insulator is

$$\frac{\delta Q^{(2)}}{L} = e \sum_{\alpha=1}^{3} \frac{\hat{\mathbf{s}} \cdot \mathbf{g}_\alpha}{2\pi} n_\alpha^{\mathrm{k}} \tag{6.52}$$

where $\hat{\mathbf{s}}$ is a unit vector that points in the direction of the skyrmion tube, $\mathbf{g}_\alpha$, $\alpha \in \{1, 2, 3\}$ are reciprocal lattice vectors, and $n_\alpha^{\mathrm{k}} \in \mathbb{Z}$ is the momentum-space winding number in the plane perpendicular to the corresponding real-space lattice vector $\mathbf{a}_\alpha$.

Part II.

Hall effect in chiral magnets with weak spin-orbit coupling

7. Hall effects in chiral magnets

One of the most striking manifestations of Berry phases in chiral magnets can be observed in measurements of transverse electron transport. It is well-known that the Berry curvature in position space leads to a large Hall response in the skyrmion lattice phase, dubbed the topological Hall effect [21, 22]. An additional contribution to the transverse current comes from the anomalous Hall effect [70, 72], whose intrinsic part is a consequence of a non-zero Berry curvature in momentum space. Both topological and anomalous Hall effect can be much larger than the ordinary Hall effect generated by the small external magnetic field that stabilizes the skyrmion lattice phase.

In this chapter, we briefly review the experimental observations of Hall effects in chiral magnets (Section 7.1). We then present a simple semiclassical derivation of the Hall conductivity that takes Berry phases in all of phase space into account (Section 7.2). In the next chapter, we go beyond the semiclassical approximation and derive the Hall response using a field-theoretical approach based on the gradient expansion introduced in Section 6.2.

7.1. Overview over experiments and theoretical methods

In measurements of the Hall response, a small current I is driven through a sample and one measures the voltage U_H that builds up perpendicular to the current direction. If the voltage is measured in x direction and the current runs through the system in y direction, the Hall resistivity is given by

$$\rho_{xy} = \frac{E_x}{j_y} = \begin{cases} U_H/I & \text{in } d = 2 \text{ dimensions} \\ L_z\, U_H/I & \text{in } d = 3 \text{ dimensions} \end{cases} \tag{7.1}$$

where E_x is the electric field that builds up perpendicular to the current direction, j_y is the current density, and L_z is the thickness of the three-dimensional sample.

Contributions to the Hall signal. The rich phase diagram of chiral magnets leads to an intricate dependency of ρ_{xy} on the external magnetic field, temperature, and sample quality. We show measurement data for the Hall resistivity in MnSi in Figure 7.1, which is taken from Ref. [30]. Here, $B_{\mathrm{a}1}$ and $B_{\mathrm{a}2}$ indicate the boundary of the Skyrmion lattice phase, and $B_{\mathrm{c}2}$ marks the transition from the conical to the field polarized state (cf., Figure 2.3). Three major contributions to the Hall resistivity can be identified: the normal Hall effect, the topological Hall effect, and the anomalous Hall effect.

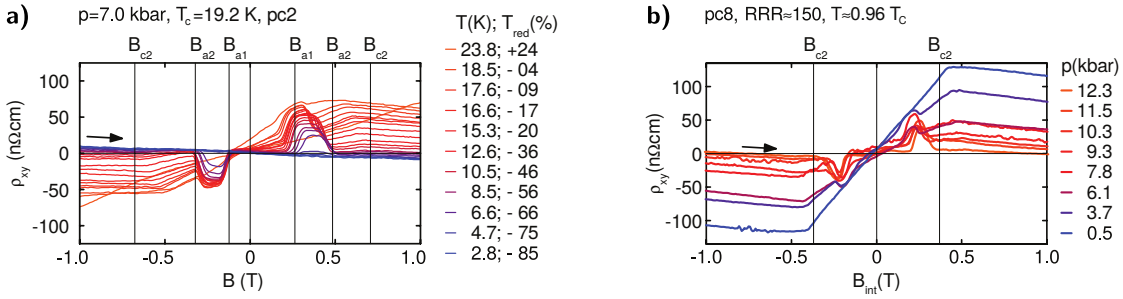

Figure 7.1.: Experimental data for the Hall resistivity in MnSi as a function of magnetic field. Both plots are taken from Ref. [30]. B_{a1} and B_{a2} indicate the boundaries of the Skyrmion lattice phase, see Figure 2.3. The transition from the conical to the field polarized state is at B_{c2}. Arrows indicate sweep direction. a) Sweeps at different temperatures and constant pressure $p = 7.0\,\mathrm{kbar}$; the reduced temperature is defined as $T_{\mathrm{red}} = (T - T_c)/T_c$ where T_c is the transition temperature at which the system orders. The large signal between B_{a1} and B_{a2} is due to the topological Hall effect. b) Sweeps at different pressures and similar temperatures close to the transition temperature; the residual resistivity ration (RRR) is a measure of the sample quality. At low pressures, there is a pronounced signal due to the anomalous Hall effect, which saturates at B_{c2}.

First, the normal Hall effect $\rho_{xy}^{\mathrm{n}} = R_0 B_z$ is proportional to the externally applied magnetic field. The Hall constant $R_0 \approx 1/(nq)$ depends on the density n and charge q of the charge carriers (electrons or holes). The normal Hall effect appears in all metals and can be explained, on a semiclassical level, by a Lorentz force $\mathbf{F}_L = q\mathbf{v} \times \mathbf{B}$ on charge carriers with group velocity $\mathbf{v}$. The Lorentz force accelerates the charge carriers in the direction perpendicular to the current until a Hall voltage U_H builds up that generates an equally strong counter force. In the steady state, the net force perpendicular to the current vanishes, which explains why the normal Hall resistivity ρ_{xy}^{n} is typically insensitive to the mean-free time τ_{el} between scattering processes, and thus independent of the impurity concentration n_{imp}. In the measurements shown in Figure 7.1, the normal Hall effect is only a small contribution. It is responsible for the small negative slope, best seen in the curve for $T = 2.8\,\mathrm{K}$ in Figure 7.1a. At low pressures, the slope of the curves due to the normal Hall effect is dwarfed by the anomalous Hall effect (see below) for magnetic fields smaller than B_{c2} (Figure 7.1b).

Second, the topological Hall effect ρ_{xy}^{top} owes its name to the topological winding number of skyrmions in the skyrmion lattice phase of chiral magnets. It can be understood in terms of the emergent magnetic field $\mathbf{B}^{\mathrm{em}}$ discussed in Section 4.1 [21, 22]. Since an emergent magnetic field influences the motion of electrons in a similar way as does a real external magnetic field, ρ_{xy}^{top} is also largely independent of the impurity concentration. Experimentally, ρ_{xy}^{top} can be distinguished from ρ_{xy}^{n} by the fact that it only exists in the skyrmion lattice phase, leading to the sharp steps in Figure 7.1a. A sudden increase of

the Hall resistivity in MnSi as a function of magnetic field was first reported by Lee and collaborators [91]. However, the effect was observed under high pressures and it remained an open question for some time whether the magnetic fields at which the increased Hall resistivity was observed corresponds to the skyrmion lattice phase [30]. Experiments by Neubauer and collaborators [10, 22] at ambient pressure showed an increase of the Hall resistivity that occurred indeed at the transition to the skyrmion lattice phase. In MnSi, the average strength of the emergent magnetic field is on the order of 13 T, which is much larger than the external field $B \approx 0.2 \ldots 0.4\,\mathrm{T}$ required to stabilize the skyrmion lattice. On the other hand, the resulting force $\mathbf{F} = q_\sigma^{\mathrm{em}} \mathbf{v} \times \mathbf{B}^{\mathrm{em}}$ on the electrons is proportional to the emergent charge $q_\sigma^{\mathrm{em}} = \pm\frac{1}{2}$, which has a different sign for majority and minority spins. The topological Hall resistivity may thus be estimated by $\rho_{xy}^{\mathrm{top}} = P R_0 B_z^{\mathrm{em}}$ where R_0 is the ordinary Hall constant and P is the average spin polarization. Despite the averaging over different signs, the topological Hall effect can become much larger than the ordinary Hall effect, see Figure 7.1a. The definition of P involves a rather complicated averaging over the Fermi surface [30], which makes calculations for real materials challenging. Recent numerical calculations of the topological Hall response from *ab-initio* can be found in Refs. [92, 93]. The emergent magnetic field is inversely proportional to the size of the magnetic unit cell. Therefore, the topological Hall effect becomes large in chiral magnets with a short pitch length, see, e.g., Ref. [94]. In the extreme limit, position-space Berry phases have also been considered in materials where the spin texture varies on the atomic length scale. This includes materials where the non-coplanar spin texture is a result of double-exchange [95, 96] or of frustration [97, 98]. In these systems, however, the adiabatic assumption breaks down and spin-flip processes, not taken into account by the Berry phase picture, become important.

Finally, the anomalous Hall effect ρ_{xy}^{AHE}, well-known from ferromagnetic materials, also appears in chiral magnets. Topological and anomalous Hall effect can be regarded as opposite limits of a coupling between the spin and a real-space structure. In the topological Hall effect, the coupling is to the effective exchange field due to the spontaneous magnetization. In chiral magnets with weak spin-orbit coupling, the latter varies on a length scale much larger than the lattice constant. In the opposite limit, electric fields due to variations of the periodic crystal potential couple to the electron spins via spin-orbit interaction, leading to a momentum-space Berry curvature and to the anomalous Hall effect. Since a (charge) Hall current is only possible for broken time-reversal symmetry, the anomalous Hall effect depends on the magnetization M and it can be distinguished from the normal Hall signal in experimental data by its hysteretic behavior and its saturation at large magnetic fields. The latter is clearly visible in Figure 7.1b. In the literature, one often finds the relation $\rho_{xy}^{\mathrm{AHE}} = R_s M$ with an anomalous Hall constant R_s. The proportionality should be taken with a grain of salt, however, and the relation between ρ_{xy}^{AHE} and M is often more complex and can even be non-monotonic [99, 100]. This can be explained by the fact that the system changes its magnetization by redistributing electrons between different bands. Since the momentum-space Berry curvature has sharp peaks in the vicinity of avoided band crossings, see Section 4.3, the anomalous Hall effect can be very sensitive to such electron redistributions. The dependency of R_s on temperature

and on impurity concentrations remained a source of debate for decades [101–104]. It is now understood that three different physical mechanisms mainly contribute to the anomalous Hall effect, which all relate differently to scattering processes. First, Berry phases in momentum space lead to an anomalous electron velocity [6] perpendicular to the applied electric field, see Section 5.1. The resulting contribution $\sigma_{xy}^{\mathrm{AHE,int}}$ to the Hall conductivity is called the intrinsic anomalous Hall effect, and is independent of impurity concentrations. In experiments, one measures the Hall resistivity $\rho_{xy} \approx -\rho_{xx}^2 \sigma_{xy}$ where ρ_{xx} is the longitudinal resistivity assumed to be much larger than ρ_{xy}. As ρ_{xx} is approximately proportional to the impurity concentration, the Hall resistivity in systems where the intrinsic contribution dominates is approximately quadratic in the impurity concentration. Second, asymmetric scattering at impurities, so-called skew-scattering, leads to a Hall resistivity approximately proportional to ρ_{xx} [105]. Third, due to spin-orbit interaction, scattering processes are accompanied with a transverse shift of the electron wave packet, which leads to the so-called side-jump contribution to the anomalous Hall effect [106]. Although side-jump is a disorder effect, the disorder strength cancels out in the contribution to the Hall conductivity in the simplest model [107]. This makes it difficult to distinguish the side jump from the intrinsic contribution in experimental data [108].

Theoretical methods. In the literature, topological and anomalous Hall effect are usually discussed independently of each other. For the anomalous Hall effect, sophisticated and field-theoretical techniques exist to calculate the transverse conductivity σ_{xy}, taking into account both intrinsic and extrinsic mechanisms [109–112]. The link between the field-theoretical approach and a semiclassical theory of the anomalous Hall effect was established by Sinitsyn and collaborators in Ref. [113]. In recent years, the existence of these field-theoretical techniques has fueled a refinement of numerical methods, which are now able to reproduce the experimentally measured Hall response in real materials on a semi-quantitative level [109,110,114]. For the topological Hall effect, however, theoretical descriptions in the literature are based on a semiclassical approach [22,63], which is difficult to combine with the field-theoretical methods for the anomalous Hall effect. We review the semiclassical approach in Section 7.2. In Chapter 8, we show that the topological Hall effect can be expressed within a field-theoretical framework by means of the gradient expansion introduced in Section 6.2.

7.2. Semiclassical theory of Hall effects in chiral magnets

There exists a vast literature on the application of semiclassical methods to both the anomalous Hall effect [105,107,115] and the topological Hall effect [21,30,63]. However, the two phenomena are usually treated in separation of each other. In this section, we provide a brief review of the semiclassical approach, using a general model that accounts for both spin-orbit coupling and an inhomogeneous magnetization texture. It turns out that the interplay between spin-orbit coupling and the inhomogeneous magnetization texture leads to an additional contribution to the Hall effect already on a semiclas-

sical level. We focus on intrinsic contributions to the Hall conductivity and consider scattering processes in the most basic relaxation time approximation. A discussion of scattering effects in the semiclassical approach of the anomalous Hall effect can be found in Ref. [107].

The derivation in this section is based on the semiclassical Boltzmann equation, which describes the evolution of a classical distribution of electrons in phase space. Quantum-mechanical corrections due to the non-commutativity of the phase space coordinates $\mathbf{r}$ and $\mathbf{p}$ are taken into account to leading order by including Berry-curvature terms in the semiclassical equations of motion, see Section 5.1. Since the semiclassical equations of motion are only valid to linear order in the gradient corrections, we retain results from the semiclassical Boltzmann equation only to linear order in the Berry curvature. A systematic gradient expansion that is not limited to the semiclassical approximation will be presented in Chapter 8.

Model and hierarchy of energy and length scales. We describe the chiral magnet by a similar model as in Section 5.1, see Eq. (7.2). The Hamiltonian is given by

$$H = H_0 + V_{\mathrm{dis}}(\mathbf{r}) \tag{7.2}$$

with

$$H_0 = \frac{(-i\hbar\boldsymbol{\nabla} + e\mathbf{A})^2}{2m} + V(\mathbf{r}) + H_{\mathrm{so}} + \mathbf{B}^{\mathrm{ex}}(\mathbf{r}) \cdot \boldsymbol{\sigma} \tag{7.3}$$

Here, V is the periodic crystal potential, H_{so} is the spin-orbit coupling, see Eq. (4.22), and $\mathbf{B}^{\mathrm{ex}}(t, \mathbf{r})$ is an effective Zeeman field that couples to the spin of the electron and includes both the usual Zeeman coupling and the exchange coupling to the background magnetization. Further, m and $-e$ are the bare mass and the charge of the electron, respectively, and $\mathbf{A}$ is the electromagnetic vector potential, where we chose a gauge in which the scalar potential vanishes. In contrast to Eq. (7.2), we include a disorder potential V_{dis} in the Hamiltonian so that the system has a well-defined conductivity.

We assume, as in Chapter 5, that $\mathbf{B}^{\mathrm{ex}}$ describes a skyrmion lattice with a skyrmion size ξ_{mod} much larger than the lattice constant a. Disorder leads to a finite life-time of excitations given by the elastic mean-free time τ_{el}. We use the simplest possible approximation of a spin and momentum-independent τ_{el}. Its value is related to the disorder strength. For example, if we assume a Gaussian white-noise disorder potential, the second moment $\langle V_{\mathrm{dis}}(\mathbf{r}) V_{\mathrm{dis}}(\mathbf{r}') \rangle_{\mathrm{dis}} \sim \frac{\hbar}{\nu_F \tau_{\mathrm{el}}} \delta(\mathbf{r} - \mathbf{r}')$ is inversely proportional to τ_{el}, where $\langle \cdots \rangle_{\mathrm{dis}}$ denotes averaging over disorder configurations and ν_F is the density of states at the Fermi level [116]. We assume that the decay rate $1/\tau_{\mathrm{el}}$ is small compared to the band width $\Delta\mathcal{E}$ so that quasi-particle excitations have a well-defined energy. On the other hand, $1/\tau_{\mathrm{el}}$ should be large compared to the cyclotron frequency $\omega_c = eB^{\mathrm{em}}/m^*$ so that the Shubnikov–de Haas effect may be neglected. Here, $B^{\mathrm{em}} \approx \Phi_0/\xi_{\mathrm{mod}}^2$ is the emergent magnetic field with one flux quantum $\Phi_0 = 2\pi\hbar/e$ per skyrmion, and m^* is the cyclotron mass of the electrons. In summary, we assume that the following hierarchy of energy scales holds,

$$\Delta\mathcal{E} \gg \frac{\hbar}{\tau_{\mathrm{el}}} \gg \hbar\omega_c. \tag{7.4}$$

This is the relevant regime for typical samples of chiral magnets with small spin-orbit coupling in the skyrmion-lattice phase. The band gap may be estimated by $\Delta\mathcal{E} \sim \hbar^2/(m^* a^2)$ where a is the lattice constant. Defining the mean-free path $\ell_{\mathrm{el}} = v_F \tau_{\mathrm{el}}$, with Fermi velocity $v_F = \frac{\partial \mathcal{E}}{\hbar \partial k} \sim \frac{a}{\hbar}\Delta\mathcal{E}$, we find that Eq. (7.4) is equivalent to the hierarchy of length scales

$$a \ll \ell_{\mathrm{el}} \lesssim \xi_{\mathrm{mod}}. \tag{7.5}$$

Hall conductivity and Hall resistivity. In experiments, one usually measures the Hall voltage U_H perpendicular to a small current I through the sample. If the current runs in y direction and U_H is measured in x direction, the Hall resistivity ρ_{xy} can be calculated from Eq. (7.1). In the experimental setup, the Hall bar has a finite width in x direction and no current can run in x direction in the steady state. In theoretical models, on the other hand, it is usually easier assume an infinite system and to calculate the transverse conductivity σ_{xy} rather than the transverse resistivity. Here, $\sigma_{xy} := \partial j_x/\partial E_y$ quantifies the current density in x direction in response to an applied electric field in y direction. Since one assumes a system without boundaries, no transverse electric counter-field E_x builds up. Both conductivity σ and resistivity ρ form a $d \times d$ tensor, and in a translationally invariant system the two are related by a simple matrix inversion, $\rho = \sigma^{-1}$. The situation is more complicated in an inhomogeneous system. Since the properties of the system depend on position, so does the conductivity, and one should expect that an inhomogeneous current density $\mathbf{j}(\mathbf{r})$ and an inhomogeneous electric field $\mathbf{E}(\mathbf{r})$ build up in the sample. We will, however, only derive expressions for the homogeneous component of the current in response to a homogeneous electric field. This is the experimentally most relevant part of the conductivity, as can be seen by the following arguments. In Fourier space, $\mathbf{j}(\mathbf{q})$ and $\mathbf{E}(\mathbf{q}')$ are related by Ohm's law

$$j_\alpha(\mathbf{q}) = \sum_\beta \sum_{\mathbf{q}'} \sigma_{\alpha\beta}(\mathbf{q}, \mathbf{q}') E_\beta(\mathbf{q}') \tag{7.6}$$

where $\alpha, \beta = 1, \ldots, d$ and, in a skyrmion lattice, $\mathbf{q}$ and $\mathbf{q}'$ are reciprocal lattice vectors of the skyrmion lattice. Assuming that the position-dependency of $\sigma(\mathbf{r})$ is weak, momentum is approximately conserved and the components of $\sigma(\mathbf{q}, \mathbf{q}')$ with $\mathbf{q} = \mathbf{q}'$ are large compared to the components with $\mathbf{q} \neq \mathbf{q}'$. In the experiment, one measures the Hall voltage $U_H \propto E_x(\mathbf{q}' = \mathbf{0})$ in response to the total current $I \propto j_y(\mathbf{q} = \mathbf{0})$ through the sample. The experimental setup imposes the additional boundary conditions that the components of the total current $\mathbf{j}(\mathbf{q} = \mathbf{0})$ perpendicular to the y direction vanish, and that the divergence $\mathbf{q} \cdot \mathbf{j}(\mathbf{q})$ vanishes in the steady state. By solving Eq. (7.6) perturbatively in the small parameter $\sigma(\mathbf{q} \neq \mathbf{q}')/\sigma(\mathbf{q} = \mathbf{q}')$ subject to the above boundary conditions, we find for the measured Hall resistivity to leading order,

$$\frac{E_x(\mathbf{q}' = \mathbf{0})}{j_y(\mathbf{q} = \mathbf{0})} \approx \left(\sigma(\mathbf{q} = \mathbf{0}, \mathbf{q}' = \mathbf{0})^{-1}\right)_{xy}. \tag{7.7}$$

We will therefore only be concerned with the homogeneous conductivity tensor $\sigma(\mathbf{q} = \mathbf{0}, \mathbf{q}' = \mathbf{0})$, and we drop the arguments $\mathbf{q}$ and $\mathbf{q}'$ in the following.

In a further simplification, we only calculate the anti-symmetric part

$$\sigma^{\mathrm{H}}_{\alpha\beta} := \frac{1}{2}(\sigma_{\alpha\beta} - \sigma_{\beta\alpha}) \tag{7.8}$$

of the conductivity tensor. In absence of cubic symmetries, the symmetric part $\sigma^{\mathrm{sym}}_{\alpha\beta} = \frac{1}{2}(\sigma_{\alpha\beta} + \sigma_{\beta\alpha})$ may in principle also have non-vanishing off-diagonal elements. However, the off-diagonal components of σ^{sym} describe a sheer conductivity, not related to broken time-reversal symmetry, which can always be avoided by cutting the sample perpendicular to the main axes of σ^{sym}.

Boltzmann Equation. Within a semiclassical framework, electronic transport is described by the Boltzmann Equation [84, 117],

$$\left(\frac{\partial}{\partial t} + \left.\frac{\mathrm{d}\mathbf{r}}{\mathrm{d}t}\right|_n \cdot \frac{\partial}{\partial \mathbf{r}} + \left.\frac{\mathrm{d}\mathbf{k}}{\mathrm{d}t}\right|_n \cdot \frac{\partial}{\partial \mathbf{k}}\right) \mathfrak{n}_n(t, \mathbf{r}, \mathbf{k}) = I_{\mathrm{coll}}[\mathfrak{n}]. \tag{7.9}$$

The Boltzmann Equation is the equation of motion for the semiclassical occupation number $\mathfrak{n}_n(t, \mathbf{r}, \mathbf{k}) \in [0, 1]$, which denotes the probability that at time t, the electron state with crystal momentum $\hbar\mathbf{k}$ in band n at position $\mathbf{r}$ is occupied. We use the name "occupation number" and the non-standard notation $\mathfrak{n}$ to avoid confusion with the distribution function f to be introduced in Chapter 10, which is related to $\mathfrak{n}$ but depends also on frequency. The left-hand side of Eq. (7.9) describes the change of the occupation number due to ballistic motion of electrons. Here, $\left.\frac{\mathrm{d}\mathbf{r}}{\mathrm{d}t}\right|_n$ and $\left.\frac{\mathrm{d}\mathbf{k}}{\mathrm{d}t}\right|_n$ are given by the semiclassical equations of motion, Eqs. (5.19)–(5.20), where we dropped the subscript "c" to improve readability. The collision integral I_{coll} on the right-hand side of Eq. (7.9) describes scattering processes that drive the system back towards equilibrium. A thorough semiclassical treatment of collisions would have to account for two effects. First, momentum transfer from impurities to the electrons leads to relaxation and, for asymmetric scattering cross-sections, to the skew-scattering contribution to the anomalous Hall effect [105]. In the literature, the momentum transfer from impurities is usually obtained from the golden rule in the lowest Born approximation [107, 113]. Second, Berry curvatures in momentum-space lead to a coordinate shift during the scattering process [106, 118], which is responsible for the side-jump contribution to the anomalous Hall effect. A gauge-invariant formula for the coordinate shift was derived by Sinitsyn and collaborators in Ref. [51]. In the present work we focus on intrinsic contributions to the Hall conductivity and use a very simple phenomenological approximation of the collision integral that describes only relaxation towards equilibrium. We set for the collision integral

$$I_{\mathrm{coll}}[\mathfrak{n}]_n(t, \mathbf{r}, \mathbf{k}) = -\frac{\mathfrak{n}_n(t, \mathbf{r}, \mathbf{k}) - \mathfrak{n}^{\mathrm{eq}}_n(\mathbf{r}, \mathbf{k})}{\tau_{\mathrm{el}}} \tag{7.10}$$

where τ_{el} is the elastic mean-free time, approximated by a momentum and spin-independent scalar, and

$$\mathfrak{n}^{\mathrm{eq}}_n(\mathbf{r}, \mathbf{k}) = n_F(\mathcal{E}_n(\mathbf{r}, \mathbf{k}) - \mu) \tag{7.11}$$

is the occupation number in equilibrium. Here, n_F is the Fermi function, μ the chemical potential, and $\mathcal{E}_n \approx \mathcal{E}_n^{(0)} + \delta\mathcal{E}_n^{(1)}$ is the expectation value of the energy of a wave packet located around position $\mathbf{r}$ and momentum $\hbar\mathbf{k}$ in phase space, which includes the gradient correction $\delta\mathcal{E}_n^{(1)}$, see Eq. (5.14).

For a constant external electric field $\mathbf{E} = -\partial\mathbf{A}/\partial t$, the system establishes a steady after time $\sim \tau_{\mathrm{el}}$ and the term $\partial\mathfrak{n}_n/\partial t$ in Eq. (7.9) vanishes. Once a solution of the Boltzmann equation is found, the charge current density is obtained from

$$\mathbf{j}(\mathbf{r}) = -e\sum_n \int \mathrm{d}^d k\, D_n(\mathbf{r},\mathbf{k})\, \frac{\mathrm{d}\mathbf{r}}{\mathrm{d}t}\bigg|_n \mathfrak{n}_n(\mathbf{r},\mathbf{k}). \tag{7.12}$$

Here, $D_n = \frac{1}{(2\pi)^d}(1 - \frac{1}{2}J_{ij}\Omega^{\mathrm{x,x}}_{n,ij})$ is the semiclassical density of states in phase space, see Eq. (5.32), with symplectic matrix J and Berry curvature tensor in phase space $\Omega_n^{\mathrm{x,x}}$. The anti-symmetric part of the conductivity tensor is then given by

$$\sigma^{\mathrm{H}}_{\alpha\beta} = \frac{1}{2V}\int \mathrm{d}^d r\, \left(\frac{\partial j_\alpha}{\partial E_\beta} - \frac{\partial j_\beta}{\partial E_\alpha}\right)_{\mathbf{E}=\mathbf{0}} \tag{7.13}$$

where V is the volume of the sample.

Perturbative solution of the Boltzmann equation. We solve Eq. (7.9) perturbatively around the equilibrium state $\mathfrak{n}_n^{\mathrm{eq}}$. Technically, we perform an expansion in the small parameter $\tau_{\mathrm{el}} \ll \hbar/(eaE)$, which is valid in the linear-response regime. It turns out to be helpful for the calculation to rewrite the Boltzmann equation, Eq. (7.9), in the steady state in a more compact form using Eqs. (5.23)–(5.24),

$$-\frac{1}{\hbar}\frac{\partial(\mathcal{E}_n(x) + e\mathbf{E}\cdot\mathbf{r})}{\partial x_i}\left(J - J\Omega'^{\mathrm{x,x}}_n(x)J\right)_{ij}\frac{\partial\mathfrak{n}_n(x)}{\partial x_j} = -\frac{\mathfrak{n}_n(x) - \mathfrak{n}_n^{\mathrm{eq}}(x)}{\tau_{\mathrm{el}}} \tag{7.14}$$

and the current density, Eq. (7.12), in the form

$$j_\alpha(\mathbf{r}) = -\frac{e}{\hbar}\sum_n \int \mathrm{d}^d k\, \left(1 - \frac{1}{2}J_{ij}\Omega'^{\mathrm{x,x}}_{n,ij}(x)\right)\left(J - J\,\Omega'^{\mathrm{x,x}}_n(x)\,J\right)_{\alpha l}\frac{\partial(\mathcal{E}_n(x) + e\mathbf{E}\cdot\mathbf{r})}{\partial x_l}\,\mathfrak{n}_n(x). \tag{7.15}$$

Here, $x \equiv (\mathbf{r},\mathbf{k})$ is the combined phase-space coordinate, J is the symplectic matrix, see Eq. (5.3), and the anti-symmetric tensor $\Omega'^{\mathrm{x,x}}_n$ is the Berry curvature in phase space that includes also the effect of an external magnetic field, see Eq. (5.23).

To zeroth order in τ_{el}, the occupation number $\mathfrak{n}_n^{\mathrm{eq}}$ is given by Eq. (7.11). We obtain the $\mathbf{q} = \mathbf{0}$ component of the current density by inserting $\mathfrak{n}_n^{\mathrm{eq}}$ into Eq. (7.15) and integrating over space. Using partial integration and the Jacobi identity, Eq. (3.14), we find that only the term proportional to $\Omega^{\mathrm{k,k}}_{n,\alpha\beta}E_\beta$ contributes and all other terms cancel. We thus obtain the Hall conductivity to zeroth order in τ_{el},

$$\sigma^{\mathrm{AHE,int}}_{\alpha\beta} = -\frac{e^2}{\hbar V}\sum_n \int \mathrm{d}^d r \int \frac{\mathrm{d}^d k}{(2\pi)^d}\,\Omega^{\mathrm{k,k}}_{n,\alpha\beta}(x)\, n_F(\mathcal{E}_n(x) - \mu) \tag{7.16}$$

Eq. (7.16) is the intrinsic part of the anomalous Hall effect, averaged over the volume. This is a well-known result.

An out-of-equilibrium electron distribution due to the applied electric field leads to corrections to Eq. (7.16). We expand the occupation number $\mathfrak{n}_n(x) \approx \mathfrak{n}_n^{\mathrm{eq}}(x) + \delta\mathfrak{n}_n^{(1)}(x) + \delta\mathfrak{n}_n^{(2)}(x)$ in orders of τ_{el}. For the first order correction $\delta\mathfrak{n}_n^{(1)}$, we obtain from Eq. (7.14),

$$\begin{aligned}\delta\mathfrak{n}_n^{(1)}(x) &= \frac{\tau_{\mathrm{el}}}{\hbar}\frac{\partial(\mathcal{E}_n(x) + e\mathbf{E}\cdot\mathbf{r})}{\partial x_i}\left(J - J\Omega'^{\mathrm{x,x}}_n(x)J\right)_{ij}\frac{\partial\mathfrak{n}_n^{\mathrm{eq}}(x)}{\partial x_j} \\ &= \frac{e\tau_{\mathrm{el}}}{\hbar}E_\beta\left(J - J\Omega'^{\mathrm{x,x}}_n(x)J\right)_{\beta j}\frac{\partial\mathcal{E}_n(x)}{\partial x_j}\,n'_F(\mathcal{E}_n(x)-\mu) \qquad (7.17)\end{aligned}$$

where β runs only over spatial directions, $n'_F(\mathcal{E}_n - \mu) := \partial n_F(\mathcal{E}_n - \mu)/\partial\mathcal{E}_n$, and we used the anti-symmetry of the matrix $(J - J\Omega'^{\mathrm{x,x}}_n J)$ in the second equality. The current j_α in response to the electric field E_β is obtained by inserting $\delta\mathfrak{n}_n^{(1)}$ into Eq. (7.15). The resulting expression is symmetric in the indices α and β to linear order in $\mathbf{E}$, and therefore does not contribute to the Hall conductivity.

We obtain the second-order term $\delta\mathfrak{n}_n^{(2)}$ by substituting $\delta\mathfrak{n}_n^{(1)}$ for $\mathfrak{n}_n$ on the left-hand side of Eq. (7.14). Neglecting terms quadratic in $\mathbf{E}$ and using the anti-symmetry of $(J - J\Omega'^{\mathrm{x,x}}_n J)$, we obtain

$$\delta\mathfrak{n}_n^{(2)} = \frac{e\tau_{\mathrm{el}}^2 E_\beta}{\hbar^2}\frac{\partial\mathcal{E}_n}{\partial x_i}\left(J - J\Omega'^{\mathrm{x,x}}_n J\right)_{ij}\frac{\partial}{\partial x_j}\left[\left(J - J\Omega'^{\mathrm{x,x}}_n J\right)_{\beta l}\frac{\partial\mathcal{E}_n}{\partial x_l}\right]n'_F(\mathcal{E}_n(x)-\mu). \quad (7.18)$$

Inserting $\delta\mathfrak{n}_n^{(2)}$ into Eq. (7.15) leads to a number of additional contributions to the current. We keep only terms up to quadratic order in the spin-orbit coupling strength λ_{so}, where we count spatial derivatives as first order in λ_{so} and, according to Eqs. (4.31)–(4.33), all components of the Berry curvature as second order in λ_{so}. We split the result into two contributions, $\sigma^{\mathrm{H},(1)}$ and $\sigma^{\mathrm{H},(2)}$. The first contribution is independent of the Berry curvature,

$$\sigma^{\mathrm{H},(1)}_{\alpha\beta} = \frac{e^2\tau_{\mathrm{el}}^2}{\hbar^3 V}J_{ij}\sum_n\int \mathrm{d}^d r\int\frac{\mathrm{d}^d k}{(2\pi)^d}\frac{\partial^2\mathcal{E}_n}{\partial k_\alpha\,\partial x_i}\frac{\partial^2\mathcal{E}_n}{\partial k_\beta\,\partial x_j}\,n_F(\mathcal{E}_n-\mu). \qquad (7.19)$$

In absence of spin-orbit coupling, the group velocity $\frac{1}{\hbar}\partial\mathcal{E}_n/\partial\mathbf{k}$ is independent of the magnetization and therefore of position. Thus, $\sigma^{\mathrm{H},(1)}$ vanishes in absence of spin-orbit coupling. The situation is different if spin-orbit coupling is taken into account. Full bands do not contribute to $\sigma^{\mathrm{H},(1)}$ because the integrand is a total derivative by x_i due to the anti-symmetry in i and j. It is easy to see that the same is not true for partially filled bands. For example, if the chemical potential in a two-dimensional system lies in a band n whose local energy is given by

$$\mathcal{E}_n(\mathbf{r},\mathbf{k}) = -\frac{\hbar^2}{ma^2}\left(\cos(k_x a) + \cos(k_y a + q r_x)\right) \qquad (7.20)$$

then $\sigma^{\mathrm{H},(1)}$ assumes a finite value. Here, $q \sim 1/\xi_{\mathrm{mod}}$ is the wave vector of some spatial modulation in x direction.

The second contribution from $\delta\mathfrak{n}_n^{(2)}$ to the Hall conductivity is proportional to the Berry curvature in position space,

$$\sigma_{\alpha\beta}^{\mathrm{H},(2)} = -\frac{e^2\tau_{\mathrm{el}}^2}{2\hbar^3 V}\sum_n \int \mathrm{d}^d r \int \frac{\mathrm{d}^d k}{(2\pi)^d}\, \Omega'^{\mathrm{r,r}}_{n,ij} \frac{\partial \mathcal{E}_n}{\partial k_i}\left(\frac{\partial \mathcal{E}_n}{\partial k_\alpha}\frac{\partial^2 \mathcal{E}_n}{\partial k_j\, \partial k_\beta} - \frac{\partial \mathcal{E}_n}{\partial k_\beta}\frac{\partial^2 \mathcal{E}_n}{\partial k_j\, \partial k_\alpha}\right) n_F'(\mathcal{E}_n - \mu) \tag{7.21}$$

where $\Omega'^{\mathrm{r,r}}_n$, is given in Eq. (5.23). For a single orbital band, we obtain from Eq. (4.14),

$$\Omega'^{\mathrm{r,r}}_{n,ij} = \frac{1}{\hbar}\epsilon_{ijl}\left(q_\sigma^{\mathrm{em}} B_l^{\mathrm{em}} - eB_l\right) \tag{7.22}$$

where $\mathbf{B}$ is the (real) magnetic field, $\mathbf{B}^{\mathrm{em}}$ is the emergent magnetic field discussed in Section 4.1, and $q_\downarrow^{\mathrm{em}} = \frac{1}{2}$ ($q_\uparrow^{\mathrm{em}} = -\frac{1}{2}$) is the emergent charge in the majority (minority) spin band. The Berry curvature $\Omega'^{\mathrm{r,r}}_n$ is already quadratic in λ_{so}. Neglecting higher orders in λ_{so} we may assume that energy $\mathcal{E}_n$ is independent of position. For a quadratic dispersion $\mathcal{E}_\sigma(\mathbf{k}) = \hbar^2 k^2/(2m^*)$ with effective electron mass m^*, Eq. (7.21) simplifies to

$$\sigma_{\alpha\beta}^{\mathrm{H},(2)} = -\frac{e^2\tau_{\mathrm{el}}^2}{m^*}\,\epsilon_{\alpha\beta\gamma}\sum_{\sigma=\downarrow,\uparrow}\left(\frac{1}{V}\int \mathrm{d}^d r\left(q_\sigma^{\mathrm{em}} B_\gamma^{\mathrm{em}} - eB_\gamma\right)\right)\left(\int \frac{\mathrm{d}^d k}{(2\pi)^d}\,\frac{v_\alpha^2 + v_\beta^2}{2}\right) n_F'(\mathcal{E}_n - \mu) \tag{7.23}$$

which describes the normal and the topological Hall effect [22].

In summary, we obtain the Hall conductivity

$$\sigma_{\alpha\beta}^{\mathrm{H}} = \sigma_{\alpha\beta}^{\mathrm{AHE,int}} + \sigma_{\alpha\beta}^{\mathrm{H},(1)} + \sigma_{\alpha\beta}^{\mathrm{H},(2)} \tag{7.24}$$

where the three contributions on the right-hand side are given in Eqs. (7.16), (7.19), and (7.23), respectively. Here, the intrinsic anomalous Hall effect $\sigma^{\mathrm{AHE,int}}$ and the topological hall effect $\sigma^{\mathrm{H},(2)}$ are well-known, while the additional contribution $\sigma^{\mathrm{H},(1)}$ only occurs if both spin-orbit interaction and the inhomogeneous magnetization texture are taken into account. We derived this result from a semiclassical theory which is only valid to leading order in the Berry curvature Ω_n. Quantum-mechanically, Ω_n can be interpreted in terms of virtual transitions into another band, see Eq. (3.18). Therefore, the semiclassical theory can only capture processes with at most a single virtual transition into a different band and it stands to reason that the results from this section may be modified by processes with more than one virtual transition. In the following chapter, we calculate the Hall conductivity from a systematic gradient expansion that goes beyond the semiclassical approximation.

8. Hall effect from a systematic gradient expansion

In this chapter, we derive the Hall conductivity in chiral magnets from a field-theoretical method based on the Kubo formula. We focus on intrinsic effects and model scattering processes by a spin and momentum-independent imaginary self-energy, and we neglect vertex corrections due to impurity scattering. As a consequence, our result for the Hall conductivity will not contain any extrinsic contributions known from the anomalous Hall effect, such as side-jump and skew scattering processes. A consistent description, based on the Kubo-Středa formula, of side-jump and skew-scattering contributions to the anomalous Hall effect was presented by Sinitsyn et al. [113]. Recently, Ado and co-workers pointed out [119] that diagrams with crossing impurity lines must also be considered as they contribute on the same order of magnitude as side-jump and skew scattering terms. The same treatment can also be applied to the formalism derived in this chapter, but this would go beyond the scope of this work.

Our calculation is based on a gradient expansion of the Kubo formula for the conductivity tensor. We identify the zeroth order term in the gradient expansion as the anomalous Hall conductivity, while the topological Hall conductivity arises at second order in spatial gradients. In addition, we obtain a contribution $\sigma_{xy}^{(1)}$ linear in spatial gradients, which is only present in systems with both spin-orbit coupling and an inhomogeneous magnetization texture.

This chapter is organized as follows. In Section 8.1, we introduce the field-theoretical description of the Hall conductivity and we briefly review how the intrinsic contribution to the anomalous Hall effect can be derived within this framework. In Section 8.2, we extend the method by a gradient expansion and we calculate the contribution to the Hall conductivity linear in spatial gradient, which turns out to confirm the term $\sigma_{xy}^{(1)}$ obtained in the semiclassical calculation of Section 7.2. In Section 8.3, we derive a general expression for the topological Hall effect from a gradient expansion to second order in the spatial gradients, neglecting terms of higher than second order in the spin-orbit coupling strength λ_{so}. We conclude in Section 8.4 with a comparison between the results obtained within the semiclassical theory and the gradient expansion.

8.1. Bastin Equation and intrinsic anomalous Hall effect

We consider the model described by Eqs. (7.2)–(7.3). Our starting point for the derivation of the Hall conductivity is the Bastin Equation [120, 121],

$$\sigma_{\alpha\beta} = \frac{e^2\hbar}{2\pi V}\int \mathrm{d}\omega\, \mathrm{Tr}\left[v_\alpha (G^R - G^A) v_\beta \frac{\partial G^A}{\partial \omega} - v_\alpha \frac{\partial G^R}{\partial \omega} v_\beta (G^R - G^A)\right] n_F(\hbar\omega - \mu). \quad (8.1)$$

Here, V is the volume of the system, $\mathrm{Tr}[\cdots]$ denotes summation over all single-particle states, $\mathbf{v}$ is the velocity operator, and $G^{R/A}$ denote the retarded and advanced Green's function, respectively. The Bastin Equation describes the homogeneous current response to a constant homogeneous electric field. It can be derived from the Kubo formula [122] in the DC limit by analytic continuation of the Matsubara Green's functions to real frequencies. In Wigner representation, the velocity operator is given by

$$\tilde{\mathbf{v}}(\mathbf{r},\mathbf{k}) = \frac{\partial \tilde{H}_0(\mathbf{r},\mathbf{k})}{\hbar\,\partial \mathbf{k}}. \quad (8.2)$$

where $\tilde{H}_{0,ml}(\mathbf{r},\mathbf{k})$ is the Wigner transform of the disorder-free Hamiltonian H_0, see Eq. (7.3). We do not consider vertex corrections from impurity scattering, as discussed in the introduction to this chapter. The Green's functions satisfy the relation (cf., Eq. (6.18))

$$\sum_l (\hbar\omega\delta_{ml} - \tilde{H}_{0,ml}(\mathbf{r},\mathbf{k}) - \tilde{\Sigma}^{R/A}) \circ \tilde{G}^{R/A}_{lj}(\omega;\mathbf{r},\mathbf{k}) = \delta_{mj} \quad (8.3)$$

where the symbol "$\circ$" denotes the Moyal product, see Eq. (6.19). In contrast to the equilibrium case, Eq. (6.18), we evaluate the Green's function here at real frequencies ω and we introduce the self-energy $\tilde{\Sigma}^{R/A}$ to include disorder effects. As in the semiclassical treatment, we restrict the discussion to intrinsic contributions to the Hall conductivity and we model disorder effects only by a momentum-independent purely imaginary self energy

$$\tilde{\Sigma}^{R/A} = \mp\frac{i\hbar}{2\tau_{\mathrm{el}}} \quad (8.4)$$

where τ_{el} is the elastic mean-free time. Approximating the self-energy by Eq. (8.4) and neglecting vertex corrections are the most serious approximations of our model.

In Wigner representation, products between velocity operators and Green's functions in Eq. (8.1) have to be replaced by Moyal products and the trace $\mathrm{Tr}[\cdots]$ is given by an integral over phase space and a sum over all bands. We obtain for the anti-symmetric part of the conductivity tensor,

$$\sigma^{\mathrm{H}}_{\alpha\beta} = \frac{e^2}{2\pi\hbar V}\int \mathrm{d}\omega \int \frac{\mathrm{d}^d x}{(2\pi)^d}\, \mathrm{Re}\,\mathrm{Tr}\left[\frac{\partial \tilde{H}_0}{\partial k_\alpha} \circ (\tilde{G}^R - \tilde{G}^A) \circ \frac{\partial \tilde{H}_0}{\partial k_\beta} \circ \frac{\partial (\tilde{G}^R + \tilde{G}^A)}{\partial \omega}\right] n_F(\hbar\omega - \mu) \quad (8.5)$$

where the trace is now only in band space. The inhomogeneous magnetization texture enters Eq. (8.5) in two places. First, the Moyal products contain derivatives in position

space. Second, in order to obtain the retarded and advanced Green's functions from Eq. (8.3), we have to perform a gradient expansion similar to the discussion in Section 6.2. To zeroth order in the spatial gradients, the Green's function is given by

$$\tilde{g}^{R/A}(\omega;\mathbf{r},\mathbf{k}) = \sum_n |n,\mathbf{k}\rangle\, \tilde{g}_n^{R/A}(\omega;\mathbf{r},\mathbf{k})\, \langle n,\mathbf{k}| \tag{8.6}$$

with

$$\tilde{g}_n^{R/A}(\omega;\mathbf{r},\mathbf{k}) = \frac{1}{\hbar\omega - \mathcal{E}_n^{(0)}(\mathbf{r},\mathbf{k}) \pm i\hbar/(2\tau_{\mathrm{el}})} \tag{8.7}$$

where $\mathcal{E}_n^{(0)}(\mathbf{r},\mathbf{k})$ is the local eigenvalue of $\tilde{H}_0(\mathbf{r},\mathbf{k})$ in band n. Using the relation $\tilde{g}_n^R - \tilde{g}_n^A \approx -2\pi i\delta(\hbar\omega - \mathcal{E}_n^{(0)})$ in the limit of large τ_{el}, we obtain from Eq. (8.5) to zeroth order in the spatial gradients

$$\begin{aligned}\sigma_{\alpha\beta}^{\mathrm{H},(0)} &\approx -\frac{2e^2}{\hbar V}\int \frac{\mathrm{d}^d x}{(2\pi)^d} \sum_{m,n} \mathrm{Im}\left[\frac{\langle n,\mathbf{k}|\frac{\partial \tilde{H}_0}{\partial k_\beta}|m,\mathbf{k}\rangle\ \langle m,\mathbf{k}|\frac{\partial \tilde{H}_0}{\partial k_\alpha}|n,\mathbf{k}\rangle}{\left(\mathcal{E}_n^{(0)}(x) - \mathcal{E}_m^{(0)}(x)\right)^2}\right] n_F(\mathcal{E}_n^{(0)}(x) - \mu) \\ &= -\frac{e^2}{\hbar V}\int \frac{\mathrm{d}^d x}{(2\pi)^d} \sum_{m,n} \Omega_{n,\alpha\beta}^{\mathrm{k,k}}(x)\, n_F(\mathcal{E}_n^{(0)}(x) - \mu)\end{aligned} \tag{8.8}$$

where we used Eq. (3.18) in the second step. A comparison with Eq. (7.16) yields $\sigma^{\mathrm{H},(0)} = \sigma^{\mathrm{AHE,int}}$ up to the fact that the energy $\mathcal{E}_n^{(0)}$ in Eq. (8.8) does not contain the energy correction $\delta\mathcal{E}_n^{(1)}$ contained in the semiclassical formula Eq. (7.16), which is of higher order in the gradient corrections. Thus, the intrinsic contribution to the anomalous Hall effect can be obtained from the Bastin Equation without vertex and gradient corrections. This is a well-known result [113]. In the following two sections, we derive contributions to the Hall conductivity due to spatial gradients up to second order.

8.2. First-order gradient corrections to the Hall conductivity

We now turn our attention to contributions to the Hall conductivity σ^{H} due to the inhomogeneous magnetization texture. We begin by rewriting the Bastin equation Eq. (8.1) in the form of the Kubo-Středa formula [123]. In the limit $T \to 0$, the conductivity

tensor is given by $\sigma_{\alpha\beta} = \sigma^{\mathrm{Ia}}_{\alpha\beta} + \sigma^{\mathrm{Ib}}_{\alpha\beta} + \sigma^{\mathrm{II}}_{\alpha\beta}$ with

$$\sigma^{\mathrm{Ia}}_{\alpha\beta} = \frac{e^2\hbar}{2\pi V} \operatorname{Tr}\left[\hat{v}_\alpha G^R \hat{v}_\beta G^A\right]_{\hbar\omega=E_F}; \tag{8.9}$$

$$\sigma^{\mathrm{Ib}}_{\alpha\beta} = -\frac{e^2\hbar}{4\pi V} \operatorname{Tr}\left[\hat{v}_\alpha G^R \hat{v}_\beta G^R + \hat{v}_\alpha G^A \hat{v}_\beta G^A\right]_{\hbar\omega=E_F}; \tag{8.10}$$

$$\begin{aligned}\sigma^{\mathrm{II}}_{\alpha\beta} &= \frac{e^2\hbar}{4\pi V} \int \mathrm{d}\omega \operatorname{Tr}\Big[\hat{v}_\alpha G^R \hat{v}_\beta \frac{\partial G^R}{\partial\omega} - \hat{v}_\alpha \frac{\partial G^R}{\partial\omega} \hat{v}_\beta G^R \\ &\qquad - \hat{v}_\alpha G^A \hat{v}_\beta \frac{\partial G^A}{\partial\omega} + \hat{v}_\alpha \frac{\partial G^A}{\partial\omega} \hat{v}_\beta G^A\Big] n_F(\hbar\omega - E_F) \\ &= -e\,\epsilon_{\alpha\beta\gamma} \left.\frac{\partial n_e}{\partial B_\gamma}\right|_{\mathbf{B}=\mathbf{0},\, E_F=\text{const.}}\end{aligned} \tag{8.11}$$

where E_F is the Fermi energy. The term $\sigma^{\mathrm{Ib}}_{\alpha\beta}$ is symmetric in α and β and therefore does not contribute to the Hall conductivity σ^{H}. The last equality in Eq. (8.11) was derived by Středa [123]. Here, $\partial n_e/\partial B_\gamma$ is the derivative of the electron density n_e by an external orbital magnetic field $\mathbf{B}$ at constant Fermi level. In this and the following section, we derive the Hall conductivity in the skyrmion lattice phase of a chiral magnet using Eqs. (8.9) and (8.11) and an expansion in spatial gradients. Assuming the hierarchy of length scales given in Eq. (7.5), the gradient expansion is equivalent to an expansion in the small parameter a/ξ_{mod}. For each order in a/ξ_{mod}, we keep only the highest order contribution in $\tau_{\mathrm{el}}\Delta\mathcal{E}/\hbar$, assuming that the hierarchy of energy scales Eq. (7.4) holds. To zeroth order in a/ξ_{mod}, the Hall conductivity is given by $\sigma^{\mathrm{H},(0)}$, Eq. (8.8). The term $\sigma^{\mathrm{II}} \propto \partial n_e/\partial B$ is an equilibrium property of the system. As argued in Ref. [113], disorder corrections to σ^{II} are small since the right-hand side of Eq. (8.11) contains poles either only above or only below the real axis. Since all contributions to σ^{H} except for the zeroth order term $\sigma^{\mathrm{H},(0)}$ turn out to be at least linear in τ_{el}, we neglect the term σ^{II} in the gradient expansion.

We thus focus on the contribution $\sigma^{\mathrm{H,Ia}}_{\alpha\beta} := \frac{1}{2}\big(\sigma^{\mathrm{Ia}}_{\alpha\beta} - \sigma^{\mathrm{Ia}}_{\beta\alpha}\big)$ to the Hall conductivity. In Wigner representation, it is given by

$$\begin{aligned}\sigma^{\mathrm{H,Ia}}_{\alpha\beta} &= \frac{e^2\hbar}{4\pi V} \int \frac{\mathrm{d}^d x}{(2\pi)^d} \operatorname{Tr}\Big[\Big(\Big(\frac{\partial \tilde{H}_0}{\hbar\,\partial k_\alpha} \circ \tilde{G}^R\Big) \circ \frac{\partial \tilde{H}_0}{\hbar\,\partial k_\beta}\Big) \circ \tilde{G}^A \\ &\qquad - \Big(\Big(\frac{\partial \tilde{H}_0}{\hbar\,\partial k_\alpha} \circ \tilde{G}^A\Big) \circ \frac{\partial \tilde{H}_0}{\hbar\,\partial k_\beta}\Big) \circ \tilde{G}^R\Big]_{\hbar\omega=E_F} \\ &\equiv \frac{e^2\hbar}{4\pi V} \Big[\tilde{v}_\alpha \overset{\overset{A}{\frown}}{\underset{\underset{R}{\smile}}{\bullet\!\bullet}} \tilde{v}_\beta \;-\; \tilde{v}_\alpha \overset{\overset{R}{\frown}}{\underset{\underset{A}{\smile}}{\bullet\!\bullet}} \tilde{v}_\beta\Big]_{\hbar\omega=E_F}\end{aligned} \tag{8.12}$$

where we added parentheses inside the trace only to make the following steps of the calculation more clear. The placement of parentheses is arbitrary since the Moyal product is associative. The last equality in Eq. (8.12) defines our conventions for Feynman

diagrams: double lines denote a full Green's function $\tilde{G}^{R/A}$, a vertex labeled $\tilde{v}_\alpha$ ($\tilde{v}_\beta$) denotes a Moyal product with the velocity operator $\partial\tilde{H}_0/\hbar\partial k_\alpha$ ($\partial\tilde{H}_0/\hbar\partial k_\beta$), and a closed Fermi loop implies integration $\int \frac{\mathrm{d}^d x}{(2\pi)^d}$ over phase space and trace over all bands.

We now expand the right-hand side of Eq. (8.12) in spatial gradients. In the Moyal product, Eq. (6.19), gradients in phase space always come as a pair of a derivative in position and a derivative in momentum space. Since the Green's function varies in momentum space on the scale of $1/a$ and in position space on the scale of ξ_{mod}, each pair of position and momentum derivatives leads to a small factor of $a/\xi_{\mathrm{mod}} \ll 1$ assuming that the hierarchy of length scales Eq. (7.5) holds. To zeroth order in a/ξ_{mod}, the Hall conductivity is given by $\sigma^{\mathrm{H},(0)}$, Eq. (8.8). We denote the contribution to first order in a/ξ_{mod} by $\sigma^{\mathrm{H},(1)} := \sigma^{\mathrm{H},(1\mathrm{A})} + \sigma^{\mathrm{H},(1\mathrm{B})}$. Here, the part $\sigma^{\mathrm{H},(1\mathrm{A})}$ comes from an expansion of the Moyal products on the right-hand side of Eq. (8.12) and $\sigma^{\mathrm{H},(1\mathrm{B})}$ comes from an expansion of the Green's functions $\tilde{G}^{R/A}$ in terms of gradients of the local Green's function $\tilde{g}^{R/A}$, see below.

We first consider the contribution due to the Moyal products in Eq. (8.12). Gradient contributions from the outermost Moyal products do not contribute since the anti-symmetric combination of position and momentum derivatives cancels by partial integration over phase space. From the inner Moyal products, we obtain

$$\sigma^{\mathrm{H},(1\mathrm{A})} = \frac{e^2\hbar}{4\pi V}\Bigg[\tilde{v}_\alpha \;\underset{R}{\overset{A}{\bigcirc}}\; \tilde{v}_\beta \;+\; \tilde{v}_\alpha \;\underset{R}{\overset{A}{\bigcirc}}\; \tilde{v}_\beta \;+\; \tilde{v}_\alpha \;\underset{R}{\overset{A}{\bigcirc}}\; \tilde{v}_\beta \;-\; \text{“}R \leftrightarrow A\text{”} \Bigg]_{E_F} \tag{8.13}$$

Here, “$R \leftrightarrow A$” denotes the term where $\tilde{g}^R$ and $\tilde{g}^A$ are swapped. As in Section 6.2, single solid lines represent a local Green's function $\tilde{g}^{R/A}$, see Eqs. (8.6)–(8.7), unlabeled vertices denote a factor of $\partial\tilde{H}_0/\partial x_i$, and a dashed line pointing from $\partial\tilde{H}_0/\partial x_i$ to $\partial\tilde{H}_0/\partial x_j$ denotes contraction with $\frac{i}{2}J_{ij}$ where J is the symplectic form, see Eq. (5.3). For example, the first diagram on the right-hand side of Eq. (8.13) is short for

$$\tilde{v}_\alpha \;\underset{R}{\overset{A}{\bigcirc}}\; \tilde{v}_\beta \equiv \frac{i}{2\hbar^2} J_{ij} \int \frac{\mathrm{d}^d x}{(2\pi)^d} \operatorname{Tr}\left[\frac{\partial^2 \tilde{H}_0}{\partial k_\alpha\, \partial x_i}\, \tilde{g}^R\, \frac{\partial \tilde{H}_0}{\partial x_j}\, \tilde{g}^R\, \frac{\partial \tilde{H}_0}{\partial k_\beta}\, \tilde{g}^A \right]_{E_F}. \tag{8.14}$$

Eq. (8.13) can be simplified by partial integration over x_i in the last diagram,

$$\tilde{v}_\alpha \;\underset{R}{\overset{A}{\bigcirc}}\; \tilde{v}_\beta \;=\; \tilde{v}_\alpha \;\underset{R}{\overset{A}{\bigcirc}}\; \tilde{v}_\beta \;-\; \tilde{v}_\alpha \;\underset{R}{\overset{A}{\bigcirc}}\; \tilde{v}_\beta\,. \tag{8.15}$$

Here, the fact that we drew one vertex as an empty circle is meant only as a guide to the eye in order to mark the derivative in phase space over which we integrated by parts. For consistency, we inverted the arrowhead in the first diagram on the right-hand side,

which led to the additional minus sign. Combining Eqs. (8.13) and (8.15) leads to

$$\sigma^{\mathrm{H},(1\mathrm{A})} = \frac{e^2\hbar}{4\pi V}\Bigg[\tilde{v}_\alpha$$ 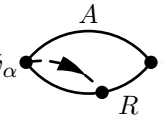 $$\tilde{v}_\beta + \tilde{v}_\alpha$$ 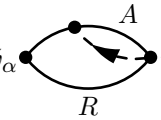 $$\tilde{v}_\beta - \text{“}R \leftrightarrow A\text{”}\Bigg]_{E_F} \tag{8.16}$$

$$= \frac{e^2}{4\pi V}\, J_{ij} \sum_{m,n,s} \int \frac{\mathrm{d}^d x}{(2\pi)^d} \left(\int \mathrm{d}\omega\ \mathrm{Im}\left[\tilde{g}^R_m\, \tilde{g}^R_n\, \tilde{g}^A_s\right] n_F'(\hbar\omega - E_F) \right) \mathrm{Re}\Bigg[\langle m|\frac{\partial \tilde{H}_0}{\partial x_j}|n\rangle \times$$
$$\times \left(\langle n|\frac{\partial \tilde{H}_0}{\partial k_\beta}|s\rangle\ \langle s|\frac{\partial^2 \tilde{H}_0}{\partial k_\alpha\, \partial x_i}|m\rangle - \langle n|\frac{\partial \tilde{H}_0}{\partial k_\alpha}|s\rangle\ \langle s|\frac{\partial^2 \tilde{H}_0}{\partial k_\beta\, \partial x_i}|m\rangle \right)\Bigg]. \tag{8.17}$$

In the second step, we evaluated the trace in the local eigenbasis using Eqs. (8.6)–(8.7). We assume that the hierarchy of energy scales Eq. (7.4) holds and that the energy difference between different bands is on the order of $\Delta\mathcal{E}$. The leading-order contribution in $\hbar/(\tau_{\mathrm{el}}\Delta\mathcal{E}) \ll 1$ is thus obtained if all bands m, n, and s are equal. Using

$$\mathrm{Im}\left[\tilde{g}^R_n\, \tilde{g}^R_n\, \tilde{g}^A_n\right] \approx -\frac{2\pi\tau_{\mathrm{el}}^2}{\hbar^2}\, \delta\big(\hbar\omega - \mathcal{E}_n^{(0)}\big). \tag{8.18}$$

we find

$$\sigma^{\mathrm{H},(1\mathrm{A})} \approx -\frac{e^2\tau_{\mathrm{el}}^2}{2\hbar^3 V} J_{ij} \sum_n \int \frac{\mathrm{d}^d x}{(2\pi)^d}\, n_F'(\mathcal{E}_n^{(0)} - E_F) \Bigg[\langle n|\frac{\partial \tilde{H}_0}{\partial x_j}|n\rangle \times$$
$$\times \left(\langle n|\frac{\partial \tilde{H}_0}{\partial k_\beta}|n\rangle\ \langle n|\frac{\partial^2 \tilde{H}_0}{\partial k_\alpha\, \partial x_i}|n\rangle - \langle n|\frac{\partial \tilde{H}_0}{\partial k_\alpha}|n\rangle\ \langle n|\frac{\partial^2 \tilde{H}_0}{\partial k_\beta\, \partial x_i}|n\rangle \right)\Bigg]. \tag{8.19}$$

We now turn to the contributions to $\sigma^{\mathrm{H},(1)}$ due to gradient corrections of the Green's functions $\tilde{G}^{R/A}$ on the right-hand side of Eq. (8.12). The first-order correction to the Green's function is given in Eq. (6.23). We thus obtain

$$\sigma^{\mathrm{H},(1\mathrm{B})}_{\alpha\beta} = \frac{e^2\hbar}{4\pi V}\Bigg[\tilde{v}_\alpha$$ 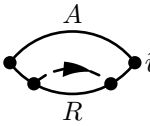 $$\tilde{v}_\beta + \tilde{v}_\alpha$$ 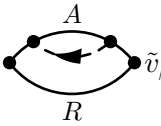 $$\tilde{v}_\beta - \text{“}R \leftrightarrow A\text{”}\Bigg]_{\hbar\omega = E_F}$$
$$= \frac{e^2}{2\pi V} J_{ij} \sum_{m,n,r,s} \int \frac{\mathrm{d}^d x}{(2\pi)^d} \left(\int \mathrm{d}\omega\ \mathrm{Im}\left[\tilde{g}^R_m\, \tilde{g}^R_n\, \tilde{g}^R_r\, \tilde{g}^A_s\right] n_F'(\hbar\omega - E_F) \right) \times$$
$$\times\, \mathrm{Re}\left[\langle m|\frac{\partial \tilde{H}_0}{\partial x_i}|n\rangle\ \langle n|\frac{\partial \tilde{H}_0}{\partial x_j}|r\rangle\ \langle r|\frac{\partial \tilde{H}_0}{\partial k_\beta}|s\rangle\ \langle s|\frac{\partial \tilde{H}_0}{\partial k_\alpha}|m\rangle \right] \tag{8.20}$$

Due to the anti-symmetry in i, j and in α, β, terms with $m = n = r$ and terms with $r = s = m$ vanish and the leading-order contribution is again quadratic in τ_{el}. We obtain to leading order in $\hbar/(\tau_{\mathrm{el}}\Delta\mathcal{E})$,

$$\mathrm{Im}\left[\tilde{g}^R_m\, \tilde{g}^R_n\, \tilde{g}^R_r\, \tilde{g}^A_s\right] \approx \frac{2\pi\tau_{\mathrm{el}}^2}{\hbar^2}\, \delta_{ns}\, \delta\big(\hbar\omega - \mathcal{E}_n^{(0)}\big) \left(\frac{\delta_{nr}}{\mathcal{E}_m^{(0)} - \mathcal{E}_n^{(0)}} + \frac{\delta_{nm}}{\mathcal{E}_r^{(0)} - \mathcal{E}_n^{(0)}} \right). \tag{8.21}$$

The total contribution to the Hall conductivity linear in a/ξ_{mod} is obtained from $\sigma^{\mathrm{H},(1)} = \sigma^{\mathrm{H},(1\mathrm{A})} + \sigma^{\mathrm{H},(1\mathrm{B})}$. Combining Eqs. (8.19)–(8.21) and using the relations

$$\frac{\partial \mathcal{E}_n^{(0)}}{\partial x_i} = \langle n| \frac{\partial \tilde{H}_0}{\partial x_i} |n\rangle \,; \tag{8.22}$$

$$\frac{\partial^2 \mathcal{E}_n^{(0)}}{\partial k_\alpha \, \partial x_i} = \langle n| \frac{\partial^2 \tilde{H}_0}{\partial k_\alpha \, \partial x_i} |n\rangle - 2 \sum_{m \neq n} \frac{\mathrm{Re}\left[\langle n| \frac{\partial \tilde{H}_0}{\partial k_\alpha} |m\rangle \, \langle m| \frac{\partial \tilde{H}_0}{\partial x_i} |n\rangle \right]}{\mathcal{E}_m^{(0)} - \mathcal{E}_n^{(0)}} \tag{8.23}$$

which follow from Eq. (3.16), we recover the result from the semiclassical analysis, see Eq. (7.19).

8.3. Topological Hall effect from the Kubo-Středa formula

We continue the gradient expansion and turn to the contribution $\sigma^{\mathrm{H},(2)}$ to the Hall conductivity quadratic in a/ξ_{mod}. In chiral magnets, the ration a/ξ_{mod} is proportional to the spin-orbit coupling strength λ_{so}, see Section 4.3. As in section 7.2, we assume $\lambda_{\mathrm{so}} \ll 1$ and consider only contributions to the Hall conductivity up to order λ_{so}^2. This means that, for the second-order term in a/ξ_{mod}, we neglect the spin-orbit coupling term H_{so} in the Hamiltonian, Eq. (7.3). In this approximation the velocity operator $\partial \tilde{H}_0/\partial \mathbf{k}$ is diagonal in the basis of local eigenstates and independent of position $\mathbf{r}$.

We obtain $\sigma^{\mathrm{H},(2)}$ by expanding the right-hand side of $\sigma^{\mathrm{H,Ia}}$, Eq. (8.12), to second order in spatial gradients. Gradient contributions come both from the Moyal products in Eq. (8.12) and from an expansion of the Green's functions $\tilde{G}^{R/A}$. For a band-diagonal position independent velocity operator, it is easy to see that contributions where either the Moyal products or the Green's functions are expanded to zeroth order do not contribute to the anti-symmetric part of the conductivity tensor. The only contributions to $\sigma^{\mathrm{H},(2)}$ are therefore terms where both the Moyal products and the Green's functions are expanded to first order. We first expand the Moyal products to first order. With the same arguments that lead to Eq. (8.16) we obtain

$$\begin{aligned}
\sigma^{\mathrm{H},(2)}_{\alpha\beta} &= -\frac{ie^2}{8\pi\hbar V} \int \frac{\mathrm{d}^d x}{(2\pi)^d} \, \mathrm{Tr} \left[\frac{\partial^2 \tilde{H}_0}{\partial k_\alpha \, \partial k_i} \frac{\partial \tilde{G}^R}{\partial r_i} \frac{\partial \tilde{H}_0}{\partial k_\beta} \tilde{G}^A + \frac{\tilde{H}_0}{\partial k_\alpha} \tilde{G}^R \frac{\partial^2 \tilde{H}_0}{\partial k_\beta \, \partial k_i} \frac{\partial \tilde{G}^A}{\partial r_i} - \text{“}R \leftrightarrow A\text{”} \right]_{E_F} \\
&= -\frac{ie^2}{8\pi\hbar V} \int \frac{\mathrm{d}^d x}{(2\pi)^d} \, \mathrm{Tr} \left[\left(\frac{\partial^2 \tilde{H}_0}{\partial k_\alpha \, \partial k_i} \frac{\partial \tilde{G}^R}{\partial r_i} \frac{\partial \tilde{H}_0}{\partial k_\beta} \tilde{G}^A - \text{“}R \leftrightarrow A\text{”} \right) - \text{“}\alpha \leftrightarrow \beta\text{”} \right]_{E_F}
\end{aligned} \tag{8.24}$$

where “$\alpha \leftrightarrow \beta$” denotes the term with α and β swapped. Expanding the Green's

functions to linear order in spatial gradients using Eq. (6.23) leads to

$$\sigma^{\mathrm{H},(2)}_{\alpha\beta} = \frac{e^2\hbar}{4\pi V}\Bigg[\tilde{v}_\alpha \;\underset{R}{\overset{A}{\bigcirc}}\; \tilde{v}_\beta + \tilde{v}_\alpha \;\underset{R}{\overset{A}{\bigcirc}}\; \tilde{v}_\beta + \tilde{v}_\alpha \;\underset{R}{\overset{A}{\bigcirc}}\; \tilde{v}_\beta + \tilde{v}_\alpha \;\underset{R}{\overset{A}{\bigcirc}}\; \tilde{v}_\beta + \tilde{v}_\alpha \;\underset{R}{\overset{A}{\bigcirc}}\; \tilde{v}_\beta + \tilde{v}_\alpha \;\underset{R}{\overset{A}{\bigcirc}}\; \tilde{v}_\beta - \text{“}R \leftrightarrow A\text{”} - \text{“}\alpha \leftrightarrow \beta\text{”} \Bigg]_{E_F} \tag{8.25}$$

where the first five diagrams originate from the gradient expansion of $\tilde{G}^R$ and the last diagram comes from the gradient expansion of $\tilde{G}^A$. Eq. (8.25) can be simplified by partial integration in phase space, which leads to the relation

$$\tilde{v}_\alpha \;\underset{R}{\overset{A}{\bigcirc}}\; \tilde{v}_\beta = - \tilde{v}_\alpha \;\underset{R}{\overset{A}{\bigcirc}}\; \tilde{v}_\beta - \tilde{v}_\alpha \;\underset{R}{\overset{A}{\bigcirc}}\; \tilde{v}_\beta - \tilde{v}_\alpha \;\underset{R}{\overset{A}{\bigcirc}}\; \tilde{v}_\beta - \tilde{v}_\alpha \;\underset{R}{\overset{A}{\bigcirc}}\; \tilde{v}_\beta + \tilde{v}_\alpha \;\underset{R}{\overset{A}{\bigcirc}}\; \tilde{v}_\beta \,. \tag{8.26}$$

Here, the fact that one vertex is drawn as an empty circle is again only a guide to the eye. We left out the diagram with a Moyal line from $\tilde{v}_\alpha$ to $\tilde{v}_\beta$, which vanishes in our approximation of position-independent velocity operators. Combining Eqs. (8.25)–(8.26) leads to

$$\begin{aligned}\sigma^{\mathrm{H},(2)}_{\alpha\beta} &= \frac{e^2\hbar}{4\pi V}\Bigg[\tilde{v}_\alpha \;\underset{R}{\overset{A}{\bigcirc}}\; \tilde{v}_\beta + \tilde{v}_\alpha \;\underset{R}{\overset{A}{\bigcirc}}\; \tilde{v}_\beta - \text{“}R \leftrightarrow A\text{”} - \text{“}\alpha \leftrightarrow \beta\text{”} \Bigg]_{E_F} \\ &= \frac{e^2\hbar}{2\pi V}\,\mathrm{Re}\Bigg[\tilde{v}_\alpha \;\underset{R}{\overset{A}{\bigcirc}}\; \tilde{v}_\beta - \text{“}R \leftrightarrow A\text{”} - \text{“}\alpha \leftrightarrow \beta\text{”} \Bigg]_{E_F} .\end{aligned} \tag{8.27}$$

The evaluation of the right-hand side of Eq. (8.27) is greatly simplified by the fact that the velocity operators $\partial\tilde{H}_0/\partial\mathbf{k}$ are diagonal in the basis of local eigenstates of $\tilde{H}_0$ if spin-orbit coupling is neglected, and therefore commute with the local Green's functions

$\tilde{g}^{R/A}$. We obtain

$$\sigma^{\mathrm{H},(2)}_{\alpha\beta} = -\frac{e^2\hbar^2}{2\pi V}\sum_{m,n}\int\frac{\mathrm{d}^d x}{(2\pi)^d}\left(\int \mathrm{d}\omega\ \mathrm{Im}\left[\tilde{g}^R_m\,\tilde{g}^A_m\big(\tilde{g}^R_n\big)^2\tilde{g}^A_n\right] n'_F(\hbar\omega - E_F)\right)\times$$
$$\times\,\tilde{v}_{n,i}\,\tilde{v}_{n,\alpha}\frac{\partial^2\mathcal{E}^{(0)}_m}{\partial k_j\,\partial k_\beta}\ \mathrm{Im}\left[\langle n|\frac{\partial\tilde{H}_0}{\partial r_i}|m\rangle\ \langle m|\frac{\partial\tilde{H}_0}{\partial r_j}|n\rangle\right] - \text{“}\alpha\leftrightarrow\beta\text{”}. \quad (8.28)$$

For terms with $m = n$, the last factor $\mathrm{Im}[\cdots]$ vanishes. For $m \neq n$, we find in the limit of small $\hbar/(\tau_{\mathrm{el}}\Delta\mathcal{E})$,

$$\mathrm{Im}\left[\tilde{g}^R_m\,\tilde{g}^A_m\big(\tilde{g}^R_n\big)^2\tilde{g}^A_n\right] = \frac{1}{2i}\,\tilde{g}^R_m\,\tilde{g}^A_m\,\tilde{g}^R_n\,\tilde{g}^A_n\big(\tilde{g}^R_n - \tilde{g}^A_n\big) = -\frac{2\pi\tau_{\mathrm{el}}^2/\hbar^2}{\big(\mathcal{E}^{(0)}_n - \mathcal{E}^{(1)}_m\big)^2}\,\delta\big(\hbar\omega - \mathcal{E}^{(0)}_n\big) \quad (8.29)$$

which leads to

$$\sigma^{\mathrm{H},(2)}_{\alpha\beta} = \frac{e^2\tau_{\mathrm{el}}^2\hbar}{V}\sum_n\sum_{m\neq n}\int\frac{\mathrm{d}^d x}{(2\pi)^d}\,n'_F\big(\mathcal{E}^{(0)}_n - E_F\big)\,\tilde{v}_{n,i}\left(\tilde{v}_{n,\alpha}\frac{\partial^2\mathcal{E}^{(0)}_m}{\partial k_j\,\partial k_\beta} - \tilde{v}_{n,\beta}\frac{\partial^2\mathcal{E}^{(0)}_m}{\partial k_j\,\partial k_\alpha}\right)\times$$
$$\times\,\mathrm{Im}\left[\frac{\langle n|\frac{\partial\tilde{H}_0}{\partial r_i}|m\rangle\ \langle m|\frac{\partial\tilde{H}_0}{\partial r_j}|n\rangle}{\big(\mathcal{E}^{(0)}_n - \mathcal{E}^{(1)}_m\big)^2}\right]. \quad (8.30)$$

Eq. (8.30) is a general expression for the topological Hall effect if spin-orbit coupling is neglected, and it is the main result of this chapter. A comparison to the semiclassical formula Eq. (7.21) follows in the next section.

8.4. Discussion

In this chapter, we derived the Hall conductivity in chiral magnets based on a systematic gradient expansion of the Kubo formula. In addition to the well-known anomalous and topological Hall effect, we obtain a contribution $\sigma^{\mathrm{H},(1)}$, Eq. (7.19), linear in spatial derivatives, which occurs only in the presence of both spin-orbit interaction and an inhomogeneous magnetization texture. The existence of $\sigma^{\mathrm{H},(1)}$ is confirmed by the semiclassical calculation in Section 7.2.

To second order in the spatial gradients, the Hall conductivity is given by Eq. (8.30). For a model with only a single orbital band, the terms $\partial^2\mathcal{E}^{(0)}_\sigma/\partial k_\alpha\partial k_i$ and $\partial^2\mathcal{E}^{(0)}_\sigma/\partial k_\beta\partial k_i$ are independent of the spin σ in absence of spin-orbit coupling, and we can identify the position-space Berry curvature using Eq. (3.18). In this case, we obtain

$$\sigma^{\mathrm{H},(2)}_{\alpha\beta} = -\frac{e^2\tau_{\mathrm{el}}^2}{2\hbar V}\sum_{\sigma=\downarrow/\uparrow}\int\frac{\mathrm{d}^d x}{(2\pi)^d}\,\Omega^{\mathrm{r,r}}_{\sigma,ij}\,\tilde{v}_i\left(\tilde{v}_\alpha\frac{\partial^2\mathcal{E}^{(0)}}{\partial k_j\,\partial k_\beta} - \tilde{v}_\beta\frac{\partial^2\mathcal{E}^{(0)}}{\partial k_j\,\partial k_\alpha}\right) n'_F\big(\mathcal{E}^{(0)}_\sigma - E_F\big) \quad (8.31)$$

in agreement with our result from the semiclassical calculation, see Eq. (7.21). For an isotropic quadratic dispersion the term in the brace is given by $\hbar^2(\tilde{v}_\alpha\delta_{j\beta} - \tilde{v}_\beta\delta_{j\alpha})/m^*$

and Eq. (8.31) simplifies to Eq. (7.23), which is more commonly used to describe the topological Hall effect. We thus identify the diagram on the right-hand side of Eq. (8.27) as the term responsible for the topological Hall effect in a perturbative expansion in $a/\xi_{\mathrm{mod}} \ll 1$ for chiral magnets with weak spin-orbit coupling.

If more than one orbital band participates in the coupling to the effective exchange field, then Eq. (8.30) suggests that the effective electron mass in the empty bands should also play a role. Physically, the diagram on the right-hand side of Eq. (8.27) sums up amplitudes of virtual transitions from occupied bands n into empty bands m and back. If no additional physical process happens while the electron is in band m, then the amplitude of such a virtual transition can be expressed in terms of the Berry curvature Ω_n, see discussion below Eq. (3.18). Here, Ω_n may be regarded as a property of the occupied band n in the sense that it can be calculated from the Bloch states in band n only. Thus, the system can in this case be described in a semiclassical picture where the physics in each band is treated in isolation. The equivalence between the Berry curvature and the amplitude of a virtual transition is what allowed us to identify the zero-order Hall conductivity $\sigma^{\mathrm{H},(0)}$, Eq. (8.8), with the anomalous Hall conductivity $\sigma^{\mathrm{AHE,int}}$, Eq. (7.16). Eq. (8.30), however, goes slightly beyond the semiclassical approximation by including additional mass operators $\partial^2\mathcal{E}_m^{(0)}/\partial k_j \partial k_\beta$ and $\partial^2\mathcal{E}_m^{(0)}/\partial k_j \partial k_\alpha$ during the virtual transition. This effect has no precise semiclassical counterpart.

Part III.

Dynamics of rigid skyrmions in the presence of spin-orbit coupling

9. Theories of magnetization dynamics

The discovery of the giant magnetoresistance (GMR) effect by Grünberg and Fert [124, 125] demonstrated that electrical currents can be efficiently manipulated by tiny magnetic structures. The GMR effect is widely used in computer hard disks today. Nowadays, one of the main goals in the field of spintronics is the reverse mechanism: the controlled manipulation of magnetic structures with currents and electric fields. There are strong indications that this goal can be achieved with so-called spin-transfer torques [126,127], a mechanism by which angular momentum is transferred from conduction electrons to the magnetization texture. Parkin and collaborators demonstrated [128] that spin-transfer torques could find use in future devices for data storage. In their prototype of a so-called racetrack memory, data is stored as a pattern of magnetic domain walls on a wire, similar to the way data is stored on magnetic tapes. In contrast to traditional magnetic tapes, however, it is not the wire itself that is moved around when the data is accessed. Instead, one pushes the domain-wall pattern along the wire by driving an electric current through the system, using the principle of spin-transfer torques. Recently, skyrmions have become increasingly popular as candidate alternatives for domain walls in race-track type memories [39]. Due to the smooth magnetization texture and the rigidness of skyrmions, pinning forces on skyrmions are weak and the current densities required to move skyrmions are around a factor of 10^5 lower than in the case of domain-walls [12].

In this part of the thesis we focus on the influence of phase-space Berry phases on the dynamics of skyrmions in an externally applied electric field. In particular, we address the question of how the electric charge of skyrmions discussed in Chapters 5 and 6 couples to an external electric field. This chapter is an introduction to the topic. We provide an overview of the most common theoretical models for magnetization dynamics in Section 9.1. In Section 9.2 we give a brief outline of the open questions that we address in Chapters 10 and Chapter 11.

9.1. The Landau-Lifshitz-Gilbert equation and the Thiele Equation

The coupling of a spin $\mathbf{S}$ to a magnetic field $\mathbf{B}$ is described by the Hamiltonian

$$H = -\gamma \mathbf{B} \cdot \mathbf{S}. \tag{9.1}$$

Here, the gyromagnetic ratio γ is the ratio between the spin expectation value and the magnetic moment $\mathbf{m} = \gamma \langle \mathbf{S} \rangle$. For a single electron, $\gamma = -ge/(2m) < 0$ follows from the Dirac equation in the non-relativistic limit, where the electron has electric charge $-e$,

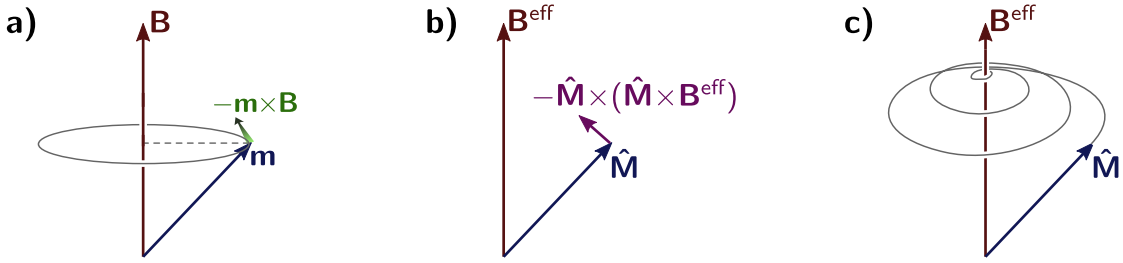

Figure 9.1.: Geometry of magnetic, magnetization, and torques in the Landau-Lifshitz-Gilbert Equation. a) The dissipationless dynamics according to Eq. (9.1). The torque $-\mathbf{m}\times\mathbf{B}$ points into the plane. b) The dissipative torque $\alpha\gamma\hat{\mathbf{M}}\times(\hat{\mathbf{M}}\times\mathbf{B}^{\text{eff}})$ points towards the magnetic field for $\gamma<0$. c) Gilbert damping leads to a relaxation of $\hat{\mathbf{M}}$ on a spiral towards parallel alignment with $\mathbf{B}^{\text{eff}}$.

mass m, and the g-factor $g\approx 2$ differs slightly from the value 2 predicted by the Dirac equation due to vertex corrections of the electromagnetic coupling. If the particle that carries the spin is more complex than a single electron, e.g., an atom in a solid, then γ is a material parameter that has to be measured or determined from bandstructure calculations. For an electron-like Fermi surface, γ typically stays negative. However, the notation in the literature is inconsistent in this regard and sometimes γ is implicitly assumed positive, leading to different signs in the Landau-Lifshitz-Gilbert Equation, see below.

The dynamics of the magnetic moment $\mathbf{m}$ for the model Eq. (9.1) follows from the commutation relations of the spin operator, $[S_i,S_j]=i\hbar\epsilon_{ijk}S_k$. One obtains

$$\frac{\partial\mathbf{m}}{\partial t}=\frac{i}{\hbar}\gamma\left\langle[H,\mathbf{S}]\right\rangle=\gamma\mathbf{m}\times\mathbf{B}. \tag{9.2}$$

Eq. (9.2) describes the precession of $\mathbf{m}$ around $\mathbf{B}$ (Figure 9.1a). The magnitude $|\mathbf{m}|$ of the magnetization is a conserved quantity, as can be seen by taking the scalar product with $\mathbf{m}$ on both sides of the equation. One therefore often rescales the equation and considers the equation of motion for the direction $\hat{\mathbf{m}}:=\mathbf{m}/|\mathbf{m}|$ of the magnetization,

$$\frac{\partial\hat{\mathbf{m}}}{\partial t}=\gamma\hat{\mathbf{m}}\times\mathbf{B}. \tag{9.3}$$

Eq. (9.3) is the equation of motion for the direction of the magnetization of a single spin. In a solid, the model has to be adapted in three regards. First, the single magnetic moment $\mathbf{m}$ is replaced by the magnetization $\mathbf{M}(\mathbf{r})$, which may vary in space. Second, the magnetization couples not only to the external magnetic field $\mathbf{B}$ but also to exchange and demagnetization fields. This is taken into account by replacing $\mathbf{B}$ with an effective magnetic field $\mathbf{B}^{\text{eff}}(\mathbf{r}):=-\frac{\delta F[\mathbf{M}]}{|\mathbf{M}(\mathbf{r})|\,\delta\hat{\mathbf{M}}(\mathbf{r})}$ where $F[\mathbf{M}(\mathbf{r})]$ is the free energy functional [36]. Second, dissipative processes become important. In Eq. (9.3), the projection of $\hat{\mathbf{m}}$ on $\mathbf{B}$ is a conserved quantity due to energy conservation (see Figure 9.1a). This is an unphysical approximation in solid state physics. Phenomenologically, dissipation is typically

described by adding a torque $\mathbf{T} = \alpha\gamma\hat{\mathbf{M}} \times (\hat{\mathbf{M}} \times \mathbf{B}^{\text{eff}})$ to the right-hand side of Eq. (9.3). This term was introduced by Landau and Lifshitz in Ref. [129]. The dimensionless parameter α is known today as the Gilbert damping parameter. For $\alpha > 0$ and $\gamma < 0$, the torque points towards the direction of $\mathbf{B}^{\text{eff}}$ (Figure 9.1b), as required for a relaxation process. For $\gamma > 0$ the torque points in the opposite direction, consistent with the fact that the energy is minimized in this case by anti-parallel alignment of $\hat{\mathbf{M}}$ and $\mathbf{B}^{\text{eff}}$. The resulting equation of motion for $\hat{\mathbf{m}}$ with damping is usually written in the form of the Landau-Lifshitz-Gilbert (LLG) Equation [130]. In the absence of currents, it is given by

$$\frac{\partial \hat{\mathbf{M}}}{\partial t} = \gamma' \, \hat{\mathbf{M}} \times \mathbf{B}^{\text{eff}} + \alpha \hat{\mathbf{M}} \times \frac{\partial \hat{\mathbf{M}}}{\partial t} \tag{9.4}$$

where $\gamma' = (1 + \alpha)\gamma$ is a renormalized gyromagnetic ratio. We will drop the prime on γ in the following and always consider the renormalized gyromagnetic ratio. As a consequence of the damping term the magnetization direction moves on a spiral towards parallel alignment with $\mathbf{B}^{\text{eff}}$ on the time scale $1/(\alpha|\gamma\mathbf{B}^{\text{eff}}|)$ (Figure 9.1c).

It has proven difficult to calculate α from microscopic theories due to the fact that any processes that does not conserve the electronic spin can contribute to α. The microscopic origin of Gilbert damping was discussed in Refs. [131–134]. Generally, a change of the magnetization is accompanied by a small deformation of the Fermi surface due to spin-orbit coupling [135, 136]. This deformation brings the system out of equilibrium and is therefore followed by relaxation processes during which phonons or magnons are emitted. In numerical calculations from *ab-initio* [136, 137], inter-band transitions have been identified as the dominant process contributing to Gilbert damping. Experimentally, the value of α can be determined from the line-width of the ferromagnetic resonance [138,139]. Typical values lie in the range of $\alpha = 10^{-3} \ldots 10^{-1}$. The LLG Equation is the basis of powerful micromagnetic simulation codes that integrate Eq. (9.4) numerically over time on a lattice [140]. Simulations with an additional stochastic torque due to thermal noise were presented in Ref. [35]. If only the final magnetization profile in the ground state or in a metastable state is of interest, then often values of α that are larger than the actual material parameters are used to speed up the calculations.

In metals, a spin current couples to the magnetization via spin-transfer torques [126, 127]. When conduction electrons traverse a smooth magnetic texture, a torque is exerted on their spin that causes the spin to follow the background magnetization. Since the total angular momentum is conserved (unless it is passed to the crystal), there has to be an opposite counter-torque on the magnetization [126, 141]. This counter-torque leads to both dissipative and non-dissipative effects. Phenomenologically, the effects of spin-transfer torques are described by the LLG Equation with two additional terms [142],

$$(\partial_t + \mathbf{v}_{\text{s}} \cdot \boldsymbol{\nabla}) \, \hat{\mathbf{M}} = \gamma \hat{\mathbf{M}} \times \mathbf{B}^{\text{eff}} + \alpha \hat{\mathbf{M}} \times \left(\partial_t + \frac{\beta}{\alpha} \mathbf{v}_{\text{s}} \cdot \boldsymbol{\nabla} \right) \hat{\mathbf{M}}. \tag{9.5}$$

Here, $\mathbf{v}_{\text{s}}$ is an effective spin velocity and β is sometimes called the non-adiabatic damping parameter. The term on the left-hand side of Eq. (9.5) is the total time derivative of the magnetization direction in the co-moving frame. For $\beta = \alpha$ the total time derivative also

appears in the Gilbert damping term on the right-hand side. This is only the correct damping term in a Galileo-invariant system. In a solid the crystal potential breaks Galileo invariance and $\beta \neq \alpha$. However, the two damping parameters are usually on the same order of magnitude. Derivations of the value of β from microscopic models can be found in Refs. [131, 134]. It can be measured by observing the motion of domain walls generated by an applied current [143].

Eq. (9.5) is the standard form of the LLG Equation. The dissipative torques proportional to α and β are phenomenological terms based on symmetry arguments. It was pointed out in Refs. [36, 62, 133] that an additional dissipative term is allowed due to spin-orbit coupling. It is described by adding the torque

$$-\alpha' \left[\hat{\mathbf{M}} \cdot \left(\partial_i \hat{\mathbf{M}} \times \left(\partial_t + \frac{\beta'}{\alpha'} \mathbf{v}_\mathrm{s} \cdot \boldsymbol{\nabla}\right) \hat{\mathbf{M}}\right)\right] \partial_i \hat{\mathbf{M}} \tag{9.6}$$

to the right-hand side of Eq. (9.5). Physically Eq. (9.6) describes the effect that the change of magnetization generates a current due to spin-orbit coupling, which leads to ohmic friction [36].

The LLG Equation is an equation of motion for the field $\hat{\mathbf{M}}(\mathbf{r})$. In absence of currents, $\mathbf{v}_\mathrm{s} = \mathbf{0}$, it describes precessing magnetic moments that ultimately relax to a local minimum of the free energy due to the Gilbert damping α. In chiral magnets, single skyrmions exist as metastable states of the magnetization texture [144]. A finite current, related to $\mathbf{v}_\mathrm{s} \neq \mathbf{0}$ drives the magnetization texture out of its static configuration. It turns out that for low current densities, deformations of the magnetic texture are weak and the current couples mainly to the translational mode of the magnetization texture [36]. The magnetization texture is thus described by a $\mathbf{M}(t, \mathbf{r}) = \mathbf{M}_0(\mathbf{r} - \mathbf{R}(t))$ where $\mathbf{M}_0(\mathbf{r})$ is a time-independent function of position, for example a domain wall or a skyrmion, and $\mathbf{R}(t)$ is the trajectory of the magnetic texture. Following Refs. [11, 36], an equation of motion for $\mathbf{R}(t)$ can be obtained from the LLG Equation by multiplying both sides with $\partial_i \hat{\mathbf{M}}$ and integrating over space. In Ref. [36], the resulting equation of motion is given in the form of a balance of forces,

$$\mathbf{G} \times (\mathbf{v}_\mathrm{s} - \dot{\mathbf{R}}) + \boldsymbol{\mathcal{D}}(\tilde{\beta}\mathbf{v}_\mathrm{s} - \tilde{\alpha}\dot{\mathbf{R}}) + \mathbf{F}_\mathrm{pin} = \mathbf{0} \tag{9.7}$$

with

$$\mathbf{G} = \int \mathrm{d}^2 r \, M(\mathbf{r}) \, \mathbf{B}^\mathrm{em}(\mathbf{r}); \tag{9.8}$$

$$\boldsymbol{\mathcal{D}}_{ij} = \int \mathrm{d}^2 r \, M(\mathbf{r}) \, (\partial_i \hat{\mathbf{M}}(\mathbf{r})) \cdot (\partial_j \hat{\mathbf{M}}(\mathbf{r})); \tag{9.9}$$

$$\mathcal{D}' = \int \mathrm{d}^2 r \, M(\mathbf{r}) \, |\mathbf{B}^\mathrm{em}(\mathbf{r})|^2; \tag{9.10}$$

$$\tilde{\alpha} = \alpha + \alpha' \mathcal{D}'/\mathcal{D}; \tag{9.11}$$

$$\tilde{\beta} = \beta + \beta' \mathcal{D}'/\mathcal{D}. \tag{9.12}$$

Here, $\mathbf{B}^\mathrm{em}$ is the emergent magnetic field due to a non-coplanar magnetization texture, see Section 4.1, and $\mathbf{F}_\mathrm{pin}$ is a pinning force due to disorder. Eq. (9.7) is known as the

Thiele equation. The first term on the left-hand side describes a gyro-coupling of the skyrmion velocity and the effective spin velocity to applied forces, and the remaining two terms are forces related to dissipation and pinning, respectively. The gyro-coupling vector $\mathbf{G}$ is proportional to the topological winding number of the magnetization texture. Therefore, skyrmions, which have a non-trivial winding number, couple efficiently to forces and external currents. According to Eq. (9.7), a current $\mathbf{v}_\mathrm{s} \neq \mathbf{0}$ or an applied force directly generate a non-zero skyrmion velocity $\dot{\mathbf{R}}$ without retardation. This is a consequence of the fact that only the translational mode was considered in the derivation of Eq. (9.7). Excitations of the magnetization texture, not taken into account by the Thiele Equation, can lead to a finite memory of the system. In Ref. [38], the authors found that, while the retardation can be large if the magnetization texture is driven by time-dependent magnetic fields, it is usually negligible in current-driven systems.

9.2. Open questions

The LLG Equation, Eq. (9.5), and the Thiele Equation, Eq. (9.7) have been successfully employed to model the magnetization dynamics of chiral magnets. Their derivation is, however, of mainly phenomenological nature based on symmetry arguments. In particular, while the gyro-coupling term in the Thiele Equation is clearly related to Berry phases in position space, other Berry phase effects in phase space are only taken into account in the prefactors of the dissipative terms. There are two reasons why Berry phases in phase space can be expected to lead to non-dissipative forces on skyrmions. First, the Berry curvature $\Omega_n^{\mathrm{r,k}}$ in mixed position/momentum space leads to a renormalization of the force on Bloch electrons in presence of an electric field, see Eq. (5.20) in Section 5.1. Due to momentum conservation, one should expect a counter-force on the magnetization texture. Second, as discussed in Chapters 5 and 6, skyrmions carry an electric charge related to a Berry-phase correction to the density of states in phase space. It is therefore a natural question to ask whether the skyrmion charge couples to an external electric field. In Chapter 10, we derive an equation of motion for skyrmions in the presence of phase-space Berry phases. We present results for metals and insulators in Chapter 11.

10. Derivation of the equation of motion for skyrmions

In this chapter, we derive a formal equation of motion for the translational mode of a single rigid skyrmion in presence of an electric field, taking into account all Berry phases in phase space. The resulting equation is given by a balance of forces, $\mathbf{F}^{\mathrm{tot}} = \mathbf{0}$, where the total force will turn out to be given by

$$F_i^{\mathrm{tot}} = \sum_{\bar{n}} \int \mathrm{d}^d \bar{r} \int \frac{\mathrm{d}^d \bar{k}}{(2\pi)^d} \Big[(1 - \Omega^{\mathrm{r,k}}_{\bar{n},jj}) \frac{\partial \mathcal{E}_{\bar{n}}}{\partial \bar{r}_i} - \Omega^{\mathrm{r,r}}_{\bar{n},ij} \left(\frac{\partial \mathcal{E}_{\bar{n}}}{\partial \bar{k}_j} - \hbar \dot{R}_j \right) + \Omega^{\mathrm{r,k}}_{\bar{n},ij} \left(\frac{\partial \mathcal{E}_{\bar{n}}}{\partial \bar{r}_j} + e E_j \right) \Big] \bar{\tilde{\mathfrak{n}}}_{\bar{n}}. \tag{10.1}$$

Here, $\Omega^{\mathrm{r,r}}_{\bar{n}}$ and $\Omega^{\mathrm{r,k}}_{\bar{n}}$ are the Berry curvature in position space and in mixed position/momentum space, respectively. Further $\bar{n}$ labels an eigenstate of a diagonalized Hamiltonian that is adiabatically connected to a Bloch band n, $\bar{\mathbf{r}}$ and $\bar{\mathbf{k}}$ are kinetic phase-space coordinates, and $\mathcal{E}_{\bar{n}}(\bar{\mathbf{r}}, \bar{\mathbf{k}})$ is the semiclassical energy that contains the gradient correction $\delta\mathcal{E}^{(1)}$, see Eq. (5.14). In Chapter 11, we will evaluate Eq. (10.1) in the case of a metal and an insulator.

10.1. Model and outline of the derivation

We consider a magnetic material with a rigid magnetization texture

$$\mathbf{M}(t, \mathbf{r}) = \mathbf{M}_0(\mathbf{r} - \mathbf{R}(t)) \tag{10.2}$$

where $\mathbf{M}_0$ is a known function of position that describes a single skyrmion in a ferromagnetic background (see, e.g., Ref. [144]), and $\mathbf{R}(t)$ is the trajectory of the skyrmion center. The goal of this chapter is to derive an equation of motion for $\mathbf{R}(t)$ in a disordered magnetic metal in presence of an electric field.

Hamiltonian. We model the electronic properties by the Hamiltonian

$$H(t) = H_{\mathrm{latt}}(t) + H_M(t) + V_{\mathrm{dis}}(\mathbf{r}). \tag{10.3}$$

where H_{latt} is the lattice-periodic part of the Hamiltonian, H_M describes the coupling to the smooth background magnetization, and V_{dis} is a random disorder potential. We

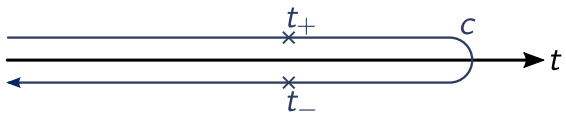

Figure 10.1.: Time evolution in the Keldysh formalism runs from $t = -\infty$ to $t = \infty$ and back to $t = -\infty$. We denote the value of a field ψ at time t on the forward (backward) branch of the time evolution by $\psi(t_+)$ ($\psi(t_-)$).

have

$$H_{\text{latt}}(t) = \frac{(-i\hbar\boldsymbol{\nabla} + e\mathbf{A}(t))^2}{2m} + V(\mathbf{r}) + H_{\text{so}}; \tag{10.4}$$

$$H_{\text{M}}(t) = -J\mathbf{M}(t, \mathbf{r}) \cdot \boldsymbol{\sigma}. \tag{10.5}$$

where m is the bare mass of the electrons with charge $-e$, $\mathbf{A}$ is a homogeneous external vector potential, which generates the electric field $\mathbf{E} = -\partial\mathbf{A}/\partial t$, V is the periodic crystal potential, H_{so} is the spin-orbit (SO) coupling term defined in Eq. (4.22), $J > 0$ is a coupling constant, and $\boldsymbol{\sigma}$ is the vector of Pauli matrices acting on the spin degree of freedom of the electrons.

Real-time action. The Hamiltonian Eq. (10.3) depends on time t due to the time-dependent vector potential $\mathbf{A}(t)$ and the skyrmion trajectory $\mathbf{R}(t)$, which enters via Eq. (10.2). Both the external electric field and the movement of the skyrmion drive the electronic system out of equilibrium, and we derive an equation of motion for $\mathbf{R}(t)$ using Keldysh formalism (see, e.g., Refs. [83, 116, 145]). In this section, we introduce the central quantities on which the derivation of the equation of motion is based. In doing so, we briefly review the required concepts from the Keldysh formalism, using conventions and notation from Ref. [145].

In Keldysh formalism, one deals with the partition function $\mathcal{Z} = \text{Tr}[U_c\, \rho(-\infty)]$ where $\rho(-\infty)$ is the density matrix at time $t \to -\infty$ and the time-evolution operator $U_c = U_-(-\infty, \infty)U_+(\infty, -\infty) = \mathcal{T}_c \exp\left[-\frac{i}{\hbar}\int_c \mathrm{d}t\, \mathcal{H}(t)\right]$ takes the system from $t \to -\infty$ to $t \to \infty$ and back to $t \to -\infty$ along the Keldysh contour "c" (Figure 10.1), where $\mathcal{T}_c$ denotes time-ordering along the Keldysh contour and $\mathcal{H}(t)$ is many-body Hamiltonian. Evidently, $U_c = \mathbb{1}$ if the Hamiltonian is identical on the forward and backward branch of the Keldysh contour, i.e., if $\mathcal{H}(t_+) = \mathcal{H}(t_-)$ for all t. Correlation functions are obtained by differentiating $\mathcal{Z}$ w.r.t. so-called source terms, which take a different value on the forward and backward branch. At the end of the calculation, one has to set all source terms to zero to restore the physical situation.

Using path integrals, the partition function is given by $\mathcal{Z} = \int \mathcal{D}[\bar{\psi}, \psi, \mathbf{R}]\, e^{iS[\bar{\psi}, \psi, \mathbf{R}]}$,

where the real-time action S for our model, Eqs. (10.2)–(10.5), is given by

$$\begin{aligned} S[\bar{\psi},\psi,\mathbf{R}] &= \int_c \mathrm{d}t\, L[\bar{\psi}(t),\psi(t),\mathbf{R}(t)] \\ &= \int_{-\infty}^{\infty} \mathrm{d}t\, L[\bar{\psi}(t_+),\psi(t_+),\mathbf{R}(t_+)] + \int_{\infty}^{-\infty} \mathrm{d}t\, L[\bar{\psi}(t_-),\psi(t_-),\mathbf{R}(t_-)]. \end{aligned} \tag{10.6}$$

Here, $\bar{\psi} \equiv (\bar{\psi}_\uparrow, \bar{\psi}_\downarrow)$ and $\psi \equiv (\psi_\uparrow, \psi_\downarrow)^T$ are spinors of Graßmann fields, the time integral runs along the Keldysh contour (Figure 10.1), t_+ (t_-) denotes that the corresponding Graßmann field is evaluated on the forward (backward) part of the Keldysh contour, and the Lagrangian is given by

$$L[\bar{\psi}(t),\psi(t),\mathbf{R}(t)] = \int \mathrm{d}^d r\, \bar{\psi}(t,\mathbf{r})\,(i\hbar\partial_t - H(t))\,\psi(t,\mathbf{r}). \tag{10.7}$$

We apply the usual Keldysh rotation for fermionic systems [145],

$$\begin{aligned} \psi_1(t,\mathbf{r}) &:= \frac{1}{\sqrt{2}}(\psi(t_+,\mathbf{r}) + \psi(t_-,\mathbf{r})); \qquad \psi_2(t,\mathbf{r}) := \frac{1}{\sqrt{2}}(\psi(t_+,\mathbf{r}) - \psi(t_-,\mathbf{r})); \\ \bar{\psi}_1(t,\mathbf{r}) &:= \frac{1}{\sqrt{2}}\big(\bar{\psi}(t_+,\mathbf{r}) - \bar{\psi}(t_-,\mathbf{r})\big); \qquad \bar{\psi}_2(t,\mathbf{r}) := \frac{1}{\sqrt{2}}(\bar{\psi}(t_+,\mathbf{r}) + \bar{\psi}(t_-,\mathbf{r})), \end{aligned} \tag{10.8}$$

which leads to

$$S[\bar{\psi},\psi,\mathbf{R}] = \int_{-\infty}^{\infty} \mathrm{d}t_1 \int_{-\infty}^{\infty} \mathrm{d}t_2 \int \mathrm{d}^d r_1 \int \mathrm{d}^d r_2\, \bar{\psi}_\alpha(t_1,\mathbf{r}_1)\, g^{-1}_{\alpha\beta}(t_1,\mathbf{r}_1;t_2,\mathbf{r}_2)\, \psi_\beta(t_2,\mathbf{r}_2) \tag{10.9}$$

where summation over repeated Keldysh indices $\alpha,\beta \in \{1,2\}$ is implied and the local inverse Green's function is given by

$$g^{-1}_{\alpha\beta} = \begin{pmatrix} \big(g^R\big)^{-1} & \big(g^{-1}\big)^K \\ 0 & \big(g^A\big)^{-1} \end{pmatrix}_{\alpha\beta}. \tag{10.10}$$

Here, R, A, and K denote the retarded, advanced, and Keldysh part, respectively. The latter is an infinitesimal regularization term that encodes the initial state at $t \to -\infty$, while the former two are given by

$$\big(g^R\big)^{-1} = g_0^{-1} + \delta(t_1 - t_2)\delta(\mathbf{r}_1 - \mathbf{r}_2)(V_{\mathrm{dis}}(\mathbf{r}_1) + i0_+); \tag{10.11}$$

$$\big(g^A\big)^{-1} = g_0^{-1} + \delta(t_1 - t_2)\delta(\mathbf{r}_1 - \mathbf{r}_2)(V_{\mathrm{dis}}(\mathbf{r}_1) - i0_+) \tag{10.12}$$

where 0_+ is an infinitesimal positive number and the disorder-free part of the inverse Green's function is

$$g_0^{-1}(t_1,\mathbf{r}_1;t_2,\mathbf{r}_2) = i\hbar\delta'(t_1 - t_2)\delta(\mathbf{r}_1 - \mathbf{r}_2) - \delta(t_1 - t_2)\delta(\mathbf{r}_1 - \mathbf{r}_2)H(t_2) \tag{10.13}$$

where δ' is the derivative of the delta distribution, defined by $\int \mathrm{d}x\, \delta'(x) f(x) := -f'(0)$, and $H(t_2)$ is understood to act as a differential operator on $\psi_\beta(t_2,\mathbf{r}_2)$ in Eq. (10.9).

Formal equation of motion. We obtain an effective action $S_{\text{eff}}[\mathbf{R}]$ for the skyrmion trajectory $\mathbf{R}(t)$ from Eq. (10.6) by integrating out the fermionic fields,

$$S_{\text{eff}}[\mathbf{R}] = -i \log\left[\int \mathcal{D}[\bar{\psi},\psi]\, e^{\frac{i}{\hbar}S[\bar{\psi},\psi,\mathbf{R}]}\right] = -i \log\left[\int \mathcal{D}[\bar{\psi},\psi]\, e^{\frac{i}{\hbar}\int_{-\infty}^{\infty}\mathrm{d}t\, L_+ + \frac{i}{\hbar}\int_{\infty}^{-\infty}\mathrm{d}t\, L_-}\right] \tag{10.14}$$

where L_+ (L_-) denotes the Lagrangian, Eq. (10.7), evaluated on the forward (backward) part of the Keldysh contour. We parameterize the skyrmion trajectory $\mathbf{R}(t)$ by a classical and a quantum component (cf., Ref. [145]),

$$\mathbf{R}(t_+) = \mathbf{R}^{\text{cl}}(t) + \mathbf{R}^{\text{q}}(t) \qquad \text{and} \qquad \mathbf{R}(t_-) = \mathbf{R}^{\text{cl}}(t) - \mathbf{R}^{\text{q}}(t). \tag{10.15}$$

The solution of the classical equation of motion is a stationary point of $S_{\text{eff}}[\mathbf{R}]$ and is identical on the forward and backward part of the time contour. The latter condition is equivalent to $\mathbf{R}^{\text{q}}(t) = 0$ for all t. To find the stationary solution, one has to solve the saddle point equations $\delta S_{\text{eff}}/\delta \mathbf{R}^{\text{cl}}(t) = 0$ and $\delta S_{\text{eff}}/\delta \mathbf{R}^{\text{q}}(t) = 0$. The former is trivially satisfied since $S_{\text{eff}}[\mathbf{R}] = 0$ as long as the quantum component $\mathbf{R}^{\text{q}}(t)$ vanishes for all t, because the forward and backward parts on the right-hand side of Eq. (10.14) cancel for a purely classical trajectory. Thus, the saddle point equation for the classical skyrmion trajectory $\mathbf{R}(t)$ is

$$\left.\frac{\delta S_{\text{eff}}[\mathbf{R}]}{\delta \mathbf{R}^{\text{q}}(t)}\right|_{\mathbf{R}^{\text{q}}=0} = 0. \tag{10.16}$$

Inserting the Hamiltonian Eqs. (10.3)–(10.5), the Lagrangian Eq. (10.7), and the Keldysh rotation Eq. (10.8), we find

$$\frac{1}{\mathcal{Z}[\mathbf{R}]}\int \mathrm{d}^d r\ \mathrm{tr}\left[\frac{\partial H(t)}{\partial \mathbf{R}(t)}\int \mathcal{D}[\bar{\psi},\psi]\, e^{\frac{i}{\hbar}S[\bar{\psi},\psi,\mathbf{R}]}\ \big(\psi_2(t,\mathbf{r})\bar{\psi}_1(t,\mathbf{r}) + \psi_1(t,\mathbf{r})\bar{\psi}_2(t,\mathbf{r})\big)\right] = 0 \tag{10.17}$$

where H_{M} is evaluated at position $\mathbf{r}$, the trace $\mathrm{tr}[\cdots]$ runs over the spin configurations, and $\mathcal{Z}[\mathbf{R}] = \int \mathcal{D}[\bar{\psi},\psi]\, e^{iS[\bar{\psi},\psi,\mathbf{R}]} = 1$ is the partition function, which is equal to 1 for a classical trajectory $\mathbf{R}(t)$ [145]. The left-hand side of Eq. (10.17) is a two-point correlation function. We denote by G the disorder-averaged Green's function,

$$G_{\alpha\beta}(t_1,\mathbf{r}_1;t_2,\mathbf{r}_2) := -\frac{i}{\hbar}\left\langle \int \mathcal{D}[\bar{\psi},\psi]\, e^{\frac{i}{\hbar}S[\bar{\psi},\psi,\mathbf{R}]}\, \psi_\alpha(t_1,\mathbf{r}_1)\bar{\psi}_\beta(t_2,\mathbf{r}_2)\right\rangle_{\text{dis}} = \begin{pmatrix} G^R & G^K \\ 0 & G^A \end{pmatrix}_{\alpha\beta} \tag{10.18}$$

where $\langle\cdots\rangle_{\text{dis}}$ denotes averaging over all disorer configurations and $\alpha,\beta \in \{1,2\}$ are Keldysh indices. The last equality in Eq. (10.18) defines the retarded (G^R), advanced (G^A), and Keldysh (G^K) component, as is customary, and the lower left component vanishes due to causality [145]. By averaging Eq. (10.17) over all disorder configurations, we obtain the formal equation of motion for the skyrmion trajectory,

$$\mathbf{F}^{\text{tot}}(t) := \frac{i\hbar}{2}\int \mathrm{d}^d r\ \mathrm{tr}\left[\frac{\partial H(t)}{\partial \mathbf{R}(t)}\, G^K(t,\mathbf{r};t,\mathbf{r})\right] = 0 \tag{10.19}$$

where we included a prefactor of $\frac{i\hbar}{2}$ in anticipation of the interpretation of $\mathbf{F}^{\mathrm{tot}}$ as the sum of all forces on the skyrmion, which have to balance, see below. The aim of this chapter is to obtain an explicit expression for $\mathbf{F}^{\mathrm{tot}}(t)$. To this end, we will transform into a basis in which the Keldysh Green's function G^K is diagonal in band space, see Section 10.2 below. In a time-dependent system, the Green's function does, in general, not commute with the single-particle Hamiltonian $H(t)$ and thus the basis that diagonalizes G^K does not necessarily diagonalize $H(t)$. Using Eq. (10.13), we can express $\mathbf{F}^{\mathrm{tot}}(t)$ in terms of only the Green's function and the inverse Green's function,

$$\begin{aligned}\mathbf{F}^{\mathrm{tot}}(t) &= -\frac{i\hbar}{2}\int \mathrm{d}^d r \int \mathrm{d}^d r' \int \mathrm{d}t' \ \mathrm{tr}\left[\frac{\partial g_0^{-1}(t,\mathbf{r};t',\mathbf{r}')}{\partial \mathbf{R}(t)}\, G^K(t',\mathbf{r}';t,\mathbf{r})\right] \\ &\equiv -\frac{i\hbar}{2}\int \mathrm{d}^d r \ \mathrm{tr}\left[\left(\frac{\partial g_0^{-1}}{\partial \mathbf{R}(t)} \otimes G^K\right)(t,\mathbf{r};t,\mathbf{r})\right] \end{aligned} \tag{10.20}$$

where, in the second step, we introduced the notation "$\otimes$", which denotes convolution in position, time, and spin space.

Dyson Equation. The disorder-averaged Keldysh Green's function G^K in Eq. (10.20) is obtained from the Dyson equation,

$$\begin{pmatrix} g_0^{-1} - \Sigma^R & -\Sigma^K \\ 0 & g_0^{-1} - \Sigma^A \end{pmatrix} \otimes \begin{pmatrix} G^R & G^K \\ 0 & G^A \end{pmatrix} = \mathbb{1} \tag{10.21}$$

where Σ is the self-energy, which encodes disorder, and $\mathbb{1}$ is the identity in the space of all parameters, i.e., position, time, spin, and Keldysh space. With the usual parametrization of the Keldysh Green's function

$$G^K = G^R \otimes f - f \otimes G^A \tag{10.22}$$

in terms of a hermitian distribution function $f(t_1,\mathbf{r}_1;t_2,\mathbf{r}_2)$, the upper-right component of Eq. (10.21) can be written as a formal transport equation (cf., [145])

$$f \otimes g_0^{-1} - g_0^{-1} \otimes f = \Sigma^K - \left(\Sigma^R \otimes f - f \otimes \Sigma^A\right) \tag{10.23}$$

and the retarded and advanced Green's functions are obtained from the diagonal parts of Eq. (10.21),

$$(g_0^{-1} - \Sigma^{R/A}) \otimes G^{R/A} = \mathbb{1}. \tag{10.24}$$

Outline of the remaining derivation. In this section, we derived a formal equation of motion $\mathbf{F}^{\mathrm{tot}} = 0$ for the skyrmion, where $\mathbf{F}^{\mathrm{tot}}$ is given by Eq. (10.20). The skyrmion trajectory $\mathbf{R}(t)$ enters in the equation of motion indirectly via the Keldysh Green's function G^K, which is given by Eq. (10.22), where f and $G^{R/A}$ are the solutions of Eqs. (10.23) and (10.24), respectively. In the remaining sections of this chapter we derive a general expression for $\mathbf{F}^{\mathrm{tot}}$ that depends explicitly on the skyrmion velocity $\dot{\mathbf{R}}$. The derivation is organized as follows. In Section 10.2, we review a method from Ref. [84] to perturbatively diagonalize the inverse Green's function. We apply this methods first to the

transport equation Eq. (10.23) in order to obtain the distribution function f (Section 10.3). It turns out that, in order to account for local particle number conservation, a position-dependent chemical potential has to be introduced. In Section 10.4, we apply the perturbative band-diagonalization to the expression for the total force on the skyrmion.

10.2. Wigner transform and diagonalized local Green's function

Wigner transform in space and time. The Hamiltonian Eq. (10.3) contains a lattice-periodic part $H_{\mathrm{latt}}(t)$, whose instantaneous eigenstates are Bloch states $|n,t,\mathbf{k}\rangle$ given by

$$\langle \mathbf{r}|n,t,\mathbf{k}\rangle = e^{i\mathbf{k}\cdot\mathbf{r}} u_{n,\mathbf{k}+\frac{e}{\hbar}\mathbf{A}(t)}(\mathbf{r}) \tag{10.25}$$

that satisfy the instantaneous eigenvalue equation

$$H_{\mathrm{latt}}(t)\,|n,t,\mathbf{k}\rangle = \epsilon_n\left(\mathbf{k}+\frac{e}{\hbar}\mathbf{A}(t)\right)|n,t,\mathbf{k}\rangle \tag{10.26}$$

where n is a band index, the canonical momentum $\mathbf{k}$ lies in the 1st Brillouin zone (BZ), $u_{n,\mathbf{k}+\frac{e}{\hbar}\mathbf{A}(t)}(\mathbf{r})$ is the lattice-periodic part of the Bloch function, and $\epsilon_n(\mathbf{k}+\frac{e}{\hbar}\mathbf{A}(t))$ is the instantaneous eigenenergy of $H_{\mathrm{latt}}(t)$ for the state with kinetic momentum $\hbar\mathbf{k}+e\mathbf{A}(t)$. Here, we chose to label the Bloch states $|n,t,\mathbf{k}\rangle$ by their *canonical* lattice momentum $\hbar\mathbf{k}$ rather than the kinetic lattice momentum $\hbar\mathbf{k}+e\mathbf{A}(t)$. In this way, Eq. (10.25) differs from our definition of Bloch states, Eq. (5.6), that we used for the semiclassical description of Section 5.1. Here, we choose to define the Bloch states in terms of the kinetic momentum in order to avoid an unbounded term $-e\mathbf{E}\cdot\mathbf{r}$ in the WT of the inverse Green's function, see Eqs. (10.31)–(10.33) below, which would complicate the treatment of a steady-state electric current in a system with open boundary conditions. With our choice of Bloch states, Eq. (10.25), we will be able to treat the influence of the electric field $\mathbf{E}=-\partial\mathbf{A}/\partial t$ within the same gradient expansion that we will also use to derive Berry-phase effects.

The magnetization $\mathbf{M}(t,\mathbf{r})$ in Eq. (10.3) breaks the discrete translation symmetry so that the states $|n,t,\mathbf{k}\rangle$ are not eigenstates of $H(t)$. Assuming that $\mathbf{M}$ varies on a large length scale $\xi_{\mathrm{mod}} \gg a$ where a is the lattice constant, correlation functions are most efficiently described in Wigner representation, see Section 6.1. The Wigner representation $\tilde{A}(\mathbf{r};\mathbf{k})$ of an operator $\hat{A}$ has the advantage that variations on the two length scales ξ_{mod} and a are separated into the dependency on a "central" position $\mathbf{r}$ and a "central" wave vector $\mathbf{k}$, respectively. For the non-equilibrium system discussed in this chapter, we define the WT in both position and time domain. Here, position and time require a different treatment due to the existence of a periodic lattice in position space, which lacks a corresponding counterpart in the time domain. We define the WT in the time domain according to Eq. (6.1) and in position domain according to Eq. (6.5),

so that the WT of a correlation function $A(t_1, \mathbf{r}_1; t_2, \mathbf{r}_2)$ is defined as

$$\tilde{A}_{mn}(t, \mathbf{r}; \omega, \mathbf{k}) := \int_{-\infty}^{\infty} \mathrm{d}\tau \int' \frac{\mathrm{d}^d q}{(2\pi)^d} \int \mathrm{d}^d r_1 \int \mathrm{d}^d r_2 \, e^{i\omega\tau + i\mathbf{q}\cdot\mathbf{r}} \times \\ \times \left\langle m, t + \frac{\tau}{2}, \mathbf{k} + \frac{\mathbf{q}}{2} \middle| \mathbf{r}_1 \right\rangle A\Big(t + \frac{\tau}{2}, \mathbf{r}_1; t - \frac{\tau}{2}, \mathbf{r}_2\Big) \left\langle \mathbf{r}_2 \middle| n, t - \frac{\tau}{2}, \mathbf{k} - \frac{\mathbf{q}}{2} \right\rangle \tag{10.27}$$

where the prime on the momentum integral is a reminder that the BZ should be chosen such that $\mathbf{k} + \frac{\mathbf{q}}{2}$ and $\mathbf{k} - \frac{\mathbf{q}}{2}$ both run over the same integration region, see discussion in Section 6.1.

Moyal product. For two correlation functions $A(t_1, \mathbf{r}_1; t_2, \mathbf{r}_2)$ and $B(t_1, \mathbf{r}_1; t_2, \mathbf{r}_2)$, the convolution $C = A \otimes B$ is defined by

$$C(t_1, \mathbf{r}_1; t_2, \mathbf{r}_2) = \int \mathrm{d}t' \int \mathrm{d}^d r' \, A(t_1, \mathbf{r}_1; t', \mathbf{r}') B(t', \mathbf{r}'; t_2, \mathbf{r}_2). \tag{10.28}$$

In Wigner representation, the convolution is given by the Moyal product

$$\begin{aligned} \tilde{C}_{mn}(t, \mathbf{r}; \omega, \mathbf{k}) &= \sum_l \tilde{A}_{ml}(t, \mathbf{r}; \omega, \mathbf{k}) \, e^{\frac{i}{2}(\overleftarrow{\partial_\omega}\overrightarrow{\partial_t} - \overleftarrow{\partial_t}\overrightarrow{\partial_\omega} + \overleftarrow{\partial_\mathbf{r}}\cdot\overrightarrow{\partial_\mathbf{k}} - \overleftarrow{\partial_\mathbf{k}}\cdot\overrightarrow{\partial_\mathbf{r}})} \, \tilde{B}_{ln}(t, \mathbf{r}; \omega, \mathbf{k}) \\ &\equiv \sum_l \tilde{A}_{ml}(t, \mathbf{r}; \omega, \mathbf{k}) \, e^{\frac{i}{2} J_{\mu\nu} \overleftarrow{\partial_\mu}\overrightarrow{\partial_\nu}} \, \tilde{B}_{ln}(t, \mathbf{r}; \omega, \mathbf{k}) \end{aligned} \tag{10.29}$$

where we introduced a short-hand notation in the second equality. Here, the derivatives $\partial_\mu \equiv (\partial_t, \partial_\mathbf{r}, \partial_\omega, \partial_\mathbf{k})_\mu$ are in the full space of time, position, frequency, and momentum, and the anti-symmetric matrix J is given by

$$J_{\mu\nu} = \begin{pmatrix} 0 & 0 & -1 & 0 \\ 0 & 0 & 0 & \mathbb{1}_{d\times d} \\ 1 & 0 & 0 & 0 \\ 0 & -\mathbb{1}_{d\times d} & 0 & 0 \end{pmatrix}_{\mu\nu} \tag{10.30}$$

where $\mathbb{1}_{d\times d}$ is the d-dimensional identity matrix. In Eq. (10.29), the exponential function is understood as a formal power series and $\overleftarrow{\partial}$ ($\overrightarrow{\partial}$) denotes a partial derivative that acts only on the factor to the left (right). We use the symbol "$\otimes$" for Moyal products in both position/momentum and time/frequency space, while the symbol "$\circ$" is reserved for Moyal products in position/momentum space only.

Local inverse Green's function. We obtain the WT of g_0^{-1} from Eqs. (10.13) and (10.27),

$$\tilde{g}^{-1}_{0,mn}(t, \mathbf{r}; \omega, \mathbf{k}) = \hbar\omega\delta_{mn} - \tilde{H}_{mn}(t, \mathbf{r}; \mathbf{k}) + \mathbf{E}(t) \cdot \tilde{\mathbf{D}}_{mn}(t, \mathbf{r}; \mathbf{k}) \tag{10.31}$$

where, in the basis of Eq. (10.25),

$$\tilde{H}_{mn}(t,\mathbf{r};\mathbf{k}) = \delta_{mn}\,\epsilon_m\left(\mathbf{k}+\frac{e}{\hbar}\mathbf{A}(t)\right) + \tilde{H}_{\mathrm{M},mn}(t,\mathbf{r};\mathbf{k}). \tag{10.32}$$

Here, $\tilde{H}_{\mathrm{M},mn}$ is the WT of H_{M}, Eq. (10.5), the electric field is $\mathbf{E}(t) = -\partial\mathbf{A}(t)/\partial t$, and $\tilde{\mathbf{D}}_{mn}(t,\mathbf{r};\mathbf{k})$ is the WT of the electric dipole operator,

$$\begin{aligned}\tilde{\mathbf{D}}_{mn}(t,\mathbf{r};\mathbf{k}) &= ie\int\frac{\mathrm{d}^d q}{(2\pi)^d}\int\mathrm{d}^d r'\,e^{i\mathbf{q}\cdot(\mathbf{r}-\mathbf{r}')}\,\frac{\partial}{\partial\mathbf{q}}\left[u^*_{m,\mathbf{k}+\frac{e}{\hbar}\mathbf{A}(t)+\frac{\mathbf{q}}{2}}(\mathbf{r}')\,u_{n,\mathbf{k}+\frac{e}{\hbar}\mathbf{A}(t)-\frac{\mathbf{q}}{2}}(\mathbf{r}')\right]\\ &= -e\int\frac{\mathrm{d}^d q}{(2\pi)^d}\,e^{i\mathbf{q}\cdot\mathbf{r}}\left\langle m,t,\mathbf{k}+\frac{\mathbf{q}}{2}\middle|(\hat{\mathbf{r}}-\mathbf{r})\middle|n,t,\mathbf{k}-\frac{\mathbf{q}}{2}\right\rangle\end{aligned} \tag{10.33}$$

where $\hat{\mathbf{r}}$ is the position operator, while $\mathbf{r}$ is the position argument of $\tilde{\mathbf{D}}_{mn}(t,\mathbf{r};\mathbf{k})$, and the subtraction $(\hat{\mathbf{r}}-\mathbf{r})$ leads to a cancellation of unbounded terms that would grow proportionally to the size of the sample. The appearance of the position coordinate $\mathbf{r}$ on the right-hand side of Eq. (10.33) is a consequence of our choice to label the Bloch states by their canonical momentum $\hbar\mathbf{k}$, see Eq. (10.25). The fact that the electric dipole energy $-\mathbf{E}\cdot\tilde{\mathbf{D}}$ appears naturally in the denominator of the Green's function, Eq. (10.31), demonstrates the benefit of using a well-defined WT, Eq. (10.27), that takes the underlying lattice into account.

So far, Eqs. (10.31)–(10.33) are exact relations. To obtain an approximate expression for $\tilde{H}_{\mathrm{M}}$, we expand in gradients of the magnetization. To linear order, we obtain from Eqs. (10.2) and (10.5),

$$\begin{aligned}\tilde{H}_{\mathrm{M},mn}(t,\mathbf{r};\mathbf{k}) \approx\ & -J\mathbf{M}_0(\mathbf{r}-\mathbf{R}(t))\cdot\langle m,t,\mathbf{k}|\boldsymbol{\sigma}|n,t,\mathbf{k}\rangle\\ & -\frac{J}{2}\frac{\partial M_{0,j}(\mathbf{r}-\mathbf{R}(t))}{\partial r_i}\left(\frac{\partial\langle m,t,\mathbf{k}|}{\partial k_i}\sigma_j\,|n,t,\mathbf{k}\rangle - \langle m,t,\mathbf{k}|\,\sigma_j\frac{\partial|n,t,\mathbf{k}\rangle}{\partial k_i}\right)\end{aligned} \tag{10.34}$$

where the second term vanishes in absence of SO coupling.

Perturbative band-diagonalization. In Wigner representation for a system with N bands, the transport equation Eq. (10.23) is a system of $N\times N$ coupled partial differential equations for the components $\tilde{f}_{mn}(t,\mathbf{r};\omega,\mathbf{k})$ of the distribution function. Even if the transport equation is expressed in the local eigenbasis of $\tilde{g}_0^{-1}(t,\mathbf{r};\omega,\mathbf{k})$, derivatives $\partial_i\tilde{g}_0^{-1}$ coming from the Moyal products in Eq. (10.23) introduce couplings between different bands. Wickles and Belzig [84] developed a method to decouple the system of $N\times N$ equations order-by-order in the gradients. It turns out that, in a system out of equilibrium, off-diagonal components of $\tilde{f}_{mn}$ in the local eigenbasis of $\tilde{g}_0^{-1}$ become finite. As we will show in Section 10.4, a gauge-invariant total force $\mathbf{F}^{\mathrm{tot}}$ on the skyrmion can only be obtained if the contribution from these off-diagonal components of $\tilde{f}_{mn}$ is taken into account.

In the following, we summarize the method from Ref. [84]. The main idea is to introduce a unitary transformation $\tilde{\mathcal{U}}$ that diagonalizes the WT $\tilde{g}_0^{-1}$ of the inverse Green's

function. For simplicity, we consider only situations where $\tilde{g}_0^{-1}$ has no degeneracies. Degeneracies can be taken into account by generalizing the diagonalization of $\tilde{g}_0^{-1}$ to a block-diagonalization, see Ref. [84]. In absence of degeneracies, $\tilde{\mathcal{U}}(t, \mathbf{r}; \omega, \mathbf{k})$ is defined such that

$$\bar{\tilde{g}}_0^{-1} := \tilde{\mathcal{U}} \otimes \tilde{g}_0^{-1} \otimes \tilde{\mathcal{U}}^\dagger \tag{10.35}$$

is diagonal in band space. We denote the N eigenstates of $\bar{\tilde{g}}_0^{-1}$ by $|\bar{n}\rangle$. Note that Eq. (10.35) is not just a pointwise diagonalization of the $(N \times N)$-matrix-valued function $\tilde{g}_0^{-1}(t, \mathbf{r}; \omega, \mathbf{k})$, but rather a diagonalization of the full inverse Green's function g_0^{-1} understood as an operator in time and single-particle Hilbert space. Due to the Moyal products on the right-hand side of Eq. (10.35), the transformation $\tilde{\mathcal{U}}(t, \mathbf{r}; \omega, \mathbf{k})$ depends not only on the value of $\tilde{g}_0^{-1}$ at the point $(t, \mathbf{r}; \omega, \mathbf{k})$, but also on its gradients. One formally expands

$$\tilde{\mathcal{U}}(t, \mathbf{r}; \omega, \mathbf{k}) = \big(\mathbb{1} + \tilde{\mathcal{U}}_1(t, \mathbf{r}; \omega, \mathbf{k}) + \tilde{\mathcal{U}}_2(t, \mathbf{r}; \omega, \mathbf{k}) + \dots\big)\, \tilde{\mathcal{U}}_0(t, \mathbf{r}; \omega, \mathbf{k}) \tag{10.36}$$

where the subscript denotes the order in spatial and temporal gradients. Unitarity $\tilde{\mathcal{U}} \otimes \tilde{\mathcal{U}}^\dagger = \mathbb{1}$ must hold to each order in the gradients, which implies

$$\tilde{\mathcal{U}}_0 \tilde{\mathcal{U}}_0^\dagger = \mathbb{1}; \qquad \text{and} \qquad \tilde{\mathcal{U}}_1 + \tilde{\mathcal{U}}_1^\dagger + \frac{i}{2} J_{\mu\nu} (\partial_\mu \tilde{\mathcal{U}}_0)(\partial_\nu \tilde{\mathcal{U}}_0^\dagger) = 0. \tag{10.37}$$

Since $\tilde{\mathcal{U}}$ is a non-local transformation, it also affects the coordinates $\mathbf{r}$, ω, and $\mathbf{k}$, which become matrices in band-space. We will refer to the coordinates in the new frame of reference as the kinetic coordinates $\bar{\mathbf{r}}$, $\bar{\omega}$, and $\bar{\mathbf{k}}$. Their diagonal components in band n are given by

$$\bar{\mathbf{r}}_{\bar{n}} := \langle \bar{n} | \tilde{\mathcal{U}} \otimes \mathbf{r} \otimes \tilde{\mathcal{U}}^\dagger | \bar{n} \rangle \approx \mathbf{r} + \boldsymbol{\mathcal{A}}^{\mathrm{k}}_{\bar{n}}; \tag{10.38}$$

$$\bar{\omega}_{\bar{n}} := \langle \bar{n} | \tilde{\mathcal{U}} \otimes \omega \otimes \tilde{\mathcal{U}}^\dagger | \bar{n} \rangle \approx \omega + \mathcal{A}^{\mathrm{t}}_{\bar{n}}; \tag{10.39}$$

$$\bar{\mathbf{k}}_{\bar{n}} := \langle \bar{n} | \tilde{\mathcal{U}} \otimes \mathbf{k} \otimes \tilde{\mathcal{U}}^\dagger | \bar{n} \rangle \approx \mathbf{k} - \boldsymbol{\mathcal{A}}^{\mathrm{r}}_{\bar{n}}\,. \tag{10.40}$$

In the second equality on each line, we expanded to linear order in the gradients using Eq. (10.37). Here, the Berry connections $\mathcal{A}^{\mathrm{t}}_{\bar{n}}$, $\boldsymbol{\mathcal{A}}^{\mathrm{r}}_{\bar{n}}$, and $\boldsymbol{\mathcal{A}}^{\mathrm{k}}_{\bar{n}}$ are the diagonal components in band $\bar{n}$ of the matrices

$$\mathcal{A}^{\mathrm{t/r/k}} := \tilde{\mathcal{U}}_0 \big(i \partial_{t/\mathbf{r}/\mathbf{k}} \tilde{\mathcal{U}}_0^\dagger\big). \tag{10.41}$$

For symmetry reasons, one would also expect a Berry-phase correction to the time, $\bar{t} = t - \mathcal{A}^{\omega}_{\bar{n}}$, but it turns out that $\mathcal{A}^{\omega}_{\bar{n}}$ vanishes in a non-interacting system [84]. Due to our choice of reference states for the WT, Eq. (10.25), the inverse Green's function $\tilde{g}_0^{-1}$ is a function of $\mathbf{k} + \frac{e}{\hbar}\mathbf{A}(t)$. Neglecting the small position-dependency of the electric dipole energy $-\mathbf{E} \cdot \tilde{\mathbf{D}}$ in Eq. (10.31), the position-dependency of $\tilde{g}_0^{-1}$ is described by a function of $\mathbf{r} - \mathbf{R}(t)$. Thus, the time dependency of $\tilde{g}_0^{-1}$, and therefore also of $\tilde{\mathcal{U}}_0$, comes from the vector potential $\mathbf{A}(t)$ and the skyrmion position $\mathbf{R}(t)$, and we find

$$\frac{\partial \tilde{\mathcal{U}}_0}{\partial t} = -\frac{e}{\hbar} \mathbf{E}(t) \cdot \frac{\partial \tilde{\mathcal{U}}_0}{\partial \mathbf{k}} - \dot{\mathbf{R}}(t) \cdot \frac{\partial \tilde{\mathcal{U}}}{\partial \mathbf{r}} \tag{10.42}$$

and therefore,

$$\mathcal{A}^{\mathrm{t}} = -\frac{e}{\hbar}\mathbf{E}(t)\cdot\boldsymbol{\mathcal{A}}^{\mathrm{k}} - \dot{\mathbf{R}}(t)\cdot\boldsymbol{\mathcal{A}}^{\mathrm{r}} \tag{10.43}$$

where we used $\mathbf{E}(t) = -\partial\mathbf{A}(t)/\partial t$.

Correlation functions $\bar{\tilde{A}}$ in the new frame of reference are most naturally expressed in terms of the kinetic coordinates. For any Wigner transformed correlation function $\tilde{A}(t,\mathbf{r};\omega,\mathbf{k})$, we define

$$\bar{\tilde{A}}(t,\bar{\mathbf{r}};\bar{\omega},\bar{\mathbf{k}}) := \tilde{\mathcal{U}}(t,\mathbf{r};\omega,\mathbf{k}) \otimes \tilde{A}(t,\mathbf{r};\omega,\mathbf{k}) \otimes \tilde{\mathcal{U}}^{\dagger}(t,\mathbf{r};\omega,\mathbf{k}). \tag{10.44}$$

In the calculations in this chapter, we will only encounter correlation functions $\bar{\tilde{A}}(t,\bar{\mathbf{r}};\bar{\omega},\bar{\mathbf{k}})$ which are band-diagonal in the new frame of reference. For the diagonal component of $\bar{\tilde{A}}$ in band $\bar{n}$, the kinetic coordinates $\bar{\mathbf{r}}_{\bar{n}}$, $\bar{\omega}_{\bar{n}}$, and $\bar{\mathbf{k}}_{\bar{n}}$ on the left-hand side of Eq. (10.44) are always understood to be evaluated in the same band and we will drop the subscript $\bar{n}$ to improve readability.

Integrals over the canonical phase-space coordinates $\mathbf{r}$ and $\mathbf{k}$ can be transformed into integrals over the kinetic coordinates using the Jacobi determinant

$$\bar{D}_{\bar{n}}(t,\bar{\mathbf{r}};\bar{\mathbf{k}}) := \frac{1}{(2\pi)^d}\det\left[\left(\frac{\partial(\bar{\mathbf{r}}_{\bar{n}},\bar{\mathbf{k}}_{\bar{n}})}{\partial(\mathbf{r},\mathbf{k})}\right)^{-1}\right] \approx \frac{1}{(2\pi)^d}\left(1 - \sum_{i=1}^{d}\Omega^{\mathrm{r,k}}_{\bar{n},ii}(t,\bar{\mathbf{r}};\bar{\mathbf{k}})\right) \tag{10.45}$$

where we included a factor of $1/(2\pi)^d$ to be consistent with Section 5.2 and Ref. [65] and we evaluated the determinant to linear order in the Berry curvature $\Omega_{\bar{n}}$. The Jacobi determinant $\bar{D}_{\bar{n}}$ is precisely the density of states in phase space discussed in Section 5.2, see Eq. (5.32). Here, $\Omega^{\mathrm{r,k}}_{\bar{n},ii}$ is the (r_i,k_i)-component of the Berry curvature tensor $\Omega_{\bar{n}}$ in time, position, and momentum,[1]

$$\Omega_{\bar{n},\mu\nu} := \partial_\mu\mathcal{A}_{\bar{n},\nu} - \partial_\nu\mathcal{A}_{\bar{n},\mu} = i\,\langle\bar{n}|(\partial_\mu\tilde{\mathcal{U}}_0)(\partial_\nu\tilde{\mathcal{U}}_0^{\dagger})|\bar{n}\rangle \tag{10.46}$$

where μ and ν are placeholders for any component of t, $\mathbf{r}$, or $\mathbf{k}$, and Berry curvatures w.r.t. frequency ω vanish in a non-interacting system. Using Eq. (10.42), we obtain for the Berry curvatures with a time component,

$$\Omega^{\mathrm{r,t}}_{\bar{n},i} = -\frac{e}{\hbar}\Omega^{\mathrm{r,k}}_{\bar{n},ij}E_j - \Omega^{\mathrm{r,r}}_{\bar{n},ij}\dot{R}_j \tag{10.47}$$

$$\Omega^{\mathrm{k,t}}_{\bar{n},i} = -\frac{e}{\hbar}\Omega^{\mathrm{k,k}}_{\bar{n},ij}E_j - \Omega^{\mathrm{k,r}}_{\bar{n},ij}\dot{R}_j \tag{10.48}$$

For completeness, we note that one can express the Moyal product "$\otimes$", Eq. (10.29), in terms of derivatives w.r.t. the kinetic coordinates. To leading order in the Berry curvature, one obtains [84],

$$(\bar{\tilde{A}}\otimes\bar{\tilde{B}})_{\bar{n}}(t,\bar{\mathbf{r}};\bar{\omega},\bar{\mathbf{k}}) = \bar{\tilde{A}}_{\bar{n}}(t,\bar{\mathbf{r}};\bar{\omega},\bar{\mathbf{k}})\, e^{\frac{i}{2}(J - J\Omega_{\bar{n}}J)_{\mu\nu}\overleftarrow{\partial_\mu}\overrightarrow{\partial_\nu}}\,\bar{\tilde{B}}_{\bar{n}}(t,\bar{\mathbf{r}};\bar{\omega},\bar{\mathbf{k}}) \tag{10.49}$$

[1] Note that our notation differs from the one in Ref. [84], where Berry curvatures are denoted by Θ and the symbol Ω is used for a different quantity.

where the matrix J is defined in Eq. (10.30) and $\overleftarrow{\partial_\mu}$ ($\overrightarrow{\partial_\nu}$) denotes the partial derivative on component μ (ν) of the kinetic coordinates $(t, \bar{\mathbf{r}}; \bar{\omega}, \bar{\mathbf{k}})$, acting on the factor to the left (right). For our calculations, however, it turns out that it is easier to perform all Moyal products in canonical coordinates, as defined in Eq. (10.29).

Diagonalized local inverse Green's function. Using kinetic coordinates and keeping gradient corrections only to leading order, the band-diagonal inverse Green's function $\bar{\tilde{g}}_0^{-1}$, Eq. (10.35), was derived in Ref. [84] for a general non-interacting system. Its component in band $\bar{n}$ is given by

$$\bar{\tilde{g}}_{0,\bar{n}}^{-1}(t, \bar{\mathbf{r}}; \bar{\omega}, \bar{\mathbf{k}}) \approx \hbar\bar{\omega}_{\bar{n}} - \mathcal{E}_{\bar{n}}(t, \bar{\mathbf{r}}; \bar{\mathbf{k}}) \tag{10.50}$$

with

$$\mathcal{E}_{\bar{n}}(t, \bar{\mathbf{r}}; \bar{\mathbf{k}}) = \mathcal{E}_{\bar{n}}^{(0)}(t, \bar{\mathbf{r}}; \bar{\mathbf{k}}) + \delta\mathcal{E}_{\bar{n}}^{(1)}(t, \bar{\mathbf{r}}; \bar{\mathbf{k}}) \tag{10.51}$$

where $\mathcal{E}_{\bar{n}}^{(0)}$ is the (local instantaneous) eigenvalue of $(\tilde{H} - \mathbf{E}\cdot\tilde{\mathbf{D}})$, see Eq. (10.31), evaluated at the kinetic coordinates $\bar{\mathbf{r}}$ and $\bar{\mathbf{k}}$, and $\delta\mathcal{E}_{\bar{n}}^{(1)}$ is the gradient correction to the local energy, which we already encountered in the semiclassical treatment of Section 5.1. The latter is given by Eqs. (5.14) and (5.15), which, in the notation of this chapter, read as

$$\begin{aligned}
\delta\mathcal{E}_{\bar{n}}^{(1)}(t, \bar{\mathbf{r}}; \bar{\mathbf{k}}) &= -\sum_{i=1}^{d} \mathrm{Im}\left[\left\langle \bar{n}\left| \frac{\partial\tilde{\mathcal{U}}_0}{\partial r_i}\left(\mathcal{E}_{\bar{n}}^{(0)} - \left(\tilde{H} - \mathbf{E}\cdot\tilde{\mathbf{D}}\right)\right)\frac{\partial\tilde{\mathcal{U}}_0^\dagger}{\partial k_i}\right|\bar{n}\right\rangle\right] \\
&= -\sum_{i=1}^{d}\sum_{\bar{m}\neq\bar{n}} \mathrm{Im}\left[\frac{\langle\bar{n}|\tilde{\mathcal{U}}_0\frac{\partial\bar{\tilde{g}}_0^{-1}}{\partial r_i}\tilde{\mathcal{U}}_0^\dagger|\bar{m}\rangle\ \langle\bar{m}|\tilde{\mathcal{U}}_0\frac{\partial\bar{\tilde{g}}_0^{-1}}{\partial k_i}\tilde{\mathcal{U}}_0^\dagger|\bar{n}\rangle}{\mathcal{E}_{\bar{n}}^{(0)} - \mathcal{E}_{\bar{m}}^{(0)}}\right].
\end{aligned} \tag{10.52}$$

10.3. Transport equation and local charge conservation

We now turn to the transport equation Eq. (10.23). In the new frame of reference defined by Eq. (10.44), the transport equation reads as

$$\bar{\bar{f}} \otimes \bar{\bar{g}}_0^{-1} - \bar{\bar{g}}_0^{-1} \otimes \bar{\bar{f}} = \bar{\bar{\Sigma}}^K - \left(\bar{\bar{\Sigma}}^R \otimes \bar{\bar{f}} - \bar{\bar{f}} \otimes \bar{\bar{\Sigma}}^A\right) \tag{10.53}$$

where the band-diagonal inverse local Green's function $\bar{\bar{g}}_0^{-1}$ is given in Eq. (10.50) and the Moyal product "$\otimes$" is defined in Eq. (10.49). The distribution function $\bar{\bar{f}}(t, \mathbf{r}; \omega, \mathbf{k})$ encodes the probability that a single-particle state with energy $\hbar\omega$, position $\mathbf{r}$, and momentum $\hbar\mathbf{k}$ (to zeroth order in the gradients) is occupied at time t. In a time-independent system, Eq. (10.53) is solved by the scalar equilibrium distribution function $\bar{\bar{f}}^{\mathrm{eq}}(\bar{\omega}) = \tanh(\hbar\bar{\omega}/(2k_BT)) = (1 - 2n_F(\hbar\bar{\omega}))$, where T is the temperature and n_F is the Fermi distribution [145]. The external electric field $\mathbf{E} = -\partial\mathbf{A}/\partial t$ and the motion of the skyrmion drive the system out of equilibrium, and the solution of the transport equation deviates from $\bar{\bar{f}}^{\mathrm{eq}}$.

The left-hand side of Eq. (10.53) describes ballistic motion of electrons. Gradient terms from the Moyal products lead to a coupling to the electric field, the skyrmion velocity $\dot{\mathbf{R}}$, and to Berry-phase effects that influence the electron trajectories. The right-hand side describes scattering processes that drive the system back towards local equilibrium. In this work, we focus on the discussion of *intrinsic* Berry-phase effects on the skyrmion dynamics, i.e., we take gradient-corrections into account only on the left-hand side of the transport equation and neglect the influence of Berry phases on scattering processes (e.g., side-jump scattering). A more more elaborate discussion that takes Berry-phase effects on scattering processes into account remains the subject for future investigations.

We further neglect inter-band scattering so that the self-energies $\bar{\tilde{\Sigma}}^{R/A/K}$ are diagonal in band space. Since the inverse Green's function $\bar{\tilde{g}}_0^{-1}$ is band-diagonal by construction, Eq. (10.53) is solved by a diagonal distribution function $\bar{\tilde{f}}_{\bar{n}}$. This is the main reason why we introduced the transformation Eq. (10.44): we started out from a transport equation Eq. (10.23) that is a system of $N \times N$ coupled partial differential equations for the components of $\tilde{f}_{mn}$; in the new frame of reference, the transport equation Eq. (10.53) reduces to N independent partial differential equations for the components of $\bar{\tilde{f}}_{\bar{n}}$. In the original frame of reference, the distribution function $\tilde{f} = \tilde{\mathcal{U}}^\dagger \otimes \bar{\tilde{f}} \otimes \tilde{\mathcal{U}}$ obtains non-vanishing off-diagonal elements, which would be difficult to obtain by solving the system of $N \times N$ partial differential equations directly. The detour to the band-diagonalized representation allows us to calculate off-diagonal elements of $\tilde{f}$ perturbatively in spatial and temporal gradients.

Left-hand side of the transport equation. The left-hand side of Eq. (10.53) has been derived to leading order in the gradients in Ref. [84]. The authors found the result

$$\begin{aligned}\text{l.h.s.} = -i\Bigg[&\hbar\partial_t + \hbar\frac{\mathrm{d}\bar{\mathbf{r}}_{\bar{n}}}{\mathrm{d}t}\cdot\frac{\partial}{\partial\bar{\mathbf{r}}} + \hbar\frac{\mathrm{d}\bar{\mathbf{k}}_{\bar{n}}}{\mathrm{d}t}\cdot\frac{\partial}{\partial\bar{\mathbf{k}}} \\ &+ \left(\frac{\partial\mathcal{E}_{\bar{n}}}{\partial t} + \left(\boldsymbol{\Omega}^{\mathrm{r,t}}_{\bar{n}} - \frac{e}{\hbar}\mathbf{E}\right)\cdot\frac{\partial\mathcal{E}_{\bar{n}}}{\partial\bar{\mathbf{k}}} - \boldsymbol{\Omega}^{\mathrm{k,t}}_{\bar{n}}\cdot\frac{\partial\mathcal{E}_{\bar{n}}}{\partial\bar{\mathbf{r}}}\right)\frac{\partial}{\partial\bar{\omega}_{\bar{n}}}\Bigg]\bar{\tilde{f}}_{\bar{n}}\end{aligned} \tag{10.54}$$

where $\frac{\mathrm{d}\bar{\mathbf{r}}_{\bar{n}}}{\mathrm{d}t}$ and $\frac{\mathrm{d}\bar{\mathbf{k}}_{\bar{n}}}{\mathrm{d}t}$ are given by the semiclassical equations of motion, see Eqs. (5.19)–(5.20); explicitly, in absence of an orbital magnetic field,

$$\frac{\mathrm{d}\bar{r}_{\bar{n},i}}{\mathrm{d}t} = \frac{\partial\mathcal{E}_{\bar{n}}}{\hbar\,\partial\bar{k}_{\bar{n},i}} - \Omega^{\mathrm{k,t}}_{\bar{n},i} - \Omega^{\mathrm{k,r}}_{\bar{n},ij}\frac{\mathrm{d}\bar{r}_{\bar{n},j}}{\mathrm{d}t} - \Omega^{\mathrm{k,k}}_{\bar{n},ij}\frac{\mathrm{d}\bar{k}_{\bar{n},j}}{\mathrm{d}t}; \tag{10.55}$$

$$\hbar\frac{\mathrm{d}\bar{k}_{\bar{n},i}}{\mathrm{d}t} = -\frac{\partial\mathcal{E}_n}{\partial\bar{r}_{\mathrm{c},i}} - eE_i + \hbar\,\Omega^{\mathrm{r,t}}_{\bar{n},i} + \hbar\,\Omega^{\mathrm{r,r}}_{\bar{n},ij}\frac{\mathrm{d}\bar{r}_{\bar{n},j}}{\mathrm{d}t} + \hbar\,\Omega^{\mathrm{r,k}}_{\bar{n},ij}\frac{\mathrm{d}\bar{k}_{\bar{n},j}}{\mathrm{d}t}. \tag{10.56}$$

Right-hand side of the transport equation. For the quadratic action Eq. (10.9), only disorder diagrams contribute to the self-energy Σ. Since our focus lies on *intrinsic* forces on the skyrmion we use a very simple approximation for the self-energy, neglecting both gradient-corrections and inter-band scattering. With these simplifications the right-hand side of Eq. (10.53) is obtained with the following standard techniques (cf., Ref. [145]). We

model the disorder potential $V_{\rm dis}(\mathbf{r}) = \sum_i V_i\,\delta(\mathbf{r}-\mathbf{r}_i)$ by a random configuration of short-ranged non-magnetic scattering centers with uncorrelated amplitudes V_i and positions $\mathbf{r}_i$. The amplitudes V_i are assumed to obey a Gaussian distribution characterized by $\langle V_i\rangle_{\rm dis} = 0$, $\langle V_i V_j\rangle_{\rm dis} = \delta_{ij}V_0^2$, and vanishing higher cumulants, where V_0 characterizes the typical amplitude of individual scattering centers (V_0 has dimension of energy times volume). Within this model, the disorder average of any quantity can be expressed by Wick's theorem in terms of the first two cumulants,

$$\langle V_{\rm dis}(\mathbf{r})\rangle_{\rm dis} = 0 \qquad \text{and} \qquad \big\langle V_{\rm dis}(\mathbf{r})V_{\rm dis}(\mathbf{r}')\big\rangle_{\rm dis} = n_{\rm imp}V_0^2\delta(\mathbf{r}-\mathbf{r}') \tag{10.57}$$

where $n_{\rm imp}$ is the impurity concentration. In the self-consistent Born approximation, the self-energy is given by

$$\Sigma_{\alpha\beta}(t_1,\mathbf{r}_1;t_2,\mathbf{r}_2) \approx G_{\alpha\beta}(t_1,\mathbf{r}_1;t_2,\mathbf{r}_2)\,\langle V_{\rm dis}(\mathbf{r}_1)V_{\rm dis}(\mathbf{r}_2)\rangle_{\rm dis} =$$

(10.58)

where α and β are Keldysh indices, the solid line indicates a disorder-averaged Green's function G, crosses denote scattering centers, and the dotted line indicates Wick contraction for the disorder average. This approximation neglects disorder diagrams with crossing impurity lines, such as

(10.59)

whose contribution to G is suppressed in good metals due to the short range of the individual scattering potentials.

Neglecting both gradient corrections and inter-band scattering, we obtain for the WT of the self-energy in the diagonalized basis,

$$\begin{aligned}\bar{\bar{\Sigma}}_{\bar{n}}(t,\bar{\mathbf{r}};\bar{\omega},\bar{\mathbf{k}}) \equiv\ & \langle\bar{n}|\tilde{\mathcal{U}}\otimes\tilde{\Sigma}(t,\mathbf{r};\omega,\mathbf{k})\otimes\tilde{\mathcal{U}}^\dagger|\bar{n}\rangle \\ &\approx n_{\rm imp}V_0^2\int \mathrm{d}^d\bar{k}'\,D_{\bar{n}}(t,\bar{\mathbf{r}};\bar{\mathbf{k}}')\,\big|\langle u_{n,\bar{\mathbf{k}}}|u_{n,\bar{\mathbf{k}}'}\rangle\big|^2\bar{\bar{G}}(t,\bar{\mathbf{r}};\bar{\omega},\bar{\mathbf{k}}')\end{aligned} \tag{10.60}$$

where $|u_{n,\bar{\mathbf{k}}}\rangle$ is the periodic part of the Bloch function in the band n that is adiabatically connected to band $\bar{n}$ in the limit of infinitely smooth modulation fields. While we neglect gradient corrections, such as side-jump scattering, in the evaluation of $\tilde{\mathcal{U}}\otimes\tilde{\Sigma}\otimes\tilde{\mathcal{U}}^\dagger$ in Eq. (10.60), we do include the phase-space volume $D_{\bar{n}}$, Eq. (10.45), in order to treat the transformation to kinetic coordinates $\bar{\mathbf{r}}$ and $\bar{\mathbf{k}}$ consistent with the left-hand-side of the Boltzmann equation. Using Eq. (10.22), we find for the right-hand side of Eq. (10.53),

$$\begin{aligned}\text{r.h.s.} = -in_{\rm imp}V_0^2\int\frac{\mathrm{d}^d\bar{k}'}{(2\pi)^d}\,\bar{D}_{\bar{n}}(t,\bar{\mathbf{r}};\bar{\mathbf{k}}')\,\big|\langle u_{n,\bar{\mathbf{k}}}|u_{n,\bar{\mathbf{k}}'}\rangle\big|^2\bar{\bar{A}}_{\bar{n}}(t,\bar{\mathbf{r}};\bar{\omega},\bar{\mathbf{k}}')\times \\ \times\Big[\bar{\bar{f}}_{\bar{n}}(t,\bar{\mathbf{r}};\bar{\omega},\bar{\mathbf{k}}')-\bar{\bar{f}}_{\bar{n}}(t,\bar{\mathbf{r}};\bar{\omega},\bar{\mathbf{k}})\Big]\end{aligned} \tag{10.61}$$

where $\bar{\bar{A}} := i(\bar{\bar{G}}^R - \bar{\bar{G}}^A)$ is the spectral function.

Boltzmann equation with Berry phases. The transport equation (Eqs. (10.54) and (10.61)) is a partial differential equation for the distribution function $\bar{\bar{f}}_{\bar{n}}(t, \bar{\mathbf{r}}; \bar{\omega}, \bar{\mathbf{k}})$. It turns out, however, that only the value of $\bar{\bar{f}}_{\bar{n}}$ at frequency $\Omega_{\bar{n}} = \mathcal{E}_{\bar{n}}/\hbar$ enters in the equation of motion for the skyrmion trajectory Eq. (10.20). This is a consequence of the well-known fact that, in physical observables, the distribution function always appears in a product with the spectral function $\bar{\bar{A}} = i(\bar{\bar{G}}^R - \bar{\bar{G}}^A)$ (see, e.g., [145]), which is strongly peaked at the eigenenergies assuming a small imaginary part of the self-energy (i.e., low impurity concentration in our non-interacting model).

Inspired by the form of the equilibrium distribution function $\bar{\bar{f}}^{\mathrm{eq}}(\bar{\omega}) = 1 - 2n_F(\hbar\bar{\omega})$, where n_F is the Fermi distribution, we define the occupation number

$$\bar{\bar{\mathfrak{n}}}_{\bar{n}}(t, \bar{\mathbf{r}}; \bar{\mathbf{k}}) := \frac{1}{2}\left(1 - \bar{\bar{f}}_{\bar{n}}(t, \bar{\mathbf{r}}; \mathcal{E}_{\bar{n}}(t, \bar{\mathbf{r}}; \bar{\mathbf{k}})/\hbar, \bar{\mathbf{k}})\right). \tag{10.62}$$

Combining Eqs. (10.54), (10.61), and (10.62) and dropping all terms quadratic in the Berry curvature $\Omega_{\bar{n}}$ one can show by direct evaluation that $\bar{\bar{\mathfrak{n}}}_{\bar{n}}$ satisfies the Boltzmann equation,

$$\left[\frac{\partial}{\partial t} + \frac{\mathrm{d}\bar{\mathbf{r}}_{\bar{n}}}{\mathrm{d}t} \cdot \frac{\partial}{\partial \bar{\mathbf{r}}} + \frac{\mathrm{d}\bar{\mathbf{k}}_{\bar{n}}}{\mathrm{d}t} \cdot \frac{\partial}{\partial \bar{\mathbf{k}}}\right] \bar{\bar{\mathfrak{n}}}_{\bar{n}}(t, \bar{\mathbf{r}}; \bar{\mathbf{k}}) = I_{\mathrm{coll}}(t, \bar{\mathbf{r}}; \bar{\mathbf{k}}) \tag{10.63}$$

where $\frac{\mathrm{d}\bar{\mathbf{r}}_{\bar{n}}}{\mathrm{d}t}$, $\frac{\mathrm{d}\bar{\mathbf{k}}_{\bar{n}}}{\mathrm{d}t}$ are given in Eqs. (10.55) and (10.56), respectively, and the collision integral is given by

$$\begin{aligned} I_{\mathrm{coll}}(t, \bar{\mathbf{r}}; \bar{\mathbf{k}}) \approx 2\pi \frac{n_{\mathrm{imp}} V_0^2}{\hbar} \int \mathrm{d}^d \bar{k}' \, \bar{D}_{\bar{n}}(t, \bar{\mathbf{r}}; \bar{\mathbf{k}}') \, \delta\big(\mathcal{E}_{\bar{n}}(t, \bar{\mathbf{r}}; \bar{\mathbf{k}}') - \mathcal{E}_{\bar{n}}(t, \bar{\mathbf{r}}; \bar{\mathbf{k}})\big) \times \\ \times \left|\langle u_{n,\bar{\mathbf{k}}} | u_{n,\bar{\mathbf{k}}'} \rangle\right|^2 \left[\bar{\bar{\mathfrak{n}}}_{\bar{n}}(t, \bar{\mathbf{r}}; \bar{\mathbf{k}}') - \bar{\bar{\mathfrak{n}}}_{\bar{n}}(t, \bar{\mathbf{r}}; \bar{\mathbf{k}})\right] \end{aligned} \tag{10.64}$$

where we used the approximation $\bar{\bar{A}}_{\bar{n}}(t, \bar{\mathbf{r}}; \bar{\omega}, \bar{\mathbf{k}}) \approx 2\pi\delta\left(\hbar\bar{\omega} - \mathcal{E}_{\bar{n}}(t, \bar{\mathbf{r}}; \bar{\mathbf{k}})\right)$. Note that, while we neglected gradient corrections to the convolutions, the self-energies, and the inversion of Eq. (10.50) in the derivation of the collision term, we evaluate the spectral function $\bar{\bar{A}}_{\bar{n}}$ in the rotated basis $\{|\bar{n}\rangle\}$ and do include the energy correction $\delta\mathcal{E}^{(1)}_{\bar{n}}$, Eq. (10.52), in the eigenenergies $\mathcal{E}_{\bar{n}}$. This makes sure that our theory conserves energy during scattering processes.

Local particle number conservation. In a time-independent system (i.e., $\dot{\mathbf{R}} = \mathbf{0}$ and $\mathbf{E} = -\partial\mathbf{A}/\partial t = \mathbf{0}$), both the left-hand-side and the right-hand-side of the Boltzmann Equation Eq. (10.63) are set to zero by any occupation number $\bar{\bar{\mathfrak{n}}}_{\bar{n}}$ that is a function only of the energy $\mathcal{E}_{\bar{n}}(\bar{\mathbf{r}}; \bar{\mathbf{k}})$. If the system is in contact with a bath at temperature T, that function of energy is the Fermi function $n_F(\epsilon) = 1/(1 + e^{\epsilon/(k_B T)})$ and the occupation number in global equilibrium is given by

$$\bar{\bar{\mathfrak{n}}}^{\mathrm{eq}}_{\bar{n}}(\bar{\mathbf{r}}; \bar{\mathbf{k}}) = n_F(\mathcal{E}_{\bar{n}}(\bar{\mathbf{r}}; \bar{\mathbf{k}})). \tag{10.65}$$

In presence of a small electric field or for a slowly moving skyrmion the occupation number will deviate from $\bar{\bar{\mathfrak{n}}}^{\mathrm{eq}}_{\bar{n}}$, but we expect that it will still be close to a *local* equilibrium.

The collision integral Eq. (10.64) drives the system back towards local equilibrium and the Boltzmann equation Eq. (10.63) may then be solved perturbatively around the local equilibrium. An important property of the collision integral is that it conserves the particle number locally in space,

$$\int \mathrm{d}^d\bar{k}\, \bar{D}_{\bar{n}}(t,\bar{\mathbf{r}};\bar{\mathbf{k}})\, I_{\mathrm{coll}}(t,\bar{\mathbf{r}};\bar{\mathbf{k}}) = 0 \tag{10.66}$$

which can be easily checked.[2] Local particle number conservation imposes a constraint on the dynamics of the system, which prevents it from smoothing out an inhomogeneous electron density and returning to the global equilibrium $\bar{\tilde{\mathbf{n}}}^{\mathrm{eq}}_{\bar{n}}$ on the short time scale of the elastic mean-free time

$$\tau_{\mathrm{el}} \sim \frac{\hbar}{\nu_F n_{\mathrm{imp}} V_0^2} \tag{10.67}$$

where ν_F is the density of states at the Fermi surface. For this reason, we expect the local equilibrium to be different from the global equilibrium $\bar{\tilde{\mathbf{n}}}^{\mathrm{eq}}_{\bar{n}}$.

Local particle number conservation is expressed by the equation of continuity

$$\frac{\partial \rho(t,\bar{\mathbf{r}})}{\partial t} + \sum_{i=1}^{d} \frac{\partial j_i(t,\bar{\mathbf{r}})}{\partial \bar{r}_i} = 0 \tag{10.68}$$

with the charge density $\rho(t,\bar{\mathbf{r}})$ and the charge current density $\mathbf{j}(t,\bar{\mathbf{r}})$. In order to find the correct expressions for ρ and $\mathbf{j}$ in presence of Berry phases in phase space, we multiply the Boltzmann equation Eq. (10.63) by $\bar{D}_{\bar{n}}$ and integrate over momentum. This leads to

$$\int \mathrm{d}^d\bar{k}\, \left[\bar{D}_{\bar{n}} \frac{\partial \bar{\tilde{\mathbf{n}}}_{\bar{n}}}{\partial t} + \bar{D}_{\bar{n}} \frac{\mathrm{d}\bar{\mathbf{r}}_{\bar{n}}}{\mathrm{d}t} \cdot \frac{\partial \bar{\tilde{\mathbf{n}}}_{\bar{n}}}{\partial \bar{\mathbf{r}}} - \frac{\partial}{\partial \bar{\mathbf{k}}} \cdot \left(\bar{D}_{\bar{n}} \frac{\mathrm{d}\bar{\mathbf{k}}_{\bar{n}}}{\mathrm{d}t} \right) \bar{\tilde{\mathbf{n}}}_{\bar{n}} \right] = \int \mathrm{d}^d\bar{k}\, \bar{D}_{\bar{n}}\, I_{\mathrm{coll}} = 0 \tag{10.69}$$

where the last term on the left-hand side is obtained by partial integration. Summing over all bands and using the defining equation for the density of states (c.f., Eq. (5.29)),

$$\frac{\partial \bar{D}_{\bar{n}}}{\partial t} + \frac{\partial}{\partial \bar{\mathbf{r}}} \cdot \left(\bar{D}_{\bar{n}} \frac{\mathrm{d}\bar{\mathbf{r}}_{\bar{n}}}{\mathrm{d}t} \right) + \frac{\partial}{\partial \bar{\mathbf{k}}} \cdot \left(\bar{D}_{\bar{n}} \frac{\mathrm{d}\bar{\mathbf{k}}_{\bar{n}}}{\mathrm{d}t} \right) = 0 \tag{10.70}$$

leads to the equation of continuity, Eq. (10.68), with

$$\rho(t,\bar{\mathbf{r}}) = -e \sum_{\bar{n}} \int \mathrm{d}^d\bar{k}\, \bar{D}_{\bar{n}}(t,\bar{\mathbf{r}};\bar{\mathbf{k}})\, \bar{\tilde{\mathbf{n}}}_{\bar{n}}(t,\bar{\mathbf{r}};\bar{\mathbf{k}}); \tag{10.71}$$

$$\mathbf{j}(t,\bar{\mathbf{r}}) = -e \sum_{\bar{n}} \int \mathrm{d}^d\bar{k}\, \bar{D}_{\bar{n}}(t,\bar{\mathbf{r}};\bar{\mathbf{k}})\, \frac{\mathrm{d}\bar{\mathbf{r}}_{\bar{n}}}{\mathrm{d}t}\, \bar{\tilde{\mathbf{n}}}_{\bar{n}}(t,\bar{\mathbf{r}};\bar{\mathbf{k}}). \tag{10.72}$$

[2] Note that side-jump scattering processes, not considered here, break the local particle number conservation of the collision integral weakly and lead to an additional term on the right-hand side of Eq. (10.72). However, side jumps only lead to a finite current proportional to the electric field. Therefore, a hydrodynamic treatment of the local chemical potential similar to the one presented here is still required even if side-jump scattering is taken into account. The influence of side-jump scattering on the steady-state distribution function in presence of an electric field has been discussed in Ref. [113].

In order to find the local equilibrium, taking local particle number conservation into account, we introduce the local chemical potential $\mu(t, \bar{\mathbf{r}})$ and make the following ansatz for the solution of the Boltzmann equation,

$$\bar{\bar{\mathfrak{n}}}_{\bar{n}}(t, \bar{\mathbf{r}}; \bar{\mathbf{k}}) = n_F(\mathcal{E}_{\bar{n}}(t, \bar{\mathbf{r}}; \bar{\mathbf{k}}) - \mu(t, \bar{\mathbf{r}})) + \delta\bar{\bar{\mathfrak{n}}}_{\bar{n}}(t, \bar{\mathbf{r}}; \bar{\mathbf{k}}). \tag{10.73}$$

Here, the first term on the right-hand side is the occupation number in local equilibrium and $\delta\bar{\bar{\mathfrak{n}}}_{\bar{n}}$ describes out-of-equilibrium electron redistribution in momentum space. We choose $\mu(t, \bar{\mathbf{r}})$ such that the charge density $\rho(t, \bar{\mathbf{r}})$ is completely determined by the local equilibrium, i.e.,

$$\sum_{\bar{n}} \int \mathrm{d}^d\bar{k}\, \bar{D}_{\bar{n}}(t, \bar{\mathbf{r}}; \bar{\mathbf{k}})\, \delta\bar{\bar{\mathfrak{n}}}_{\bar{n}}(t, \bar{\mathbf{r}}; \bar{\mathbf{k}}) = 0. \tag{10.74}$$

In principle, one should expect to have a different chemical potential $\mu_{\bar{n}}$ for each band $\bar{n}$ since Eq. (10.66) holds for each band separately. This is, however, an artifact of our approximation to neglect inter-band scattering. In real materials, inter-band (i.e., spin-flip) scattering processes balance out the individual chemical potentials on a short time scale, and only the global chemical potential μ defined by Eqs. (10.73)–(10.74) is a good hydrodynamic quantity. We expect $\delta\bar{\bar{\mathfrak{n}}}_{\bar{n}} \sim \mathcal{O}(\tau_{\mathrm{el}})$ to be small since scattering processes can redistribute electrons in momentum space on the short time scale of τ_{el}. In position space, on the other hand, fast equilibration is prohibited by local particle conservation and we expect that the deviation from global equilibrium is more pronounced in position space, i.e., $|\mu\, n_F'| \gg |\delta\bar{\bar{\mathfrak{n}}}_{\bar{n}}|$.

Local equilibrium in the steady-state. For a constant skyrmion velocity $\dot{\mathbf{R}}$ and constant electric field $\mathbf{E}$, the charge density in the steady state moves with the skyrmion. Therefore, the first term in the equation of continuity Eq. (10.68) is given by $\frac{\partial \rho}{\partial t} = -\frac{\partial \rho}{\partial \bar{\mathbf{r}}} \cdot \dot{\mathbf{R}}$. We expand the current $\mathbf{j} = \sigma\mathbf{E} + \frac{\sigma'}{e}\boldsymbol{\nabla}\mu$ in Eq. (10.68) to linear order in the electric field and in the gradient of the chemical potential. Here, σ is the usual conductivity tensor, while σ' describes diffusive transport towards global equilibrium $\mu(\bar{\mathbf{r}}) = \text{const}$ (recall that the electron charge is $-e$ in our conventions). In general, σ and σ' are not the same since the term $\sigma\mathbf{E}$ contains, for example, the intrinsic anomalous Hall current $\mathbf{j}_{\mathrm{anom}} = -\frac{e^2}{\hbar}\sum_{\bar{n}} \int \frac{\mathrm{d}^d\bar{k}}{(2\pi)^d}\, n_F\, \Omega^{\mathrm{k,k}}_{\bar{n}}\mathbf{E}$, see Eq. (10.56), which has no diffusive counterpart. Here, we use only the simplest approximation of a scalar conductivity, assuming that the Hall angle is small. The consideration of the topological and anomalous Hall effect at this point remains an open topic. In total, we obtain from Eq. (10.68) for the steady state,

$$\frac{\partial}{\partial \bar{\mathbf{r}}} \cdot \left(\frac{\sigma'}{e} \frac{\partial \mu}{\partial \bar{\mathbf{r}}} - \rho\dot{\mathbf{R}} + \sigma\mathbf{E} \right) = 0 \tag{10.75}$$

To obtain a deeper understanding of the steady-state solution we assume that only two bands are partially filled and that the spin configuration of the majority (minority) band is parallel (anti-parallel) to the magnetization $\mathbf{M}(t, \bar{\mathbf{r}})$, thus neglecting the weak position-dependency of the spin-orbit coupling. We also neglect the weak dependency of

the dipole operator $\tilde{\mathbf{D}}$ on position, so that we obtain from Eq. (10.34) to lowest order,

$$\frac{\partial \mathcal{E}^{(0)}_{\downarrow/\uparrow}(t,\bar{\mathbf{r}};\bar{\mathbf{k}})}{\partial \bar{\mathbf{r}}} \approx \mp J \frac{\partial M(t,\bar{\mathbf{r}})}{\partial \bar{\mathbf{r}}} \tag{10.76}$$

where $M(t,\bar{\mathbf{r}}) = |\mathbf{M}(t,\bar{\mathbf{r}})|$ and the upper (lower) sign is for majority band $\downarrow$ (minority band $\uparrow$). Within this model, we obtain for the gradient of the charge density from Eq. (10.71),

$$\frac{\partial \rho}{\partial \bar{\mathbf{r}}} \approx -e\nu_F \frac{\partial \mu}{\partial \bar{\mathbf{r}}} + \frac{\partial(\delta\rho^{(0)} + \delta\rho^{(1)})}{\partial \bar{\mathbf{r}}}. \tag{10.77}$$

Here, $\nu_F = \nu_{F,\downarrow} + \nu_{F,\uparrow}$ is the local density of states at the Fermi level[3]with

$$\nu_{\downarrow/\uparrow}(t,\bar{\mathbf{r}}) = -\int \frac{\mathrm{d}^d\bar{k}}{(2\pi)^d}\, n_F'\big(\mathcal{E}^{(0)}_{\downarrow/\uparrow}(t,\bar{\mathbf{r}};\bar{\mathbf{k}}) - \mu(t,\bar{\mathbf{r}})\big). \tag{10.78}$$

Further, $\delta\rho^{(1)}(t,\bar{\mathbf{r}})$ is the Berry-phase contribution to the skyrmion charge density discussed in Sections 5.3 and 6.3, see Eq. (5.36). It is obtained from an expansion of Eq. (10.71) to first order in the gradient corrections. Apart from phase-space Berry phases, an inhomogeneous magnitude of the magnetization also causes charges to accumulate at the skyrmion. Within our model Eq. (10.76), this effect is described by

$$\delta\rho^{(0)}(t,\bar{\mathbf{r}}) = -e\nu_F JP(M(t,\bar{\mathbf{r}}) - M_\infty) \tag{10.79}$$

where M_∞ is the magnetization far away from the skyrmion and $P = (\nu_{F,\downarrow} - \nu_{F,\uparrow})/\nu_F$ is the average spin polarization of the Fermi surface.

Inserting Eq. (10.77) into Eq. (10.75) leads to a partial differential equation for the chemical momentum in the steady state,

$$\frac{\partial}{\partial \bar{\mathbf{r}}} \cdot \left(\frac{\sigma'}{e} \frac{\partial \mu}{\partial \bar{\mathbf{r}}} + \left(e\nu_F \mu - \delta\rho^{(0)} - \delta\rho^{(1)} \right) \dot{\mathbf{R}} + \sigma \mathbf{E} \right) = 0 \tag{10.80}$$

where we neglected the dependency of ν_F on position. Far away from the skyrmion, the magnetization is constant and $\delta\rho^{(0)}$ and $\delta\rho^{(1)}$ vanishe so that Eq. (10.80) is solved by a constant chemical potential μ_∞. In the vicinity of the skyrmion, two mechanisms cause a gradient of the chemical potential to build up in the steady state. First, a moving skyrmion drags along excess charges $\delta\rho^{(0)} + \delta\rho^{(1)}$, which lag behind the skyrmion trajectory because of ohmic friction. For a skyrmion that carries extra (fewer) electrons than its environment the lagging of the electrons is described by a decrease (increase) of $\mu(\bar{\mathbf{r}})$ ahead of the skyrmion and an increase (decrease) of $\mu(\bar{\mathbf{r}})$ in its wake (Figure 10.2). Second, the conductivities σ and σ' depend on position. In the Drude model σ and σ' are described by the same scalar quantity that is proportional to the density $n(\bar{\mathbf{r}}) = -\rho(\bar{\mathbf{r}})/e$ of conduction electrons. Therefore,

$$\frac{\partial \sigma}{\partial \bar{\mathbf{r}}} \approx \frac{\partial \sigma'}{\partial \bar{\mathbf{r}}} \approx -\frac{1}{e}\frac{\partial \rho}{\partial \bar{\mathbf{r}}}\frac{\partial \sigma}{\partial n}. \tag{10.81}$$

[3]Note that, if the long-range Coulomb interaction between the electrons is taken into account, the relation between μ and ρ is given by the compressibility rather than the density of states ν_F at the Fermi level.

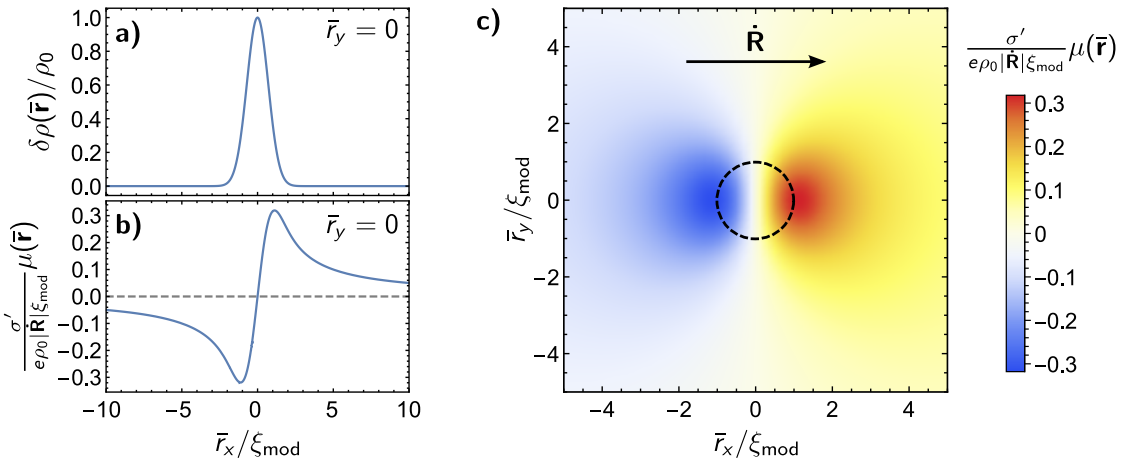

Figure 10.2.: Chemical potential in the steady state for an impurity with a Gaussian charge density profile, see Eq. (10.83). The impurity moves with constant velocity $\dot{\mathbf{R}}$ from left to right through the two-dimensional system. The same figures apply for the case of an applied electric field instead of a moving impurity. a) Excess charge density $\delta\rho(\bar{\mathbf{r}}) = \rho_0 e^{-|\bar{\mathbf{r}}|^2/\xi_{\mathrm{mod}}}$ of the rotationally symmetric impurity for a cut along the x-axis. b) Chemical potential along the x-axis. c) Chemical potential in the plane; the dashed circle indicates the position of the impurity and the standard deviation of its charge profile.

In presence of an electric field, an inhomogeneous conductivity causes charges to pile up (deplete) in front of regions of lower (higher) conductivity. By inserting Eq. (10.81) into Eq. (10.80), we obtain to linear order in $\dot{\mathbf{R}}$, $\mathbf{E}$, and $(\delta\rho^{(0)} + \delta\rho^{(1)})$,

$$\Delta\mu \approx \frac{1}{\sigma'}\left(e\dot{\mathbf{R}} + \frac{\partial\sigma}{\partial n}\mathbf{E}\right)\cdot\boldsymbol{\nabla}\left(\delta\rho^{(0)} + \delta\rho^{(1)}\right) \tag{10.82}$$

where Δ and $\boldsymbol{\nabla}$ are the Laplace operator and the gradient in the kinetic coordinates $\bar{\mathbf{r}}$, respectively. In the step from Eq. (10.80) to Eq. (10.81) we neglected the terms proportional to $\dot{\mathbf{R}}\cdot\boldsymbol{\nabla}\mu$ and $\mathbf{E}\cdot\boldsymbol{\nabla}\mu$. This is a valid approximation in the limit of a good metal, small skyrmion velocity, and small external electric field. More precisely, we assumed $e^2\xi_{\mathrm{mod}}|\dot{\mathbf{R}}|\nu_F/\sigma' \ll 1$ and $e^2\xi_{\mathrm{mod}}|\mathbf{E}|\nu_F/\rho \ll 1$ where ξ_{mod} is the length scale of the skyrmion. We obtain the solution of Eq. (10.82) by convolution of the right-hand side with the fundamental solution $F(\bar{\mathbf{r}})$ of the Laplacian, which is defined by $\Delta F(\bar{\mathbf{r}}) = \delta^d(\bar{\mathbf{r}})$. In $d = 2$ dimensions or, equivalently, in a three dimensional system that is translationally invariant in z direction, we have $F(\bar{\mathbf{r}}) = \frac{1}{4\pi}\ln\left(\bar{r}_x^2 + \bar{r}_y^2\right)$ and we obtain

$$\mu(\bar{\mathbf{r}}) = \mu_\infty + \frac{1}{2\pi\sigma'}\left(e\dot{\mathbf{R}} + \frac{\partial\sigma}{\partial n}\mathbf{E}\right)\cdot\int \mathrm{d}^2\bar{r}'\left(\delta\rho^{(0)}(\bar{\mathbf{r}}') + \delta\rho^{(1)}(\bar{\mathbf{r}}')\right)\frac{\bar{\mathbf{r}} - \bar{\mathbf{r}}'}{|\bar{\mathbf{r}} - \bar{\mathbf{r}}'|^2}. \tag{10.83}$$

In case of a three-dimensional system, $\bar{\mathbf{r}}'$ runs over the plane perpendicular to the symmetry axis that contains the point $\bar{\mathbf{r}}$, i.e., $\bar{\mathbf{r}} - \bar{\mathbf{r}}'$ is always perpendicular to the skyrmion

tube.

In Figure 10.2, we show the chemical $\mu(\bar{\mathbf{r}})$ in the steady state of a two-dimensional system in the case that a local peak of the charge density moves from left to right. The same figure applies to the case of an applied electric field that points to the right. The excess charge density is modeled by a Gaussian peak $\delta\rho^{(0)}(\bar{\mathbf{r}}) + \delta\rho^{(1)}(\bar{\mathbf{r}}) = \rho_0\, e^{-|\bar{\mathbf{r}}|/\xi_{\mathrm{mod}}}$ (Figure 10.2a). For $\rho_0 > 0$, the impurity repels (negatively charged) electrons. When it moves from left to right, excess electrons from the environment are pushed into the impurity, resulting in a rise of the chemical potential at the right side. The impurity leaves behind a region of depleted electron density, corresponding to a decrease of μ on the left side.

10.4. Formal equation of motion

We now turn to the dynamics of the skyrmion. The general equation of motion for the skyrmion trajectory $\mathbf{R}(t)$ is $\mathbf{F}^{\mathrm{tot}} = \mathbf{0}$ where $\mathbf{F}^{\mathrm{tot}}$ is given in Eq. (10.20). In Wigner representation, we obtain

$$\mathbf{F}^{\mathrm{tot}}(t) = \frac{i\hbar}{2}\int \mathrm{d}^d r \int \frac{\mathrm{d}^d k}{(2\pi)^d}\int \frac{\mathrm{d}\omega}{2\pi}\ \mathrm{Tr}\left[\frac{\partial \tilde{g}_0^{-1}(t,\mathbf{r};\omega,\mathbf{k})}{\partial \mathbf{r}} \otimes \tilde{G}^K(t,\mathbf{r};\omega,\mathbf{k})\right] \tag{10.84}$$

where we used that $\partial\tilde{g}_0^{-1}/\partial\mathbf{R} \approx -\partial\tilde{g}_0^{-1}/\partial\mathbf{r}$. We remark that this approximation neglects the weak position-dependency of the electric dipole energy $-\mathbf{E}\cdot\tilde{\mathbf{D}}$ in Eq. (10.31), which is lattice-periodic but may have a non-vanishing overlap with $\tilde{G}^K$ if not forbidden by symmetries of the atomic lattice. In order to calculate $\mathbf{F}^{\mathrm{tot}}$ in the electron distribution obtained in Section 10.3, we transform Eq. (10.84) into the frame of reference in which $\bar{\tilde{g}}_0^{-1}$ is diagonal in band space. Using Eq. (10.44), we obtain,

$$\begin{aligned}\frac{\partial \tilde{g}_0^{-1}(t,\mathbf{r};\omega,\mathbf{k})}{\partial \mathbf{r}} &= \frac{\partial(\tilde{\mathcal{U}}^\dagger(t,\mathbf{r};\omega,\mathbf{k}) \otimes \bar{\tilde{g}}_0^{-1}(t,\bar{\mathbf{r}};\bar{\omega},\bar{\mathbf{k}}) \otimes \tilde{\mathcal{U}}(t,\mathbf{r};\omega,\mathbf{k}))}{\partial \mathbf{r}} \\ &= \frac{\partial \tilde{\mathcal{U}}^\dagger}{\partial \mathbf{r}} \otimes \bar{\tilde{g}}_0^{-1} \otimes \tilde{\mathcal{U}} + \tilde{\mathcal{U}}^\dagger \otimes \bar{\tilde{g}}_0^{-1} \otimes \frac{\partial \tilde{\mathcal{U}}}{\partial \mathbf{r}} + \tilde{\mathcal{U}}^\dagger \otimes \frac{\partial \bar{\tilde{g}}_0^{-1}(t,\bar{\mathbf{r}};\bar{\omega},\bar{\mathbf{k}})}{\partial \mathbf{r}} \otimes \tilde{\mathcal{U}}.\end{aligned} \tag{10.85}$$

Here, the last term contains a derivative of $\bar{\tilde{g}}_0^{-1}$, which is a function of the kinetic coordinates $\bar{\mathbf{r}}$, $\bar{\omega}$, and $\bar{\mathbf{k}}$, by the canonical position $\mathbf{r}$. Using the inverse of Eqs. (10.38)–(10.40), we obtain in band $\bar{n}$,

$$\frac{\partial \bar{\tilde{g}}_{0,\bar{n}}^{-1}(t,\bar{\mathbf{r}};\bar{\omega},\bar{\mathbf{k}})}{\partial r_i} = \frac{\partial \bar{\tilde{g}}_{0,\bar{n}}^{-1}}{\partial \bar{r}_j}\left(\delta_{ij} + \frac{\partial \mathcal{A}^{\mathrm{k}}_{\bar{n},j}}{\partial r_i}\right) + \frac{\partial \bar{\tilde{g}}_{0,\bar{n}}^{-1}}{\partial \bar{\omega}}\frac{\partial \mathcal{A}^{\mathrm{t}}_{\bar{n}}}{\partial r_i} - \frac{\partial \bar{\tilde{g}}_{0,\bar{n}}^{-1}}{\partial \bar{k}_j}\frac{\partial \mathcal{A}^{\mathrm{r}}_{\bar{n},j}}{\partial r_i}. \tag{10.86}$$

Combining Eqs. (10.84)–(10.85) and writing the WT of the Keldysh Green's function as $\tilde{G}^K = \tilde{\mathcal{U}}^\dagger \otimes \bar{\tilde{G}}^K \otimes \tilde{\mathcal{U}}$, we find

$$\mathbf{F}^{\mathrm{tot}}(t) = \mathbf{F}^{(0)}(t) + \mathbf{F}^{(1\mathrm{a})}(t) + \mathbf{F}^{(1\mathrm{b})}(t) \tag{10.87}$$

with

$$\mathbf{F}^{(0)}(t) = \frac{i\hbar}{2}\int \mathrm{d}^d r \int \frac{\mathrm{d}^d k}{(2\pi)^d}\int \frac{\mathrm{d}\omega}{2\pi}\ \mathrm{Tr}\left[\frac{\partial \bar{\tilde{g}}_0^{-1}}{\partial \bar{\mathbf{r}}} \otimes \bar{\tilde{G}}^K\right]; \tag{10.88}$$

$$\mathbf{F}^{(1a)}(t) = \frac{i\hbar}{2}\int \mathrm{d}^d r \int \frac{\mathrm{d}^d k}{(2\pi)^d}\int \frac{\mathrm{d}\omega}{2\pi}\ \mathrm{Tr}\left[\tilde{\mathcal{U}} \otimes \frac{\partial \tilde{\mathcal{U}}^\dagger}{\partial \mathbf{r}} \otimes \left(\bar{\tilde{g}}_0^{-1} \otimes \bar{\tilde{G}}^K - \bar{\tilde{G}}^K \otimes \bar{\tilde{g}}_0^{-1}\right)\right]; \tag{10.89}$$

$$\mathbf{F}^{(1b)}(t) = \frac{i\hbar}{2}\int \mathrm{d}^d r \int \frac{\mathrm{d}^d k}{(2\pi)^d}\int \frac{\mathrm{d}\omega}{2\pi}\sum_{\bar{n}}\left[\left(\frac{\partial \bar{\tilde{g}}_{0,\bar{n}}^{-1}}{\partial \bar{r}_j}\frac{\partial \mathcal{A}^{\mathrm{k}}_{\bar{n},j}}{\partial \mathbf{r}} + \frac{\partial \bar{\tilde{g}}_{0,\bar{n}}^{-1}}{\partial \bar{\omega}}\frac{\partial \mathcal{A}^{\mathrm{t}}_{\bar{n}}}{\partial \mathbf{r}} - \frac{\partial \bar{\tilde{g}}_{0,\bar{n}}^{-1}}{\partial \bar{k}_j}\frac{\partial \mathcal{A}^{\mathrm{r}}_{\bar{n},j}}{\partial \mathbf{r}}\right)\bar{\tilde{G}}^K_{\bar{n}}\right]. \tag{10.90}$$

Here, we used in the expression for $\mathbf{F}^{(1a)}$ that $\tilde{\mathcal{U}}\otimes\tilde{\mathcal{U}}^\dagger = \mathbb{1}$, which implies $(\partial\tilde{\mathcal{U}}/\partial r_i)\otimes\tilde{\mathcal{U}}^\dagger = -\tilde{\mathcal{U}}\otimes(\partial\tilde{\mathcal{U}}^\dagger/\partial r_i)$. Further, we used that $\mathbf{F}^{(1b)}$ is already of first order in the Berry curvatures and neglected higher-order gradient corrections. Finally, in the derivation of all Eqs. (10.88)–(10.90), we used the cyclicity of the trace

$$\int \mathrm{d}^d r \int \frac{\mathrm{d}^d k}{(2\pi)^d}\int \frac{\mathrm{d}\omega}{2\pi}\ \mathrm{Tr}\Big[\tilde{A}\otimes\tilde{B} - \tilde{B}\otimes\tilde{A}\Big] = 0 \qquad \text{(in steady state)} \tag{10.91}$$

which can be shown by writing out the Moyal product in canonical coordinates, Eq. (10.29), and integrating by parts. Since there is no integration over time, Eq. (10.91) is only valid if temporal derivatives can be expressed in terms of gradients in position and momentum space. In our model, this is the case for all terms that depend only on the spectral properties of the system, i.e., $\tilde{\mathcal{U}}$, $\tilde{\mathcal{U}}^\dagger$, $\bar{\tilde{g}}_0^{-1}$, and the Berry connections $\mathcal{A}^{\mathrm{t/r/k}}$, see, e.g., Eq. (10.42). For $\bar{\tilde{G}}^K$, which depends on the distribution function, a similar relation holds only in the steady state with constant skyrmion velocity $\dot{\mathbf{R}}$.

Force to zeroth order in gradient corrections. The term $\mathbf{F}^{(0)}$, Eq. (10.88), describes a force on the skyrmion due to pressure from an out-of-equilibrium electron distribution. In the steady state, the Moyal product between $\partial\bar{\tilde{g}}_0^{-1}/\partial\bar{\mathbf{r}}$ and $\bar{\tilde{G}}^K$ can be replaced by a simple pointwise product in Wigner representation since gradient terms cancel each other out by partial integration. From Eq. (10.22) we obtain for the Keldysh Green's function,

$$\bar{\tilde{G}}^K_{\bar{n}} = \bar{\tilde{G}}^R_{\bar{n}}\otimes\bar{\tilde{f}}_{\bar{n}} - \bar{\tilde{f}}_{\bar{n}}\otimes\bar{\tilde{G}}^A_{\bar{n}} = \frac{1}{2}\left\{\bar{\tilde{G}}^R_{\bar{n}} - \bar{\tilde{G}}^A_{\bar{n}} \mathbin{\overset{\otimes}{,}} \bar{\tilde{f}}_{\bar{n}}\right\} + \frac{1}{2}\left[\bar{\tilde{G}}^R_{\bar{n}} + \bar{\tilde{G}}^A_{\bar{n}} \mathbin{\overset{\otimes}{,}} \bar{\tilde{f}}_{\bar{n}}\right] \tag{10.92}$$

where the notation $\{\bar{\tilde{A}} \mathbin{\overset{\otimes}{,}} \bar{\tilde{B}}\} := \bar{\tilde{A}}\otimes\bar{\tilde{B}} + \bar{\tilde{B}}\otimes\bar{\tilde{A}}$ denotes the anti-commutator under the Moyal product and $[\bar{\tilde{A}} \mathbin{\overset{\otimes}{,}} \bar{\tilde{B}}] := \bar{\tilde{A}}\otimes\bar{\tilde{B}} - \bar{\tilde{B}}\otimes\bar{\tilde{A}}$ is the commutator. Since $\bar{\tilde{G}}^R$, $\bar{\tilde{G}}^A$, and $\bar{\tilde{f}}$ are all diagonal in band space, only gradient terms contribute to the commutator term on the right-hand side of Eq. (10.92). It turns out that this term is suppressed in clean systems since it is proportional to a small factor of $n_{\mathrm{imp}}V_0^2$, which is not compensated by any additional momentum integrations. This can be seen by rewriting its contribution

to $\mathbf{F}^{(0)}$ using the exact relation

$$\begin{aligned}
&\frac{i\hbar}{4}\int \mathrm{d}^d r \int \frac{\mathrm{d}^d k}{(2\pi)^d}\int \frac{\mathrm{d}\omega}{2\pi}\ \mathrm{Tr}\left[\frac{\partial \bar{\bar{g}}_0^{-1}}{\partial \bar{\mathbf{r}}} \otimes \left[\bar{\bar{G}}_{\bar{n}}^R + \bar{\bar{G}}_{\bar{n}}^A \mathbin{\overset{\otimes}{,}} \bar{\bar{f}}_{\bar{n}}\right]\right] = \\
&= \frac{i\hbar}{4}\int \mathrm{d}^d r \int \frac{\mathrm{d}^d k}{(2\pi)^d}\int \frac{\mathrm{d}\omega}{2\pi}\ \mathrm{Tr}\Bigg[\left(\left[\bar{\bar{G}}_{\bar{n}}^R \mathbin{\overset{\otimes}{,}} \bar{\bar{\Sigma}}_{\bar{n}}^R\right] + \left[\bar{\bar{G}}_{\bar{n}}^A \mathbin{\overset{\otimes}{,}} \bar{\bar{\Sigma}}_{\bar{n}}^A\right]\right) \otimes \frac{\partial \bar{\bar{f}}_{\bar{n}}}{\partial \bar{\mathbf{r}}} \\
&\qquad\qquad - \left(\bar{\bar{\Sigma}}_{\bar{n}}^K - \bar{\bar{\Sigma}}_{\bar{n}}^R \otimes \bar{\bar{f}}_{\bar{n}} + \bar{\bar{f}}_{\bar{n}} \otimes \bar{\bar{\Sigma}}_{\bar{n}}^A\right) \otimes \frac{\partial (\bar{\bar{G}}_{\bar{n}}^R + \bar{\bar{G}}_{\bar{n}}^A)}{\partial \bar{\mathbf{r}}}\Bigg] \qquad (10.93)
\end{aligned}$$

which follows from Eqs. (10.23), (10.24), and (10.91). The force described by Eq. (10.93) can be attributed to the influence of the skyrmion on the cross section of impurity scattering, and it vanishes in the limit of dilute impurities $n_{\mathrm{imp}} V_0^2 \to 0$, see Eq. (10.60). In this work, we focus on intrinsic forces on the skyrmion and leave the discussion of extrinsic forces such as Eq. (10.93) open for future work.

In the anti-commutator term on the right-hand sice of Eq. (10.92), only even orders of the Moyal product contribute. Thus, if we neglect terms beyond linear order in the Gradient corrections, only the zero-order term survives. We obtain

$$\mathbf{F}^{(0)}(t) \approx \frac{i\hbar}{2}\int \mathrm{d}^d r \int \frac{\mathrm{d}^d k}{(2\pi)^d}\int \frac{\mathrm{d}\omega}{2\pi}\sum_{\bar{n}}\left[\frac{\partial \bar{\bar{g}}_{0,\bar{n}}^{-1}}{\partial \bar{\mathbf{r}}}\left(\bar{\bar{G}}_{\bar{n}}^R - \bar{\bar{G}}_{\bar{n}}^A\right)\bar{\bar{f}}_{\bar{n}}\right] \qquad (10.94)$$

Due to the product with the spectral function $i(\bar{\bar{G}}^R - \bar{\bar{G}}^A)$, the distribution function $\bar{\bar{f}}$ is only evaluated at quasi-particle energies of the system. The advanced and retarded Green's function $\bar{\bar{G}}^{R/A}$ are obtained from $(\bar{\bar{g}}_0^{-1} - \bar{\bar{\Sigma}}^{R/A}) \otimes \bar{\bar{G}}^{R/A} = \mathbb{1}$. We focus, as before, on intrinsic forces on the skyrmion and neglect off-diagonal components of the self-energy $\bar{\bar{\Sigma}}^{R/A}$. Thus, using Eq. (10.50), the Green's function is given by

$$\bar{\bar{G}}_{\bar{n}}^{R/A}(t, \bar{\mathbf{r}}; \bar{\omega}, \bar{\mathbf{k}}) = \frac{1}{\hbar\bar{\omega} - \mathcal{E}_{\bar{n}}(t, \bar{\mathbf{r}}; \bar{\mathbf{k}}) - \bar{\bar{\Sigma}}_n^{R/A}}. \qquad (10.95)$$

The fact that we work in the band-diagonalized frame of reference leads to two differences between Eq. (10.95) and treatment of the Green's function in Section 6.2. First, the position of the pole at $\hbar\bar{\omega} = \mathcal{E}_{\bar{n}} + \bar{\bar{\Sigma}}_n^{R/A} \approx \mathcal{E}_{\bar{n}}^{(0)} + \delta\mathcal{E}_{\bar{n}}^{(1)} + \bar{\bar{\Sigma}}_n^{R/A}$ already accounts for the gradient correction $\delta\mathcal{E}_{\bar{n}}^{(1)}$ to the quasi-particle energy. Second, a gradient expansion of the Green's function $\bar{\bar{G}}^{R/A}$ as presented in Section 6.2 is not necessary. Indeed, since $\bar{\bar{g}}_0^{-1}(t, \bar{\mathbf{r}}; \bar{\omega}, \bar{\mathbf{k}})$ is by definition diagonal for all t, $\bar{\mathbf{r}}$, $\bar{\omega}$, and $\bar{\mathbf{k}}$, the gradient expansion of $\bar{\bar{G}}^{R/A}$ terminates after the zero-order term given in Eq. (10.95).

In the limit of small impurity concentration, $\bar{\bar{\Sigma}}_{\bar{n}}^{R/A} \to \pm i0_+$, the spectral function is $i(\bar{\bar{G}}_{\bar{n}}^R - \bar{\bar{G}}_{\bar{n}}^A) \to 2\pi\delta(\hbar\omega - \mathcal{E}_{\bar{n}})$ and we obtain from Eq. (10.94),

$$\mathbf{F}^{(0)}(t) = \sum_{\bar{n}}\int \mathrm{d}^d \bar{r} \int \mathrm{d}^d \bar{k}\, \bar{D}_{\bar{n}}(t, \bar{\mathbf{r}}; \bar{\mathbf{k}}) \frac{\partial \mathcal{E}_{\bar{n}}(t, \bar{\mathbf{r}}; \bar{\mathbf{k}})}{\partial \bar{\mathbf{r}}}\, \bar{\bar{\mathfrak{n}}}_{\bar{n}}(t, \bar{\mathbf{r}}; \bar{\mathbf{k}}) \qquad (10.96)$$

where we used the definition Eq. (10.62) of the occupation number $\bar{\tilde{\mathfrak{n}}}_{\bar{n}}$, and we transformed the integrals into kinetic coordinates, thus introducing the density of states $\bar{D}_{\bar{n}}$, see Eq. (10.45). Neglecting for the moment all gradient corrections, the density of states $D_{\bar{n}}$ is approximately constant and the zeroth order force is given by

$$\mathbf{F}^{(0)}(t) \approx -\sum_{\bar{n}} \int \mathrm{d}^d\bar{r} \int \frac{\mathrm{d}^d\bar{k}}{(2\pi)^d} \frac{\partial \mathcal{E}_{\bar{n}}(t,\bar{\mathbf{r}};\bar{\mathbf{k}})}{\partial \mathbf{R}} \bar{\tilde{\mathfrak{n}}}_{\bar{n}}(t,\bar{\mathbf{r}};\bar{\mathbf{k}}) + \mathcal{O}(\Omega^{\mathrm{r,k}}) \tag{10.97}$$

where we used $\partial\mathcal{E}_{\bar{n}}/\partial\bar{\mathbf{r}} = -\partial\mathcal{E}_{\bar{n}}/\partial\mathbf{R}$. Thus, if the skyrmion position $\mathbf{R}$ moves by $\mathrm{d}\mathbf{R}$ in the direction of $\mathbf{F}^{(0)}$, the total energy of the system is reduced by $\mathbf{F}^{(0)} \cdot \mathrm{d}\mathbf{R}$ to zeroth order in the gradient corrections. This explains our choice of prefactors in the definition Eq. (10.20) of the total force $\mathbf{F}^{\mathrm{tot}}$. The role of the gradient corrections due to the non-constant density of states $D_{\bar{n}}$ in Eq. (10.96) will become clear when we combine $\mathbf{F}^{(0)}$ with $\mathbf{F}^{(1a)}$ and $\mathbf{F}^{(1b)}$ below.

First-order gradient corrections. The terms $\mathbf{F}^{(1a)}$ and $\mathbf{F}^{(1b)}$, Eqs. (10.89)–(10.90) describe corrections to Eq. (10.96) due to Berry phases. We consider only gradient corrections to linear order in the Berry curvature $\Omega_{\bar{n}}$. In Eq. (10.90), the factor $(\bar{\tilde{g}}_0^{-1} \otimes \bar{\tilde{G}}^K - \bar{\tilde{G}}^K \otimes \bar{\tilde{g}}_0^{-1})$ vanishes to zeroth order in the Moyal product. Therefore, the leading-order contribution to $\mathbf{F}^{(1a)}$ is

$$\mathbf{F}^{(1a)}(t) = -\frac{\hbar}{2} J_{\mu\nu} \int \mathrm{d}^d r \int \frac{\mathrm{d}^d k}{(2\pi)^d} \int \frac{\mathrm{d}\omega}{2\pi} \operatorname{Tr}\left[\tilde{\mathcal{U}}_0 \frac{\partial \tilde{\mathcal{U}}_0^\dagger}{\partial \mathbf{r}} (\partial_\mu \bar{\tilde{g}}_0^{-1})(\partial_\nu \bar{\tilde{G}}^K)\right] \tag{10.98}$$

where we evaluated the Moyal products between $\bar{\tilde{g}}_0^{-1}$ and $\bar{\tilde{G}}^K$ in canonical coordinates, see Eq. (10.29). Since $\bar{\tilde{g}}_0^{-1}$ and $\bar{\tilde{G}}^K$ are band-diagonal for all points in Wigner representation, so are their derivatives. Therefore, only the diagonal components $\langle\bar{n}|\tilde{\mathcal{U}}_0 \frac{\partial \tilde{\mathcal{U}}_0^\dagger}{\partial \mathbf{r}}|\bar{n}\rangle = -i\boldsymbol{\mathcal{A}}^{\mathrm{r}}_{\bar{n}}$ of the first factor contribute. By integrating by parts, which is allowed in the steady state, we obtain

$$\mathbf{F}^{(1a)}(t) = -\frac{i\hbar}{2} \sum_{\bar{n}} \int \mathrm{d}^d r \int \frac{\mathrm{d}^d k}{(2\pi)^d} \int \frac{\mathrm{d}\omega}{2\pi} \left[\left(\frac{\partial \bar{\tilde{g}}_{0,\bar{n}}^{-1}}{\partial r_j} \frac{\partial \boldsymbol{\mathcal{A}}^{\mathrm{r}}_{\bar{n}}}{\partial k_j} + \frac{\partial \bar{\tilde{g}}_{0,\bar{n}}^{-1}}{\partial \omega} \frac{\partial \boldsymbol{\mathcal{A}}^{\mathrm{r}}_{\bar{n}}}{\partial t} - \frac{\partial \bar{\tilde{g}}_{0,\bar{n}}^{-1}}{\partial k_j} \frac{\partial \boldsymbol{\mathcal{A}}^{\mathrm{r}}_{\bar{n}}}{\partial r_j}\right) \bar{\tilde{G}}^K_{\bar{n}}\right] \tag{10.99}$$

where we used $\partial\boldsymbol{\mathcal{A}}^{\mathrm{r}}/\partial\omega = 0$. Since $\mathbf{F}^{(1a)}(t)$ is already linear in the Berry curvatures, we may replace derivatives w.r.t. canonical coordinates by derivatives w.r.t. kinetic coordinates, e.g., $\partial\bar{\tilde{g}}_0^{-1}/r_j \approx \partial\bar{\tilde{g}}_0^{-1}/\bar{r}_j$. Combining with $\mathbf{F}^{(1b)}$, Eq. (10.90), and using $\bar{\tilde{G}}^K_{\bar{n}} \approx (\bar{\tilde{G}}^R_{\bar{n}} - \bar{\tilde{G}}^A_{\bar{n}})(1 - 2\bar{\tilde{\mathfrak{n}}}_{\bar{n}})$ to zeroth order in the gradient corrections, we obtain to leading order

$$F_i^{(1a)}(t) + F_i^{(1b)}(t) = \sum_{\bar{n}} \int \mathrm{d}^d\bar{r} \int \frac{\mathrm{d}^d\bar{k}}{(2\pi)^d} \left[\Omega^{\mathrm{r,k}}_{\bar{n},ij} \frac{\partial \mathcal{E}_{\bar{n}}}{\partial \bar{r}_j} - \Omega^{\mathrm{r,r}}_{\bar{n},ij} \frac{\partial \mathcal{E}_{\bar{n}}}{\partial \bar{k}_j} - \hbar\Omega^{\mathrm{r,t}}_{\bar{n},i}\right] \bar{\tilde{\mathfrak{n}}}_{\bar{n}}. \tag{10.100}$$

Here, we transformed the integrals from canonical to kinetic coordinates, neglecting the gradient corrections in $D_{\bar{n}}$ since $\mathbf{F}^{(1)}$ is already linear in the Berry curvatures.

Combining Eqs. (10.87), (10.96), and (10.100) and using Eqs. (10.45) and (10.47), we obtain the total force on the skyrmion to leading order in $\mathbf{E}$, $\dot{\mathbf{R}}$, and Ω,

$$F_i^{\mathrm{tot}}(t) = \sum_{\bar{n}} \int \mathrm{d}^d\bar{r} \int \frac{\mathrm{d}^d\bar{k}}{(2\pi)^d} \left[(1 - \Omega^{\mathrm{r,k}}_{\bar{n},jj}) \frac{\partial \mathcal{E}_{\bar{n}}}{\partial \bar{r}_i} - \Omega^{\mathrm{r,r}}_{\bar{n},ij} \left(\frac{\partial \mathcal{E}_{\bar{n}}}{\partial \bar{k}_j} - \hbar \dot{R}_j \right) + \Omega^{\mathrm{r,k}}_{\bar{n},ij} \left(\frac{\partial \mathcal{E}_{\bar{n}}}{\partial \bar{r}_j} + eE_j \right) \right] \bar{\tilde{\mathfrak{n}}}_{\bar{n}}. \tag{10.101}$$

Eq. (10.101) is a central result of this chapter. In Chapter 11, we evaluate $\mathbf{F}^{\mathrm{tot}}$ in metals and in insulators.

Vanishing force in global equilibrium. In absence of an electric field, the equation of motion $\mathbf{F}^{\mathrm{tot}} = \mathbf{0}$ must be solved by a resting skyrmion if the electronic system is in global equilibrium and the skyrmion is located at a minimum of the potential energy. This is a consequence of the fact that, for $\dot{\mathbf{R}} = \mathbf{0}$ and $\mathbf{E} = \mathbf{0}$, the Hamiltonian is time-independent, and the equation of motion Eq. (10.16) is solved exactly by a time-independent Hamiltonian that commutes with the density matrix at time $t \to -\infty$. This can be seen as follows. The formal classical equation of motion for the skyrmion coordinate is given by the saddlepoint equation, Eq. (10.16), which is equivalent to

$$\left. \frac{\delta \mathcal{Z}[\mathbf{R}]}{\delta \mathbf{R}^{\mathrm{q}}(t)} \right|_{\mathbf{R}^{\mathrm{q}}=0} = 0. \tag{10.102}$$

Here, $\mathcal{Z}[\mathbf{R}] = -i \log(S_{\mathrm{eff}}[\mathbf{R}])$ is the partition function of the electronic system for a given skyrmion trajectory $\mathbf{R}(t)$, where S_{eff} is the effective action defined in Eq. (10.14), and $\mathbf{R}^{\mathrm{q}}(t) = \frac{1}{2}(\mathbf{R}(t_+) - \mathbf{R}(t_-))$ is the quantum component of the skyrmion trajectory. In the Keldysh formalism, the partition function for a fixed skyrmion trajectory is given by

$$\mathcal{Z}[\mathbf{R}] = \mathrm{Tr}[U_-(-\infty, \infty)\, U_+(\infty, -\infty)\, \rho(-\infty)] \tag{10.103}$$

where $U_\pm$ is the time-evolution operator for the electronic subsystem on the forward (backward) branch of the Keldysh contour, $\rho(-\infty)$ is the density matrix at time $t \to -\infty$, and the trace is over the full many-particle Hilbert space (Fock space). The time evolution of the electronic degrees of freedom depends on the skyrmion trajectory, and we find, on the two branches,

$$\begin{aligned} \frac{\delta U_+(\infty, -\infty)}{\delta \mathbf{R}^{\mathrm{q}}(t)} &= -iU_+(\infty, t) \frac{\partial \mathcal{H}(t_+)}{\partial \mathbf{R}(t_+)} U_+(t, -\infty); \\ \frac{\delta U_-(-\infty, \infty)}{\delta \mathbf{R}^{\mathrm{q}}(t)} &= -iU_-(-\infty, t) \frac{\partial \mathcal{H}(t_-)}{\partial \mathbf{R}(t_-)} U_-(t, \infty). \end{aligned} \tag{10.104}$$

where $\mathcal{H}(t_\pm)$ is the Hamiltonian in second-quantized form evaluated on the forward (backward) branch of the Keldysh contour. Inserting into Eq. (10.103), we obtain

$$\left. \frac{\delta \mathcal{Z}[\mathbf{R}]}{\delta \mathbf{R}^{\mathrm{q}}(t)} \right|_{\mathbf{R}^{\mathrm{q}}=0} = -2i\, \mathrm{Tr} \left[U(-\infty, t) \frac{\partial \mathcal{H}(t)}{\partial \mathbf{R}(t)} U(t, -\infty)\, \rho(-\infty) \right]_{\mathbf{R}^{\mathrm{q}}=0} \tag{10.105}$$

where we used the fact that for $\mathbf{R}^{\mathrm{q}} = \mathbf{0}$ the time evolution is identical on the forward and backward branch. To solve Eq. (10.102), one has to set the right-hand side of Eq. (10.105) to zero. In the presence of an electric field or for an out-of-equilibrium initial density matrix $\rho(-\infty)$, this may in general only be achieved by a moving skyrmion. For $\mathbf{E} = \mathbf{0}$, however, we can make $\mathcal{H}$ independent of time by choosing a constant skyrmion position $\mathbf{R}(t) = \text{const}$. This trivial trajectory solves the equation of motion if the initial state is given by the equilibrium density matrix $\rho(-\infty) = \mathcal{Z}_0^{-1} e^{-\mathcal{H}/(k_B T)}$, since the right-hand side of Eq. (10.105) reduces in this case to $-2i \frac{\partial}{\partial \mathbf{R}} \langle \mathcal{H} \rangle$ where $\langle \mathcal{H} \rangle = \mathrm{Tr}[\mathcal{H}\rho(-\infty)]$ denotes thermal and quantum-mechanical averaging. Impurities render the energy landscape $\langle \mathcal{H} \rangle$ position-dependent, which leads to pinning forces, but we assumed that the skyrmion is in a minimum of the potential energy so that $\frac{\partial}{\partial \mathbf{R}} \langle \mathcal{H} \rangle = \mathbf{0}$.

Thus, in an equilibrium system with $\mathbf{E} = \mathbf{0}$, a resting skyrmion solves the equation of motion $\mathbf{F}^{\mathrm{tot}} = \mathbf{0}$ exactly. In praxis, $\mathbf{F}^{\mathrm{tot}}$ can only be obtained within some set of approximations, and a consistent approximation must not violate $\mathbf{F}^{\mathrm{tot}} = \mathbf{0}$ for a resting skyrmion and equilibrium electron distribution. In our above derivation of $\mathbf{F}^{\mathrm{tot}}$, Eq. (10.1), our main approximations were (i) the assumption of non-interacting electrons, (ii) a gradient expansion to linear order in all components of the Berry curvature tensor $\Omega_{\bar{n}}$, and (iii) the limit of dilute impurities, $n_{\mathrm{imp}} V_0^2 \to 0$. To check that we did not inadvertently break translational invariance within our approximations, we evaluate $\mathbf{F}^{\mathrm{tot}}$ in global equilibrium, characterized by an occupation number $\bar{\bar{\mathfrak{n}}}_{\bar{n}}(\bar{\mathbf{r}}; \bar{\mathbf{k}}) \equiv n_F(\mathcal{E}_{\bar{n}}(\bar{\mathbf{r}}; \bar{\mathbf{k}}))$ that depends only on energy. Inserting $\bar{\bar{\mathfrak{n}}}_{\bar{n}}(\bar{\mathbf{r}}; \bar{\mathbf{k}})$ into Eq. (10.1) and integrating by parts, we obtain for the total force in equilibrium,

$$F_i^{\mathrm{eq}} = \sum_{\bar{n}} \int \mathrm{d}^d \bar{r} \int \frac{\mathrm{d}^d \bar{k}}{(2\pi)^d} \left[\frac{\partial \Omega^{\mathrm{r,k}}_{\bar{n},jj}}{\partial \bar{r}_i} + \frac{\partial \Omega^{\mathrm{r,r}}_{\bar{n},ij}}{\partial \bar{k}_j} - \frac{\partial \Omega^{\mathrm{r,k}}_{\bar{n},ij}}{\partial \bar{r}_j} \right] \bar{\bar{N}}^{\mathrm{eq}}_{\bar{n}}(\mathcal{E}_{\bar{n}}) = 0 \tag{10.106}$$

where $\bar{\bar{N}}^{\mathrm{eq}}(\mathcal{E}_{\bar{n}})$ is the antiderivative of the Fermi function, i.e., $\partial \bar{\bar{N}}^{\mathrm{eq}}(\mathcal{E}_{\bar{n}})/\partial \mathcal{E}_{\bar{n}} = n_F(\mathcal{E}_{\bar{n}})$. The terms in the bracket cancel, as they should, due to the Jacobi identity, Eq. (3.14). Here, the first term in the bracket originates from the density of states $D_{\bar{n}}(\bar{\mathbf{r}}; \bar{\mathbf{k}})$ in phase space, while the other two terms come from forces due to Berry phases in position and in mixed position/momentum space, respectively. Not surprisingly, the Berry-phase correction to the density of states in phase space, related to Liouville's theorem, is essential to restore the correct behavior in equilibrium by canceling forces due to Berry phases. We encountered a similar cancellation of unphysical terms in the discussion of particle-number conservation in section 5.2, where the use of the correct density of states in phase space was also key.

11. Results in Metals and insulators

In this chapter, we apply the general Equation of motion derived in the preceding chapter (Eq. (10.101)) and evaluate it for the case of a metal and an insulator. In the metal, we obtain a result that is similar to the Thiele Equation, Eq. (9.7),

$$\mathbf{G} \times (\mathbf{v}_\mathrm{s} - \dot{\mathbf{R}}) + \mathbf{F}^\mathrm{so} + \mathbf{F}^\mathrm{Ohm} + \mathbf{F}^\mathrm{drag} = \mathbf{0}. \tag{11.1}$$

Here, $\mathbf{G}$ is the gyro-coupling vector, $\mathbf{v}_\mathrm{s}$ is the effective spin velocity, and the last three terms describe a new kind of force due to Berry phases in mixed position/momentum space, ohmic friction, and current drag, respectively. The equation of motion does not contain the damping terms proportional to the Gilbert damping parameter $\tilde{\alpha}$ of the standard Thiele equation Eq. (9.7).

In an insulator, the forces described above vanish and instead the electric field couples directly to the charge of the skyrmion. The equation of motion will turn out to be given by

$$-\mathbf{G} \times \dot{\mathbf{R}} + \delta Q^{(2)} \mathbf{E} = \mathbf{0}. \tag{11.2}$$

11.1. Equation of motion for skyrmions in metals

Forces in local equilibrium. We insert the occupation number $\bar{\tilde{\mathfrak{n}}}_{\bar{n}}$ obtained in Section 10.3 into Eq. (10.1) for the total force on the skyrmion. Our ansatz Eq. (10.73) for $\bar{\tilde{\mathfrak{n}}}_{\bar{n}}$, is a sum of the occupation number in local equilibrium and an out-of-equilibrium redistribution of electrons in momentum space. In local equilibrium, $\bar{\tilde{\mathfrak{n}}}_{\bar{n}}(t, \bar{\mathbf{r}}; \bar{\mathbf{k}}) = n_F(\mathcal{E}_{\bar{n}}(t, \bar{\mathbf{r}}; \bar{\mathbf{k}}) - \mu(t, \bar{\mathbf{r}}))$, we obtain the force

$$\begin{aligned} F_i^\mathrm{leq}(t) &= \sum_{\bar{n}} \int \mathrm{d}^d \bar{r} \int \frac{\mathrm{d}^d \bar{k}}{(2\pi)^d} \left[\hbar \Omega^{\mathrm{r,r}}_{\bar{n},ij} \dot{R}_j + \Omega^{\mathrm{r,k}}_{\bar{n},ij} \left(e E_j + \frac{\partial \mu}{\partial \bar{r}_j} \right) + (1 - \Omega^{\mathrm{r,k}}_{\bar{n},jj}) \frac{\partial \mu}{\partial \bar{r}_i} \right] n_F(\mathcal{E}_{\bar{n}} - \mu) \\ &= F_i^{\mathrm{gyro,R}}(t) + F_i^\mathrm{so}(t) + F_i^\mathrm{Ohm}(t) + F_i^\mathrm{drag}(t) \end{aligned} \tag{11.3}$$

where the first equality follows from partial integration and the Jacobi identity, Eq. (3.14), similar to the derivation of Eq. (10.106). In second equality, we split the total force into four different physical contributions. First, the term proportional to $\Omega^{\mathrm{r,r}}_{\bar{n}}$ leads to the well-known gyro-coupling force $\mathbf{F}^{\mathrm{gyro,R}}$. For our simple model of a chiral magnet with a single orbital band and weak SO coupling, cf., Eq. (10.76), it is given by

$$\mathbf{F}^{\mathrm{gyro,R}}(t) = -\mathbf{G} \times \dot{\mathbf{R}} \qquad \text{with} \qquad \mathbf{G} \approx \frac{1}{2} J \nu_F \sum_{\bar{n}} \int \mathrm{d}^d \bar{r}\, M(\bar{\mathbf{r}}) \mathbf{B}^\mathrm{em}(\bar{\mathbf{r}}). \tag{11.4}$$

Here, $\mathbf{G}$ is the gyro-coupling vector, M is the magnetization, and $\mathbf{B}^{\mathrm{em}}$ is the emergent magnetic field defined in Eq. (4.13), which carries a quantized flux.

The force $\mathbf{F}^{\mathrm{so}}$ comes from the term proportional to $\Omega^{\mathrm{r,k}}_{\bar{n},ij}$ in Eq. (11.3),

$$F_i^{\mathrm{so}}(t) = \sum_{\bar{n}} \int \mathrm{d}^d\bar{r} \int \frac{\mathrm{d}^d\bar{k}}{(2\pi)^d}\, \Omega^{\mathrm{r,k}}_{\bar{n},ij} \left(eE_j + \frac{\partial \mu}{\partial \bar{r}_j} \right) n_F(\mathcal{E}_{\bar{n}} - \mu). \tag{11.5}$$

This force is a new result not previously considered to our knowledge. The force is non-zero only in presence of spin-orbit coupling. Semiclassically, $\mathbf{F}^{\mathrm{so}}$ can be understood as the recoil-force on the skyrmion due to the additional force $-e\Omega^{\mathrm{r,k}}_{\bar{n},ij}E_j$ in the equation of motion of electrons, see Eq. (10.55). With the considerations from section 4.3, we estimate its magnitude to be on the order of $F^{\mathrm{so}} \sim eE$, which is consistent with numerical results for MnSi [65].

The remaining two forces on the right-hand side of Eq. (11.3) come from the term proportional to $(1 - \Omega^{\mathrm{r,k}}_{\bar{n},jj})$. expanding to leading order in the the variation of $M(\bar{\mathbf{r}})$ and in the gradient corrections leads to

$$\begin{aligned} F_i^{\mathrm{Ohm}} + F_i^{\mathrm{drag}} &= -\frac{1}{e} \int \mathrm{d}^d\bar{r}\, (\delta\rho^{(0)} + \delta\rho^{(1)}) \frac{\partial \mu}{\partial \bar{r}_i} \\ &\approx -\frac{1}{4\pi\sigma'} \left(\dot{R}_j + \frac{1}{e}\frac{\partial \sigma}{\partial n} E_j \right) \int \mathrm{d}^d\bar{r} \int \mathrm{d}^2\bar{r}'\, \delta\rho(\bar{\mathbf{r}})\, \delta\rho(\bar{\mathbf{r}}')\, \frac{\partial^2 \ln\big(|\bar{\mathbf{r}} - \bar{\mathbf{r}}'|^2\big)}{\partial \bar{r}_i\, \partial \bar{r}_j} \end{aligned} \tag{11.6}$$

where $\delta\rho^{(0)}$ ($\delta\rho^{(1)}$) is the excess charge density of the skyrmion due to variations in the magnitude of M of the magnetization (phase-space Berry phases). In the last step, we inserted the chemical potential in the steady state from Eq. (10.83) and we used the short-hand notation $\delta\rho = \delta\rho^{(0)} + \delta\rho^{(1)}$. In a three-dimensional system the integration region of $\bar{\mathbf{r}}'$ is again restricted to the plane perpendicular to the symmetry axis of the skyrmion that contains the point $\bar{\mathbf{r}}$. The integral can be simplified if the charge density is rotationally symmetric. Terms with $i \neq j$ vanish since the integrand is odd under the combined mirror reflection $\bar{r}_i \to -\bar{r}_i$, $\bar{r}'_i \to -\bar{r}'_i$. For the remaining contribution with $i = j$, we use the symmetry of the integrand under exchange of $\bar{r}_x$ with $\bar{r}_y$ and $\bar{r}'_x$ with $\bar{r}'_y$ to replace $\partial^2_{\bar{r}_i} \ln\big(|\bar{\mathbf{r}} - \bar{\mathbf{r}}'|^2\big)$ by $\frac{1}{2}(\partial^2_{\bar{r}_x} + \partial^2_{\bar{r}_y}) \ln\big(|\bar{\mathbf{r}} - \bar{\mathbf{r}}'|^2\big) = 2\pi\delta^2(\bar{\mathbf{r}} - \bar{\mathbf{r}}')$. We thus identify the two forces

$$\mathbf{F}^{\mathrm{Ohm}}(t) = -\frac{1}{2\sigma'} \int \mathrm{d}^d\bar{r}\, (\delta\rho^{(0)} + \delta\rho^{(1)})^2\, \dot{\mathbf{R}}; \tag{11.7}$$

$$\mathbf{F}^{\mathrm{drag}}(t) = \frac{1}{-2e\sigma'} \frac{\partial \sigma}{\partial n} \int \mathrm{d}^d\bar{r}\, (\delta\rho^{(0)} + \delta\rho^{(1)})^2\, \mathbf{E}. \tag{11.8}$$

Here, $\mathbf{F}^{\mathrm{Ohm}}$ points in the direction opposite to the skyrmion velocity $\dot{\mathbf{R}}$ and describes Ohmic friction due to the fact that the skyrmion drags along electrons. The force $\mathbf{F}^{\mathrm{drag}}$ points approximately in the direction of the particle current $\frac{\sigma}{-e}\mathbf{E}$ and accounts for the fact an external electric field leads to a drift velocity of the electrons, which exerts a drag

force on the skyrmion. Both $\mathbf{F}^{\mathrm{Ohm}}$ and $\mathbf{F}^{\mathrm{drag}}$ are quadratic in the excess charge density $\delta\rho^{(0)}+\delta\rho^{(1)}$. This is consistent with the requirement that the dissipated power $\dot{\mathbf{R}}\cdot\mathbf{F}^{\mathrm{Ohm}}$ due to Ohmic friction always has to be negative (see also discussion in Section 11.3). The prefactor of $\frac{1}{2}$ in Eqs. (11.7)–(11.8) results from the substitution of $\partial^2_{\bar{r}_i}\ln\big(|\bar{\mathbf{r}}-\bar{\mathbf{r}}'|^2\big)$ by $\frac{1}{2}(\partial^2_{\bar{r}_x}+\partial^2_{\bar{r}_y})\ln\big(|\bar{\mathbf{r}}-\bar{\mathbf{r}}'|^2\big)$, which is specific to a charge distribution with cylindrical symmetry. More generally, the corresponding prefactor in case of a rotationally symmetric charge distribution in d dimensions is $1/d$. This prefactor accounts for the fact that the presence of a local inhomogeneity (skyrmion) influences the flow of electrons and, for $d>1$, electrons can evade the local inhomogeneity (see Figure 10.2). Since electrons that evade the local inhomogeneity do not contribute to Ohmic friction or current drag, $\mathbf{F}^{\mathrm{Ohm}}$ and $\mathbf{F}^{\mathrm{drag}}$ are suppressed by a factor of $1/d$.

Force out of local equilibrium. In our ansatz for the occupation number, Eq. (10.73), we includes a term $\delta\bar{\tilde{\mathfrak{n}}}_{\bar{n}}(t,\bar{\mathbf{r}};\bar{\mathbf{k}})$ that accounts for electron re-distribution in momentum space out of local equilibrium. For a low skyrmion velocity and small electric field, we expect that the system is always close to local equilibrium and that $\delta\bar{\tilde{\mathfrak{n}}}_{\bar{n}}$ is small. In addition, $\delta\bar{\tilde{\mathfrak{n}}}_{\bar{n}}$ by definition does not contribute to the charge density $\rho(t,\bar{\mathbf{r}})$. We therefore only consider the the contribution from $\delta\bar{\tilde{\mathfrak{n}}}_{\bar{n}}$ to $\mathbf{F}^{\mathrm{tot}}$ that comes from the term proportional to $\partial\mathcal{E}_{\bar{n}}/\partial\bar{\mathbf{k}}$ in Eq. (10.1), which has the stronges momentum-dependency. The out-of-local-equilibrium correction $\delta\bar{\tilde{\mathfrak{n}}}_{\bar{n}}$ thus leads to the remaining part of the gyro-coupling force,

$$F_i^{\mathrm{gyro,s}}(t)=-\sum_{\bar{n}}\int \mathrm{d}^d\bar{r}\int\frac{\mathrm{d}^d\bar{k}}{(2\pi)^d}\,\Omega^{\mathrm{r,r}}_{\bar{n},ij}\frac{\partial\mathcal{E}_{\bar{n}}}{\partial\bar{k}_j}\delta\bar{\tilde{\mathfrak{n}}}_{\bar{n}}(t,\bar{\mathbf{r}};\bar{\mathbf{k}})\approx(\mathbf{G}\times\mathbf{v}_{\mathrm{s}})_i \tag{11.9}$$

where $\mathbf{v}_{\mathrm{s}}$ is an effective spin velocity. In the toy model with only a single orbital band, it is given by

$$\mathbf{v}_{\mathrm{s}}=\frac{\int\mathrm{d}^d\bar{r}\int\frac{\mathrm{d}^d\bar{k}}{(2\pi)^d}\left(\frac{\partial\mathcal{E}_\downarrow}{\hbar\,\partial\mathbf{k}}\delta\bar{\tilde{\mathfrak{n}}}_\downarrow-\frac{\partial\mathcal{E}_\uparrow}{\hbar\,\partial\mathbf{k}}\delta\bar{\tilde{\mathfrak{n}}}_\uparrow\right)}{\int\mathrm{d}^d\bar{r}\int\frac{\mathrm{d}^d\bar{k}}{(2\pi)^d}\left(n_F(\mathcal{E}_\downarrow-\mu)-n_F(\mathcal{E}_\uparrow-\mu)\right)} \tag{11.10}$$

where we neglected the small position-dependency of $\delta\bar{\tilde{\mathfrak{n}}}_{\downarrow/\uparrow}$.

11.2. Equation of motion for skyrmions in insulators

In insulators, all forces on the skyrmion to first order in the gradient expansion vanish, except for the gyro-coupling term $\mathbf{F}^{\mathrm{gyro,R}}=-\mathbf{G}\cdot\dot{\mathbf{R}}$ in Eq. (11.1). This is evident for the the forces $\mathbf{F}^{\mathrm{gyro,s}}$, $\mathbf{F}^{\mathrm{Ohm}}$, and $\mathbf{F}^{\mathrm{drag}}$, Eqs. (11.9), (11.7), and (11.8), respectively, which occur only for an out-of-equilibrium electron distribution. The force $\mathbf{F}^{\mathrm{so}}$, Eq. (11.5), vanishes in insulators by the same arguments that the first-order skyrmion charge $\delta Q^{(1)}$ vanishes, see Section 6.3. For example, for an electric field in y direction, the x-component of $\mathbf{F}^{\mathrm{so}}$ is proportional to the integral $\int\mathrm{d}\bar{r}_x\int\mathrm{d}\bar{k}_y\,\Omega^{\mathrm{r,k}}_{xy}$, which is quantized (first Chern number). Since the integral vanishes for positions $\bar{r}_y$ far away from the skyrmion, it vanishes everywhere.

The leading order contribution to the force on skyrmions in insulators is quadratic in spatial derivatives and linear in the electric field. The evaluation of $\mathbf{F}^{\mathrm{tot}}$, Eq. (10.84), is simplified in insulators since it is not necessary to apply transformation Eq. (10.44) in order to obtain a band-diagonal distribution function $\tilde{\bar{f}}$. In spite of the external driving due to the electric field $\mathbf{E}$, all states below (above) the Fermi energy are always occupied (empty) in an insulator. Therefore, the distribution function $\tilde{f}(\omega) = 1 - 2n_F(\hbar\omega - \mu)$ is a scalar function of frequency only and trivially band-diagonal. Here, n_F is the Fermi function and μ is the chemical potential, which lies in a band gap. The Keldysh Green's function is thus readily obtained in canonical coordinates,

$$\tilde{G}^K(t, \mathbf{r}; \omega, \mathbf{k}) = \big(\tilde{G}^R(t, \mathbf{r}; \omega, \mathbf{k}) - \tilde{G}^A(t, \mathbf{r}; \omega, \mathbf{k})\big)(1 - 2n_F(\hbar\omega - \mu)). \tag{11.11}$$

On the other hand, staying in the canonical frame of reference comes at the cost that the retarded and advanced Green's functions depend in a non-trivial way on the inverse local Green's function $\tilde{g}_0^{-1}$. We obtain $\tilde{G}^R$ and $\tilde{G}^A$ from a gradient expansion similar to the discussion in Section 6.2. Here, the gradient expansion has to be performed in space and time. In our model, temporal derivatives translate into gradients in position and momentum space via the relation

$$\frac{\partial \tilde{g}_0^{-1}}{\partial t} = -\frac{e}{\hbar}\mathbf{E} \cdot \frac{\partial \tilde{g}_0^{-1}}{\partial \mathbf{k}} - \dot{\mathbf{R}} \cdot \frac{\partial \tilde{g}_0^{-1}}{\partial \mathbf{r}} \tag{11.12}$$

where we assumed again that external electric field $\mathbf{E}$ is homogeneous in space. We refer to Appendix B for the calculation, which is rather technical. To leading order in $\mathbf{E}$, $\dot{\mathbf{R}}$, and spatial gradients, we obtain the equation of motion

$$-\mathbf{G} \times \dot{\mathbf{R}} + \delta Q^{(2)}\mathbf{E} = \mathbf{0}. \tag{11.13}$$

Here, $\delta Q^{(2)}$ is the quantized electric charge of the skyrmion, see Eq. (6.45). The charge couples to the electric field in the expected way, leading to the force $\mathbf{F}^{\mathrm{c}} = \delta Q^{(2)}\mathbf{E}$. Due to the gyro-coupling $-\mathbf{G} \times \dot{\mathbf{R}}$, the skyrmion velocity $\dot{\mathbf{R}}$ is perpendicular to the force and the dissipated power $\dot{\mathbf{R}} \cdot \mathbf{F}^{\mathrm{c}}$ vanishes, as it should in an insulator.

For a single occupied band in $d = 2$ dimensions, the force $\mathbf{F}^{\mathrm{c}}$ due to the electric charge of the skyrmion admits an alternative semiclassical interpretation. In this case, the skyrmion charge $\delta Q^{(2)} = \sigma_{xy}\Phi_0$ factorizes into a product of the quantized Hall conductivity σ_{xy} and the quantized total emergent magnetic flux Φ_0, see Eqs. (6.50) and (6.51), respectively. An external electric field $\mathbf{E} = E_y\hat{\mathbf{e}}_y$ in y direction generates a Hall current $j_x = \sigma_{xy}E_y$ in x direction. This current leads to the force $F_y = -\frac{\hbar}{e}\int \mathrm{d}^2 r\, \Omega^{\mathrm{r,r}}_{yx} j_x = \Phi_0 j_x$ in y direction via a process similar to the force $\mathbf{F}^{\mathrm{gyro,s}}$ in metals, see Eq. (11.9). In total, one obtains again the force $\mathbf{F}^{\mathrm{c}} = \delta Q^{(2)}\mathbf{E}$. This interpretation breaks down if more than one band is occupied. In this case, the second Chern number $\delta Q^{(2)}$ is given in terms of non-Abellian Berry curavtures in Eq. (6.48), and it does not factorize into a product of first Chern numbers Φ_0 and σ_{xy} in position and momentum space, respectively. Nevertheless, even if $\delta Q^{(2)}$ does not factorize into real-space and momentum-space winding numbers, it still couples to the electric field in the usual way via Eq. (11.13).

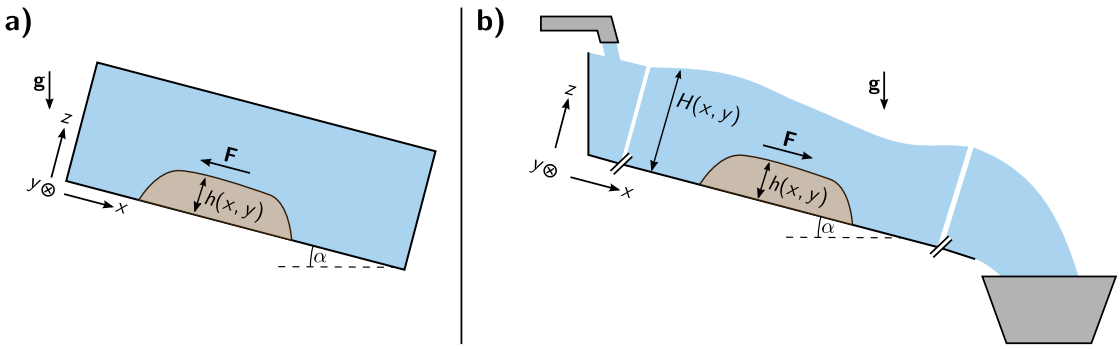

Figure 11.1.: Classical hydrodynamic analogy to the force $\mathbf{F}^{\mathrm{c}} = \delta Q^{(2)}\mathbf{E}$ in insulators and the drag force $\mathbf{F}^{\mathrm{drag}}$ in metals. a) Insulating case: in a closed container filled with water, a submerged object experiences a lifting force linear in its volume. b) Analogy to a metal: in an open gutter, a submerged object diverts the flow of water, leading to a change of the water level linear in the height of the object. The resulting drag force on the object is quadratic in its height.

11.3. Discussion of the coupling to the electric charge

In chapters 5 and 6, we argued that skyrmions carry an electric charge due to Berry phases in phase space. In presence of an electric field, the skyrmion charge influences the equation of motion of the skyrmion, see Eqs. (11.8) and (11.13). The coupling of the skyrmion charge to the electric field is, however, of different nature in metals than it is in insulators. In insulators, the skyrmion behaves much like a usual particle with a quantized electric charge $\delta Q^{(2)} = ne$, $n \in \mathbb{Z}$, which experiences a force $\mathbf{F}^{\mathrm{c}} = \delta Q^{(2)}\mathbf{E}$ in presence of an electric field. The situation in metals is different in two regards. First, the skyrmion charge in metals is not quantized, and for a skyrmion that is much larger than the unit cell, the charge density $\delta\rho^{(1)}$ due to Berry phases is typically dwarfed by the additional charge density $\delta\rho^{(0)}$ that originates from an inhomogeneous magnitude $|\mathbf{B}^{\mathrm{ex}}(\bar{\mathbf{r}})|$ of the exchange field, see Eq. (10.79). Second, the electric field does not couple to the total charge $\delta Q = \int \mathrm{d}^d\bar{r}\,(\delta\rho^{(0)} + \delta\rho^{(1)})$ in metals. Instead, it leads to a drag force $\mathbf{F}^{\mathrm{drag}}$ that is quadratic in $(\delta\rho^{(0)} + \delta\rho^{(1)})$, see Eq. (11.8).

In order to take some of the mystery out of these differences between metals and insulators we use a simple analogy to classical fluid dynamics. Instead of electrons in a solid, we consider an elongated container that is filled with water (Figure 11.1). The bottom of the container is the coordinate plane $z = 0$. The container is tilted by an angle α to the horizontal plane so that the gravitational constant $\mathbf{g}$ has a component g_x in the direction x along the elongation. This results in a gravitational force on the water, reminiscent of the electric force $-e\mathbf{E}$ on electrons in a solid. On the bottom of the container, there is a submerged object that can move without friction. The object displaces an amount of water proportional to its volume V, which is analogous to a change of the charge density $\rho(\mathbf{r})$ due to the presence of a skyrmion in a metal or

insulator. We denote the height profile of the object by $h(x, y)$. Our aim is to calculate the force in direction x that acts on the submerged object due to differences in the water pressure $p(\mathbf{r})$ on its two ends. From simple geometric considerations, the force is given by

$$F_x = \int \mathrm{d}x \int \mathrm{d}y \, p(x, y, h(x, y)) \frac{\partial h(x, y)}{\partial x}. \tag{11.14}$$

The submerged object also experiences a gravitational force proportional to its mass, but this is only a shortcoming of the analogy and we are not interested in the gravitational force on the object.

The closest classical analogy to an insulator is obtained if the container is closed to all sides and completely filled (Figure 11.1a). In this case, the pressure field $p(\mathbf{r})$ is obtained from the Bernouilli Equation,

$$p(\mathbf{r}) - \rho_\mathrm{w} \mathbf{g} \cdot \mathbf{r} + \frac{1}{2} \rho_\mathrm{w} v(\mathbf{r})^2 = \mathrm{const}, \tag{11.15}$$

where ρ_w is the density of water, assumed to be constant, and $\mathbf{v}(\mathbf{r}) = \mathbf{0}$ is the velocity of the water at position $\mathbf{r}$, which vanishes in equilibrium. We thus obtain $p(\mathbf{r}) = \rho_\mathrm{w} \mathbf{g} \cdot \mathbf{r}$, and, by Eq. (11.14), the force $F_x = -V \rho_\mathrm{w} g_x$ is just the usual lifting force. This result is analogous to the force $\mathbf{F}^\mathrm{c} = \delta Q^{(2)} \mathbf{E}$ in insulators, recalling that the presence of the submerged object changes the total mass of the water in the container by $-V \rho_\mathrm{w}$.

Let us now consider a different setup, in which the upper and lower ends of the container are connected to a constant source and sink of water, respectively, and the top of the container is open (Figure 11.1b). This is analogous to a metal that is connected to a battery, where the role of the local chemical potential $\mu(\mathbf{r})$ is taken by the distance $H(x, y)$ of the water surface measured from the bottom of the container. Water flows down the pipe and the system can establish a steady state only in presence of friction, described by the viscosity η in the Navier-Stokes Equation

$$\rho_\mathrm{w} \frac{\partial \mathbf{v}}{\partial t} + \left(\mathbf{v} \cdot \boldsymbol{\nabla} - \eta \boldsymbol{\nabla}^2 \right) \mathbf{v} = -\boldsymbol{\nabla} p + \rho_\mathrm{w} \mathbf{g}. \tag{11.16}$$

If the submerged object is held at a fixed position, the steady state is defined by $\partial \mathbf{v} / \partial t = \mathbf{0}$. The object influences the velocity and pressure fields via the boundary conditions. For non-slip boudary conditions at the bottom, one has,

$$\mathbf{v} = 0 \qquad \text{at the bottom, } z = h(x, y) \tag{11.17}$$

$$p = 0 \qquad \text{at the water surface, } z = H(x, y). \tag{11.18}$$

We assume that the water level H is large compared to the height h of the submerged object. To zeroth order in h/H, Eqs. (11.16)–(11.18) are solved by a constant filling $H(x, y) = H_0$ and

$$p_0(\mathbf{r}) = \rho_\mathrm{w} g_z (z - H_0); \tag{11.19}$$

$$\mathbf{v}_0(\mathbf{r}) = \frac{\rho_\mathrm{w} g_x}{2\eta} \left(H_0^2 - (z - H_0)^2 \right) \hat{\mathbf{e}}_x. \tag{11.20}$$

Since p_0 is independent of x, the force F_x, Eq. (11.14), generated by p_0 vanishes. Corrections to p_0 are of linear order in h, and thus the leading contribution to F_x is quadratic in h. This is analogous to the fact that $\mathbf{F}^{\mathrm{drag}}$, Eq. (11.8), is quadratic in the change of the charge density. Physically, the submerged object is an obstacle for the flow of water, leading to a rise (lowering) of the water level $H(x, y)$ linear in h in front of (behind) the object, as indicated in Figure 11.1b. In the metal, this corresponds to the non-constant local chemical potential $\mu(\mathbf{r})$, which is linear in the excess charge density $\delta\rho^{(0)}+\delta\rho^{(1)}$, see Eq. (10.83). The gradient of the water level is associated with a pressure gradient, which leads to a drag force quadratic in h on the submerged object. Similar arguments can be made if the object moves with a constant velocity, leading a frictional force analogous to $\mathbf{F}^{\mathrm{Ohm}}$, Eq. (11.7).

12. Conclusions and outlook

We studied the effects of phase-space Berry phases in chiral magnets with weak spin-orbit coupling. Chiral magnets develop a smooth magnetization textures at low temperatures due to a competition between ferromagnetic exchange and Dzyaloshinskii-Moriya *DM) interaction. Most notably, topologically protected whirls, so-called skyrmions, are thermodynamically stable in a small pocket of the phase diagram and exist as metastable objects in a wider range of the phase diagram. Based on a minimal analytic model, we argued that the combination of spin-orbit coupling and smooth magnetic textures in position space leads a non-vanishing Berry curvature in mixed position/momentum space.

In part I, we showed that the Berry curvature in mixed position/momentum space leads to an electric charge of skyrmions due to an accumulation of electrons. We estimated the charge to be on the order of one electron charge per skyrmion if screening is neglected. This was confirmed in numerical calculations for MnSi by our collaborators. In insulators, the electric charge of skyrmions is quantized (second Chern number). If all non-abelian Berry curvatures vanishes, the charge is equal to the product of the quantized Hall conductivity and the quantized total flux of emergent magnetic field. We also showed that the strength of DM interactions can be expressed in terms of the Berry curvature in mixed position/momentum space if the magnetic texture varies on a long length scale. Numerical results by our collaborators for the DM interaction strength in MnSi agree well with experimental data.

In part II, we showed that the combination of spin-orbit coupling and smooth magnetic textures leads to an additional contribution to the Hall conductivity in chiral magnets. We developed a diagrammatic theory for the topological Hall effect based on a gradient expansion of the Kubo-Středa formula and derived a correction to the semiclassical formula.

In part III, we studied the dynamics of rigid skyrmions in chiral magnets. We derive an equation of motion for the translational mode, taking into account Berry phases in all of phase space. In presence of an externally applied electric field, the Berry curvature in mixed position/momentum space leads to a dissipationless momentum transfer from conduction electrons to the skyrmions, which is independent of the current. In metals, the electric charge of skyrmions influences the motion of the skyrmion in two ways. First, a moving electron carries along excess charges, which leads to ohmic friction. Second, if an electric field is applied, a spacially inhomogeneous conductivity leads to a pile-up up of charge carriers at one side of the skyrmion and to a depletion of charge carriers on the other side. This imbalance leads to a drag force on the skyrmion. The electric charge of skyrmions in metallic chiral magnets does, however, not couple directly to the electric field. The situation is different in insulators. Here, both drag and ohmic friction

vanish, and the quantized electric charge couples instead directly to the electric field.

Outlook. In a recent series of experiments, Hsu and collaborators were able to selectively create and destroy skyrmions in a three atomic layer thick film of Iron on an Ir(111) substrate using only the electric field from the tip of a scanning tunneling microscope [43]. While it is not yet definitely settled that no current flowed from the tip to the sample, switching the sign of the tip voltage allowed to change from skyrmion creation to skyrmion destruction, indicating that the electric field is the main driving force of the process. It is possible that these experiments can be explained by the electric charge of skyrmions discussed in part I of this thesis. The voltage difference between the tip and the substrate leads to electric fields with an in-plane component that points radially either towards the tip or away from it, depending on the sign of the voltage. Once electrons accumulate or deplete below the tip, the system may be able to lower its energy by building a skyrmion, as this is accompanied with a change of the density of states in phase space. In order to investigate if the Berry-phase effect is indeed responsible for the creation an destruction skyrmions, numerical data for the phase-space Bery curvature in the materials used in the experiment are necessary.

The quantized skyrmion charge in insulators promises an exciting method to manipulate skyrmions with electric fields without the losses accompanied by ohmic friction in metals. In order to achieve this, an insulating chiral magnet with a non-trivial topology in momentum space would be required.

Finally, we presented a method to derive an equation of motion for the translational mode of skyrmions in part III of this thesis. The method is general in that it is not limited to electron-skyrmion interaction. Recently, the interaction between skyrmions and magnons due to a temperature gradient has been in the focus of a number of publications [144, 146, 147]. Due to a combination of two gyro-couplings, it turns out that skyrmions move towards the heat source. Adapting the method presented in part III of this thesis would allow to account for spin-orbit effects in the magnon-skyrmion coupling. We point out, however, that the separation between magnon modes and the translational mode of the skyrmion is more subtle than in the case of electron-magnon interaction.

Bibliography

[1] M. V. Berry, *Quantal Phase Factors Accompanying Adiabatic Changes*, Proceedings of the Royal Society of London. A. Mathematical and Physical Sciences **392**, 45 (1984).

[2] D. Xiao, M.-C. Chang, and Q. Niu, *Berry phase effects on electronic properties*, Reviews of Modern Physics **82**, 1959 (2010).

[3] J. A. Jones, V. Vedral, A. Ekert, and G. Castagnoli, *Geometric quantum computation using nuclear magnetic resonance*, Nature **403**, 869 (2000).

[4] A. Y. Smirnov, *The geometrical phase in neutrino spin precession and the solar neutrino problem*, Physics Letters B **260**, 161 (1991).

[5] G. Sundaram and Q. Niu, *Wave-packet dynamics in slowly perturbed crystals: Gradient corrections and Berry-phase effects*, Physical Review B **59**, 14915 (1999).

[6] R. Karplus and J. M. Luttinger, *Hall Effect in Ferromagnetics*, Physical Review **95**, 1154 (1954).

[7] D. Xiao, J. Shi, and Q. Niu, *Berry Phase Correction to Electron Density of States in Solids*, Physical Review Letters **95**, 137204 (2005).

[8] D. J. Thouless, M. Kohmoto, M. P. Nightingale, and M. den Nijs, *Quantized Hall Conductance in a Two-Dimensional Periodic Potential*, Physical Review Letters **49**, 405 (1982).

[9] S. Mühlbauer et al., *Skyrmion Lattice in a Chiral Magnet*, Science **323**, 915 (2009).

[10] A. Neubauer, C. Pfleiderer, R. Ritz, P. G. Niklowitz, and P. Böni, *Hall effect and magnetoresistance in MnSi*, Physica B: Condensed Matter **404**, 3163 (2009).

[11] A. A. Thiele, *Steady-State Motion of Magnetic Domains*, Physical Review Letters **30**, 230 (1973).

[12] F. Jonietz et al., *Spin Transfer Torques in MnSi at Ultralow Current Densities*, Science **330**, 1648 (2010).

[13] S. L. Sondhi, A. Karlhede, S. A. Kivelson, and E. H. Rezayi, *Skyrmions and the crossover from the integer to fractional quantum Hall effect at small Zeeman energies*, Physical Review B **47**, 16419 (1993).

[14] S. E. Barrett, G. Dabbagh, L. N. Pfeiffer, K. W. West, and R. Tycko, *Optically Pumped NMR Evidence for Finite-Size Skyrmions in GaAs Quantum Wells near Landau Level Filling ν=1*, Physical Review Letters **74**, 5112 (1995).

[15] T. H. R. Skyrme, *A Non-Linear Field Theory*, Proceedings of the Royal Society of London A: Mathematical, Physical and Engineering Sciences **260**, 127 (1961).

[16] N. Manton and P. Sutcliffe, *Topological Solitons*, Cambridge University Press, Cambridge, 1 edition, 2007.

[17] A. Bogdanov and D. Yablonskii, *Thermodynamically stable "vortices" in magnetically ordered crystals. The mixed state of magnets*, Journal of Experimental and Theoretical Physics **68**, 101 (1988).

[18] A. Bogdanov and A. Hubert, *Thermodynamically stable magnetic vortex states in magnetic crystals*, Journal of Magnetism and Magnetic Materials **138**, 255 (1994).

[19] X. Z. Yu et al., *Real-space observation of a two-dimensional skyrmion crystal*, Nature **465**, 901 (2010).

[20] P. Milde et al., *Unwinding of a Skyrmion Lattice by Magnetic Monopoles*, Science **340**, 1076 (2013).

[21] B. Binz and A. Vishwanath, *Chirality induced anomalous-Hall effect in helical spin crystals*, Physica B: Condensed Matter **403**, 1336 (2008).

[22] A. Neubauer et al., *Topological Hall Effect in the A Phase of MnSi*, Physical Review Letters **102**, 186602 (2009).

[23] W. Münzer et al., *Skyrmion lattice in the doped semiconductor $Fe_{1-x}Co_xSi$*, Physical Review B **81**, 041203 (2010).

[24] X. Z. Yu et al., *Near room-temperature formation of a skyrmion crystal in thin-films of the helimagnet FeGe*, Nature Materials **10**, 106 (2011).

[25] G. Chen, A. Mascaraque, A. T. N'Diaye, and A. K. Schmid, *Room temperature skyrmion ground state stabilized through interlayer exchange coupling*, Applied Physics Letters **106**, 242404 (2015).

[26] O. Boulle et al., *Room-temperature chiral magnetic skyrmions in ultrathin magnetic nanostructures*, Nature Nanotechnology **11**, 449 (2016).

[27] S. Seki, X. Z. Yu, S. Ishiwata, and Y. Tokura, *Observation of Skyrmions in a Multiferroic Material*, Science **336**, 198 (2012).

[28] I. Dzyaloshinsky, *A thermodynamic theory of "weak" ferromagnetism of antiferromagnetics*, Journal of Physics and Chemistry of Solids **4**, 241 (1958).

[29] T. Moriya, *Anisotropic Superexchange Interaction and Weak Ferromagnetism*, Physical Review **120**, 91 (1960).

[30] R. Ritz et al., *Giant generic topological Hall resistivity of MnSi under pressure*, Physical Review B **87**, 134424 (2013).

[31] M. Janoschek et al., *Fluctuation-induced first-order phase transition in Dzyaloshinskii-Moriya helimagnets*, Physical Review B **87**, 134407 (2013).

[32] Y. Ishikawa, K. Tajima, D. Bloch, and M. Roth, *Helical spin structure in manganese silicide MnSi*, Solid State Communications **19**, 525 (1976).

[33] S. V. Grigoriev et al., *Magnetic structure of MnSi under an applied field probed by polarized small-angle neutron scattering*, Physical Review B **74**, 214414 (2006).

[34] K. Everschor, *Current-Induced Dynamics of Chiral Magnetic Structures : Skyrmions, Emergent Electrodynamics and Spin-Transfer Torques*, Doctoral thesis, Universität zu Köln, 2012.

[35] C. Schütte and A. Rosch, *Dynamics and energetics of emergent magnetic monopoles in chiral magnets*, Physical Review B **90**, 174432 (2014).

[36] K. Everschor et al., *Rotating skyrmion lattices by spin torques and field or temperature gradients*, Physical Review B **86**, 054432 (2012).

[37] A. P. Malozemoff and J. C. Slonczewski, *Magnetic domain walls in bubble materials*, 1979.

[38] C. Schütte, J. Iwasaki, A. Rosch, and N. Nagaosa, *Inertia, diffusion, and dynamics of a driven skyrmion*, Physical Review B **90**, 174434 (2014).

[39] A. Fert, V. Cros, and J. Sampaio, *Skyrmions on the track*, Nature Nanotechnology **8**, 152 (2013).

[40] J. Iwasaki, M. Mochizuki, and N. Nagaosa, *Current-induced skyrmion dynamics in constricted geometries*, Nature Nanotechnology **8**, 742 (2013).

[41] N. Romming et al., *Writing and Deleting Single Magnetic Skyrmions*, Science **341**, 636 (2013).

[42] J. Sampaio, V. Cros, S. Rohart, A. Thiaville, and A. Fert, *Nucleation, stability and current-induced motion of isolated magnetic skyrmions in nanostructures*, Nature Nanotechnology **8**, 839 (2013).

[43] P.-J. Hsu et al., *Electric field driven switching of individual magnetic skyrmions*, arXiv:1601.02935 [cond-mat] (2016).

[44] S. Pancharatnam, *Generalized theory of interference, and its applications*, Proceedings of the Indian Academy of Sciences - Section A **44**, 247 (1956).

[45] M. Born and V. Fock, *Beweis des Adiabatensatzes*, Zeitschrift für Physik **51**, 165 (1928).

[46] T. Kato, *On the Adiabatic Theorem of Quantum Mechanics*, Journal of the Physical Society of Japan **5**, 435 (1950).

[47] B. Simon, *Holonomy, the Quantum Adiabatic Theorem, and Berry's Phase*, Physical Review Letters **51**, 2167 (1983).

[48] F. Haldane, *Model for a Quantum Hall Effect without Landau Levels: Condensed-Matter Realization of the "Parity Anomaly"*, Physical Review Letters **61**, 2015 (1988).

[49] J. E. Avron and R. Seiler, *Quantization of the Hall Conductance for General, Multiparticle Schrödinger Hamiltonians*, Physical Review Letters **54**, 259 (1985).

[50] M. I. Krivoruchenko, *Rotation of the swing plane of Foucault's pendulum and Thomas spin precession: two sides of one coin*, Physics-Uspekhi **52**, 821 (2009).

[51] N. A. Sinitsyn, Q. Niu, and A. H. MacDonald, *Coordinate shift in the semiclassical Boltzmann equation and the anomalous Hall effect*, Physical Review B **73**, 075318 (2006).

[52] Y. Aharonov and D. Bohm, *Significance of Electromagnetic Potentials in the Quantum Theory*, Physical Review **115**, 485 (1959).

[53] J. Zak, *Berry's phase for energy bands in solids*, Physical Review Letters **62**, 2747 (1989).

[54] M. Atala et al., *Direct measurement of the Zak phase in topological Bloch bands*, Nature Physics **9**, 795 (2013).

[55] R. Bott and S. S. Chern, *Hermitian vector bundles and the equidistribution of the zeroes of their holomorphic sections*, Acta Mathematica **114**, 71 (1965).

[56] S. Kobayashi and K. Nomizu, *Foundations of Differential Geometry, Vol. 2*, Wiley-Interscience, New York, volume 2 edition edition, 1996.

[57] C. Zener, *Non-Adiabatic Crossing of Energy Levels*, Proceedings of the Royal Society of London. Series A **137**, 696 (1932).

[58] L. D. Landau, *Zur theorie der energieubertragung. II*, Physics of the Soviet Union **2**, 28 (1932).

[59] E. Stueckelberg, *Theorie der unelastischen Stösse zwischen Atomen*, Helvetica Physica Acta **5**, 369 (1932).

[60] E. Majorana, *Atomi orientati in campo magnetico variabile*, Il Nuovo Cimento **9**, 43 (1932).

[61] C. Wittig, *The Landau–Zener Formula*, The Journal of Physical Chemistry B **109**, 8428 (2005).

[62] S. Zhang and S. S.-L. Zhang, *Generalization of the Landau-Lifshitz-Gilbert Equation for Conducting Ferromagnets*, Physical Review Letters **102**, 086601 (2009).

[63] T. Schulz et al., *Emergent electrodynamics of skyrmions in a chiral magnet*, Nature Physics **8**, 301 (2012).

[64] G. E. Volovik, *Linear momentum in ferromagnets*, Journal of Physics C: Solid State Physics **20**, L83 (1987).

[65] F. Freimuth, R. Bamler, Y. Mokrousov, and A. Rosch, *Phase-space Berry phases in chiral magnets: Dzyaloshinskii-Moriya interaction and the charge of skyrmions*, Physical Review B **88**, 214409 (2013).

[66] N. W. Ashcroft and N. Mermin, *Solid State Physics*, Cengage Learning, Inc, 1976.

[67] M.-C. Chang and Q. Niu, *Berry Phase, Hyperorbits, and the Hofstadter Spectrum*, Physical Review Letters **75**, 1348 (1995).

[68] D. R. Hofstadter, *Energy levels and wave functions of Bloch electrons in rational and irrational magnetic fields*, Physical Review B **14**, 2239 (1976).

[69] Y. Ishikawa, G. Shirane, J. A. Tarvin, and M. Kohgi, *Magnetic excitations in the weak itinerant ferromagnet MnSi*, Physical Review B **16**, 4956 (1977).

[70] N. Nagaosa, J. Sinova, S. Onoda, A. H. MacDonald, and N. P. Ong, *Anomalous Hall effect*, Reviews of Modern Physics **82**, 1539 (2010).

[71] T. Jeong and W. E. Pickett, *Implications of the B20 crystal structure for the magnetoelectronic structure of MnSi*, Physical Review B **70**, 075114 (2004).

[72] M. Lee, Y. Onose, Y. Tokura, and N. P. Ong, *Hidden constant in the anomalous Hall effect of high-purity magnet MnSi*, Physical Review B **75**, 172403 (2007).

[73] R. Cheng and Q. Niu, *Electron dynamics in slowly varying antiferromagnetic texture*, Physical Review B **86**, 245118 (2012).

[74] C. Duval, Z. Horváth, P. A. Horváthy, L. Martina, and P. C. Stichel, *Comment on "Berry Phase Correction to Electron Density of States in Solids"*, Physical Review Letters **96**, 099701 (2006).

[75] S. Lang, *Algebra*, Springer, New York, 3rd rev. ed. 2002. corr. 4th printing 2005 edition, 2005.

[76] A. Altland and B. D. Simons, *Condensed Matter Field Theory*, Cambridge University Press, Cambridge, 2010.

[77] F. Freimuth, S. Blügel, and Y. Mokrousov, *Berry phase theory of Dzyaloshinskii–Moriya interaction and spin–orbit torques*, Journal of Physics: Condensed Matter **26**, 104202 (2014).

[78] T. Adams et al., *Long-Range Crystalline Nature of the Skyrmion Lattice in MnSi*, Physical Review Letters **107**, 217206 (2011).

[79] R. Jones, *Density functional theory: Its origins, rise to prominence, and future*, Reviews of Modern Physics **87**, 897 (2015).

[80] P. Hohenberg and W. Kohn, *Inhomogeneous Electron Gas*, Physical Review **136**, B864 (1964).

[81] M. Levy, *Universal variational functionals of electron densities, first-order density matrices, and natural spin-orbitals and solution of the v-representability problem*, Proceedings of the National Academy of Sciences **76**, 6062 (1979).

[82] W. Kohn and L. J. Sham, *Self-Consistent Equations Including Exchange and Correlation Effects*, Physical Review **140**, A1133 (1965).

[83] J. Rammer and H. Smith, *Quantum field-theoretical methods in transport theory of metals*, Reviews of Modern Physics **58**, 323 (1986).

[84] C. Wickles and W. Belzig, *Effective quantum theories for Bloch dynamics in inhomogeneous systems with nontrivial band structure*, Physical Review B **88**, 045308 (2013).

[85] M. Genske and A. Rosch, *Floquet-Boltzmann equation for periodically driven Fermi systems*, Physical Review A **92**, 062108 (2015).

[86] H. J. Groenewold, *On the principles of elementary quantum mechanics*, Physica **12**, 405 (1946).

[87] X.-L. Qi, T. L. Hughes, and S.-C. Zhang, *Topological field theory of time-reversal invariant insulators*, Physical Review B **78**, 195424 (2008).

[88] H. A. Fertig, L. Brey, R. Côté, and A. H. MacDonald, *Charged spin-texture excitations and the Hartree-Fock approximation in the quantum Hall effect*, Physical Review B **50**, 11018 (1994).

[89] D.-H. Lee and C. L. Kane, *Boson-vortex-Skyrmion duality, spin-singlet fractional quantum Hall effect, and spin-1/2 anyon superconductivity*, Physical Review Letters **64**, 1313 (1990).

[90] L. Brey, H. A. Fertig, R. Côté, and A. H. MacDonald, *Skyrme Crystal in a Two-Dimensional Electron Gas*, Physical Review Letters **75**, 2562 (1995).

[91] M. Lee, W. Kang, Y. Onose, Y. Tokura, and N. P. Ong, *Unusual Hall Effect Anomaly in MnSi under Pressure*, Physical Review Letters **102**, 186601 (2009).

[92] C. Franz et al., *Real-Space and Reciprocal-Space Berry Phases in the Hall Effect of* $Mn_{1-x}Fe_xSi$, Physical Review Letters **112**, 186601 (2014).

[93] J. Gayles et al., *Dzyaloshinskii-Moriya Interaction and Hall Effects in the Skyrmion Phase of* $Mn_{1-x}Fe_xGe$, Physical Review Letters **115**, 036602 (2015).

[94] N. Kanazawa et al., *Large Topological Hall Effect in a Short-Period Helimagnet MnGe*, Physical Review Letters **106**, 156603 (2011).

[95] H. Yanagihara and M. B. Salamon, *Skyrmion Strings and the Anomalous Hall Effect in* CrO_2, Physical Review Letters **89**, 187201 (2002).

[96] S. A. Baily and M. B. Salamon, *Berry-phase contribution to the anomalous Hall effect in gadolinium*, Physical Review B **71**, 104407 (2005).

[97] Y. Taguchi, Y. Oohara, H. Yoshizawa, N. Nagaosa, and Y. Tokura, *Spin Chirality, Berry Phase, and Anomalous Hall Effect in a Frustrated Ferromagnet*, Science **291**, 2573 (2001).

[98] B. G. Ueland et al., *Controllable chirality-induced geometrical Hall effect in a frustrated highly correlated metal*, Nature Communications **3**, 1067 (2012).

[99] Z. Fang et al., *The Anomalous Hall Effect and Magnetic Monopoles in Momentum Space*, Science **302**, 92 (2003).

[100] H. Zhang, C. Lazo, S. Blügel, S. Heinze, and Y. Mokrousov, *Electrically Tunable Quantum Anomalous Hall Effect in Graphene Decorated by* 5*d Transition-Metal Adatoms*, Physical Review Letters **108**, 056802 (2012).

[101] C. Kooi, *Hall Effect in Ferromagnetics*, Physical Review **95**, 843 (1954).

[102] P. N. Dheer, *Galvanomagnetic Effects in Iron Whiskers*, Physical Review **156**, 637 (1967).

[103] Y. Tian, L. Ye, and X. Jin, *Proper Scaling of the Anomalous Hall Effect*, Physical Review Letters **103**, 087206 (2009).

[104] L. Ye, Y. Tian, X. Jin, and D. Xiao, *Temperature dependence of the intrinsic anomalous Hall effect in nickel*, Physical Review B **85**, 220403 (2012).

[105] J. Smit, *The spontaneous hall effect in ferromagnetics I*, Physica **21**, 877 (1955).

[106] L. Berger, *Side-Jump Mechanism for the Hall Effect of Ferromagnets*, Physical Review B **2**, 4559 (1970).

[107] N. A. Sinitsyn, *Semiclassical theories of the anomalous Hall effect*, Journal of Physics: Condensed Matter **20**, 023201 (2008).

[108] J. Kötzler and W. Gil, *Anomalous Hall resistivity of cobalt films: Evidence for the intrinsic spin-orbit effect*, Physical Review B **72**, 060412 (2005).

[109] J. Weischenberg, F. Freimuth, J. Sinova, S. Blügel, and Y. Mokrousov, *Ab Initio Theory of the Scattering-Independent Anomalous Hall Effect*, Physical Review Letters **107**, 106601 (2011).

[110] D. Ködderitzsch, K. Chadova, J. Minár, and H. Ebert, *Impact of finite temperatures and correlations on the anomalous Hall conductivity from ab initio theory*, New Journal of Physics **15**, 053009 (2013).

[111] P. Czaja, F. Freimuth, J. Weischenberg, S. Blügel, and Y. Mokrousov, *Anomalous Hall effect in ferromagnets with Gaussian disorder*, Physical Review B **89**, 014411 (2014).

[112] S. Lowitzer, D. Ködderitzsch, and H. Ebert, *Coherent Description of the Intrinsic and Extrinsic Anomalous Hall Effect in Disordered Alloys on an Ab Initio Level*, Physical Review Letters **105**, 266604 (2010).

[113] N. A. Sinitsyn, A. H. MacDonald, T. Jungwirth, V. K. Dugaev, and J. Sinova, *Anomalous Hall effect in a two-dimensional Dirac band: The link between the Kubo-Streda formula and the semiclassical Boltzmann equation approach*, Physical Review B **75**, 045315 (2007).

[114] I. Turek, J. Kudrnovský, and V. Drchal, *Ab initio theory of galvanomagnetic phenomena in ferromagnetic metals and disordered alloys*, Physical Review B **86**, 014405 (2012).

[115] J. Schliemann and D. Loss, *Anisotropic transport in a two-dimensional electron gas in the presence of spin-orbit coupling*, Physical Review B **68**, 165311 (2003).

[116] A. Kamenev, *Field Theory of Non-Equilibrium Systems*, Cambridge University Press, first edition, 2011.

[117] J. M. Ziman, *Electrons and Phonons: The Theory of Transport Phenomena in Solids*, Oxford University Press, 2001.

[118] N. A. Sinitsyn, Q. Niu, J. Sinova, and K. Nomura, *Disorder effects in the anomalous Hall effect induced by Berry curvature*, Physical Review B **72**, 045346 (2005).

[119] I. A. Ado, I. A. Dmitriev, P. M. Ostrovsky, and M. Titov, *Anomalous Hall effect with massive Dirac fermions*, EPL (Europhysics Letters) **111**, 37004 (2015).

[120] A. Bastin, C. Lewiner, O. Betbeder-matibet, and P. Nozieres, *Quantum oscillations of the hall effect of a fermion gas with random impurity scattering*, Journal of Physics and Chemistry of Solids **32**, 1811 (1971).

[121] A. Crépieux and P. Bruno, *Theory of the anomalous Hall effect from the Kubo formula and the Dirac equation*, Physical Review B **64**, 014416 (2001).

[122] G. D. Mahan, *Many Particle Physics*, Springer, 3rd ed. 2000 edition, 2000.

[123] P. Streda, *Theory of quantised Hall conductivity in two dimensions*, Journal of Physics C: Solid State Physics **15**, L717 (1982).

[124] M. N. Baibich et al., *Giant Magnetoresistance of (001)Fe/(001)Cr Magnetic Superlattices*, Physical Review Letters **61**, 2472 (1988).

[125] G. Binasch, P. Grünberg, F. Saurenbach, and W. Zinn, *Enhanced magnetoresistance in layered magnetic structures with antiferromagnetic interlayer exchange*, Physical Review B **39**, 4828 (1989).

[126] J. C. Slonczewski, *Current-driven excitation of magnetic multilayers*, Journal of Magnetism and Magnetic Materials **159**, L1 (1996).

[127] L. Berger, *Emission of spin waves by a magnetic multilayer traversed by a current*, Physical Review B **54**, 9353 (1996).

[128] S. S. P. Parkin, M. Hayashi, and L. Thomas, *Magnetic Domain-Wall Racetrack Memory*, Science **320**, 190 (2008).

[129] L. D. Landau and E. Lifshitz, *On the theory of the dispersion of magnetic permeability in ferromagnetic bodies*, Phys. Z. Sowjetunion **8**, 101 (1935).

[130] T. L. Gilbert, *A phenomenological theory of damping in ferromagnetic materials*, IEEE Transactions on Magnetics **40**, 3443 (2004).

[131] S. Zhang and Z. Li, *Roles of Nonequilibrium Conduction Electrons on the Magnetization Dynamics of Ferromagnets*, Physical Review Letters **93**, 127204 (2004).

[132] M. C. Hickey and J. S. Moodera, *Origin of Intrinsic Gilbert Damping*, Physical Review Letters **102**, 137601 (2009).

[133] Y. Tserkovnyak and C. H. Wong, *Theory of spin magnetohydrodynamics*, Physical Review B **79**, 014402 (2009).

[134] R. A. Duine, A. S. Núñez, J. Sinova, and A. H. MacDonald, *Functional Keldysh theory of spin torques*, Physical Review B **75**, 214420 (2007).

[135] L. Hodges, D. R. Stone, and A. V. Gold, *Field-Induced Changes in the Band Structure and Fermi Surface of Nickel*, Physical Review Letters **19**, 655 (1967).

[136] J. Kuneš and V. Kamberský, *First-principles investigation of the damping of fast magnetization precession in ferromagnetic* 3*d metals*, Physical Review B **65**, 212411 (2002).

[137] K. Gilmore, Y. U. Idzerda, and M. D. Stiles, *Identification of the Dominant Precession-Damping Mechanism in Fe, Co, and Ni by First-Principles Calculations*, Physical Review Letters **99**, 027204 (2007).

[138] S. M. Bhagat and P. Lubitz, *Temperature variation of ferromagnetic relaxation in the* 3*d transition metals*, Physical Review B **10**, 179 (1974).

[139] D. J. Twisselmann and R. D. McMichael, *Intrinsic damping and intentional ferromagnetic resonance broadening in thin Permalloy films*, Journal of Applied Physics **93**, 6903 (2003).

[140] *OOMMF Project at NIST, http://math.nist.gov/oommf/, accessed May 2016.*

[141] G. Tatara and H. Kohno, *Theory of Current-Driven Domain Wall Motion: Spin Transfer versus Momentum Transfer*, Physical Review Letters **92**, 086601 (2004).

[142] M. E. Lucassen, H. J. van Driel, C. M. Smith, and R. A. Duine, *Current-driven and field-driven domain walls at nonzero temperature*, Physical Review B **79**, 224411 (2009).

[143] C. Burrowes et al., *Non-adiabatic spin-torques in narrow magnetic domain walls*, Nature Physics **6**, 17 (2010).

[144] C. Schütte and M. Garst, *Magnon-skyrmion scattering in chiral magnets*, Physical Review B **90**, 094423 (2014).

[145] A. Kamenev and A. Levchenko, *Keldysh technique and non-linear sigma-model: basic principles and applications*, Advances in Physics **58**, 197 (2009).

[146] M. Mochizuki et al., *Thermally driven ratchet motion of a skyrmion microcrystal and topological magnon Hall effect*, Nature Materials **13**, 241 (2014).

[147] S. Schroeter and M. Garst, *Scattering of high-energy magnons off a magnetic skyrmion*, Low Temperature Physics **41**, 817 (2015).

[148] B.-J. Yang and N. Nagaosa, *Skyrmion quantum numbers and quantized pumping in two-dimensional topological chiral magnets*, Physical Review B **84**, 245123 (2011).

[149] S. Ryu, A. P. Schnyder, A. Furusaki, and A. W. W. Ludwig, *Topological insulators and superconductors: tenfold way and dimensional hierarchy*, New Journal of Physics **12**, 065010 (2010).

A. Derivation of the quantized skyrmion charge in insulators

In this appendix, we provide details for the calculations of the skyrmion charge in insulators, see section 6.3 of the main text. In Sections A.1–A.3, we derive Eqs. (6.45), (6.49), and (6.52) of the main text for the quantized electric charge of skyrmions in insulators. We have published these derivations in Appendix C of Ref. [65].

A.1. General expression for the skyrmion charge in insulators

We follow arguments similar to Appendix 2 of Ref. [148] in order to derive of Eq. (6.45) of the main text, using the pictorial notation introduced in Eqs. (6.23) and (6.26) of the main text. In an insulator, the Green's function $\tilde{G}(\omega)$ is analytical at $\hbar\omega = \mu$. In the following, we assume without restriction that the chemical potential $\mu = 0$. In the limit $T \to 0$, the expression for the (coarse-grained) charge density, Eq. (6.38) of the main text simplifies to

$$\rho(\mathbf{R}) = -e\hbar \int \frac{\mathrm{d}^d k}{(2\pi)^d} \int_{-\infty}^{\infty} \frac{\mathrm{d}\omega}{2\pi} \ \mathrm{Tr}\Big[\tilde{G}(i\omega; \mathbf{R}, \mathbf{k})\Big]. \tag{A.1}$$

As argued in the main text (section 6.3), terms linear in the spatial gradients do not contribute to the total electric charge of skyrmions in insulators. The second order contribution to the charge density is obtained by inserting $\tilde{G}^{(2)}$, Eq. (6.25) of the main text, into Eq. (A.1). The contribution from the last term in Eq. (6.25) is proportional to

$$\begin{aligned}
\hbar \int \frac{\mathrm{d}\omega}{2\pi} \ \mathrm{Tr}\Big[\quad \Big] &= \hbar J_{ij} J_{kl} \int \frac{\mathrm{d}\omega}{2\pi} \ \mathrm{Tr}\Big[\tilde{g}(\partial_i\partial_k \tilde{H})\tilde{g}(\partial_j\partial_l \tilde{H})\tilde{g}\Big] \\
&= - J_{ij} J_{kl} \int \frac{\mathrm{d}\omega}{2\pi} \ \mathrm{Tr}\left[(\partial_i\partial_k \tilde{H})\tilde{g}(\partial_j\partial_l \tilde{H})\frac{\partial \tilde{g}}{\partial \omega}\right] \\
&= J_{ij} J_{kl} \int \frac{\mathrm{d}\omega}{2\pi} \ \mathrm{Tr}\left[(\partial_i\partial_k \tilde{H})\frac{\partial \tilde{g}}{\partial \omega}(\partial_j\partial_l \tilde{H})\tilde{g}\right] \\
&= J_{ij} J_{kl} \int \frac{\mathrm{d}\omega}{2\pi} \ \mathrm{Tr}\left[(\partial_j\partial_l \tilde{H})\tilde{g}(\partial_i\partial_k \tilde{H})\frac{\partial \tilde{g}}{\partial \omega}\right]
\end{aligned} \tag{A.2}$$

where all local Green's functions are evaluated at frequency $i\omega$ and we used cyclicity of the trace in the second and in the last equality, the relation $\partial\tilde{g}/\partial\omega = -\hbar\tilde{g}^2$ in the

second equality and integration by parts in the third equality. By relabeling indices and using $J_{ij} = -J_{ji}$ one sees that the last line of Eq. (A.2) is the negative of the second line and hence vanishes. Thus, the last term in Eq. (6.25) does not contribute to the charge density in insulators,

$$\int \frac{\mathrm{d}\omega}{2\pi}\ \mathrm{Tr}\Big[$$ 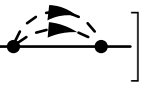 $$\Big] = 0. \tag{A.3}$$

In a similar way one can show the relations

$$\int \frac{\mathrm{d}\omega}{2\pi}\ \mathrm{Tr}\Big[$$ 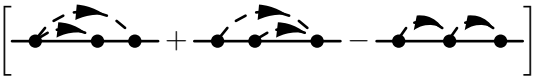 $$\Big] = 0 \tag{A.4}$$

and

$$\int \frac{\mathrm{d}\omega}{2\pi}\ \mathrm{Tr}\Big[$$  $$\Big] = 0. \tag{A.5}$$

Combining Eqs. (A.1), (A.3)-(A.5), and Eq. (6.25) of the main text leads to a simplified expression for the second order correction to the charge density in insulators,

$$\delta\rho^{(2)}(\mathbf{R}) = -e\hbar \int \frac{\mathrm{d}^d k}{(2\pi)^d} \int \frac{\mathrm{d}\omega}{2\pi}\ \mathrm{Tr}\Big[$$ 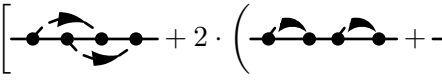 $$\Big]. \tag{A.6}$$

To make further progress we now focus on the contribution of $\delta\rho^{(2)}$ to the total charge of a skyrmion, given by $\delta Q^{(2)} = \int \mathrm{d}^d r\, \delta\rho^{(2)}(\mathbf{r})$. The expression for $\delta Q^{(2)}$ can be simplified by means of integration by parts in phase space. The last diagram on the right-hand side of Eq. (A.6) represents the term $\left(\frac{i}{2}\right)^2 J_{ij}J_{kl}\,\tilde{g}(\partial_i\tilde{H})\tilde{g}(\partial_j\partial_k\tilde{H})\tilde{g}(\partial_l\tilde{H})\tilde{g}$. It is structurally different from the other two diagrams in that it contains a second order derivative in phase space. Integration by parts over the phase-space direction x_j or x_k, respectively, leads to the relations

$$\int \frac{\mathrm{d}^{2d} x}{(2\pi)^d}\ \mathrm{Tr}\Big[$$  $$\Big] = -\int \frac{\mathrm{d}^{2d} x}{(2\pi)^d}\ \mathrm{Tr}\Big[$$ 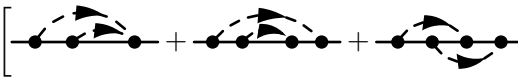 $$\Big]$$

$$= -\int \frac{\mathrm{d}^{2d} x}{(2\pi)^d}\ \mathrm{Tr}\Big[$$  $$\Big]. \tag{A.7}$$

Combining Eqs.(A.4)-(A.7) leads to

$$\delta Q^{(2)} = \frac{e\hbar}{3} \int \frac{\mathrm{d}^{2d} x}{(2\pi)^d} \int \frac{\mathrm{d}\omega}{2\pi}\ \mathrm{Tr}\Big[$$ 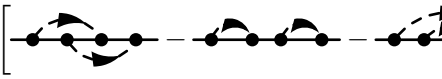 $$\Big] =$$

$$= \frac{e\hbar}{3} \left(\frac{i}{2}\right)^2 \int \frac{\mathrm{d}^{2d} x}{(2\pi)^d} \int \frac{\mathrm{d}\omega}{2\pi}\, \mathcal{I}_{ijkl}\, \mathcal{B}_{ijkl}(i\omega, x) \tag{A.8}$$

with

$$\mathcal{I}_{ijkl} = J_{ik}J_{jl} - J_{ij}J_{kl} - J_{il}J_{jk} \tag{A.9}$$

$$\mathcal{B}_{ijkl}(i\omega, x) = \mathrm{Tr}\Big[\tilde{g}(\partial_i\tilde{H})\tilde{g}(\partial_j\tilde{H})\tilde{g}(\partial_k\tilde{H})\tilde{g}(\partial_l\tilde{H})\tilde{g}\Big]. \tag{A.10}$$

Evidently, $\mathcal{I}_{ijkl}$ is totally anti-symmetric in all indices. For $d = 2$ and $d = 3$ dimensions, one finds that $\mathcal{I}_{ijkl}$ is given by Eq. (6.46) of the main text. This concludes the derivation of Eq. (6.45) of the main text.

A.2. Factorization of the skyrmion charge in two-dimensional insulators with Abelian Berry curvature

In this section we show that the Berry curvature contribution to the charge in a two-dimensional insulator with Abelian Berry curvature is given by the product of the quantized Hall conductivity σ_{xy} and the skyrmion number Φ_0, see Eq. (6.49) of the main text. A purely Abelian Berry curvature arises, e.g., if only a single band is occupied.

For a two-dimensional system with only one occupied band, Eq. (6.47) of the main text reduces to

$$\delta Q^{(2)} = \frac{e}{8}\,\epsilon_{ijkl}\int \frac{\mathrm{d}^4x}{(2\pi)^2}\,\Omega_{ij}\Omega_{kl} = \frac{e}{4}\,\epsilon_{ijkl}\left(\int \frac{\mathrm{d}x_j\,\mathrm{d}x_k\,\mathrm{d}x_l}{(2\pi)^2}\mathcal{A}_j\Omega_{kl}\right)_{x_i=-\infty}^{x_i=+\infty} \tag{A.11}$$

where, for a space (momentum) direction x_i, the symbols $\pm\infty$ denote positions far away from the skyrmion (the boundaries of the Brillouin zone). In the second equality of Eq. (A.11), we used the relation

$$\frac{\epsilon_{ijkl}}{8}\Omega_{ij}\Omega_{kl} = \frac{\epsilon_{ijkl}}{2}\frac{\partial\mathcal{A}_j}{\partial x_i}\frac{\partial\mathcal{A}_l}{\partial x_k} = \frac{\epsilon_{ijkl}}{2}\frac{\partial}{\partial x_i}\left(\mathcal{A}_j\frac{\partial\mathcal{A}_l}{\partial x_k}\right) = \frac{\epsilon_{ijkl}}{4}\frac{\partial}{\partial x_i}\left(\mathcal{A}_j\Omega_{kl}\right) \tag{A.12}$$

where $\mathcal{A}$ is the Berry connection.

In Eq. (A.11), Ω_{kl} only enters at the boundary of the x_i coordinate. At the boundary in a spatial direction (i.e., far away from the skyrmion), the magnetization is collinear and therefore $\Omega^{\mathrm{r,r}} = 0 = \Omega^{\mathrm{r,k}}$. Thus, if x_i is a spatial coordinate, only terms of the form $\mathcal{A}_j^{\mathrm{r}}\Omega_{kl}^{\mathrm{k,k}}$ contribute to the integrand in Eq. (A.11). If x_i is a momentum coordinate, Ω_{kl} is evaluated at the boundary of the Brillouin zone. In an insulator, the charge must be quantized and we can adiabatically deform the Bloch functions such that they are independent of momentum in a narrow stripe around the Brillouin zone boundary. This is always possible since, in absence of further symmetries, all non-interacting Hamiltonians of one-dimensional insulators are adiabatically connected [149]. Therefore, only terms of the form $\mathcal{A}_j^{\mathrm{k}}\Omega_{kl}^{\mathrm{r,r}}$ contribute if x_i is a momentum coordinate. In total, Eq. (A.11) can be written as $\delta Q^{(2)} = \delta Q^{(2),\mathrm{r}} + \delta Q^{(2),\mathrm{k}}$ where

$$\delta Q^{(2),\mathrm{r}} = \frac{e}{2}\,\epsilon_{ij}\left(\int \frac{\mathrm{d}r_j\,\mathrm{d}^2k}{(2\pi)^2}\mathcal{A}_j^{\mathrm{r}}\Omega_{xy}^{\mathrm{k,k}}\right)_{r_i=-\infty}^{r_i=+\infty} \tag{A.13}$$

and $\delta Q^{(2),\mathrm{k}}$ is defined by formally exchanging all r and k. As the Berry curvature $\Omega_{xy}^{\mathrm{k,k}}$ in Eq. (A.13) is gauge independent, it cannot depend on r_j for a collinear magnetization

at $r_i = \pm\infty$. This implies

$$\begin{aligned}\delta Q^{(2),\mathrm{r}} &= \frac{e}{2}\,\epsilon_{ij}\int\frac{\mathrm{d}^2k}{(2\pi)^2}\left(\Omega^{\mathrm{k,k}}_{xy}\int \mathrm{d}r_j(\mathcal{A}^{\mathrm{r}}_j)_{r_i=-\infty}^{r_i=+\infty}\right)\\ &= \frac{e}{2}\int\frac{\mathrm{d}^2k}{(2\pi)^2}\left(\Omega^{\mathrm{k,k}}_{xy}\int \mathrm{d}^2r\,\epsilon_{ij}\frac{\partial\mathcal{A}^{\mathrm{r}}_j}{\partial r_i}\right)\\ &= \frac{e}{2}\int\frac{d^2k}{(2\pi)^2}\left(\Omega^{\mathrm{k,k}}_{xy}\int \mathrm{d}^2r\,\Omega^{\mathrm{r,r}}_{xy}\right)\\ &= \frac{1}{2}\sigma_{xy}\Phi_0\end{aligned} \tag{A.14}$$

where σ_{xy} (Φ_0) is the quantized integral over $\frac{e^2}{\hbar}\Omega^{\mathrm{k,k}}_{xy}$ ($\frac{\hbar}{e}\Omega^{\mathrm{r,r}}_{xy}$) defined in Eqs. (6.50) and (6.51) of the main text. An analogous calculation leads to the same value for $\delta Q^{(2),\mathrm{k}}$. Thus, we conclude that the Berry curvature contribution to the skyrmion charge in a two-dimensional insulator with Abelian Berry curvature is given by Eq. (6.49) of the main text.

A.3. Skyrmion charge per length in three-dimensional insulators with Abelian Berry curvature

In three dimensional systems, skyrmions form line defects. In this section, we derive an expression for the charge per length of a skyrmion line, see Eq. (6.52) of the main text. From Eqs. (6.46) and (6.47) of the main text, the Berry curvature contribution to the charge in a three dimensional insulator is given by

$$\delta Q^{(2)} = e\frac{\epsilon_{ijklqr}J_{qr}}{16}\int\frac{\mathrm{d}^6x}{(2\pi)^3}\,\mathrm{Tr}\left[\hat{\Omega}_{ij}\hat{\Omega}_{kl}\right] \tag{A.15}$$

We introduce dimensionless phase-space coordinates $\tilde{x} \equiv (\tilde{\mathbf{r}}, \tilde{\mathbf{k}})$ such that $\mathbf{r} = \tilde{r}_\alpha \mathbf{a}_\alpha$ and $\mathbf{k} = \tilde{k}_\alpha \mathbf{g}_\alpha/(2\pi)$. Here, latin indices run from 1 to 6 while greek indices run from 1 to 3, the vectors $\mathbf{a}_\alpha$ are lattice vectors of the atomic lattice and $\mathbf{g}_\alpha$ are the corresponding reciprocal lattice vectors. We chose the coordinates $\tilde{x}$ such that momentum space is periodic in the three coordinate directions $\tilde{k}_\alpha$ and the Jacobian of the transformation $\tilde{x} = \tilde{x}(x)$ is one. Thus, in the dimensionless coordinates, Eq. (A.15) becomes

$$\begin{aligned}\delta Q^{(2)} &= \frac{e\,\epsilon_{ijklqr}}{16}\int\frac{\mathrm{d}^6\tilde{x}}{(2\pi)^3}\,\tilde{\Omega}_{ij}\tilde{\Omega}_{kl}J_{qr}\\ &= e\sum_{\alpha=1}^{3}\int\mathrm{d}\tilde{r}_\alpha\int\frac{\mathrm{d}\tilde{k}_\alpha}{2\pi}\frac{\epsilon_{ijkl\alpha(\alpha+3)}}{8}\int\frac{\mathrm{d}^4\tilde{x}}{(2\pi)^2}\,\tilde{\Omega}_{ij}\tilde{\Omega}_{kl}\\ &= e\sum_{\alpha=1}^{3}\int\mathrm{d}\tilde{r}_\alpha\int\frac{\mathrm{d}\tilde{k}_\alpha}{2\pi}\,n^{\mathrm{r}}_\alpha n^{\mathrm{k}}_\alpha\end{aligned} \tag{A.16}$$

with[1]

$$n_\alpha^{\mathrm{r}} = \frac{\epsilon_{\alpha\beta\gamma}}{4\pi} \int \mathrm{d}\tilde{r}_\beta \mathrm{d}\tilde{r}_\gamma \, \tilde{\Omega}_{\beta\gamma}^{\mathrm{r,r}} \in \mathbb{Z}; \qquad n_\alpha^{\mathrm{k}} = \frac{\epsilon_{\alpha\mu\nu}}{4\pi} \int \mathrm{d}\tilde{k}_\mu \mathrm{d}\tilde{k}_\nu \, \tilde{\Omega}_{\mu\nu}^{\mathrm{k,k}} \in \mathbb{Z}. \tag{A.17}$$

In the first line of Eq. (A.16), $\tilde{\Omega}_{ij}$ denotes the elements of the Berry curvature tensor in coordinates $\tilde{x}$. The components of the symplectic tensor J_{qr} are invariant under the transformation from coordinates x to $\tilde{x}$ due to the relation $\mathbf{a}_\alpha \cdot \mathbf{g}_\beta = 2\pi\delta_{ij}$. This allowed us to set $\beta = \alpha + 3$ in the second line of Eq. (A.16). The last integral in the second line of Eq. (A.16) runs over the four dimensional subspace of phase space perpendicular to $(\mathbf{0}, \mathbf{a}_\alpha)$ and $(\mathbf{g}_\alpha, \mathbf{0})$. Its value is given by the product of the real-space and the momentum-space winding numbers, n_α^{r} and n_α^{k}, by the same arguments that lead to the factorization of winding numbers in the two-dimensional case discussed in Appendix A.2.

The remaining integral over $\tilde{k}_\alpha$ in Eq. (A.16) equates to a factor of 1 and the integral over $\tilde{r}_\alpha$ gives

$$\int \mathrm{d}\tilde{r}_\alpha = \frac{\partial \tilde{r}_\alpha}{\partial r_\beta} \int \mathrm{d}r_\beta = \frac{(\mathbf{g}_\alpha)_\beta}{2\pi} L_\beta = \frac{\hat{\mathbf{s}} \cdot \mathbf{g}_\alpha}{2\pi} L \tag{A.18}$$

where the unit vector $\hat{\mathbf{s}}$ points along along the skyrmion line and $L_\beta = L\hat{s}_\beta$ is the projection of the length L of the skyrmion line onto the coordinate direction r_β. For a generic skyrmion line that pierces all three position-space coordinate planes, the skyrmion number is $n_\alpha^{\mathrm{r}} = 1$ for all α. Combining Eqs. (A.16) and (A.18), we arrive at Eq. (6.52) of the main text.

[1] In Appendix C.4 of Ref. [65], we defined n_α^{r} and n_α^{k} with different prefactors. Here, we opted for prefactors that make both winding numbers integer quantities.

B. Coupling of the quantized skyrmion charge to an electric field

In this appendix, we derive the equation of motion for a skyrmion in an insulator in presence of an electric field, see (11.13) of the main text. We start from the equation $\mathbf{F}^{\mathrm{tot}} = \mathbf{0}$ where $\mathbf{F}^{\mathrm{tot}}$ is given by Eq. (10.84), with Keldysh Green's function $\tilde{G}^K$ given by Eq. (11.11). Thus,

$$\mathbf{F}^{\mathrm{tot}}(t) = \frac{i\hbar}{2} \int \mathrm{d}^d r \int \frac{\mathrm{d}^d k}{(2\pi)^d} \int_{-\infty}^{\infty} \frac{\mathrm{d}\omega}{2\pi} \, \mathrm{Tr} \left[\frac{\partial \tilde{g}_0^{-1}}{\partial \mathbf{r}} \otimes \left(\tilde{G}^R - \tilde{G}^A \right) \right] (1 - 2n_F(\hbar\omega)) \tag{B.1}$$

Here, $\tilde{g}_0^{-1}$, $\tilde{g}^R$, and $\tilde{g}^A$ are all evaluated at $(t, \mathbf{r}; \omega, \mathbf{k})$, the trace is over all bands, the symbol "$\otimes$" denotes the Moyal product in position/momentum space as well as in frequency/time space, and we assumed without restriction that he chemical potential $\mu = 0$. The term without the Fermi function vanishes, since the integrand is a sum of two terms that have poles either only above or only below the real axis. For the the term proportional to the Fermi function, the frequency integral over $\tilde{G}^R - \tilde{G}^A$ along the real is equivalent to an integral just above the real axis from $-\infty$ to $+\infty$, followed by an integral just below the real axis from ∞ to $-\infty$ (left-hand side of Figure B.1). Using the fact that the integrand vanishes for $\hbar\omega > 0$ (for $T \to 0$) and the fact that there are no poles at $\hbar\omega = 0$ in an insulator, we obtain

$$\mathbf{F}^{\mathrm{tot}} = -\hbar \int \mathrm{d}^d r \int \frac{\mathrm{d}^d k}{(2\pi)^d} \oint \frac{\mathrm{d}\omega}{2\pi i} \, \mathrm{Tr} \left[\frac{\partial \tilde{g}_0^{-1}}{\partial \mathbf{r}} \otimes \tilde{G}^{(\mathrm{T})} \right]. \tag{B.2}$$

Here, the symbol $\oint \mathrm{d}\omega$ denotes integration along the closed contour that runs counterclockwise around the negative real axis (right-hand side of Figure B.1), and $\tilde{G}^{(\mathrm{T})}$ is the Green's function in the limit of vanishing self-energy. The superscript "(T)" serves as a reminder that $\tilde{G}^{(\mathrm{T})}$ is the Green's function of a time-dependent system, not to be confused with the equilibrium Green's function $\tilde{G}$ used in Eq. (A.1). The Green's function satisfies the relation

$$\mathbb{1} = \tilde{g}_0^{-1} \otimes \tilde{G}^{(\mathrm{T})} = \tilde{g}_0^{-1} \; e^{\frac{i}{2} J_{ij} \overleftarrow{\partial_i} \overrightarrow{\partial_j}} e^{\frac{i}{2} (\overleftarrow{\partial_\omega} \overrightarrow{\partial_t} - \overleftarrow{\partial_t} \overrightarrow{\partial_\omega})} \; \tilde{G}^{(\mathrm{T})} \tag{B.3}$$

where, in the last equality, i and j run only over position and momentum. We are interested in forces to linear order in $\mathbf{E} = -\partial \mathbf{A}/\partial t$ and $\dot{\mathbf{R}}$, i.e., to linear order in temporal derivatives. Therefore, we expand $\tilde{G}^{(\mathrm{T})} \approx \tilde{G}^{(\mathrm{T}0)} + \tilde{G}^{(\mathrm{T}1)} + \mathcal{O}(\partial_t^2)$ where the superscript

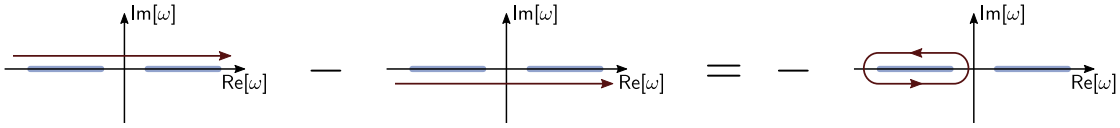

Figure B.1.: Transformation of the interal $\int_{-\infty}^{\infty} \mathrm{d}\omega\, (G^R - G^A)$ into an integral around a closed contour, see Eqs. (B.1)–(B.2). The blue shaded regions indicate the positions of poles of the Green's function.

denotes the order in temporal derivatives. From Eq. (B.3), we obtain

$$\mathbb{1} = \tilde{g}_0^{-1} \circ \tilde{G}^{(\mathrm{T0})}; \tag{B.4}$$

$$0 = \tilde{g}_0^{-1} \circ \tilde{G}^{(\mathrm{T1})} + \frac{i}{2}\left(\hbar \frac{\partial \tilde{G}^{(\mathrm{T0})}}{\partial t} - \frac{\partial \tilde{g}_0^{-1}}{\partial t} \circ \frac{\partial \tilde{G}^{(\mathrm{T0})}}{\partial \omega}\right). \tag{B.5}$$

Here, the symbol "$\circ$" denotes the Moyal product in position/momentum space only, and we used $\partial \tilde{g}_0^{-1}/\partial\omega = \hbar$. Eq. (B.4) is equivalent to the the defining equation of the equilibrium Green's function $\tilde{G}$ in a time-independent system, see Eq. (6.18) of the main text, and therefore $\tilde{G}^{(T0)} = \tilde{G}$. Inserting $\tilde{G}$ into Eq. (B.2), one obtains the force on a resting skyrmion in absence of an electric field, which vanishes as argued at the end of Section 10.4 of the main text. By solving Eqs. (B.4)–(B.5) for $\tilde{G}^{(\mathrm{T1})}$ and inserting into Eq. (B.3), we obtain after some partial integrations,

$$F_\alpha^{(\mathrm{T1})} = -\frac{i\hbar^2}{2}\int \mathrm{d}^d r \int \frac{\mathrm{d}^d k}{(2\pi)^d} \oint \frac{\mathrm{d}\omega}{2\pi i}\, \mathrm{Tr}\left[\tilde{G} \circ \left(\frac{\partial \tilde{g}_0^{-1}}{\partial r_\alpha} \circ \frac{\partial \tilde{G}}{\partial t} - \frac{\partial \tilde{g}_0^{-1}}{\partial t} \circ \frac{\partial \tilde{G}}{\partial r_\alpha}\right)\right]. \tag{B.6}$$

In the derivation of Eq. (B.6), we used $\tilde{g}_0^{-1} \circ \tilde{G} = \mathbb{1}$, cf., Eq. (B.4), $\partial \tilde{g}_0^{-1}/\partial\omega = \hbar$, and partial integration. While there is no integral over time, we can nevertheless use partial integration for temporal derivatives, since they are equivalent to derivatives in position and momentum space via the relation

$$\partial_t = -\frac{e}{\hbar}\mathbf{E}\cdot\partial_{\mathbf{k}} - \dot{\mathbf{R}}\cdot\partial_{\mathbf{r}}. \tag{B.7}$$

We now expand $F_\alpha^{(\mathrm{T1})} = F_\alpha^{(\mathrm{T1},0)} + F_\alpha^{(\mathrm{T1},1)} + \ldots$ in spatial gradients. The lowest order contribution is

$$\begin{aligned} F_\alpha^{(\mathrm{T1},0)} &= -\frac{i\hbar^2}{2}\int \mathrm{d}^d r \int \frac{\mathrm{d}^d k}{(2\pi)^d} \oint \frac{\mathrm{d}\omega}{2\pi i}\, \mathrm{Tr}\left[\tilde{g}_0\left(\frac{\partial \tilde{g}_0^{-1}}{\partial r_\alpha}\frac{\partial \tilde{g}_0}{\partial t} - \frac{\partial \tilde{g}_0^{-1}}{\partial t}\frac{\partial \tilde{g}_0}{\partial r_\alpha}\right)\right] \\ &= +\frac{i\hbar}{2}\int \mathrm{d}^d r \int \frac{\mathrm{d}^d k}{(2\pi)^d} \oint \frac{\mathrm{d}\omega}{2\pi i}\, J'_{ij}\, \mathrm{Tr}\left[\tilde{g}_0(\partial_i \tilde{H})\tilde{g}_0(\partial_j \tilde{H})\tilde{g}_0\right]. \end{aligned} \tag{B.8}$$

Here, i and j run over position, momentum, time, and frequency, and J' is an anti-symmetric tensor whose only non-vanishing components are

$$J'_{r_\alpha,t} = 1 \qquad \text{and} \qquad J'_{t,r_\alpha} = -1. \tag{B.9}$$

We evaluate the frequency integral using residue theorem and the relation

$$\tilde{g}_0(t,\mathbf{r};\omega,\mathbf{k}) = \sum_n \frac{|u_{n,t,\mathbf{k}}\rangle\langle u_{n,t,\mathbf{k}}|}{\hbar\omega - \mathcal{E}^{(0)}(t,\mathbf{r};\omega,\mathbf{k})}. \tag{B.10}$$

Finally, using Eq. (3.18) of the main text, we obtain

$$F_\alpha^{(\mathrm{T1},0)} = \sum_{n\ \mathrm{occ.}} \int \mathrm{d}^d r \int \frac{\mathrm{d}^d k}{(2\pi)^d} \left(\hbar \Omega^{\mathrm{r,r}}_{n,\alpha j} \dot{R}_j + e \Omega^{\mathrm{r,k}}_{n,\alpha j} E_j \right) \tag{B.11}$$

where the sum runs over all occupied bands n. The first term on the right-hand side of Eq. (B.11) is the gyro-coupling $-\mathbf{G}\times\dot{\mathbf{R}}$, cf., Eqs. (11.3) and (11.4) of the main text. The second term is the first chern number in the plane spanned by r_α and k_j. As argued in the main text, this term vanishes if position space can be compactified, i.e., if the magnetization is collinear far away from the skyrmion.

Gradient corrections to $F_\alpha^{(\mathrm{T1},0)}$ come in two varieties. First gradient corrections to the Green's functions $\tilde{G}$ in Eq. (B.6) are given to first order by Eq. (6.23) of the main text. Second, the Moyal products in Eq. (B.6) contain gradient corrections. Here, only the inner Moyal products have to be takein into account, since all gradient contributions from the outer Moyal product vanish by partial integration. We obtain for the leading correction to $F_\alpha^{(\mathrm{T1},0)}$,

$$F_\alpha^{(\mathrm{T1},1)} = \hbar^2 \int \mathrm{d}^d r \int \frac{\mathrm{d}^d k}{(2\pi)^d} \oint \frac{\mathrm{d}\omega}{2\pi i}\ \mathrm{Tr}\Big[$$

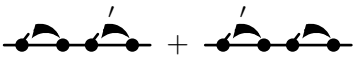

$$+\frac{1}{2}\Big($$

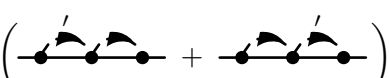

$$\Big)\Big]. \tag{B.12}$$

Here, we used again the pictorial notation introduced in Section 6.2 with one additional building block: a primed line with an arrow denotes contraction with the matrix J' instead of J, see Eq. (B.9). For example, the last diagram on the right-hand side of Eq. (B.12) denotes the term

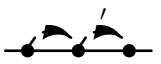

$$\equiv \left(\frac{i}{2}\right)^2 J_{ij} J'_{kl}\, \tilde{g}_0(-\partial_i \tilde{H}) \tilde{g}_0(-\partial_j\partial_k \tilde{H}) \tilde{g}_0(-\partial_l \tilde{H}) \tilde{g}_0. \tag{B.13}$$

One can easily generalize Eqs. (A.4), (A.5), and (A.7) to the situation where the two Moyal contractions are performed with different matrices J and J'. Using these relations, we find

$$F_\alpha^{(\mathrm{T1},1)} = -\frac{\hbar^2}{3} \int \mathrm{d}^d r \int \frac{\mathrm{d}^d k}{(2\pi)^d} \oint \frac{\mathrm{d}\omega}{2\pi i}\ \mathrm{Tr}\Big[$$

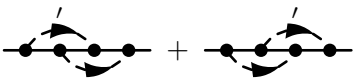

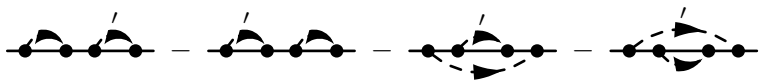

$$= -\frac{\hbar^2}{3}\left(\frac{i}{2}\right)^2 \int \mathrm{d}^d r \int \frac{\mathrm{d}^d k}{(2\pi)^d} \oint \frac{\mathrm{d}\omega}{2\pi i}\ \mathcal{I}'_{ijkl}\, \mathcal{B}_{ijkl}(t,\mathbf{r};\omega,\mathbf{k}) \tag{B.14}$$

where $\mathcal{B}_{ijkl}$ is given in Eq. (A.10) and

$$\mathcal{I}'_{ijkl} = J'_{ik}J_{jl} + J_{ik}J'_{jl} - J'_{ij}J_{kl} - J_{ij}J'_{kl} - J'_{il}J_{jk} - J_{il}J'_{jk}. \tag{B.15}$$

Evidently, $\mathcal{I}'_{ijkl}$ is totally antisymmetric in all indices. Of the coordinates i, j, k, and l, exactly one is the time, one is r_α, and the other two are a pair (r_β, k_β) of conjugated position and momentum directions, with $\alpha \neq \beta$ due to the anti-symmetry. When we express the temporal derivative in terms of position and momentum derivatives via Eq. (B.7), only the term $-\frac{e}{\hbar}E_\alpha \partial_{k_\alpha}$ survives the anti-symmetrization in a two-dimensional system. This is also true for a skyrmion tube in a three-dimensional system if we assume that the electric field is perpendicular to the skyrmion tube, since spatial derivatives along the symmetry axis of the skyrmion tube vanish. Thus, we obtain

$$F_\alpha^{(\mathrm{T1,1})} = \frac{e\hbar}{3}\left(\frac{i}{2}\right)^2 E_\alpha \int \mathrm{d}^d r \int \frac{\mathrm{d}^d k}{(2\pi)^d} \oint \frac{\mathrm{d}\omega}{2\pi i}\, \mathcal{I}_{ijkl}\mathcal{B}_{ijkl}(t, \mathbf{r}; \omega, \mathbf{k}) \tag{B.16}$$

where the indices i, j, k, and l run over position and momentum and $\mathcal{I}_{ijkl}$ is given in Eq. (A.9). Opening the integration contour at $\omega \to -\infty$ and deforming it to run along the imaginary axis from $-i\infty$ to $+i\infty$ leads to

$$F_\alpha^{(\mathrm{T1,1})} = -\delta Q^{(2)} E_\alpha \tag{B.17}$$

where $\delta Q^{(2)}$ is given in Eq. (A.8). Eqs. (B.11) and (B.17) conclude the derivation of Eq. (11.13) of the main text.

Acknowledgments

I would like to thank my thesis supervisor Prof. Dr. Achim Rosch for his invaluable support and guidance during the past years. It has been a great pleasure to work with him and to learn from him about physics and beyond. His deeply respectful treatment of any questions and his clearly visible joy in both identifying and solving physical problems have provided great conditions for working on this thesis. Fruitful discussions with PD Dr. Markus Garst, Dr. Dmitry Bagrets, and Prof. Dr. Philipp Strack at the Institute for Theoretical Physics in Cologne have cleared up many problems, for which I am thankful. I thank Dr. Frank Freimuth and Prof. Dr. Yuriy Mokrousov for the constructive cooperation and their openness for exchanging ideas. Discussions with Prof. Dr. Christian Pfleiderer, Prof. Dr. Jairo Sinova, and Prof. Dr. Stefan Blügel have helped me stay focused on the right topics. I also thank Prof. Dr. Alexander Altland and Prof. Dr. Paul van Loosdrecht for reviewing this thesis.

I am grateful for financial and intellectual support by Deutsche Telekom Stiftung and I would like to express my thanks to Christiane Frense-Heck for providing personal guidance. I am equally grateful to the Bonn-Cologne Graduate School of Physics and Astronomy, and to Dr. Petra Neubauer-Guenther.

Over the past years, I have had exchanges with many fellow students at the physics institute and I have greatly enjoyed the working environment and the team spirit that arises from our joint seminars and activities. Of the many people, I would like to mention in particular the ones I shared an office with: Karin Everschor-Sitte, Stephan Mandt, Christoph Schütte, Maximilian Genske, Sarah Schroeter, Laura Köhler, and Johannes Waizner, in order of appearance. It has been a pleasure working with you all! Thanks especially to Karin, who helped me getting started during my first weeks in Cologne, and Maximilian, who has been a great colleague both at the physics institute and at physics outreach programs.

Thanks to Mariela Boevska, Ute Graffenberger, Dorothea Hochscheid, Birgit Micheel, and Yasemin Tieben for great administrative support, to Dr. Andreas Sindermann for technical support and for so efficiently coordinating all correspondence with the central administration, and to Torsten Held and Daniel Klemmer for managing the supply of the Joyful Coffee Community of the University of Cologne.

Finally, I would like to express my sincere thanks to all my friends, my brother Richard Bamler, and my parents for their unconditional support.

Erklärung

Ich versichere, dass ich die von mir vorgelegte Dissertation selbständig angefertigt, die benutzten Quellen und Hilfsmittel vollständig angegeben und die Stellen der Arbeit – einschließlich Tabellen, Karten und Abbildungen –, die anderen Werken im Wortlaut oder dem Sinn nach entnommen sind, in jedem Einzelfall als Entlehnung kenntlich gemacht habe; dass diese Dissertation noch keiner anderen Fakultät oder Universität zur Prüfung vorgelegen hat; dass sie – abgesehen von unten angegebenen Teilpublikationen – noch nicht veröffentlicht worden ist sowie, dass ich eine solche Veröffentlichung vor Abschluss des Promotionsverfahrens nicht vornehmen werde. Die Bestimmungen der Promotionsordnung sind mir bekannt. Die von mir vorgelegte Dissertation ist von Prof. Dr. Achim Rosch betreut worden.

Köln, den 22. August 2016

Teilpublikationen

- R. Ritz, M. Halder, C. Franz, A. Bauer, M. Wagner, R. Bamler, A. Rosch, and C. Pfleiderer,
  Giant generic topological Hall resistivity of MnSi under pressure,
  Phys. Rev. B **87**, 134424 (2013)
- F. Freimuth, R. Bamler, Y. Mokrousov, and A. Rosch,
  Phase-space Berry phases in chiral magnets: Dzyaloshinskii-Moriya interaction and the charge of skyrmions,
  Phys. Rev. B **88**, 214409 (2013)
- R. Bamler and A. Rosch,
  Equilibration and approximate conservation laws: Dipole oscillations and perfect drag of ultracold atoms in a harmonic trap,
  Phys. Rev. A **91**, 063604 (2015)